Global Translational Medicine

ACCSCIENCE PUBLISHING

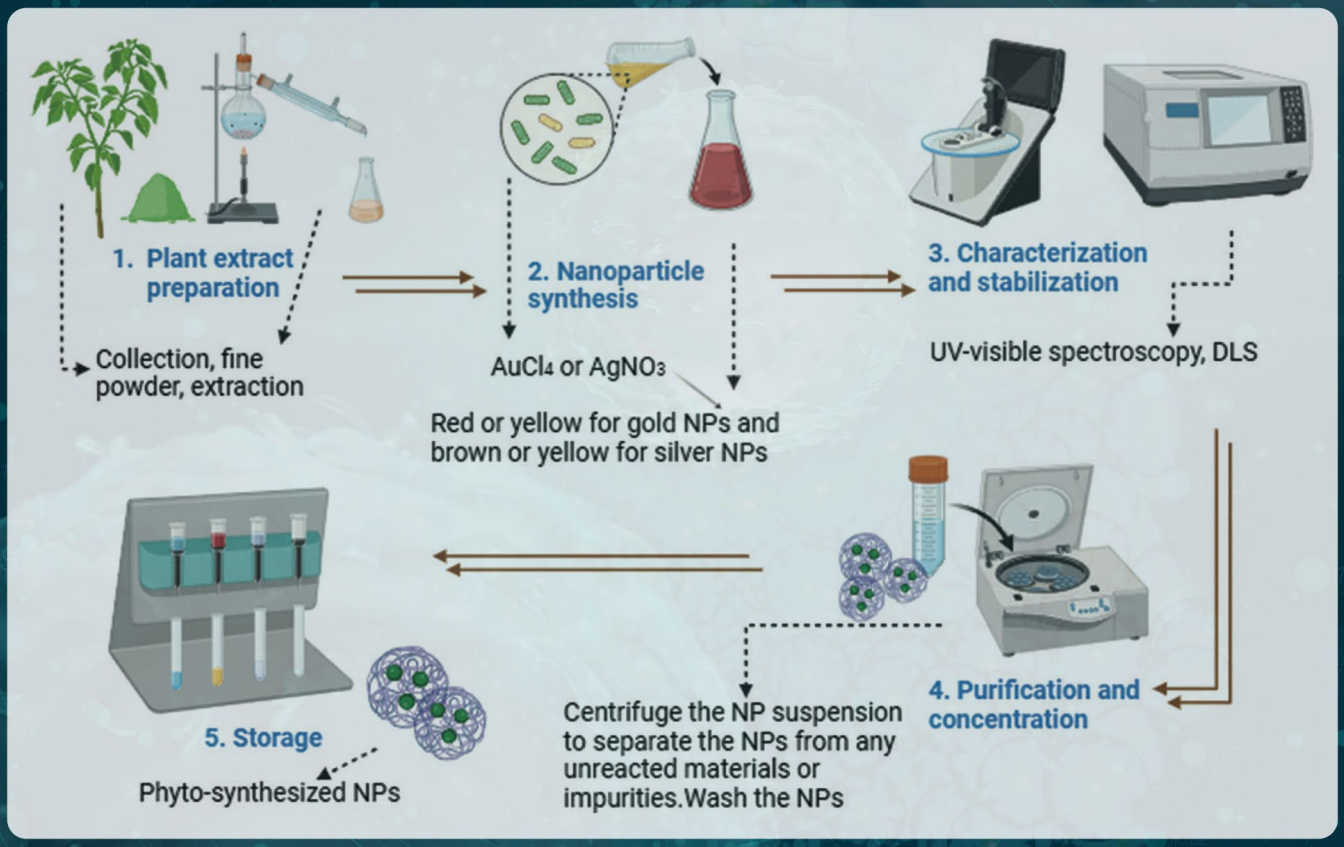

Synergizing phytonanotherapy and complementary medicine: Future horizons in cancer and diabetes care

ISSN: 3060-8600 (Print)
ISSN: 2811-0021 (Online)
Volume 4 · Issue 1
March 2025

Global Translational Medicine

Print ISSN: 3060-8600
Online ISSN: 2811-0021

Global Translational Medicine is a quarterly journal that focuses on medicine, biological sciences, and biomaterials engineering. *Global Translational Medicine* provides a platform to fill the gaps in preclinical and inter-disciplinary research, to promote clinical translation of scientific research results, and to contribute to the conception of new and improved preventive measures as well as diagnostic and therapeutic techniques of diseases.

About the Publisher

AccScience Publishing is a publishing company based in Singapore. We publish a range of high-quality, open-access, peer-reviewed journals and books from a broad spectrum of disciplines.

Contact Us

Managing Editor
gtm.office@accscience.sg

AccScience Publishing
8 Burn Road, #15-03 Trivex, Singapore 369977.

Volume 4 • Issue 1 • March 2025
ISSN 3060-8600 (print) ISSN 2811-0021 (online)

GLOBAL TRANSLATIONAL MEDICINE

ACCSCIENCE PUBLISHING

Access Science Without Barriers

GLOBAL TRANSLATIONAL MEDICINE

ISSN: 3060-8600 (print)
ISSN: 2811-0021 (online)

Editorial and Production Credits

Publisher: AccScience Publishing
Managing Editor: Alice Liu
Production Editor: Sharmila Velapasamy
Article Layout and Typeset: Sinjore Technologies (India)

For all advertising queries, contact gtm.office@accscience.sg.

Supplementary file

Supplementary files of articles can be obtained at https://accscience.com/journal/GTM/4/1.

About the Cover

An abstract illustration of human brain

Disclaimer

AccScience Publishing is not liable to the statements, perspectives, and opinions contained in the publications. The appearance of advertisements in the journal shall not be construed as a warranty, endorsement, or approval of the products or services advertised and/or the safety thereof. AccScience Publishing disclaims responsibility for any injury to persons or property resulting from any ideas or products referred to in the publications or advertisements. AccScience Publishing remains neutral with regard to jurisdictional claims in published maps and institutional affiliations.

Global Translational Medicine

Editorial Board

Assistant Editor

Youth Editorial Board Members

*Editorial Board Members as of March 27, 2025

ACCSCIENCE PUBLISHING

Volume 4 | Issue 1 | March 2025 | Page 1 – 143 |

Global Translational Medicine

https://accscience.com/journal/gtm

CONTENTS

REVIEW ARTICLES

1 **Advancements in cardiac regenerative therapy: Scalable human iPSC-derived cardiomyocyte differentiation and maturation**
Tadahisa Sugiura, Dhienda C. Shahannaz, Brandon E. Ferrell, Taizo Yoshida

16 **Synergizing phytonanotherapy and complementary medicine: Future horizons in cancer and diabetes care**
Faheem Patwekar, Mohsina Patwekar, Mohammad Amjad Kamal

PERSPECTIVE ARTICLES

35 **Patient-oriented and clinical considerations supporting the single-incision subepithelial connective tissue harvest**
Han S. Kim, Denise M. Cacho, Alan R. George, Joseph K. Retrum, Carsen R. McDaniel, Adam R. Lincicum, Kimberly Ann Inouye, Brian W. Stancoven, Thomas M. Johnson

47 **State-of-the-art perspective: Advances in incretin-based therapy targeting progression of diabetes and cardiovascular-kidney-metabolic syndrome**
Samar A. Nasser, Anuhya V. Pulapaka, Shaveta Gupta, Keith C. Ferdinand

56 **Overestimation of the cardiovascular consequences of low-dose radiation exposures**
Sergei V. Jargin

ORIGINAL RESEARCH ARTICLES

67 **Optimization of gelatin-based cell carriers for tooth-germ organoids**
Anisha Jackson, Cemile Bektas, Yong Mao

80 **Morphological signs of neurodegenerative and inflammatory processes in the brain of rats on a high-calorie diet**
Tatyana E. Kuznetsova, Tatyana A. Mityukova, Anastasia A. Basalai, Olga Y. Poluliakh

90 **Comparative evaluation of the therapeutic effects of *Schisandra chinensis* and *Schisandra sphenanthera* on vascular cognitive impairment and their drug-like compounds**
Yucen Zou, Bin Li, Meiqi Wang, Xiaomeng Xie, Jianuo Zhang, Qi Xiao, Chunyan Yang, Jiushi Liu, Haitao Sun, Bengang Zhang, Pei Ma, Haitao Liu

104 **Systemic and gastrointestinal amyloid A amyloidosis in rheumatoid arthritis: A post-mortem clinicopathologic study of 161 cases**
Miklós Bély, Ágnes Apáthy

126 **Predicting magnetic resonance imaging-guided focused ultrasound sonication parameters beyond skull density ratio**
Alsu Narkisovna Khatmullina, Diana Shamilevna Avzaletdinova, Dinara Ilgizovna Nabiullina, Sergey Nikolaevich Illarioshkin, Guzaliya Minvazykhovna Sakharova, Naufal Shamilevich Zagidullin, Nadezhdina Ekaterina Andreevna, Shamil Makhmutovich Safin, Rezida Maratovna Galimova

MINI-REVIEW

136 **The potential impact of weight control management on metabolic health during healthy aging**
Onur Oral, Mudasir Maqbool, Pramila Thapa, Pinar Tatlibal, Mumtaz Enser

LETTER TO EDITOR

142 Comment to the manuscript “chronic positive mass balance is the actual etiology of obesity: A living review”
Nikolaos Theodorakis

ACCSCIENCE PUBLISHING

Global Translational Medicine

REVIEW ARTICLE

Advancements in cardiac regenerative therapy: Scalable human iPSC-derived cardiomyocyte differentiation and maturation

Tadahisa Sugiura[1†*], Dhienda C. Shahannaz[1†], Brandon E. Ferrell[1], and Taizo Yoshida[2]

[1]Department of Cardiothoracic and Vascular Surgery, Montefiore Medical Center/Albert Einstein College of Medicine, New York, United States of America

[2]Department of Surgery, Montefiore Medical Center/Albert Einstein College of Medicine, New York, United States of America

(This article belongs to the *Special Issue: Exploring Cardiovascular Regenerative Therapy Using Induced Pluripotent Stem Cells*)

Abstract

The demand for mass production of induced pluripotent stem cell-derived cardiomyocytes (iPSC-CMs) is escalating, driven by their potential to revolutionize cardiac regenerative therapies. The development of large-scale production protocols for iPSC-CMs is crucial to attain their therapeutic potential, enabling the treatment of millions of patients' worldwide suffering from cardiovascular diseases. However, the scalable production of iPSC-CMs hinges on overcoming several critical challenges, including cellular differentiation and maturation. In pursue of tackling these challenges, researchers are investigating novel strategies such as prolonged culture periods, mechanical stimulation, and co-culture with supporting cell types. Overcoming these challenges is essential for unlocking the full potential of iPSC-CMs and paving the way for a new era in cardiac regenerative medicine. In this review, following topics are covered: (1) improvement of differentiation and maturation of iPSC-CMs and (2) scalable production of iPSC-CMs.

Keywords: Induced pluripotent stem cell; Cardiac regenerative therapy; Cardiomyocyte; Stem cell maturation; Clinical translation

[†]These authors contributed equally to this work.

***Corresponding author:**
Tadahisa Sugiura
(tsugiura@montefiore.org)

Citation: Sugiura T, Shahannaz DC, Ferrell BE, Yoshida T. Advancements in cardiac regenerative therapy: Scalable human iPSC-derived cardiomyocyte differentiation and maturation. *Global Transl Med*. 2025:4(1):1-15. doi: 10.36922/gtm.5745

Received: November 1, 2024

Revised: November 20, 2024

Accepted: November 27, 2024

Published online: January 8, 2025

1. Introduction

The human heart possesses a limited capacity for regeneration, characterized by a modest annual turnover rate of cardiomyocytes (CMs), which decreases with age, from approximately 1% at 25 years to 0.45% by 75 years, indicating a decline in regenerative potential over the lifespan.[1] The remarkable longevity of adult human CMs results in almost 50% being replaced over a 75-year lifespan, in stark contrast to the high mitotic and cytokinetic activity observed in infant CMs reaching 40%,[1] which drives cardiac growth and development, indicating a pronounced regenerative capacity in pediatric heart. Research investigations which incorporate findings based on animal model findings have consistently demonstrated that CMs undergo a developmental shift from a mononucleate to a binucleate state, concomitant with cell cycle withdrawal and

the loss of postnatal proliferative capacity.[2] In the context of prevalent cardiovascular diseases, such in myocardial infarction (MI), which results in the sudden loss of approximately one billion CMs, the inherent regenerative capacity is markedly insufficient. This limitation leads to structural repair through scar formation rather than functional repair through contractile restoration, potentially culminating in adverse ventricular remodeling and heart failure post-MI. Nevertheless, the discovery of adult CM repopulation suggests that native cell populations, both cardiac progenitor cells (CPCs) and existing CMs, may serve as viable sources for myocardial regeneration following injuries.[1]

Regenerative medicine requires a constant supply of cell sources, such as induced pluripotent stem cells (iPSCs), including those differentiated into CMs and other functional progenies. First founded in 2006 through reprogramming through the "Yamanaka Factors" (octamer-binding transcription factor 4 [OCT 4], sex-determining region Y-box 2 [Sox 2], Kruppel-like factor 4 [KLF4], and c-Myc protein; all abbreviated as OSKM), these somatic cells are collectively referred to as iPSCs, which can differentiate into all three embryonic germ layers.[3] As the research has been relying on the advancement of these iPSCs, their production should be resilient, financially feasible, and ultimately standardized by lab-scale protocols for iPSC expansion and cardiomyogenic differentiation toward more controlled processing in industry-compatible culture platforms. Here, advanced strategies for the cultivation and differentiation of iPSC will be reviewed by focusing on stirred bioreactor-based techniques for process-upscaling. The generation of CM mass from iPSCs could be enhanced by cardiovascular progenitor state, with equally important processes of cell fate control (differentiation and maturation). Finally, remaining challenges will be highlighted specifically regarding the adoption of three-dimensional (3D) iPSC suspension culture techniques for process-upscaling and critical safety issues ahead of clinical translation.

2. Differentiation and maturation of iPSC-CMs

2.1. Cardiac differentiation of iPSCs

The long-held notion that CMs are terminally differentiated, post-mitotic cells with negligible regenerative capacity after birth has recently been challenged. Bergmann *et al.* have provided evidence that CMs do indeed undergo renewal, although at a remarkably low rate. Their findings suggest that approximately 50% of CMs are replaced throughout an individual's lifetime, substantiating the concept of lifelong CM repopulation and overturning the previous understanding of CMs as a static cell population.[4]

Cardiac development is a complex, multidimensional process orchestrated by the sophisticated interplay of signaling pathways and gene transcriptional regulation. The quest for generating CMs has undergone a significant transformation. Formerly, embryonic stem cells were employed, but this approach was beset by ethical concerns. However, in 2006, Yamanaka pioneered an innovative method, harnessing iPSCs to reprogram terminally differentiated human fibroblasts,[5,6] obtained from skin or connective tissue biopsies, or human hair follicle keratinocyte, using four transcription factors (OSKM).[7-9] This reprogramming process yields iPSCs that can be further directed toward a cardiac fate through cardiac differentiation/induction, involving the activation of cardiac-specific transcription factors (T-box transcription factor 5 [TBX5], heart and neural crest derivatives expressed 1 [HAND1), GATA binding protein 4 [GATA4], and NK2 homeobox 5 [NKX2-5]).[10,11] This process generates reprogrammed cardiac precursors, including CPCs, which have the ability to differentiate into multiple cardiac cell types, such as CMs, smooth muscle cells, and endothelial cells.

In iPSC-CM development, differentiation and maturation are two distinct processes that occur sequentially: (1) the process of differentiation refers to the process by which iPSCs are coaxed to undergo a series of molecular and cellular changes, acquiring a CM-like phenotype and expressing cardiac-specific markers and genes. This process is characterized by the activation of cardiac-specific transcriptional programs and the suppression of pluripotency genes.[12,13] It results in the formation of immature CMs with primitive structural and functional properties, which then will need to undergo (2) maturation process to acquire advanced structural and functional properties. This second process is characterized by the further development of sarcomeres, contractile apparatus, and mitochondrial density, leading to enhanced contractility and electrophysiological function. This results in the formation of mature CMs with improved functionality and resemblance to native adult CMs.

The capacity of allowing stem cells to differentiate into specific human cell types of interest facilitates the discovery of compounds that selectively influence the activity of these cells while exhibiting minimal effects on alternative cell types, thereby facilitating elucidation of cell-type-specific responses.[14] The differentiation process involves the orchestrated activation of transcriptional programs,

signaling pathways, and epigenetic modifications that ultimately lead to the formation of functional CMs with the ability to contract, propagate action potentials (APs), and respond to physiological stimuli. Differentiation protocols also enhance the expression of cardiac-specific markers and ion channels, improving their electrophysiological properties.[15,16] This process also promotes the development of sarcomeres, contractile apparatus, and mitochondrial density, leading to enhanced contractility and calcium handling.[17,18] In addition, differentiation promotes the formation of functional gap junctions, enabling proper cell-cell coupling and synchronous beating.[19,20] Moreover, differentiated iPSC-CMs exhibit an improved response to beta-adrenergic stimulation and increased sensitivity to pharmacological agents.[21,22] This process also reduces the activation of pluripotency markers and tumorigenic potential.[23,24]

The maintenance and differentiation of cardiac stem cells from *in vitro* iPSCs rely on the recreation of the heart's intrinsic signaling microenvironment, achieving through the targeted use of growth factors (GFs), neurotransmitters, epigenetic modulators, and extracellular matrix proteins, which necessitates the selective activation or suppression of distinct signaling cascades.[25] Various differentiation protocols have been developed, including modulation of Wnt/β-catenin signaling, ACTIVIN/NODAL activation, BMP signaling activation, and the application of small molecules that trigger mesodermal specification. This is followed by the inhibition of Wnt signaling to form cardiac mesoderm and, consequently, cardiac-specific progenitors, culminating in the expression of cardiac markers, including structure genes which encode sarcomeric proteins characteristic of terminally differentiated CMs.[26-29]

Inadequate differentiation of iPSCs into CMs can result in immature or partially differentiated cells, leading to reduced contractility, abnormal electrophysiology, increased susceptibility to disease modeling, limited response to pharmacological agents, reduced engraftment and survival, and tumorigenic potential. These immature CMs may exhibit decreased contractile force and velocity (less effective for contractility to pump blood), aberrant electrical activity (leading to arrhythmia), and decreased response to drugs targeting mature CM functions. Furthermore, they may be more prone to disease-related phenotypes, such as hypertrophy or fibrosis, and have lower survival rates and engraftment efficiency when transplanted into the heart. The use of iPSC-CMs with immature properties may also result in the development of teratomas or other kinds of tumor.[30-32]

2.2. iPSC differentiation into cardiac subtypes

Differentiating iPSCs into specific cardiac subtypes: atrial, ventricular, Purkinje fibers, nodal cells, and endothelial cells involves manipulating distinct signaling pathways and environmental conditions, which leads to the development of cells with specialized structural and functional properties. Below is an elaboration of how differentiation occurs for each subtype:

For atrial CM (iPSC-aCMs), a key factor is the addition of retinoic acid (RA), which is pivotal for atrial differentiation. RA helps to guide progenitor cells toward the atrial phenotype by influencing atrial-specific gene expression, such as atrial natriuretic peptide.[33] Compared to ventricular CMs (vCMs), aCM's exhibit functional differences, including a shorter AP duration and faster beating rates. iPSC-aCMs also show distinctive triangular-shaped APs, reflecting faster repolarization and higher beating frequencies, which are essential for their role in controlling the atrial contraction rhythm.[34,35]

In attaining vCMs, differentiation involves the inhibition of RA and the enhancement of Wnt signaling. The absence of RA guides cells away from an atrial fate and toward the ventricular lineage. The iPSC-vCMs display longer APs with a prominent plateau phase, reflecting the sustained contraction necessary for ventricular pumping as its functional differences. These cells also have a slower beating frequency and demonstrate different calcium transient kinetics, which are crucial for the forceful and sustained contractions of the ventricles.[36,37]

Nodal (Pacemaker) cells are induced by high levels of cyclic adenosine monophosphate (cAMP) and the transcription factor T-box 3 (TBX3), which suppresses typical chamber-specific genes, thus enabling pacemaker characteristics. Bone morphogenetic protein (BMP) pathway is also involved in their specification. Nodal cells exhibit automaticity, meaning they generate spontaneous APs to regulate the heartbeat. This pacemaker activity is a defining feature, where nodal cells exhibit slower AP upstrokes and lack the fast sodium current seen in working CMs.[38,39]

Differentiation into Purkinje fibers is less commonly studied in iPSC research. However, these cells can be derived by modulating Notch signaling and transforming GF-beta (TGF-β) pathways, which influence the specialized conduction system. Purkinje fibers are specialized for fast transmission of electrical signals in the heart. They have unique AP profiles with a quick rise velocity, essential for coordinating timely ventricular contraction. Their primary function is fast conduction

rather than contraction, distinguishing them from atrial and ventricular cells.[40]

Endothelial cells, crucial for blood vessel formation, can be differentiated from iPSCs by inducing basic fibroblast GF and vascular endothelial GF (VEGF). These GFs stimulate the cells to develop endothelial-specific characteristics. Unlike CMs, endothelial cells do not contract but are essential for forming the lining of blood vessels and maintaining vascular integrity. They produce nitric oxide, which helps to regulate blood vessel dilation and blood pressure, and contributes to angiogenesis, the formation of new blood vessels.[41]

Each of these subtypes, though derived from a common progenitor (iPSC-CPCs), displays unique molecular markers, ion channel properties, and electrophysiological characteristics that define their specific roles within the heart.

To further fine-tune the differentiation process, purification is essential. Post-differentiation, CM purification ensures a homogeneous cell population for therapeutic applications. Techniques such as metabolic selection (e.g., using lactate-based media) or immunomagnetic sorting (targeting cTnT or SIRPA) are commonly employed, with purities reaching up to 95%. This purification step is critical, as undifferentiated cells or non-cardiac lineages can pose risks such as tumor formation or other complications *in vivo*. During differentiation, purification helps to enrich specific cardiac subtypes with two ways: (1) surface marker-based selection: cells are sorted based on specific surface markers expressed during differentiation, such as c-kit, fetal liver kinase 1, or vascular cell adhesion molecule 1 and (2) intracellular marker-based selection: cells are sorted based on intracellular markers, such as troponin or myosin, using techniques like fluorescence-activated cell sorting.

2.3. Maturation of iPSC-CPCs

The natural maturation process of CMs is intricate and extends into human development, culminating around 6 years of age when CMs attain the specialized characteristics necessary for effective cardiac contraction and relaxation.[42] This maturation begins during the early postnatal period, marked by the cessation of cell division and the initiation of physiological hypertrophy, which enhances cell size and functional capacity, enabling adaptation to the dynamic hemodynamic environment. This process is driven by the orchestrated releases of specific transcription factors, structural protein isoforms, and ion channels, which collectively delineate the functional identity of each CM subtype. Understanding the mechanisms governing these processes is vital for elucidating human heart development and function, while also leveraging the clinical potential of iPSC-CMs in cardiac disease modeling, drug discovery, and regenerative medicine.[42]

The maturation of iPSCs into CPCs involves several overlapping pathways and factors. Critical signaling pathways, including BMP, Wnt and FGF, alongside pivotal transcription factors such as NKX2-5, TBX5, and GATA4, play significant roles in this differentiation process. In addition, epigenetic modifications refine these cellular transitions, emphasizing their shared relevance in both the differentiation of iPSCs into CPCs and the subsequent maturation of these progenitors into fully functional CMs.

During the differentiation phase, the primary focus lies in inducing cardiac lineage commitment and suppressing alternative cell fates. In contrast, the maturation phase of CPCs into CMs emphasizes refining cardiac subtypes,[43] enhancing electrophysiological properties, and improving contractile functionality.[44] This transition illustrates a nuanced interplay between signaling pathways and epigenetic regulation, where factors pivotal to CPC differentiation are subsequently modulated to facilitate CM maturation. For instance, the Wnt/β-catenin pathways instrumental in promoting formation of CPCs undergoes suppression as maturation progresses.[45] Conversely, the BMP/Smad pathway, initially inhibitory to CPC differentiation, becomes activated to further define cardiac subtype identity.[46] In addition, microRNAs (miRNAs) such as miR-1 and miR-133 are dynamically regulated during the maturation process, meticulously tuning the expression of essential ion channels and contractile proteins.[47,48] These nuanced shifts in gene regulation and signaling are crucial for achieving mature CM phenotypes, highlighting the necessity for precise control over these processes *in vitro*.

Recent advancements have led researchers to develop maturation strategies that simulate *in vivo* cardiac conditions, utilizing a variety of biochemical and biophysical techniques. These strategies aim to enhance the maturation of iPSC-CMs, as summarized in Table 1, which highlights progress in recapitulating the complex processes associated with cardiac maturation, evaluated through the presentation of developed sarcomeric and ion/electrolyte channel proteins in high-throughput screening assays.

Table 1. iPSC-CM maturation and characteristics

Method	Approach	Maturation duration (day)	Mature CM features	Recent Findings (2018 – 2024)
Physical[50]	Prolonged culture time	360	(Day 30 as comparison) Expanded cellular dimension Sarcomere elongation Reduced rate of beating Decreased dual MCL22α/v expression Greater sarcomere-alignment	Prolonged culture leads to improved sarcomere alignment and functionality.[51]
Metabolic (hormone treatment)	Media +Triiodothyronine (T3) +Glucocorticoid +Dexamethasone	7 – 14	Expanded cellular dimension Reduced roundness Enhanced MHC-α and SERCA2a expression Suppressed β-MHC expression Decline of proliferative activity Boost in contractile strength and dynamics Accelerated calcium signaling Heightened mitochondrial activity for energy production	Hormone treatments significantly enhance cardiac maturation markers.[52]
Metabolic (glucose replacement)	Media Remove Glucose +palmitate +oleic acid +carnitine	≥3 – ≤20	Expanded cellular dimension Reduced roundness Elongated contractile unit (sarcomere) Enhanced mitochondrial quantity and respiratory activity Boost in contractile strength and dynamics Rise of velocity rate and membrane electrostatic storage	Replacement of glucose with fatty acids improves metabolic activity.[53]
Physical (substrate modification)	Substrate stiffness increase in: polydimethylsiloxane (PDMS)/polyacrylic acid (PAA) (6~10 kPa)	3 – 9	Regulates sarcomere stress and contractile activity Enhanced force production More elongated form adoption	Stiffer substrates enhance contractility and structural maturity.[54]
Physical (electrical stimulation)	Continuous electrical stimulation (6.6 V/cm and 1 Hz in 2 ms duration)	4	Enhanced expression of HCN1, MLCV, SCN5A, SERCA, Kv4.3 and GATA4 Rise of $TNNT^{+}$ cells Cell extension Ventricular-like action potential Increased action potential duration Improved calcium regulation In conjunction with mechanical stimulation through photoactivated PDMS: amplified surface N-cadherin signaling and sarcomere contraction	Electrical stimulation promotes maturation and improves action potential characteristics.[55]
Biochemical/physical	CM-fibroblast/MSC co-culture and static-cyclic stretching	2 × 7	Enhanced contraction speed Larger twitch amplitude Elevated tensile modulus More developed sarcomere architecture Connexin 43 aggregation Surface localization of n-cadherin Reduced cell proliferation capacity Improved upregulation of MYL2/7 and MYH7/6 including MLC2, CACNA1C, NPPA, and SERCA2 Stretching further amplified these effects, especially with cyclic stress	Co-culture with FB/MSC enhances functional properties of iPSC-CMs.[56]

(Cont'd...)

Table 1. ***(Continued)***

Method	Approach	Maturation duration (day)	Mature CM features	Recent Findings (2018 – 2024)
Metabolic/ biochemical/physical	Media+ Thyroid hormone-dexamethasone-IGF-1 (TDI) formed in microtissue	7	Enhanced cellular alignment Lengthened sarcomere structure Elevated expression of ATP2A2, MYH7, SLCBA1, PLN, PPARG, ADRB1, CHRM2, and p-AKT Reduced level of MYH6, TNNI1 Boosted contractile strength Prolonged time to peak Extended relaxation phase	Microtissue formats improve cellular alignment and contractility.[57]
Metabolic/biochemical	EHT-based media culture	3 – 5 × 7	Elevated fatty acid oxidation Greater sensitivity to tetrodotoxin Enhanced aerobic metabolic activity Mitochondria aligned in sarcomere structure Improved calcium regulation Increased density of I_{k1} Reduced diastolic membrane potential	EHT Formats enhance metabolic activity and functional maturation.[58]
3D Bioprinting	3D printing of cardiac tissue	2 – 4 × 7	Vascularization of tissues Enhanced cell alignment Mimics native heart structure and function	3D bioprinting advances functional cardiac tissue engineering.[59]
Genetic Modification	CRISPR/Cas9 and other gene editing technologies	Editing: 2 × 7 Further iPSC maturation: 2 – 4 × 7	Enhanced expression of cardiac markers Improved metabolic functions Enhanced cell survival	Genetic modifications using CRISPR enhance cardiac differentiation.[60,61]
ECM Engineering	Modifications to ECM properties	~30	Improved cell-matrix interactions Enhanced mechanical properties Mimics native ECM composition	ECM engineering improves cardiac patch integration[62]
Integration with Devices	Connection with electronic and sensing devices	As early as 48 h	Real-time monitoring of cardiac activity Enhanced integration with engineered tissues Feedback mechanisms for stimulation	Device integration enhances functionality of engineered cardiac tissues[63,64]

Note: This table is adapted and updated from Thomas *et al.*[49]
Abbreviations: MHC-α: Alpha-myosin heavy chain; SERCA2a: Sarcoplasmic reticulum $Ca^{[2]+}$ ATPase; β-MHC: Beta-myosin heavy chain; HCN1: Hyperpolarization activated cyclic nucleotide-gate potassium channel 1; SCN5A: Sodium voltage-gated channel alpha subunit 5; GATA4: GATA binding protein 4; TNNT: Troponin T; CM: Cardiomyocyte; FB: Fibroblast; MSC: Mesenchymal stem cell; MLCV: iPSC: Induced pluripotent stem cell; MYL: Myosin light chain; MYH: Myosin heavy chain; CACNA1C: Calcium voltage-gated channel subunit alpha 1C; NPPA: Natriuretic peptide precursor A; ATP2A2: ATPase sarcoplasmic/endoplasmic reticulum $Ca^{[2]+}$ transporting 2; PLN: Phospholamban; PPARG: Peroxisome proliferator-activated receptor gamma; ADRB1: Adrenoceptor beta 1; CHRM2: Cholinergic receptor muscarinic 2; EHT: Engineered heart tissue; ECM: Extracellular matrix.

One of the methods used to further mature CPCs is electrical stimulation (ES). ES promotes cardiac repair by recruiting stem cells to injury sites through cardioprotective extracellular vesicles (EVs) and exosomes released from CPCs. These EVs carry bioactive molecules, including VEGF, cytokines (such as interleukin [IL]-6, IL-8, and tumor necrosis factor-alpha), matrix metalloproteinases, tissue inhibitors of metalloproteinases, stromal cell-derived factor 1, and heat shock proteins, which support angiogenesis, remodeling, and inflammation resolution, including in Q-waves denervation.[64,65] EVs also contain peptides, mRNA, and miRNAs that modulate recipient cell function and protect CMs from hypoxia-induced cell death, aiding tissue repair and regeneration.[64,65] Neutral sphingomyelinase 2 (nSMase2) assists in ceramide formation, further promoting EV biogenesis under ES and enhancing cell survival. In addition, cAMP is involved in signaling to support stem cell survival.[66,67]

In cell culture, ES promotes the differentiation of CPCs into mature CMs by driving calcium ion (Ca^{2+}) influx through voltage-gated channels. This influx activates calmodulin and calcineurin, leading to the nuclear translocation of transcription factors. Key pathways, such as AKT and GSK3β phosphorylation, along with focal

adhesion kinase and MAPK/ERK signaling, enhance cell adhesion, growth, and migration. Connexin-43 gap junctions also form under ES, promoting electromechanical coupling and cell alignment for synchronized contraction, which is essential for mature cardiac tissue formation.[66,67]

In addition to promoting stem cell recruitment, ES helps prevent atrophy caused by denervation, which occurs when nerve supply to tissues is lost. By maintaining heart contractility and enhancing cellular responsiveness to electrical signals, ES can counteract the effects of denervation. ES activates pathways involved in muscle protein synthesis and cell survival, including the mechanistic target of rapamycin pathway, which is crucial for maintaining muscle mass.[67,68] Furthermore, ES has a neurogenic effect, influencing the autonomic nervous system to regulate neurotransmitter release and modulate cardiac function.[65,68] This interaction supports tissue repair by improving the heart's electrical activity in response to injury. Findings highlight the potential of ES in enhancing stem cell homing to cardiac injury sites, supporting tissue repair, and preventing atrophy due to denervation.

In large MIs with Q-waves and denervation, pulsed electromagnetic fields (PEMF) simulate EM forces,[69] potentially aiding sympathetic re-innervation and autonomic regulation. PEMF has shown benefits in experimental studies, improving metrics such as ejection fraction and supporting myocardial healing. At the biomolecular level, PEMF promotes VEGFR-mediated angiogenesis, nerve GF for re-innervation, and IL-10 to reduce chronic inflammation, all of which are essential for controlled tissue repair. In addition, piezoelectric materials are being investigated to localize electrical signals, improving stem cell migration to the infarct site without invasive power sources. Further studies employing 3D visualization methods, such as CUBIC and CLARITY,[70] have made strides in clarifying sympathetic nerve remodeling in post-MI contexts. This technology has enabled detailed mapping of cardiac sympathetic networks, which could help in monitoring EM treatment effectiveness and improving nerve regeneration post-MI. Together, these biomolecular mechanisms position ES and EM therapies as potent tools for cardiac repair

3. Scalable production of iPSC-CMs

The discovery of iPSCs has revolutionized the field of regenerative medicine, enabling the generation of diverse cell types for therapeutic applications. However, the high costs associated with generating and validating iPSC lines pose a significant obstacle to their widespread adoption. Consequently, there is an urgent need for the establishment of cell banks that provide access to high-quality, validated iPSC lines, serving as repositories to cater the various requirements of clinical research communities. This would facilitate the widespread adoption of iPSCs in therapeutic research, ultimately advancing the regenerative medicine field. Clinical trials have begun utilizing human iPSCs to address debilitating diseases. For instance, iPSC-derived retinal-pigment epithelial cells have been transplanted to tackle macular degeneration (MD),[71] while β-like cells are being differentiated to overcome insulin dependence in type 1 diabetes mellitus patients.[72] These advancements highlight the need for large-scale, clinically compliant iPSC production to support these innovations. Several key factors must be optimized, including bioreactor design, culture conditions, and cell differentiation protocols. The goal is to achieve rejection-free cell transplants without needing lifelong immunosuppressive therapy (that comes with direct organ transplantation as earlier therapy finding).

From a bioprocess perspective, the autologous method necessitates modestly sized, condition-targeted treatment doses for each individual patient. This approach may also require extra cells for quality assurance, efficacy assays, and reserved dosages for subsequent transplantation, if applicable. For instance, estimates suggest that retinal-pigment epithelium cells from approximately 50,000 iPSCs would suffice to treat MD in one patient, as demonstrated in a successful case using human iPSCs.[73] To accommodate therapeutic cell production on such a limited scale, automation, facility space with minimal good manufacturing practice (GMP) standards, and the simultaneous production of various patient samples in single-use culture systems are crucial to the continuing of this production.[74]

These facts collectively strongly advocate for an allogeneic approach, wherein a "universal cell source" is intended for transplantation into non-related recipients, likely requiring immunosuppressive therapy similar to traditional organ transplants. However, the degree of immunosuppression needed will depend on human leukocyte antigen compatibility, which can be achieved through the strategic deployment of multiple iPSC lines to cater to specific patient populations within a given region or country, as discussed in greater detail elsewhere.[75] This allogeneic "off-the-shelf" strategy also ensures timely cell availability to meet pressing clinical demands. This highlights the need for robust, cost-effective, and reliable GMP-compliant protocols for scaling up iPSC cultivation and differentiation into specialized cell types (including iPSC-CMs), ensuring consistency and reproducibility in research applications, without displaying heterogeneous behaviors.

Culture medium is a critical component for large-scale production, impacting both cost and quality control. Standard iPSC culture media, such as mTeSR™1 or Essential 8™, are commonly used, but their high costs present a bottleneck for scalability. On average, these media cost \$500 – \$700/L, with daily consumption in large-scale bioreactors ranging from 1 – 2 L, depending on cell density and bioreactor volume.[76] Thus, media optimization, including potential shifts toward serum-free or chemically defined formulations, is a key strategy for cost reduction. Studies have shown that adjusting key components such as GFs (e.g., fibroblast growth factor 2 [FGF2] and TGF-β) can reduce media consumption by 20 – 30% while maintaining high cell viability and pluripotency.[77,78]

Scalable production of iPSC-CMs requires meticulous optimization of biomolecular and process factors to drive differentiation toward CPCs mimicking the complexity and multipotentiality of first heart field and second heart field.[79-81] Key factors include: (1) transcription factors: Essential cardiac-specific marker genes such as GATA4-6,[82,83] HAND1/2,[84] NKX2-5,[85] TBX5,[85,86] and cardiac troponin T (cTnT) must be expressed to initiate cardiac development;[10,11] (2) signaling pathways: activation of pathways such as activin A, Wnt/β-catenin, and BMP/TGF-β to regulate lineage specification;[87] (3) GFs and cytokines: supplementation with FGF,[88] VEGF,[89] BMP4,[90] and cytokines such as IL-6[91] and IL-11[92] supports directed differentiation; (4) extracellular matrix (ECM) components: collagen, fibronectin, and laminin in synthetic scaffolds or decellularized matrices create an ideal cellular environment, enhancing maturation;[93-95] (5) cell culture conditions: controlled oxygen levels, pH, and nutrient flow are crucial for maintaining cell viability;[96,97] (6) timing and duration: the schedule and length of exposure to these cues directly impact differentiation efficiency;[98] (7) iPSC line quality: the initial quality and pluripotency of the iPSC line affect differentiation outcomes;[99,100] (8) reprogramming method: the method of iPSC generation shapes the epigenetic profile and influences differentiation potential;[101,102] (9) epigenetic modifications: DNA methylation and histone modifications regulate cardiac gene expression throughout differentiation;[103] and (10) mechanical forces and biophysical cues: shear stress and ES enhance maturation and functional rhythm.[104-107]

The use of stirred tank bioreactors (STBs) remains a widely employed method for scalable iPSC-CM production, particularly for generating high-yield quantities. Parameters such as medium composition, ECM scaffold selection, and precise biochemical signaling are essential to ensure consistency and reproducibility. In current large-scale differentiation protocols, optimized conditions involving factors such as activin A (100 ng/mL) and BMP4 (10 ng/mL) have demonstrated the potential to generate 10^8 – 10^{10} iPSC-CMs (one to two folds of which are required per patient) in a single run, yielding sufficient quantities of iPSC-CMs for therapeutic applications in 5 – 10 L volumes within a 2 – 3 week timeframe. Differentiation efficiencies of 70 – 90% are achieved through these optimized protocols, meaning 7 – 9 out of every 10 iPSCs successfully differentiate into CMs, depending on the initial seeding density and bioreactor volume.[20,108] The estimated cost for generating these cells, including reagents, media, and labor, ranges from \$10,000 to \$20,000 per patient dose, with ongoing efforts aimed to reduce this cost through process optimization and economies of scale.[63,109,110]

As for process dimensions, estimates indicate that approximately 1 – 10 × 10^9 (1 – 10 billions) functional active cells for each patient are required for solid organ restoration, including substituting hepatocytes, pancreatic β-cells, or CMs. However, significantly larger quantities are required in producing "*in vitro* blood," with calculations suggesting that around 2 – 3 × 10^{13} human iPSC-derived red blood cells (iPSC-RBCs) are required to match 5 L of blood in adults, considering that 1 millimeter of blood contains approximately 5 billion erythrocytes.[43]

Calculations derived from experimental data indicate that current production of one billion human iPSC-CMs demands a bioprocess scale of 1 – 2.5 L.[110] This implies that even with substantial future advancements, mass production of iPSC progenies will demand industrial-level procedures, which have already been developed for producing recombinant proteins or vaccines in mammalian cell cultures at scales of approximately 1,000 L.[111] In contrast, bioprocess development for iPSCs remains in its nascent stage, requiring the further advancement to meet industrial demands.

However, it is worth noting that STBs are not 3D systems in the same way as other bioreactor types, such as 3D suspension bioreactors. While STBs remain useful for large-scale production, advancements in 3D cultures have been increasingly explored to enhance the differentiation and maturation of iPSC-derived cells. These systems allow for more complex interactions, potentially improving both the yields and functionalities of differentiated cells, though STBs still provide a reliable and scalable approach for achieving high-yield production. Some of the latest scalable methods include: (1) vertical-wheel bioreactors: designed to reduce shear stress using a gentler mixing mechanism compared to traditional impeller-based stirred tanks, potentially improving cell viability and differentiation consistency, (2) microcarrier-based systems: By allowing iPSCs to attach and grow on microcarriers, these systems

help increase cell density in the bioreactor, enhancing yield without significantly increasing reactor size, and (3) perfusion bioreactors: by continuously supplying fresh medium while removing waste, perfusion bioreactors maintain optimal conditions for cell growth, supporting longer culture durations and higher cell densities, and (4) 3D suspension culture systems: enabling cells to grow as aggregates or spheroids, which can better mimic *in vivo* environments, potentially leading to more mature cell phenotypes and scalable expansion.[111]

3D suspension culture systems have emerged as a powerful method for scalable iPSC-CM production, offering significant advantages over traditional 2D culture systems by better mimicking the *in vivo* environment. In these systems, iPSCs aggregate into spheroids, fostering enhanced cell-cell and cell-matrix interactions and creating a more uniformed cellular microenvironment, promoting CPCs differentiation into functional CMs. This setup supports key signaling pathways, such as gap junction maturation. 3D cultures generate CMs with better electrophysiological properties, contractile function, and drug response, making them ideal for drug screening and regenerative medicine. In addition, 3D cultures are more likely to exhibit a mature phenotype, including better synchronization of cell contractions and enhanced responses to pharmacological agents, making them more suitable for drug screening and regenerative medicine applications. Their scalability is crucial for therapeutic applications, supporting heart disease modeling, personalized medicine, and autologous therapies with improved consistency.

To optimize these systems for scalable production, bioreactor design plays a pivotal role. Maintaining continuous nutrient flow and removing waste through continuous perfusion are crucial for supporting large-scale cell cultures. For instance, spinner flasks, wave-induced motion systems, and perfusion-based platforms have been used to maintain optimal cell health and growth while ensuring uniform differentiation. These bioreactor systems allow the maintenance of large volumes of spheroids, streamlining the process of expanding iPSC-CMs. The success of these cultures also hinges on controlling key parameters, such as shear forces, agitation speed, and seeding density, all of which can influence cell viability and differentiation outcomes.

While scalable production is crucial for iPSC-based therapies, it is equally important to ensure cell fate control of the mature cell phenotype and its functional rhythm control. By combining optimized bioreactor conditions with precise biochemical cues, these systems are advancing the field of iPSC-derived cardiac models, enabling the development of more effective, scalable, and clinically relevant platforms for heart disease modeling, drug discovery, and regenerative medicine. The development of economically and methodologically efficient large-scale iPSC-CM culture is closely tied to understanding and promoting cell maturation, whereas optimization of rhythm control in CMs requires a comprehensive approach which incorporates advances in scalable production and cellular maturation, underscoring the importance of these three pillars.[112]

4. Conclusion

Substantial advancements have been made in leveraging iPSC-CMs for cardiac regenerative medicine, with current bioreactor systems capable of producing up to 10^{11} cells per batch. To enhance predictive power and recapitulate population-level cardiovascular risks, further refinements are required, such as implementing robust quality control endpoints, scalable differentiation protocols with minimized variability, and nutrient-driven maturation strategies. Notably, 3D bioprinting and microphysiological systems enable the replication of complex tissue structures and interactions, facilitating more accurate disease modeling and drug screening. Such bidirectional scalability is crucial for translating iPSC-CMs into large-scale regenerative applications. Efforts to harmonize patient iPSC banking and generation of cardiovascular cell types with reduced batch-to-batch variability will support personalized treatment approaches. These advancements set the foundation for population-based studies and pharmacogenetic tools, and, importantly, potential autologous transplant therapies to address myocardial repair in clinical settings. Continued progress on cost reduction, iPSC-CM maturation, and safety protocols will be pivotal for making iPSC-CM-based therapies a viable option in clinical practice.

Acknowledgments

None.

Funding

None.

Conflict of interest

Tadahisa Sugiura is the Editorial Board Member of this journal and Guest Editor of this special issue, but was not in any way involved in the editorial and peer-review process conducted for this paper, directly or indirectly. Separately, other authors declared that they have no known competing financial interests or personal relationships that could have influenced the work reported in this paper.

Author contributions

Conceptualization: Tadahisa Sugiura
Writing – original draft: Dhienda C. Shahannaz
Writing – review & editing: Tadahisa Sugiura, Brandon E. Ferrel, Taizo Yoshida

Ethics approval and consent to participate

Not applicable.

Consent for publication

Not applicable.

Availability of data

Not applicable.

References

1. Kasai-Brunswick TH, Carvalho AB, De Carvalho ACC. Cardiac stem cells: Fact or fiction? In: *Resident Stem Cells and Regenerative Therapy*. Amsterdam, Netherlands: Elsevier; 2023. p. 5-21.

   doi: 10.1016/b978-0-443-15289-4.00006-8

2. Beisaw A, Wu C. Cardiomyocyte maturation and its reversal during cardiac regeneration. *Dev Dyn*. 2022;253(1):8-27.

   doi: 10.1002/dvdy.557

3. Sugiura T, Shahannaz DC, Ferrell BE. Current status of cardiac regenerative therapy using induced pluripotent stem cells. *Int J Mol Sci*. 2024;25(11):5772.

   doi: 10.3390/ijms25115772

4. Bergmann O, Bhardwaj RD, Bernard S, *et al*. Evidence for cardiomyocyte renewal in humans. *Science*. 2009;324(5923):98-102.

   doi: 10.1126/science.1164680

5. Takahashi K, Yamanaka S. Induction of pluripotent stem cells from mouse embryonic and adult fibroblast cultures by defined factors. *Cell*. 2006;126(4):663-676.

   doi: 10.1016/j.cell.2006.07.024

6. Takahashi K, Tanabe K, Ohnuki M, *et al*. Induction of pluripotent stem cells from adult human fibroblasts by defined factors. *Cell*. 2007;131(5):861-872.

   doi: 10.1016/j.cell.2007.11.019

7. Mohit G, Mohammed JMS, Akbarsha MA, Rohini G. Cellular reprogramming, transdifferentiation and alleviation of the aging pathology. *Res J Biotechnol*. 2023;19(2):127-139.

   doi: 10.25303/1902rjbt1270139

8. Liu Q, Feng W, Yang T, Yi T, Li F. Upconversion luminescence imaging of cells and small animals. *Nat Protoc*. 2013;8(10):2033-2044.

   doi: 10.1038/nprot.2013.114

9. Hasan A, Mohammadi N, Nawaz A, *et al*. Age-dependent maturation of IPSC-CMs leads to the enhanced compartmentation of B2AR-CAMP signalling. *Cells*. 2020;9(10):2275.

   doi: 10.3390/cells9102275

10. Grunert M, Dorn C, Rickert-Sperling S. Cardiac transcription factors and regulatory networks. *Adv Exp Med Biol*. 2024;1441:295-311.

    doi: 10.1007/978-3-031-44087-8_16

11. Robbe ZL, Shi W, Wasson LK, *et al*. CHD4 is recruited by GATA4 and NKX2-5 to repress noncardiac gene programs in the developing heart. *Genes Dev*. 2022;36(7-8):468-482.

    doi: 10.1101/gad.349154.121

12. Morris SA, Daley GQ. A blueprint for engineering cell fate: Current technologies to reprogram cell identity. *Cell Res*. 2013;23:33-48.

    doi: 10.1038/cr.2013.1

13. Correia CD, Ferreira A, Fernandes MT, *et al*. Human Stem cells for cardiac disease modeling and preclinical and clinical applications-are we on the road to success? *Cells*. 2023;12:1727.

    doi: 10.3390/cells12131727

14. Eglen RM, Reisine T. Human IPS Cell-derived patient tissues and 3D cell culture part 1: Target identification and lead optimization. *SLAS Technol*. 2018;24(1):3-17.

    doi: 10.1177/2472630318803277

15. Afjeh-Dana E, Naserzadeh P, Moradi E, Hosseini N, Seifalian AM, Ashtari B. Correction to: Stem cell differentiation into cardiomyocytes: Current methods and emerging approaches. *Stem Cell Rev Rep*. 2022;18(6):2202.

    doi: 10.1007/s12015-022-10395-z

16. Clancy CE, Santana LF. Advances in induced pluripotent stem cell-derived cardiac myocytes: Technological breakthroughs, key discoveries and new applications. *J Physiol*. 2024;602(16):3871-3892.

    doi: 10.1113/jp282562

17. Correia C, Christoffersson J, Tejedor S, *et al*. Enhancing maturation and translatability of human pluripotent stem cell-derived cardiomyocytes through a novel medium containing acetyl-CoA carboxylase 2 inhibitor. *Cells*. 2024;13(16):1339.

    doi: 10.3390/cells13161339

18. Bhattacharya S, Burridge PW, Kropp EM, *et al*. High efficiency differentiation of human pluripotent stem cells to cardiomyocytes and characterization by flow cytometry. *J Vis Exp*. 2014;91:52010.

    doi: 10.3791/52010

19. Hamad S, Derichsweiler D, Papadopoulos S, *et al*. Generation of human induced pluripotent stem cell-derived cardiomyocytes in 2D monolayer and scalable 3D suspension bioreactor cultures with reduced batch-to-batch variations. *Theranostics*. 2019;9(24):7222-7238.

doi: 10.7150/thno.32058

20. Ma J, Guo L, Fiene SJ, *et al*. High purity human-induced pluripotent stem cell-derived cardiomyocytes: Electrophysiological properties of action potentials and ionic currents. *Am J Physiol Heart Circ Physiol*. 2011;301(5):H2006-H2017.

doi: 10.1152/ajpheart.00694.2011

21. Kiss E, Fischer C, Sauter JM, Sun J, Ullrich ND. The structural and the functional aspects of intercellular communication in IPSC-Cardiomyocytes. *Int J Mol Sci*. 2022;23(8):4460.

doi: 10.3390/ijms23084460

22. Li X, Zeng D, Chen Y, *et al*. Role of alpha-and beta-adrenergic receptors in cardiomyocyte differentiation from murine-induced pluripotent stem cells. *Cell Prolif*. 2016;50(1):e12310.

doi: 10.1111/cpr.12310

23. Liang P, Lan F, Lee AS, *et al*. Drug screening using a library of human induced pluripotent stem cell-derived cardiomyocytes reveals disease-specific patterns of cardiotoxicity. *Circulation*. 2013;127(16):1677-1691.

doi: 10.1161/circulationaha.113.001883

24. Lemmens M, Perner J, Potgeter L, *et al*. Identification of marker genes to monitor residual iPSCs in iPSC-derived products. *Cytotherapy*. 2022;25(1):59-67.

doi: 10.1016/j.jcyt.2022.09.010

25. Cho S, Lee C, Skylar-Scott MA, Heilshorn SC, Wu JC. Reconstructing the heart using iPSCs: Engineering strategies and applications. *J Mol Cellu Cardiol*. 2021;157:56-65.

doi: 10.1016/j.yjmcc.2021.04.006

26. Yamamoto T, Sato Y, Yasuda S, *et al*. Correlation between genetic abnormalities in induced pluripotent stem Cell-Derivatives and abnormal tissue formation in tumorigenicity tests. *Stem Cells Transl Med*. 2022;11(5):527-538.

doi: 10.1093/stcltm/szac014

27. Ye C, Yang C, Zhang H, *et al*. Canonical Wnt signaling directs the generation of functional human PSC-derived atrioventricular canal cardiomyocytes in bioprinted cardiac tissues. *Cell Stem Cell*. 2024;31(3):398-409.e5.

doi: 10.1016/j.stem.2024.01.008

28. Wang F, Yin L, Zhang W, Tang Y, Wang X, Huang C. The method of sinus node-like pacemaker cells from human induced pluripotent stem cells by BMP and Wnt signaling. *Cell Biol Toxicol*. 2023;39(6):2725-2741.

doi: 10.1007/s10565-023-09797-7

29. Burridge PW, Matsa E, Shukla P, *et al*. Chemically defined generation of human cardiomyocytes. *Nat Methods*. 2014;11(8):855-860.

doi: 10.1038/nmeth.2999

30. Burridge PW, Li YF, Matsa E, *et al*. Human induced pluripotent stem cell-derived cardiomyocytes recapitulate the predilection of breast cancer patients to doxorubicin-induced cardiotoxicity. *Nat Med*. 2016;22(5):547-556.

doi: 10.1038/nm.4087

31. Garbern JC, Lee RT. Mitochondria and metabolic transitions in cardiomyocytes: Lessons from development for stem cell-derived cardiomyocytes. *Stem Cell Res Ther*. 2021;12(1):177.

doi: 10.1186/s13287-021-02252-6

32. Zhao MT, Shao NY, Garg V. Subtype-specific cardiomyocytes for precision medicine: Where are we now? *Stem Cells*. 2020;38(7):822-833.

doi: 10.1002/stem.3178

33. Zhou Y, Zhou R, Huang W, *et al*. Gene expression, morphology, and electrophysiology during the dynamic development of human induced pluripotent stem cell-derived atrial- and ventricular-like cardiomyocytes. *Biologics*. 2024;18:115-127.

doi: 10.2147/btt.s448054

34. Shiti A, Arbil G, Shaheen N, Huber I, Setter N, Gepstein L. Utilizing human induced pluripotent stem cells to study atrial arrhythmias in the short QT syndrome. *J Mol Cell Cardiol*. 2023;183:42-53.

doi: 10.1016/j.yjmcc.2023.08.003

35. Joshi J, Albers C, Smole N, Guo S, Smith SA. Human induced pluripotent stem cell-derived cardiomyocytes (iPSC-CMs) for modeling cardiac arrhythmias: Strengths, challenges and potential solutions. *Front Physiol*. 2024;15:1475152.

doi: 10.3389/fphys.2024.1475152

36. Seibertz F, Rubio T, Springer R, *et al*. Atrial fibrillation-associated electrical remodelling in human induced pluripotent stem cell-derived atrial cardiomyocytes: A novel pathway for antiarrhythmic therapy development. *Cardiovasc Res*. 2023;119(16):2623-2637.

doi: 10.1093/cvr/cvad143

37. Cyganek L, Tiburcy M, Sekeres K, *et al*. Deep phenotyping of human induced pluripotent stem cell-derived atrial and ventricular cardiomyocytes. *JCI Insight*. 2018;3(12):e99941.

doi: 10.1172/jci.insight.99941

38. Li J, Wiesinger A, Fokkert L, *et al*. Modeling the atrioventricular conduction axis using human pluripotent stem cell-derived cardiac assembloids. *Cell Stem Cell*. 2024;31:1667-1684.e6.

doi: 10.1016/j.stem.2024.08.008

39. Kim JJ, Yang L, Lin B, *et al*. Mechanism of automaticity in cardiomyocytes derived from human induced pluripotent stem cells. *J Mol Cell Cardiol*. 2015;81:81-93.

doi: 10.1016/j.yjmcc.2015.01.013

40. Gonzalez DM, Dariolli R, Moyett J, *et al*. Transient notch activation converts pluripotent stem cell-derived cardiomyocytes towards a purkinje fiber fate. *bioRxiv* [Preprint]. 2024.

doi: 10.1101/2024.09.22.614353

41. Loh KM, Ang LT. Building human artery and vein endothelial cells from pluripotent stem cells, and enduring mysteries surrounding arteriovenous development. *Semin Cell Dev Biol*. 2023;155:62-75.

doi: 10.1016/j.semcdb.2023.06.004

42. Salameh S, Ogueri V, Posnack NG. Adapting to a new environment: Postnatal maturation of the human cardiomyocyte. *J Physiol*. 2023;601(13):2593-2619.

doi: 10.1113/jp283792

43. Prondzynski M, Berkson P, Trembley MA, *et al*. Efficient and reproducible generation of human iPSC-derived cardiomyocytes and cardiac organoids in stirred suspension systems. *Nat Commun*. 2024;15(1):5929.

doi: 10.1038/s41467-024-50224-0

44. Rapöhn M, Cyganek L, Voigt N, Hasenfuß G, Lehnart SE, Wegener JW. Noninvasive analysis of contractility during identical maturations revealed two phenotypes in ventricular but not in atrial iPSC-CM. *Am J Physiol Heart Circ Physiol*. 2024;326(3):H599-H611.

doi: 10.1152/ajpheart.00527.2023

45. Lu A, Gu R, Chu C, *et al*. Inhibition of Wnt/β-catenin signaling upregulates Nav1.5 channels in Brugada syndrome iPSC-derived cardiomyocytes. *Physiol Rep*. 2023;11(10):e15696.

doi: 10.14814/phy2.15696

46. Sánchez-Duffhues G, Hiepen C. Human IPSCs as model systems for BMP-related rare diseases. *Cells*. 2023;12(17):2200.

doi: 10.3390/cells12172200

47. Røsand Ø, Wang J, Scrimgeour N, Marwarha G, Høydal MA. Exosomal preconditioning of human IPSC-Derived cardiomyocytes beneficially alters cardiac electrophysiology and micro RNA expression. *Int J Mol Sci*. 2024;25(15):8460.

doi: 10.3390/ijms25158460

48. Martyniak A, Jeż M, Dulak J, Stępniewski J. Adaptation of cardiomyogenesis to the generation and maturation of cardiomyocytes from human pluripotent stem cells. *IUBMB Life*. 2022;75(1):8-29.

doi: 10.1002/iub.2685

49. Thomas D, Cunningham NJ, Shenoy S, Wu JC. Human-induced pluripotent stem cells in cardiovascular research: current approaches in cardiac differentiation, maturation strategies, and scalable production. *Cardiovasc Res*. 2021;118(1):20-36.

doi: 10.1093/cvr/cvab115

50. Kamakura T, Makiyama T, Sasaki K, *et al*. Ultrastructural maturation of human-induced pluripotent stem cell-derived cardiomyocytes in a long-term culture. *Circ J*. 2013;77(5):1307-1314.

doi: 10.1253/circj.cj-12-0987

51. Satsuka A, Ribeiro AJS, Kawagishi H, *et al*. Contractility assessment using aligned human iPSC-derived cardiomyocytes. *J Pharmacol Toxicol Methods*. 2024;128:107530.

doi: 10.1016/j.vascn.2024.107530

52. Hamledari H, Asghari P, Jayousi F, *et al*. Using human induced pluripotent stem cell-derived cardiomyocytes to understand the mechanisms driving cardiomyocyte maturation. *Front Cardiovasc Med*. 2022;9:967659.

doi: 10.3389/fcvm.2022.967659

53. Yoshida A, Sekine W, Homma J, *et al*. Development of appropriate fatty acid formulations to raise the contractility of constructed myocardial tissues. *Regen Ther*. 2022;21:413-423.

doi: 10.1016/j.reth.2022.09.006

54. Young KM, Reinhart-King CA. Cellular mechanosignaling for sensing and transducing matrix rigidity. *Curr Opin Cell Biol*. 2023;83:102208.

doi: 10.1016/j.ceb.2023.102208

55. Dai Y, Mu J, Zhou F. The use of electrical stimulation to induce cardiac differentiation of stem cells for the treatment of myocardial infarction. *Rev Cardiovasc Med*. 2021;22(4):1167-1171.

doi: 10.31083/j.rcm2204125

56. Sandora N, Putra MA, Busro PW, *et al*. Preparation of cell-seeded heart patch *in vitro*; Co-culture of adipose-derived mesenchymal stem cell and cardiomyocytes in amnion bilayer patch. *Cardiovasc Eng Technol*. 2021;13(2):193-206.

doi: 10.1007/s13239-021-00565-4

57. Vivas A, IJspeert C, Pan JY, *et al*. Generation and culture of cardiac microtissues in a microfluidic chip with a reversible open top enables electrical pacing, dynamic drug dosing and endothelial cell co-culture. *Adv Mater Technol*. 2022;7(7):2101355.

doi: 10.1002/admt.202101355

58. Rupert C, López JE, Cortez-Toledo E, *et al*. Increased length-dependent activation of human engineered heart tissue after chronic α1A-adrenergic agonist treatment: Testing a novel heart failure therapy. *Am J Physiol Heart Circ Physiol*.

2023;324(3):H293-H304.

doi: 10.1152/ajpheart.00279.2022

59. Mir A, Lee E, Shih W, *et al*. 3D bioprinting for vascularization. *Bioengineering* (*Basel*). 2023;10(5):606.

doi: 10.3390/bioengineering10050606

60. Friedman MJ, Wagner T, Lee H, Rosenfeld MG, Oh S. Enhancer-promoter specificity in gene transcription: Molecular mechanisms and disease associations. *Exp Mol Med*. 2024;56(4):772-787.

doi: 10.1038/s12276-024-01233-y

61. Guo Y, Cao Y, Jardin BD, *et al*. Ryanodine receptor 2 (RYR2) dysfunction activates the unfolded protein response and perturbs cardiomyocyte maturation. *Cardiovasc Res*. 2022;119(1):221-235.

doi: 10.1093/cvr/cvac077

62. Mesquita FCP, Morrissey J, Monnerat G, Domont GB, Nogueira FCS, Hochman-Mendez C. Decellularized extracellular matrix powder accelerates metabolic maturation at early stages of cardiac differentiation in human induced pluripotent stem cell-derived cardiomyocytes. *Cells Tissues Organs*. 2021;212(1):32-44.

doi: 10.1159/000521580

63. Clarke GA, Hartse BX, Asli AEN, *et al*. Advancement of sensor integrated organ-on-chip devices. *Sensors* (*Basel*). 2021;21(4):1367.

doi: 10.3390/s21041367

64. Seibertz F, Rubio T, Springer R, *et al*. Atrial fibrillation-associated electrical remodelling in human induced pluripotent stem cell-derived atrial cardiomyocytes: a novel pathway for antiarrhythmic therapy development. *Cardiovasc Res*. 2023;119:2623-2637.

doi: 10.1093/cvr/cvad143

65. Balbi C, Vassalli G. Exosomes: Beyond stem cells for cardiac protection and repair. *Stem Cells*. 2020;38(11):1387-1399.

doi: 10.1002/stem.3261

66. Kim SW, Kim HW, Huang W, *et al*. Cardiac stem cells with electrical stimulation improve ischaemic heart function through regulation of connective tissue growth factor and miR-378. *Cardiovasc Res*. 2013;100(2):241-251.

doi: 10.1093/cvr/cvt192

67. Zhang H, Shen Y, Kim IM, *et al*. Electrical stimulation increases the secretion of cardioprotective extracellular vesicles from cardiac mesenchymal stem cells. *Cells*. 2023;12(6):875.

doi: 10.3390/cells12060875

68. Omer SA, McKnight KH, Young LI, Song S. Stimulation strategies for electrical and magnetic modulation of cells and tissues. *Cell Regen*. 2023;12(1):21.

doi: 10.1186/s13619-023-00165-8

69. Wang Y, Chen L, Wang L, *et al*. Pulsed electromagnetic fields combined with adipose-derived stem cells protect ischemic myocardium by regulating miR-20a-5p/E2F1/p73 signaling. *Stem Cells*. 2023;41(7):724-737.

doi: 10.1093/stmcls/sxad037

70. Yokoyama T, Lee JK, Miwa K, *et al*. Quantification of sympathetic hyperinnervation and denervation after myocardial infarction by three-dimensional assessment of the cardiac sympathetic network in cleared transparent murine hearts. *PLoS One*. 2017;12(7):e0182072.

doi: 10.1371/journal.pone.0182072

71. Seah I, Goh D, Banerjee A, Su X. Modeling inherited retinal diseases using human induced pluripotent stem cell derived photoreceptor cells and retinal pigment epithelial cells. *Front Med* (*Lausanne*). 2024;11:1328474.

doi: 10.3389/fmed.2024.1328474

72. Zhang H, Wei Y, Wang Y, *et al*. Emerging diabetes therapies: Regenerating pancreatic β cells. *Tissue Eng Part B Rev*. 2024;30:644-656.

doi: 10.1089/ten.teb.2024.0041

73. Dehghan S, Mirshahi R, Shoae-Hassani A, Naseripour M. Human-induced pluripotent stem cells-derived retinal pigmented epithelium, a new horizon for cells-based therapies for age-related macular degeneration. *Stem Cell Res Ther*. 2022;13(1):217.

doi: 10.1186/s13287-022-02894-0

74. Novoa JJ, Westra IM, Steeneveld E, *et al*. Good manufacturing practice-compliant human induced pluripotent stem cells: From bench to putative clinical products. *Cytotherapy*. 2024;26(6):556-566.

doi: 10.1016/j.jcyt.2024.02.021

75. Fang Y, Wang SPH, Liao I, *et al*. HLA-E^{high}/HLA-G^{high}/HLA-II^{low} Human iPSC-derived cardiomyocytes exhibit low immunogenicity for heart regeneration. *Adv Healthc Mater*. 2023;12(29):e2301186.

doi: 10.1002/adhm.202301186

76. Kuo HH, Gao X, DeKeyser JM, *et al*. Negligible-cost and weekend-free chemically defined human IPSC culture. *Stem Cell Reports*. 2020;14(2):256-270.

doi: 10.1016/j.stemcr.2019.12.007

77. Lotz S, Goderie S, Tokas N, *et al*. Sustained levels of FGF2 maintain undifferentiated stem cell cultures with biweekly feeding. *PLoS One*. 2013;8(2):e56289.

doi: 10.1371/journal.pone.0056289

78. Mossahebi-Mohammadi M, Quan M, Zhang JS, Li X. FGF signaling pathway: A key regulator of stem cell pluripotency. *Front Cell Dev Biol*. 2020;8:79.

doi: 10.3389/fcell.2020.00079

79. Kelly RG. The heart field transcriptional landscape at single-cell resolution. *Dev Cell*. 2023;58(4):257-266.

doi: 10.1016/j.devcel.2023.01.010

80. Farah EN, Hu RK, Kern C, *et al*. Spatially organized cellular communities form the developing human heart. *Nature*. 2024;627(8005):854-864.

doi: 10.1038/s41586-024-07171-z

81. Zhang Q, Carlin D, Zhu F, *et al*. Unveiling complexity and multipotentiality of early heart fields. *Circ Res*. 2021;129(4):474-487.

doi: 10.1161/circresaha.121.318943

82. Bisson JA, Gordillo M, Kumar R, *et al*. GATA6 regulates WNT and BMP programs to pattern precardiac mesoderm during the earliest stages of human cardiogenesis. *bioRxiv* [Preprint]. 2024.

doi: 10.1101/2024.07.09.602666

83. Sharma A, Wasson LK, Willcox JA, *et al*. GATA6 mutations in hiPSCs inform mechanisms for maldevelopment of the heart, pancreas, and diaphragm. *Elife*. 2020;9:e53278.

doi: 10.7554/elife.53278

84. Guo H, Hang C, Lin B, *et al*. HAND factors regulate cardiac lineage commitment and differentiation from human pluripotent stem cells. *Stem Cell Res Ther*. 2024;15(1):31.

doi: 10.1186/s13287-024-03649-9

85. Pezhouman A, Engel JL, Nguyen NB, *et al*. Isolation and characterization of human embryonic stem cell-derived heart field-specific cardiomyocytes unravels new insights into their transcriptional and electrophysiological profiles. *Cardiovasc Res*. 2021;118(3):828-843.

doi: 10.1093/cvr/cvab102

86. Pezhouman A, Nguyen NB, Sercel AJ, *et al*. Transcriptional, electrophysiological, and metabolic characterizations of HESC-Derived first and second heart fields demonstrate a potential role of TBX5 in cardiomyocyte maturation. *Front Cell Dev Biol*. 2021;9:787684.

doi: 10.3389/fcell.2021.787684

87. Singh BN, Yucel D, Garay BI, *et al*. Proliferation and maturation: Janus and the art of cardiac tissue engineering. *Circ Res*. 2023;132(4):519-540.

doi: 10.1161/circresaha.122.321770

88. Shouman S, Zaher A, Abdelhameed A, *et al*. Cardiac progenitor cells. *Adv Exp Med Biol*. 2020;1312:51-73.

doi: 10.1007/5584_2020_594

89. Yan W, Xia Y, Zhao H, Xu X, Ma X, Tao L. Stem cell-based therapy in cardiac repair after myocardial infarction: Promise, challenges, and future directions. *J Mol Cell Cardiol*. 2024;188:1-14.

doi: 10.1016/j.yjmcc.2023.12.009

90. Lee CS, Kim J, Cho HJ, Kim HS. Cardiovascular regeneration via stem cells and direct reprogramming: A review. *Korean Circ J*. 2022;52(5):341.

doi: 10.4070/kcj.2022.0005

91. Almuwaqqat Z, Kim JH, Garcia M, *et al*. Associations between inflammation, cardiovascular regenerative capacity, and cardiovascular events: A cohort study. *Arterioscler Thromb Vasc Biol*. 2021;41(11):2814-2822.

doi: 10.1161/atvbaha.121.316574

92. Kastlmeier MT, Gonzalez-Rodriguez E, Cabanis P, *et al*. Cytokine signaling converging on IL11 in ILD fibroblasts provokes aberrant epithelial differentiation signatures. *Front Immunol*. 2023;14:1128239.

doi: 10.3389/fimmu.2023.1128239

93. Barnes AM, Holmstoen TB, Bonham AJ, Rowland TJ. Differentiating human pluripotent stem cells to cardiomyocytes using purified extracellular matrix proteins. *Bioengineering* (*Basel*). 2022;9(12):720.

doi: 10.3390/bioengineering9120720

94. Napiwocki BN, Stempien A, Lang D, *et al*. Micropattern platform promotes extracellular matrix remodeling by human PSC-derived cardiac fibroblasts and enhances contractility of co-cultured cardiomyocytes. *Physiol Rep*. 2021;9(19):e15045.

doi: 10.14814/phy2.15045

95. Brown GE, Han YD, Michell AR, *et al*. Engineered cocultures of iPSC-derived atrial cardiomyocytes and atrial fibroblasts for modeling atrial fibrillation. *Sci Adv*. 2024;10(3):eadg1222.

doi: 10.1126/sciadv.adg1222

96. Henn AD, Pereira T, Hunsberger J, *et al*. Cytocentric measurement for regenerative medicine. *Front Med Technol*. 2023;5:1154653.

doi: 10.3389/fmedt.2023.1154653

97. Sebastião MJ, Abecasis B, Carrondo MJT, Alves PM, Gomes-Alves P, Serra M. 3D strategies for expansion of human cardiac stem/progenitor cells. In: *Bioreactors for Stem Cell Expansion and Differentiation*. United States: CRC Press; 2018. p. 63-95.

doi: 10.1201/9780429453144-4

98. Pianezzi E, Altomare C, Bolis S, *et al*. Role of somatic cell sources in the maturation degree of human induced pluripotent stem cell-derived cardiomyocytes. *Biochim Biophys Acta Mol Cell Res*. 2019;1867(3):118538.

doi: 10.1016/j.bbamcr.2019.118538

99. Yasui R, Sekine K, Taniguchi H. Clever experimental designs: Shortcuts for better IPSC differentiation. *Cells*.

2021;10(12):3540.

doi: 10.3390/cells10123540

100. Chen CXQ, Abdian N, Maussion G, *et al*. Standardized quality control workflow to evaluate the reproducibility and differentiation potential of human iPSCs into neurons. *bioRxiv* [*Preprint*]. 2021.

doi: 10.1101/2021.01.13.426620

101. He X, Liang J, Paul C, Huang W, Dutta S, Wang Y. Advances in cellular reprogramming-based approaches for heart regenerative repair. *Cells*. 2022;11(23):3914.

doi: 10.3390/cells11233914

102. Derish I, Cecere R. Multifaceted role of induced pluripotent stem cells in preclinical cardiac regeneration research. In: *Handbook of Stem Cell Applications*. Singapore: Springer; 2024. p. 787-847.

doi: 10.1007/978-981-99-7119-0_33

103. Li N, Nguyen BT, Stitt EA, Zhang Z, MacLellan WR, Zhang Y. Dynamic visualization of DNA methylation in cell cycle genes during iPSC cardiac differentiation. *Epigenomics*. 2024;16:1407-1414.

doi: 10.1080/17501911.2024.2430171

104. Zieliński PS, Gudeti PKR, Rikmanspoel T, Włodarczyk-Biegun MK. 3D printing of bio-instructive materials: Toward directing the cell. *Bioact Mater*. 2022;19:292-327.

doi: 10.1016/j.bioactmat.2022.04.008

105. Körner A, Mosqueira M, Hecker M, Ullrich ND. Substrate stiffness influences structural and functional remodeling in induced pluripotent stem cell-derived cardiomyocytes. *Front Physiol*. 2021;12:710619.

doi: 10.3389/fphys.2021.710619

106. Qin J, Van Mil A, Sluijter JPG. Biophysical stretch induced differentiation and maturation of induced pluripotent stem cell-derived cardiomyocytes. In: *Cardiac and Vascular Biology*. Cham: Springer; 2023. p. 141-179.

doi: 10.1007/978-3-031-23965-6_7

107. Wan X, Liu Z, Li L. Manipulation of stem cells Fates: The master and multifaceted roles of biophysical cues of biomaterials. *Adv Funct Mater*. 2021;31(23):2010626.

doi: 10.1002/adfm.202010626

108. Cho S, Discher DE, Leong KW, Vunjak-Novakovic G, Wu JC. Challenges and opportunities for the next generation of cardiovascular tissue engineering. *Nat Methods*. 2022;19(9):1064-1071.

doi: 10.1038/s41592-022-01591-3

109. Nogueira DES, Cabral JMS, Rodrigues CAV. Single-use bioreactors for human pluripotent and adult stem cells: Towards regenerative medicine applications. *Bioengineering*. (*Basel*). 2021;8(5):68.

doi: 10.3390/bioengineering8050068

110. Ackermann M, Saleh F, Abdin SM, *et al*. Standardized generation of human iPSC-derived hematopoietic organoids and macrophages utilizing a benchtop bioreactor platform under fully defined conditions. *Stem Cell Res Ther*. 2024;15(1):171.

doi: 10.1186/s13287-024-03785-2

111. Bachhav B, De Rossi J, Llanos CD, Segatori L. Cell factory engineering: Challenges and opportunities for synthetic biology applications. *Biotechnol Bioeng*. 2023;120(9): 2441-2459.

doi: 10.1002/bit.28365

112. Carvalho AB, Kasai-Brunswick TH, De Carvalho ACC. Advanced cell and gene therapies in cardiology. *EBioMedicine*. 2024;103:105125.

doi: 10.1016/j.ebiom.2024.105125

ACCSCIENCE PUBLISHING

Global Translational Medicine

REVIEW ARTICLE

Synergizing phytonanotherapy and complementary medicine: Future horizons in cancer and diabetes care

Faheem Patwekar[1]*, Mohsina Patwekar[2]*, and Mohammad Amjad Kamal[3,4,5,6]

[1]Department of Pharmacognosy, Luqman College of Pharmacy, PB 86, old Jewargi Road, Gulbarga, Karnataka, India

[2]Department of Pharmacology, Luqman College of Pharmacy, PB 86, old Jewargi Road, Gulbarga, Karnataka, India

[3]Department of Pharmaceutical Sciences, College of Pharmacy, Princess Nourah bint Abdul rahman, University, Riyadh 11671, Saudi Arabia

[4]Department of Pharmacy, Faculty of Health and Life Sciences, Daffodil International University, Birulia, Savar, Dhaka -1216, Bangladesh

[5]Centre for Global Health Research, Saveetha Medical College and Hospital, Saveetha Institute of Medical and Technical Sciences, Chennai,

Tamil Nadu, India

[6]Novel Global Community Educational Foundation, Australia

***Corresponding authors:**
Faheem Patwekar (ifaheemp@gmail.com);
Mohsina Patwekar (mohsina.patwekar@gmail.com)

Citation: Patwekar F, Patwekar M, Kamal MA. Synergizing phytonanotherapy and complementary medicine: Future horizons in cancer and diabetes care. *Global Transl Med*. 2025:4(1):16-34. doi: 10.36922/gtm.5840

Received: November 11, 2024

Revised: December 24, 2024

Accepted: January 3, 2025

Published online: January 22, 2025

Abstract

The intersection of phytonanotherapy, complementary and alternative medicine (CAM), and nanoparticles (NPs) promises an exciting new area in cancer and diabetes treatment. The CAM has attracted international recognition, emphasizing natural therapies and holistic health. Phytonanotherapy uses the promise of environmentally safe and sustainable green synthesis processes to develop NPs rich in bioactive chemicals originating from plants. These NPs provide a novel approach to targeted drug delivery, diagnostics, and therapy. Personalized medicine, tailoring therapies to individual genetic profiles and illness features, will most certainly be a cornerstone of these approaches in the future. The accuracy of NP-based drug delivery systems offers improved treatment outcomes while lowering systemic toxicity. Advanced diagnostics based on NPs and biosensors will enable early disease identification and real-time therapy response monitoring. Furthermore, combining CAM principles with NP-based therapies has great promise for holistic care. Combination therapies combining traditional medicine with cutting-edge nanomedicine have the potential to revolutionize cancer and diabetes care. These medicines will become more widely available provided an improvement in the regulatory approval process and accessibility. Individual preferences and well-being will be prioritized in patient-centered care, promoting a range of treatment options. Collaboration between practitioners of traditional medicine, researchers, artificial intelligence experts, and healthcare providers will improve complete and integrative health care. Green synthesis technologies will improve the efficiency and scalability of NP production. However, greater public and professional awareness is needed through educational initiatives to highlight the benefits and potential of CAM, phytonanotherapy, and NP-based treatments. To summarize, the future of CAM, phytonanotherapy, and NPs in cancer and diabetes treatment is bright since they provide patients with a variety of options while also contributing to more effective, sustainable, and patient-centered

health care. To realize the full potential of these novel techniques, rigorous research, comprehensive clinical trials, and regulatory support will be required.

Keywords: Phytonanotherapy; Complementary and alternative medicine; Nanoparticles; Cancer treatment; Diabetes management

1. Introduction

The World Health Organization emphasizes the importance of indigenous medicinal plants in the search for eco-friendly, non-hazardous, and cost-effective healthcare solutions. These plants have been used to treat a variety of maladies, including acquired immune deficiency syndrome, tuberculosis, diabetes mellitus, malaria, and cancer. A considerable fraction of the population in many developing nations combines complementary and alternative medicines (CAMs) with conventional prescription pharmaceuticals, mirroring a global trend. Notably, in China, traditional alternative medicine accounts for 30-50% of medical use, whereas in Africa, CAM accounts for an astounding 80% of primary health care.[1,2] Even in the United States, around 158 million individuals use CAM. This increased interest in CAM can be ascribed to three basic factors: the desire to improve one's quality of life, reduce symptoms, and avoid long-term problems. Despite advances in conventional medications, they often bear the burden of long-term side effects and the danger of ineffectiveness in treating chronic conditions such as cancer and diabetes.[3,4]

The biosynthesis of metal nanoparticles (NPs) without the use of hazardous chemical and physical synthetic processes is a promising way to harness the healing potential of medicinal plants. These plants have unique metal tolerance mechanisms that allow them to produce NPs, particularly gold and silver NPs. This strategy is made even more enticing by the fact that medicinal plants include a complex mixture of chemical constituents such as proteins, vitamins, enzymes, amino acids, polysaccharides, and organic compounds. Because of their chemical diversity, they are both ecologically friendly and chemically complex, making them appropriate for a variety of medical uses. Terpenoids, polysaccharides, polyols, and flavones are phytocompounds that play critical roles in the bioreduction, stabilization, and biocapping processes that result in the creation of stable gold and silver NPs. Furthermore, as indicated by enzyme inhibitor kinetics and *in silico* docking investigations, these plant compounds have inhibitory potential against specific diabetic targets, offering light on their inhibitory actions.

This review explores the promising potential of phytosynthesized gold and silver NPs, particularly as anticancer and antidiabetic medicines. We present a new combination of plant-derived compounds and metal NPs in phytonanotherapy, delivering therapeutic qualities that potentially rival synthetic medications in clinical efficacy while minimizing adverse effects. This paradigm change has the potential to revolutionize therapy for chronic diseases by allowing medicinal plant therapies to supplement existing synthetic medicines and ushering in a new era of clinical research in both non-communicable and communicable diseases.[5-7]

2. CAM and NPs

CAM and NPs represent two distinct topics that have received considerable interest in the domains of health care and biotechnology. Recent research has investigated the junction of these two realms, leading to fresh approaches in health care and therapeutic interventions. In this section, we look at this interesting intersection. Nano-based drug delivery in CAM is one important area where CAM and NPs collide in medication delivery. Because of their small size and unique features, NPs can be created to encapsulate therapeutic chemicals sourced from medicinal plants or other CAM sources. NPs have the potential to improve the bioavailability and targeted administration of CAM-based therapies, potentially increasing efficacy while decreasing negative effects.[8,9] This method has been used to give plant extracts, essential oils, and other CAMs.

Medicinal herbs, a cornerstone of CAM, have been exploited to create eco-friendly NPs. Phytochemicals found in plant extracts can act as reducing and stabilizing agents in NP production. Plant extracts containing polyphenols, flavonoids, and terpenoids, for example, have been used to create NPs such as gold and silver. These photosynthesized NPs have the potential to be used in a variety of applications, including medication delivery and diagnostics.

The combination of CAM with NPs has the potential to improve therapeutic outcomes. NPs, for example, can increase the solubility and stability of CAM-derived chemicals, making them more appropriate for therapeutic usage. This synergy could lead to more effective treatments for disorders like cancer, diabetes, and inflammatory diseases.

NPs have also been used in CAM to aid with diagnosis.[10,11] Functionalized NPs can be used as contrast agents in imaging techniques such as magnetic resonance imaging (MRI) or as drug carriers. This approach facilitates the visualization and precise treatment of diseases, aligning with the holistic principles commonly linked with CAM.

Nevertheless, the combination of CAM and NPs raises concerns about safety and regulatory oversight. Ensuring the safety and quality of CAM-derived NPs is crucial before they acceptance and application in health care. Regulatory bodies must adapt to facilitate the comprehensive evaluation and approval of these novel therapeutics.[12]

3. Phytonanotherapy and green synthesis

Phytonanotherapy and green synthesis represent two innovative and eco-friendly approaches in the fields of health care and nanotechnology. Their individual concepts and their potential intersections are described in the following sections. Table 1 shows the pros and cons of both these approaches.

3.1. Phytonanotherapy

Phytonanotherapy is a cutting-edge method of treatment that blends the healing characteristics of medicinal plants with nanotechnology. It entails using NPs produced from plant-derived chemicals or extracts for targeted medication delivery and improved therapeutic effects. Figure 1 describes some of the most important components of phytonanotherapy.[13]

3.1.1. NP synthesis

In phytonanotherapy, NPs are synthesized utilizing phytochemicals extracted from medicinal plants, and these NPs can include gold, silver, or other materials and function as carriers for therapeutic medicines.[14]

3.1.2. Targeted drug delivery

Drugs or therapeutic compounds originating from medicinal plants can be encapsulated in phytosynthesized NPs. These NPs can then be targeted at specific disease areas in the body, boosting therapeutic efficacy while decreasing side effects.[15]

3.1.3. Improved bioavailability

NPs can improve plant-derived drug solubility and bioavailability, making them more useful as therapies for cancer, diabetes, and inflammatory illnesses.[16]

3.1.4. Reduced toxicity

Phytonanotherapy tries to lessen the toxicity associated with some synthetic medications by utilizing natural plant chemicals, hence promoting safer therapies.[15]

3.2. Green synthesis of NPs

Green synthesis, also known as environmentally friendly or eco-friendly synthesis, is a technique for creating NPs from biocompatible and sustainable ingredients. Green synthesis, as opposed to standard chemical processes, which frequently entail hazardous chemicals and severe settings, focuses on natural supplies and benign reaction conditions.

Table 1. Pros and cons of phytonanotherapy and green synthesis

Pros	Phytonanotherapy	Green Synthesis
Enhanced drug delivery	Improved bioavailability of plant-based therapies	Synthesis of NPs with customized characteristics under controlled conditions
Targeted therapy	Precise distribution to specific disease locations.	Possibility of customizing functionality for individual applications
Reduced toxicity	Uses natural, less harmful substances	Avoids the usage of potentially dangerous chemicals
Sustainable materials	Uses plant-derived chemicals	Uses ecologically friendly precursors.
Biocompatibility	NPs are generally biocompatible	Produces frequently biocompatible NPs
Diverse therapeutic options	Access to a diverse array of therapeutic plants	Material versatility (metals, oxides, and so on)
Eco-friendly approach	Complies with environmental and sustainable principles	Low environmental effect
Cons	**Phytonanotherapy**	**Green Synthesis**
Limited plant availability	Varying plant availability (seasonal)	Reliance on the availability of appropriate plant sources
Standardization challenges	Difficulty in maintaining consistency in phytochemical composition	Varying reproducibility of green synthesis methods.
Safety concerns	Allergic reactions to plant-based ingredients	Varying biocompatibility and toxicity
Regulatory hurdles	Strict guidelines for herbal medicine and NP-based treatments	Complicated regulatory approval process

Abbreviation: NP: Nanoparticles.

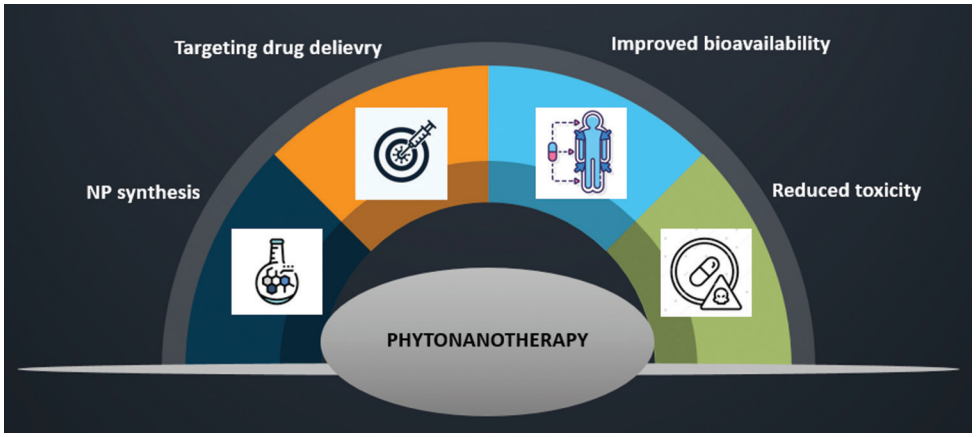

Figure 1. Key aspects pf phytonanotherapy. Figure created using Biorender.com.

Green synthesis often uses natural sources as precursors for NP synthesis, such as plant extracts, microbiological species, or even waste products.[17] By avoiding the use of hazardous chemicals, this strategy reduces environmental impact and makes it more sustainable. Green synthesized NPs are frequently biocompatible, making them useful for a variety of biomedical applications such as drug delivery and medical imaging. Green synthesis may create NPs made of a variety of materials, including metals (such as gold and silver), metal oxides, and organic compounds. Green-synthesized NPs have a wide range of applications, including agriculture, water treatment, and environmental cleanup.[18,19]

3.3. Intersection of phytonanotherapy and green synthesis

The use of plant-derived chemicals or extracts in the environmentally friendly production of NPs specifically suited for medical applications is at the junction of phytonanotherapy and green synthesis. This synergy blends medicinal plants' therapeutic potential with the sustainability of green synthesis technologies. It produces NPs that are not only biocompatible and effective for drug delivery, but are also ecologically friendly. This convergence has the potential to result in a new generation of green nanomedicine with lower environmental impact, better patient outcomes, and broader uses in health care and beyond. However, efforts are being made to optimize these approaches, ensuring their safety and efficacy in clinical settings.[20]

Despite its potential, phytonanotherapy faces many obstacles as it moves from research to clinical use. The composition and potency of bioactive compounds in plant-derived chemicals can vary significantly due to factors such as plant species, geographic location, cultivation methods, and extraction techniques. This variability contributes to the unpredictability and inconsistency of these compounds. Standardization is consequently more challenging, making it difficult to guarantee therapeutic efficacy and repeatability in NP manufacturing. Clinical studies on phytonanotherapy must also address the complexities of maximizing dosage, delivery systems, and treatment plans while reducing possible toxicity and adverse effects. In addition, obtaining regulatory permission poses a significant challenge, as the complex composition of plant-derived NPs necessitates thorough safety and effectiveness testing to meet current pharmaceutical requirements. To make phytonanotherapy a practical and scalable treatment option for real-world applications, several issues must be resolved.[13-20]

4. The preparation of phytosynthesized gold and silver NPs for the treatment of cancer and diabetes

The preparation of phytosynthesized gold and silver NPs typically involves a green and eco-friendly approach (Figure 2 and Table 2). A general method for synthesizing these NPs using plant extracts for potential therapeutic applications is described below.

4.1. Materials needed

4.1.1. Medicinal plant extract

A plant containing anticancer or antidiabetic phytochemicals or substances is selected. Turmeric (curcumin), green tea (catechins), aloe vera, neem, and bitter melon are some popular options.

4.1.2. Gold or silver salt

Gold chloride ($AuCl_4$) is commonly used for gold NPs and silver nitrate ($AgNO_3$) for silver NPs.

Table 2. Summary of the preparation method of phytosynthesized gold and silver NPs utilized for cancer and diabetes treatment

Materials needed	Medicinal plant extract, Gold or silver salt ($AuCl_4$ or $AgNO_3$), Reducing agent from plant extract, Stabilizing agent (optional)
Procedure	
Plant extract preparation	1. Gather and thoroughly clean medicinal plant parts. 2. Finely grind or crush the plant material. 3. Construct an aqueous extract. 4. To aid extraction, heat or stir. 5. Strain and filter the extract to produce a clear extract.
NP synthesis	1. Make a solution of gold or silver salt in distilled water. 2. Stir in the plant extract gradually to the salt solution. 3. Keep an eye on the color changes (red/yellow for gold, brown/yellow for silver). Allow the reaction to continue at room temperature.
Characterization and stabilization	1. Use UV-visible spectroscopy, DLS, and TEM to characterize NPs. 2. If necessary, add a stabilizing agent.
Purification and concentration	1. Separate the NPs by centrifugation. 2. Separate the NPs from the supernatant. 3. Use distilled water to clean the NPs.
Storage	Purified NPs should be stored in a suitable solution.

Abbreviations: DLS: Dynamic light scattering; NP: Nanoparticles; TEM: Transmission electron microscopy; UV: Ultraviolet.

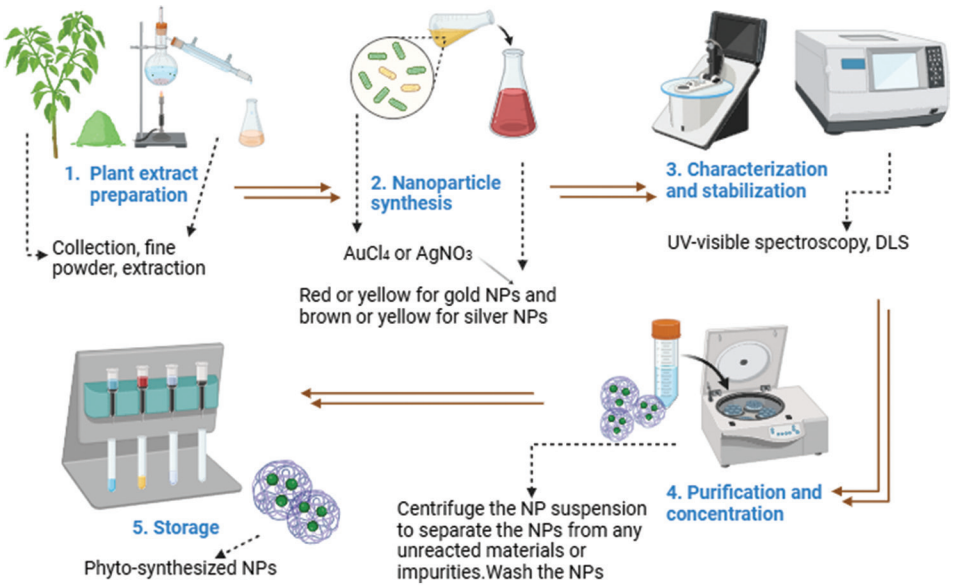

Figure 2. The preparation of phytosynthesized gold and silver NPs. Figure created using Biorender.com.
Abbreviations: $AgNO_3$: Silver nitrate; $AuCl_4$: Gold chloride; DLS: Dynamic light scattering; NP: Nanoparticles; UV: Ultraviolet.

4.1.3. Reducing agent

A moderate and biocompatible reducing agent is frequently included in the chosen plant extract. Plant chemicals such as flavonoids, polyphenols, and terpenoids can act as reducing agents.

4.1.4. Stabilizing agent (optional)

A stabilizing agent such as polyvinylpyrrolidone (PVP) or polyethylene glycol (PEG) is optionally employed to avoid aggregation and improve stability.[21-23]

4.2. The procedure

4.2.1. Plant extract preparation

The necessary medicinal plant parts (leaves, stems, or roots) are collected and thoroughly washed and dried. To make a fine powder, the plant material is ground or crushed. The plant powder is then mixed with distilled water or an organic solvent (e.g., ethanol) to make an aqueous extract. To promote phytochemical extraction, the mixture is gently heated or stirred. To achieve a clear solution, the extract is then strained and filtered.[24]

4.2.2. NP synthesis

The gold or silver salt ($AuCl_4$ or $AgNO_3$) is dissolved in distilled water in a separate container. The plant extract is then gradually added to the salt solution while swirling or shaking. The plant extract functions as a reducing agent, causing metal ions to be reduced and NPs to form. The color change in the solution is observed; for gold NPs, the solution will typically change to hues of red or yellow, while for silver NPs, it will typically change to shades of brown or yellow. The reaction is allowed to occur for a predetermined time at an acceptable temperature (typically at or near room temperature).[25]

4.2.3. Characterization and stabilization

To assess the size, shape, and stability of the synthesized NPs, techniques such as ultraviolet-visible spectroscopy, dynamic light scattering, and transmission electron microscopy are used. A stabilizing agent (e.g., PVP or PEG) is added if necessary to improve stability and prevent aggregation.[26]

4.2.4. Concentration and purification

To remove the NPs from any unreacted materials or contaminants, the suspension is centrifuged. The NPs from the centrifuge tube are removed and the supernatant is discarded. To eliminate any remaining plant extract or byproducts, the NPs are washed with distilled water.

4.2.5. Storage

To guarantee the stability, the purified phytosynthesized NPs are stored in a suitable storage solution.[27]

These photosynthesized gold and silver NPs will subsequently be characterized and assessed for efficacy in cancer and diabetes treatment. The NPs can be functionalized and adapted for diverse uses based on the individual phytochemicals contained in the plant extract and the desired therapeutic characteristics. Thorough study and testing are required to establish their usefulness and safety for medical usage.[26,27]

Table 3 addresses the need for real-world examples and research findings by presenting specific case studies and treatment examples of plants combined with NPs that have demonstrated success in treating cancer and diabetes. It adds tangible information on the impacts of NPs and phytonanotherapy to the theoretical backdrop, presenting study findings that show their efficacy.

5. Anticancer phytomedicine

The use of phytochemicals from medicinal plants in the manufacture of gold and silver NPs has tremendous promise, particularly in their role as anticancer drugs. Anticancer medicines or therapeutic chemicals derived from medicinal plants can be encapsulated in phytosynthesized NPs. These NPs can then be selectively targeted to cancer cells while causing minimal damage to healthy tissues. This focused drug delivery can improve cancer treatment efficacy while lowering negative effects. Because NPs have a high surface area-to-volume ratio, they can greatly increase the solubility and bioavailability of anticancer drugs that are weakly water soluble. This means more therapeutic ingredient is delivered to cancer cells, thereby enhancing the efficacy of the therapy.

Medicinal plants include a varied range of phytochemicals.[28-30] Combining these plants' medicinal chemicals with the unique properties of NPs can result in synergistic effects, potentially boosting their anticancer potency. Toxicity is frequently reduced in phytosynthesized NPs, as opposed to some standard chemotherapeutic medicines, which can have severe adverse effects. As a result, cancer patients may find the phytosynthesized NP treatment more acceptable.

Cancer cells can develop resistance to chemotherapy treatments over time. Phytosynthesized NPs may provide a fresh strategy for combating drug resistance, making them potentially useful against drug-resistant cancer cells.

Some phytosynthesized NPs can be potentially employed in cancer imaging and diagnostics. They can be used as contrast agents in imaging techniques, such as MRI, for the early diagnosis and monitoring of malignant growths.

The use of phytosynthesized NPs is consistent with green and sustainable medical concepts. Being derived from natural sources, they often exhibit fewer adverse effects compared to synthetic alternatives. Phytosynthesized NPs can also be used in combination with other cancer treatments, such as radiation therapy or immunotherapy, to develop comprehensive cancer treatment methods.[28] The adaptability of phytosynthesized NPs enables treatment to be tailored to individual patients and cancer types, potentially leading to more personalized and effective therapies.[31]

5.1. Developments in the field of green NPs for cancer treatment

To synthesize green NPs for cancer therapy, researchers have been investigating various plant-based materials, such as extracts from medicinal plants and agricultural waste. These plant-based NPs have shown potential in targeted medication delivery and cancer cell imaging.[32]

Green NPs produced from biodegradable materials, such as chitosan, alginate, or cellulose, have gained

Table 3. Research of plant-based NPs in diabetes and cancer treatment

Disease	Plant used	NP type	Mechanism of action	Research findings	References
Diabetes	*Gymnema sylvestre*	AuNPs	Enhances insulin secretion and glucose uptake	Improved glucose uptake in diabetic animal models	5,21,25
	Momordica charantia	AgNPs	Inhibits alpha-glucosidase and improves insulin sensitivity	Reduced post-prandial glucose spikes in studies	5,21,25.
	Moringa oleifera	AuNPs	Protects pancreatic beta cells and enhances antioxidant action	Enhanced beta-cell survival and reduced oxidative stress in diabetic rats	5,21,25
Cancer	*Catharanthus roseus*	AuNPs	Induces apoptosis in cancer cells through ROS generation	Selectively killed breast cancer cells *in vitro*	21,35,49,58
	Curcuma longa	AuNPs	Enhances drug delivery to tumors and reduces inflammation	Enhanced tumor targeting and reduced systemic toxicity	21,35,49,58
	Azadirachta indica	AgNPs	Triggers mitochondrial dysfunction in cancer cells	Effective in lung and colon cancer models	21,35,49,58

Abbreviations: AuNPs: Gold NPs; AgNPs: Silver NPs; NPs: Nanoparticles; ROS: Reactive oxygen species.

popularity. These nanocarriers can encapsulate anticancer medications and gradually release them at the tumor site, therefore decreasing systemic toxicity.

Green NPs are increasingly being used in combination therapy for cancer treatment. They have the ability to transport numerous therapeutic agents, such as chemotherapeutic medicines, immunotherapeutic, and gene therapies, thereby increasing the overall efficacy of cancer treatments.[33]

Green NPs with dual therapeutic and diagnostic properties (theranostics) have appeared. These NPs can be utilized to deliver targeted drugs while also providing imaging contrast for enhanced tumor visualization and monitoring therapy response.

5.1.1. Targeted delivery

Advances in the functionalization of green NPs with targeting ligands and antibodies have enabled more accurate and effective therapeutic payload delivery to cancer cells. This lowers off-target effects while improving treatment outcomes.[34]

5.1.2. Immunomodulation

Certain green NPs have immunomodulatory qualities that can be used to stimulate the body's immune response against cancer cells. This strategy offers promise when combined with immunotherapies.

5.1.3. Green algae NPs

Algae-based NPs have received attention due to their natural abundance and biocompatibility. Green NPs generated from algae are being investigated for application in cancer therapy, including photothermal and photodynamic therapies.[35]

5.1.4. Clinical research

Some green NP-based cancer therapeutics have advanced to early-stage clinical studies.[35,36] The purpose of these trials is to evaluate the safety and efficacy of these innovative medicines in human patients.

5.1.5. Considerations for biosafety and regulation

The biosafety and regulatory elements of green NPs have also been assessed, guaranteeing that these medicines fulfill rigorous safety and quality criteria for clinical application.[36]

While these new results are encouraging, it is crucial to highlight that translating green NP-based cancer treatments from the laboratory to clinical practice may take many years, with extensive testing required to verify their safety and efficacy in humans. As a result, ongoing research and clinical trials will play a crucial role in defining the future of cancer therapeutics based on green NPs. Table 4 shows the most recent breakthroughs in this field, encompassing current scientific literature and clinical trial databases.

6. Antidiabetic phytomedicine

The use of phytochemicals from medicinal plants in the manufacture of gold and silver NPs (NPs) offers great promise, notably in their role as possible antidiabetic medicines. Medicinal plants are high in bioactive components such as polyphenols, flavonoids, terpenoids, and alkaloids, all of which have antidiabetic characteristics. The NP synthesis procedure is both sustainable and environmentally friendly because it uses natural substances.

Gold and silver NPs can boost the bioavailability of antidiabetic phytochemicals that are poorly water soluble. This means that a greater proportion of these beneficial substances will be absorbed by the body, perhaps leading

Table 4. Recent developments in the field of green NPs for cancer treatment

Development	Descriptions
Plant-based green NPs	Plant extracts and phytochemicals are used in the synthesis of green NPs with anticancer effects. Plant-derived NPs have the potential for biocompatibility and low toxicity.
Biodegradable nanocarriers	Biodegradable nanocarriers, such as chitosan, alginate, and cellulose-based NPs, are being developed to encapsulate and deliver anticancer medicines with regulated release profiles.
Combination therapies	For improved efficacy, green NPs carrying several therapeutic agents, such as chemotherapeutic medicines, immunotherapeutic, and gene treatments, are being investigated.
Theranostic NPs	Design and application of green NPs with dual therapeutic and diagnostic properties (theranostics), enabling targeted medication administration while providing image contrast for cancer detection.
Targeted delivery	Green NPs are being functionalized with targeting ligands or antibodies to ensure precision delivery of therapeutic payloads to cancer cells while minimizing off-target effects.
Immunomodulation	Exploration of green NPs with immunomodulatory capabilities, with the goal of potentially activating the body's immune response against cancer cells and improving the efficacy of immunotherapies.
Algae-derived green NPs	Due to their natural abundance and biocompatibility, algae-based green NPs are being researched for possible applications in photothermal and photodynamic cancer therapy.
Clinical trials	Some green NP-based medicines are being advanced to early-phase clinical studies to examine their safety and efficacy in human beings as potential cancer treatments.
Biosafety and regulation considerations	Green NPs' biosafety and regulatory elements were evaluated in order to ensure their compliance with safety and quality criteria for clinical application in cancer treatment.

Abbreviation: NP: Nanoparticles.

to improved therapeutic effects. Functionalized NPs can be created to encapsulate antidiabetic medicines generated from medicinal plants for targeted drug delivery. These NPs can then be specifically targeted to pancreatic cells or other key diabetes tissues, improving medication delivery while minimizing off-target effects.[37] When compared to some synthetic antidiabetic medications, phytosynthesized NPs may have lower toxicity and fewer side effects. This can contribute to a better safety profile for diabetics, especially when employed in long-term therapies.

Medicinal plants frequently contain many bioactive substances that may work synergistically to fight diabetes. By encapsulating these chemicals in NPs, their combined therapeutic effects for improved glucose control and insulin regulation can be realized. Some plant-derived chemicals have the ability to target various diabetes pathways, including enhancing insulin sensitivity, decreasing inflammation, and protecting pancreatic beta cells.[38] This multitarget action may be useful in treating the complexities of diabetes.

Because of the diversity of medicinal plants and their bioactive ingredients, personalized antidiabetic medicines can be developed. Based on the plant source and phytochemical composition, NPs can be adjusted to individual patient needs. The synthesis of NPs from medicinal plants adheres to green and sustainable principles, minimizing the environmental impact of typical chemical synthesis methods.

Combining several phytochemicals within NPs may help lessen the possibility of drug resistance, which can arise with some synthetic antidiabetic medicines. While the promise of phytosynthesized gold and silver NPs for diabetes treatment is exciting, more research, pre-clinical studies, and clinical trials are required to establish their safety and efficacy in humans. Individual responses to various medications may differ, and careful scientific study is required to assure their dependability and therapeutic efficacy in diabetes management.[37,39]

6.1. Developments in the field of green NPs for diabetic treatment

The developments in the field of green NPs for diabetic treatment entail the use of biocompatible and environmentally friendly nanomaterials synthesized from natural sources, typically plant extracts or phytochemicals. These green NPs show considerable promise for efficiently managing diabetes.

Researchers have used medicinal plants and their bioactive components to create green NPs. These NPs can either incorporate antidiabetic medicines or have natural glucose-lowering effects. The plant extract used determines the medicinal characteristics of the NPs, providing a variety of alternatives.[40] Green NPs are intended to boost the bioavailability of antidiabetic phytochemicals that are poorly water soluble. This implies that the medicinal chemicals are more easily absorbed by the body, enhancing their effectiveness in diabetes management.

6.1.1. Targeted drug administration

One of the most significant benefits of green NPs is their capacity to assist targeted drug administration. NPs can be guided to specific areas in the body by functionalizing them with certain ligands or antibodies, such as pancreatic cells or insulin-sensitive tissues.[15] This reduces off-target effects while increasing therapeutic impact.

6.1.2. Biocompatibility and safety

Green NPs are frequently biocompatible and have lower toxicity than synthetic counterparts. Because of this, they are acceptable for long-term usage in diabetes control because they have a decreased risk of side effects.[41] Researchers are investigating the synergistic effects of mixing various antidiabetic phytochemicals within green NPs.[35,41] These combinations can target various pathways involved in diabetes, providing comprehensive diabetic therapy.

Green NPs can be created to affect a variety of biological pathways relevant to diabetes. This includes increasing insulin sensitivity, decreasing inflammation, preserving pancreatic beta cells, and better regulating blood glucose levels.[35,41] Because of the wide diversity of medicinal plants and their distinct phytochemical compositions, personalized antidiabetic treatments are possible. Patients can receive therapy that is tailored to their individual needs and responses.

6.1.3. Eco-friendly approach

Green NP synthesis adheres to eco-friendly principles, decreasing the environmental effect associated with standard chemical synthesis processes. This encourages sustainability and green initiatives in health care. Green NPs may lower the possibility of drug resistance by mixing several phytochemicals, a concern commonly associated with certain synthetic antidiabetic drugs.[42]

6.1.4. Clinical trials

Ongoing pre-clinical and clinical research is being conducted to assess the safety and efficacy of green NPs for diabetes treatment.[36] Some medicines have advanced to human trials, raising the prospect of new therapeutic choices for diabetes patients. Research is being conducted to evaluate the biosafety and regulatory aspects of green NPs. It is critical for their clinical usage in diabetes treatment to ensure compliance with safety and quality criteria.

These advancements, summarized in Table 5, point to a promising move toward more effective, personalized, and ecologically responsible diabetes management utilizing green NPs.[43]

7. Algae-derived green NPs

Algae-derived green NPs are gaining interest for their potential use in the treatment of cancer and diabetes. Algae are abundant, sustainable, and rich in bioactive substances that can be used to treat patients.[44] In this section, we present an in-depth overview of research on algae-derived green NPs for the treatment of medical conditions.

7.1. Cancer treatment with algae-derived green NPs

7.1.1. NP production

Algae, particularly microalgae and macroalgae (seaweed), contain polysaccharides, polyphenols, and pigments that can act as reducing and stabilizing agents in the production of NPs. These algae-derived chemicals can be used to synthesize green NPs, particularly gold and silver NPs.[45-48] (Table 6).

7.1.2. Photothermal therapy

Photothermal therapy using gold NPs synthesized with algae extracts has demonstrated promise for cancer treatment. When exposed to near-infrared (NIR) light, these NPs produce heat, killing cancer cells while sparing healthy tissue[49] (Table 7).

7.1.3. Photodynamic therapy (PDT)

Chlorophyll and other pigments generated from algae can be utilized to make photosensitizing NPs. When activated by precise wavelengths of light, these NPs release reactive oxygen species (ROS), mainly singlet oxygen, which causes oxidative stress and damage to cancer cells in a process known as PDT. Photosensitizing NPs loaded with these natural substances are selectively delivered to tumor locations in this novel technique.[50-52]

This localized and focused therapy has various advantages, including the ability to treat superficial as well as deeper tumors by light penetration and causing minimum injury to surrounding healthy tissue. PDT using algae-derived NPs holds great potential as a non-invasive and precise treatment strategy for numerous forms of cancer, offering a viable alternative to conventional therapies with fewer side effects. More research and clinical studies, however, are required to optimize this strategy and prove its efficacy in clinical practice.[53-57]

7.1.4. Drug delivery

Green NPs generated from algae can be functionalized to transport chemotherapeutic medicines or therapeutic substances. Due to their biocompatibility and controlled drug release characteristics, they are well-suited for targeted drug administration to malignant areas while minimizing systemic side effects.[58] The NPs can be

Table 5. Recent developments in the field of green NPs for diabetic treatment

Development	Description
Plant-derived green NPs	Phytochemicals from medicinal plants are used to create green NPs for diabetic therapy. These NPs may include antidiabetic drugs or have intrinsic glucose-lowering effects.
Enhanced bioavailability	Green NPs increase the bioavailability of weakly water-soluble antidiabetic phytochemicals, ensuring that a greater proportion of the therapeutic molecules reach the bloodstream for improved efficacy.
Targeted drug delivery	Green NPs have been functionalized for targeted drug delivery to specific diabetes tissues or cells, decreasing off-target effects and increasing the therapeutic effectiveness of antidiabetic medicines.
Biocompatibility and safety	Biocompatible green NPs show lower toxicity than synthetic medication carriers, making them safer for long-term usage in diabetes control.
Synergistic combinations	Combining various antidiabetic phytochemicals within green NPs maximizes synergistic effects to target numerous diabetes pathways for complete therapy.
Multitarget action	Green NPs are designed to influence numerous biological pathways connected to diabetes, including insulin sensitivity, inflammation reduction, and pancreatic beta cell protection.
Personalized medicine	Based on phytochemical composition, the vast spectrum of medicinal plants and their bioactive components enables personalized antidiabetic therapy customized to individual patient needs.
Eco-friendly approach	Green NP synthesis adheres to environmentally friendly concepts, decreasing the environmental impact of standard chemical synthesis procedures and increasing sustainability.
Reduced risk of drug resistance	Combining different phytochemicals into green NPs may help lessen the potential of drug resistance, which is a significant concern in some synthetic antidiabetic drugs.
Clinical research and trials	Pre-clinical and clinical research is being conducted to assess the safety and efficacy of green NPs for diabetes treatment, with several therapies moving to human trials in diabetic patients.
Biosafety and regulatory considerations	Efforts are taken to analyze the biosafety and regulatory aspects of green NPs, assuring their compliance with clinical usage in diabetes treatment safety and quality criteria.

Abbreviation: NP: Nanoparticle.

Table 6. Advantages and disadvantages of green algae-derived NPs

Advantages	Disadvantages
Environmentally friendly	Limited scalability
• Use algae that is renewable and sustainable. • Difficulties in scaling up production for huge volumes. • Minimize the environmental impact of NP production.	• May not fulfill high-demand specifications.
Biocompatibility	Variable composition
• Generally biocompatible, making it useful for biomedical applications. • Composition varies depending on algal species, resulting in inconsistency.	• Lower risk of negative reactions in biological systems. • Standardization can be difficult.
Low toxicity	Complexity of formulation
• Non-toxic components are frequently used in synthesis methods. • Creating stable and effective formulas can be difficult. • Reduce health risks to researchers and consumers.	• It can be difficult to ensure reproducibility and quality control.
Customization	Regulatory hurdles
• Adapted to individual uses by modifying algae species and growth conditions. • Application versatility, including drug administration and therapy.	• -Gaining regulatory approval for innovative therapies can be difficult. • Adherence to high regulatory norms is critical.

Abbreviation: NP: Nanoparticle.

steered to tumor areas by functionalizing them with specific ligands or antibodies that recognize cancer cell surface antigens. Once there, the NPs slowly and steadily release the chemotherapeutic medicines or therapeutic substances. This tailored drug delivery method not only improves the treatment's efficiency against cancer cells, but also decreases the drug's exposure to healthy tissues, reducing the often debilitating side effects associated with conventional chemotherapy.

Green NPs generated from algae represent a viable avenue for improving the precision and efficiency of cancer

Table 7. Advantages and disadvantages of photothermal therapy

	Advantages	Disadvantages
Precise tumor targeting	Targets cancer cells selectively, causing minimal damage to healthy tissue.	Limited penetration depth; works best on surface tumors.
Minimal side effects	Reduces the systemic side effects of conventional chemotherapy.	In places with weak blood flow, efficacy may be diminished.
Rapid treatment	Rapid heating of NPs and tumor tissue results in shorter treatment sessions.	Complete tumor ablation may necessitate many therapy sessions.
Controlled activation	Using a laser or light, it is possible to precisely control the activation of NPs.	Laser or light delivery requires specialized equipment.
Minimal invasive	The use of a non-invasive or minimally invasive method lowers patient discomfort.	Not appropriate for all cancer kinds or stages.
Versatile applications	Possibility of combining with other cancer treatments.	Photothermal agents are few and difficult to get.

Abbreviation: NP: Nanoparticle.

therapies while improving the overall quality of life of cancer patients. However, additional research and clinical validation are required to optimize this drug delivery approach and verify its safety and efficacy in clinical practice.[59,60]

7.1.5. Imaging

Certain algae-derived NPs have inherent imaging capabilities, making them useful instruments for cancer detection and treatment monitoring. These NPs can be used as contrast agents in a variety of imaging modalities, including MRI, computed tomography (CT), and fluorescence imaging.[61,62] Because of their size and surface features, these NPs concentrate preferentially in tumor tissues when delivered to patients. This selective accumulation enables precise tumor visualization, which aids in cancer identification and localization. Furthermore, during cancer treatment, these imaging NPs can aid in the monitoring of treatment response by measuring changes in tumor size, shape, and vascularization over time. This real-time imaging capabilities is especially beneficial for guiding treatment decisions and optimizing therapy tactics. Hence, algae-derived NPs with inherent imaging capabilities offer a non-invasive and highly informative method for cancer diagnosis, therapy planning, and patient care. More research and clinical validation are needed to fully realize the promise of these imaging NPs in oncology.[63,64]

7.2. Diabetes treatment with algae-derived green NPs

7.2.1. Glucose control

Algae-derived chemicals, notably alginate and fucoxanthin, which are common in brown algae, have demonstrated remarkable promise in the regulation of blood glucose levels, making them appealing candidates for diabetes management. The NPs containing these chemicals could be used as oral or injectable diabetic control medications.

Alginate, a natural polysaccharide, can create gels that block the absorption of glucose from the digestive tract, allowing for more stable blood sugar levels following meals.[65,66] Fucoxanthin, a carotenoid pigment, has been linked to enhanced insulin sensitivity and decreased inflammation, both of which are key aspects of diabetes management. Researchers are leveraging these bioactive molecules to create NPs that may be delivered orally or by injection to enable controlled and prolonged release of these diabetes-controlling substances. This method has the potential to enhance glucose control, minimize dependency on traditional drugs, and improve overall diabetes care. More research and clinical trials, however, are required to evaluate the safety and efficacy of these algae-derived NP-based treatments in diabetic patients.[67,68]

7.2.2. Insulin mimicry

Some polysaccharides generated from algae have insulin-like characteristics, boosting cell glucose absorption. These polysaccharide-containing NPs may imitate the effect of insulin, thereby assisting in diabetes treatment (Table 8).[69-71]

7.2.3. Anti-inflammatory effects

Algae-derived NPs may have anti-inflammatory characteristics, which may aid in the reduction of chronic inflammation associated with diabetes and its consequences. Algae, particularly microalgae and macroalgae (seaweed), contain a diverse range of bioactive chemicals, such as polyphenols, carotenoids, polysaccharides, and fatty acids, all of which have anti-inflammatory characteristics.[72,73] Algae-derived NPs can be designed to release or distribute bioactive chemicals that have been found to inhibit the synthesis of pro-inflammatory mediators. These mediators, such as cytokines and chemokines, play an important role in the initiation and maintenance of inflammation.

Table 8. Advantages and disadvantages of algae-derived NPs for diabetes management

Advantages	Disadvantages
Algae-derived NPs can imitate insulin's effect, allowing cells to take in more glucose.	Research is still in its infancy, and clinical validation is required.
This method may benefit people with insulin resistance or type 2 diabetes by reducing their dependency on exogenous insulin.	Efficacy may differ across individuals, necessitating personalized dosing.
Algae are a renewable and abundant source of NPs that adhere to eco-friendly principles.	It can be difficult to standardize and control the quality of algae-derived NPs.
Algae-derived NPs can be prepared for oral administration, giving a non-invasive and simple therapy option.	Stability and bioavailability of the formulation must be optimized.
NPs can be tailored to deliver drugs to specific diabetic tissues while minimizing off-target effects.	Targeted formulation development and optimization can be difficult.
	Long-term safety and potential negative effects necessitate extensive research.
	Potential allergic responses or side effects must be evaluated.
	Ensuring production reproducibility and scalability might be difficult.
	It is critical to adhere to regulatory standards for safety and quality.

Abbreviation: NP: Nanoparticle.

Chronic inflammation is intimately linked to oxidative stress, which arises when there is an imbalance between the body's ability to neutralize ROS. Algae-derived chemicals frequently contain antioxidant capabilities, which aid in the reduction of oxidative stress and inflammation. Algae-derived NPs can influence the immune system, assisting in the regulation of the immune response and the prevention of excessive inflammation. This regulation may be particularly crucial in reducing immune-related tissue and organ damage in diabetes.

As chronic inflammation can harm the microvasculature, leading to problems including diabetic retinopathy and nephropathy, compounds derived from algae may help support the function of small blood arteries, hence reducing these issues.[74,75]

Chronic inflammation in type 1 diabetes can contribute to the death of pancreatic beta cells, which produce insulin. NPs generated from algae may help protect these cells from inflammatory damage. By lowering chronic inflammation, algae-derived NPs may help prevent or reduce diabetes-related complications such as cardiovascular disease, neuropathy, and nephropathy. Algae-derived NPs can be used to supplement traditional anti-inflammatory treatments, providing a natural and perhaps safer alternative to synthetic medications.[76-79]

7.2.4. Antioxidant activity

Algae contain antioxidants, including astaxanthin and phlorotannin, that can help fight oxidative stress, which is linked to the development and progression of diabetes. These antioxidants may be therapeutically beneficial when encapsulated in NPs.

When there is an imbalance between the creation of ROS and the body's ability to neutralize them with antioxidants, oxidative stress arises.[80,81] Diabetes can increase oxidative stress due to a variety of causes, including raised blood glucose levels, increased ROS generation, and reduced antioxidant defense mechanisms. This oxidative stress can cause cellular damage, inflammation, and the development of diabetic problems.

Astaxanthin, a carotenoid pigment found in microalgae and shellfish, is well known for its antioxidant qualities. It can neutralize free radicals, scavenge ROS, and minimize oxidative damage to cells and tissues. Phlorotannin, on the other hand, are polyphenolic chemical found in brown algae (seaweed) that possess high antioxidant activity. Researchers have investigated the encapsulating of astaxanthin, phlorotannin, or other algae-derived antioxidants into NPs to harness the therapeutic effects of these antioxidants for diabetes treatment.[82-84] NPs can boost these antioxidants' solubility and bioavailability, ensuring that a greater proportion reaches target tissues and cells.

NPs can be tailored to progressively release antioxidants, giving long-term protection against oxidative stress. Functionalized NPs can be directed to specific areas inside the body, such as pancreatic cells or vascular endothelium, where oxidative stress is particularly apparent in diabetes. By encapsulating antioxidants within NPs, the risk of side effects or interactions with other drugs may be reduced.

Combining multiple antioxidants within NPs may result in synergistic effects, offering comprehensive oxidative damage protection. The utilization of algae-derived antioxidants encapsulated in NPs is a viable path

for diabetic treatment. However, research is ongoing, and clinical trials are required to evaluate the safety and efficacy of these NP-based antioxidant treatments in diabetes patients. Furthermore, aspects such as algal species selection, NP formulation, and dose must be carefully studied to optimize therapeutic benefits.[85]

7.2.5. Biosensors

Algae-based NPs have the potential to be used to create biosensors for monitoring blood glucose levels. These biosensors provide a non-invasive, possibly more pleasant alternative to typical glucose monitoring methods like fingerstick tests. The distinct qualities of algae-derived NPs, such as their biocompatibility and flexibility, make them ideal for the development of sensitive and selective glucose biosensors.[86]

NPs can be functionalized in these biosensors with glucose-specific receptors or enzymes that interact with glucose molecules in the bloodstream. When glucose attaches to NPs, it causes observable changes in electrical conductivity, fluorescence, or color. This signal may be identified and quantified, allowing for real-time monitoring of blood glucose levels.

The non-invasive nature of algae-based NP biosensors has the potential to improve patient compliance, decrease discomfort, and enable continuous glucose monitoring, hence enhancing diabetes treatment and overall quality of life for diabetic patients. More research and clinical validation, however, are required to verify the accuracy and reliability of these biosensors for routine clinical usage.[87,88]

7.2.6. Pancreatic protection

NPs generated from algae may protect pancreatic beta cells from injury, retaining their insulin-producing ability and potentially reducing diabetes progression. In both type 1 and type 2 diabetes, chronic inflammation and oxidative stress in the pancreas might contribute to the degeneration of these vital cells. Algae-derived NPs, which are frequently high in antioxidants and anti-inflammatory substances, may assist in alleviating this damage by lowering oxidative stress, inflammation, and immune-related attacks on beta cells.

Furthermore, NPs can be designed for targeted medication delivery, targeting these protective chemicals to the pancreatic tissue selectively.[89,90] Algae-derived NPs provide a possible therapeutic pathway for maintaining insulin secretion and better glucose control by sustaining beta cell activity, thus improving the long-term outlook for people with diabetes. While algae-derived green NPs show promise for cancer and diabetes treatment, further study is needed, and clinical trials are required to establish their safety and efficacy in humans. Furthermore, aspects such as algal species selection, extraction methods, and NP synthesis techniques all play a role in the efficacy of these therapies.[91,92]There are major safety issues and regulatory obstacles when CAM and NPs are combined. Because of their small size and strong reactivity, NPs might have unpredictable toxicity that can cause inflammation, oxidative stress, or organ damage. Furthermore, bioactive substances with varying potencies may be present in plant-based NPs, raising the possibility of allergic reactions or unfavorable interactions with prescription medications. The absence of defined procedures for quality control and NP manufacturing makes safety assessments even more difficult. On the regulatory front, the approval, clinical studies, and post-market surveillance for these integrative medicines are hampered by regionally disparate and inconsistent rules. Establishing quality standards, guaranteeing reproducibility in the production of NPs, and evaluating long-term impacts are among the challenges.[92,93]

8. Conclusion and future prospects

This review focuses at the exciting junction of phytonanotherapy, CAM, and NPs in the treatment of cancer and diabetes. CAM, particularly the utilization of medicinal plants, has attracted global attention. Phytosynthesized NPs, produced using green synthesis, provide a sustainable, environmentally friendly approach. These NPs include a wide range of bioactive chemicals that participate in bioreduction and stabilization processes, making them ideal tools for anticancer and antidiabetic therapy. Recent advances in green NPs are opening up new avenues for cancer and diabetes treatment, providing precision tactics such as photothermal therapy, PDT, drug delivery, and biosensors.[93,94] Furthermore, algae-derived green NPs show great promise in these fields, since they can help with imaging, preserve pancreatic beta cells, and provide antioxidant and anti-inflammatory benefits.

Overall, the convergence of CAM, phytonanotherapy, green synthesis, and novel NP-based techniques is transforming the landscape of cancer and diabetes management, promising more sustainable, effective, and patient-friendly therapeutic choices. Further study and clinical validation, however, are required to fully realize their promise and ensure their safety and efficacy in clinical practice.[95]

Advances in nanotechnology and knowledge of individual genetic variations will very certainly allow for the development of personalized medicines. Patients may receive personalized medicines based on their individual genetic profiles and illness characteristics, improving

therapeutic effectiveness while minimizing negative effects. Additional study on NP-based drug delivery systems will lead to more efficient and precise targeting of malignant cells or specific diabetic areas. These advancements may result in improved therapeutic efficacy and less systemic toxicity. As NPs and biosensors evolve, they will provide more sensitive and specialized diagnostic instruments. Early cancer and diabetes identification, as well as real-time monitoring of therapy responses, will become more practical. By combining CAM concepts with NP-based therapies, innovative combination treatments may be developed. These medicines may combine the benefits of traditional therapy with cutting-edge nanomedicine, allowing for more holistic approaches to cancer and diabetes control.[96]

As research advances and the safety and efficacy of these therapies are confirmed, regulatory agencies may approve and regulate CAM-based NP medicines, giving patients access to alternative and complementary treatments in addition to traditional choices. Future health care may priorities patient-centered care, delivering a range of treatment options that match with individual ideas and values, with a focus on patient preferences and overall well-being. Efforts to promote the eco-friendliness and cost-effectiveness of these therapies may make them more accessible, especially in resource-limited places where CAM and sustainable treatments are popular. Continued developments in green synthesis processes will increase the efficiency and scalability of NP manufacturing, making these medicines more realistic for wider clinical usage. Educating the general public and healthcare professionals on the benefits, risks, and possibilities of CAM, phytonanotherapy, and NP-based treatments will be critical for making informed treatment decisions.[97-101]

Overall, integrating CAM, phytonanotherapy, and NPs in cancer and diabetes treatment offers great promise, providing patients with a varied range of options and contributing to more effective, sustainable, and patient-centered health care. However, further research, rigorous clinical trials, and regulatory backing will be required to fully realize the potential of these novel treatments.

Acknowledgments

None.

Funding

None.

Conflict of interest

The authors declare they have no competing interests.

Author contributions

Conceptualization: Faheem Patwekar
Investigation: Faheem Patwekar, Mohsina Patwekar
Writing – original draft: Faheem Patwekar, Mohsina Patwekar
Writing – review & editing: All authors

Ethics approval and consent to participate

Not applicable.

Consent for publication

Not applicable.

Availability of data

Not applicable.

References

1. Fuad NF, Ching SM, Dzulkarnain DH, Cheong AT, Zakaria ZA. Complementary alternative medicine use among postpartum mothers in a primary care setting: A cross-sectional study in Malaysia. *BMC Complement Med Ther*. 2020;20:197.

   doi: 10.1186/s12906-020-02984-7

2. Frawley JE, McKenzie K, Janosi J, Forssman B, Sullivan E, Wiley K. The role of complementary and alternative medicine practitioners in the information-seeking pathway of vaccine-hesitant parents in the Blue Mountains area, Australia. *Health Soc Care Community.* 2021;29(6):e368-e376.

   doi: 10.1111/hsc.13361

3. Upamali S, Rathnayake S. Perspectives of older people with uncontrolled type 2 diabetes mellitus towards medication adherence: A qualitative study. *PLoS One*. 2023;18(8):e0289834.

   doi: 10.1371/journal.pone.0289834

4. Kristoffersen AE, Nilsen JV, Stub T, *et al.* Use of Complementary and Alternative Medicine in the context of cancer; prevalence, reasons for use, disclosure, information received, risks and benefits reported by people with cancer in Norway. *BMC Complement Med Ther*. 2022;22(1):202.

   doi: 10.1186/s12906-022-03606-0

5. Vijayakumar S, Vinayagam R, Anand MA, *et al.* Green synthesis of gold nanoparticle using Eclipta alba and its antidiabetic activities through regulation of Bcl-2 expression in pancreatic cell line. *J Drug Deliv Sci Technol*. 2020;58:101786.

   doi: 10.1016/j.jddst.2020.101786

6. Singh H, Desimone MF, Pandya S, *et al.* Revisiting the green synthesis of nanoparticles: Uncovering influences of plant extracts as reducing agents for enhanced synthesis

efficiency and its biomedical applications. *Int J Nanomed*. 2023;18:4727-4750.

doi: 10.2147/IJN.S419369

7. Taifa S, Muhee A, Bhat RA, *et al*. Evaluation of therapeutic efficacy of copper nanoparticles in *Staphylococcus aureus*-induced rat mastitis model. *J Nanomater*. 2022;2022:7124114.

doi: 10.1155/2022/7124114

8. Elnawasany S, Haggag YA, Shalaby SM, *et al*. Anti-cancer effect of nano-encapsulated boswellic acids, curcumin and naringenin against HepG-2 cell line. *BMC Complement Med Ther*. 2023;23(1):270.

doi: 10.1186/s12906-023-04096-4

9. Butler KS, Brinker CJ, Leong HS. Bridging the *in vitro* to *in vivo* gap: Using the chick embryo model to accelerate nanoparticle validation and qualification for *in vivo* studies. *ACS Nano*. 2022;16(12):19626-19650.

doi: 10.1021/acsnano.2c03990

10. Devi N, Rani K, Kharb P, Prasad M. Herbal medicine for urinary tract infections with the blazing nanotechnology. *J Nanosci Nanotechnol*. 2021;21(6):3495-3512.

doi: 10.1166/jnn.2021.19002

11. Zhang H, Han G, Litscher G. Traditional acupuncture meets modern nanotechnology: opportunities and perspectives. *Evid Based Complement Alternat Med*. 2019;2019:2146167.

doi: 10.1155/2019/2146167

12. De Jong WH, Borm PJ. Drug delivery and nanoparticles: Applications and hazards. *Int J Nanomedicine*. 2008; 3(2):133-149.

doi: 10.2147/ijn.s596

13. Javed R, Ghonaim R, Shathili A, Khalifa SA, El-Seedi HR. Phytonanotechnology: A greener approach for biomedical applications. In: *Biogenic Nanoparticles for Cancer Theranostics*. Amsterdam: Elsevier; 2021. p. 43-86.

doi: 10.1016/B978-0-12-821467-1.00009-4

14. Rana N, Singh SK, Banu NA, Hjazi A, Vamanu E, Singh MP. The ethnopharmacological properties of green-engineered metallic nanoparticles against metabolic disorders. *Medicina* (*Kaunas*). 2023;59(6):1022.

doi: 10.3390/medicina59061022

15. Meydan I, Burhan H, Gür T, Seçkin H, Tanhaei B, Sen F. Characterization of *Rheum ribes* with ZnO nanoparticle and its antidiabetic, antibacterial, DNA damage prevention and lipid peroxidation prevention activity of *in vitro*. *Environ Res*. 2022;204:112363.

doi: 10.1016/j.envres.2021.112363

16. Mohamed HE, Khalil AT, Hkiri K, *et al*. Physicochemical and nanomedicine applications of phyto-reduced erbium oxide (Er2O3) nanoparticles. *AMB Exp*. 2023;13(1):24.

doi: 10.1186/s13568-023-01527-w

17. Ehtesabi H, Fayaz M, Hosseini-Doabi FS, Rezaei P. The application of green synthesis nanoparticles in wound healing: A review. *Mater Today Sustain*. 2022;2022:100272.

doi: 10.1016/j.mtsust.2022.100272

18. Mahanty S, Bakshi M, Ghosh S, *et al*. Green synthesis of iron oxide nanoparticles mediated by filamentous fungi isolated from Sundarban mangrove ecosystem, India. *BioNanoScience*. 2019;9:637-651.

doi: 10.1007/s12668-019-00644-w

19. Ojo OA, Olayide II, Akalabu MC, *et al*. Nanoparticles and their biomedical applications. *Biointerface Res Appl Chem*. 2021;11(1):8431-8445.

doi: 10.33263/BRIAC111.84318445

20. Navada KM, Nagaraja GK, D'Souza JN, *et al*. Synthesis of phyto-functionalized nano hematite for lung cancer suppressive activity and paracetamol sensing by electrochemical studies. *Process Biochem*. 2022;123:76-90.

doi: 10.1016/j.procbio.2022.10.033

21. Abd El-Moaty HI, Soliman NA, Hamad RS, Ismail EH, Sabry DY, Khalil MM. Comparative therapeutic effects of *Pituranthos tortuosus* aqueous extract and phyto-synthesized gold nanoparticles on *Helicobacter pylori*, diabetic and cancer proliferation. *South Afr J Bot*. 2021;139:167-174.

doi: 10.1016/j.sajb.2021.02.009

22. Venkatadri B, Shanparvish E, Rameshkumar MR, *et aL*. Green synthesis of silver nanoparticles using aqueous rhizome extract of *Zingiber officinale* and *Curcuma longa: In-vitro* anti-cancer potential on human colon carcinoma HT-29 cells. *Saudi J Biol Sci*. 2020;27(11):2980-2986.

doi: 10.1016/j.sjbs.2020.09.021

23. Shashiraj KN, Hugar A, Kumar RS, *et al*. Exploring the antimicrobial, anticancer, and apoptosis inducing ability of biofabricated silver nanoparticles using *Lagerstroemia speciosa* flower buds against the Human Osteosarcoma (MG-63) cell line via flow cytometry. *Bioengineering*. 2023;10(7):821.

doi: 10.3390/bioengineering10070821

24. Said A, Abu-Elghait M, Atta HM, Salem SS. Antibacterial activity of green synthesized silver nanoparticles using *lawsonia inermis* against common pathogens from urinary tract infection. *Appl Biochem Biotechnol*. 2023;196:85-98.

doi: 10.1007/s12010-023-04482-1

25. Baldea I, Florea A, Olteanu D, *et al*. Effects of silver and gold nanoparticles phytosynthesized with *Cornus mas* extract on oral dysplastic human cells. *Nanomedicine*. 2020;15(1):55-75.

doi: 10.2217/nnm-2019-0290

26. Hublikar LV, Ganachari SV, Patil VB. Phytofabrication of silver nanoparticles using *Averrhoa bilimbi* leaf extract for

anticancer activity. *Nanoscale Adv*. 2023;5(16):4149-4157.

doi: 10.1039/D3NA00313B

27. Halkai KR, Mudda JA, Shivanna V, Patil V, Rathod V, Halkai R. Cytotoxicity evaluation of fungal-derived silver nanoparticles on human gingival fibroblast cell line: An *in vitro* study. *J Conserv Dent*. 2019;22(2):160.

28. Ogidi CO, Oyetayo VO, Akinyele BJ. *Wild Medicinal Mushrooms: Potential Applications in Phytomedicine and Functional Foods. An Introduction to Mushroom*. London: Intechopen; 2020. p. 118-i26.

29. Zheng X, Yang X, Lin J, Song F, Shao Y. Low curcumin concentration enhances the anticancer effect of 5-fluorouracil against colorectal cancer. *Phytomedicine*. 2021;85:153547.

doi: 10.1016/j.phymed.2021.153547

30. Naqvi SA, Ali S, Sherazi TA, *et al*. Antioxidant, antibacterial, and anticancer activities of bitter gourd fruit extracts at three different cultivation stages. *J Chem*. 2020;2020:1.

doi: 10.1155/2020/7394751

31. Zhu Z, Cui L, Yang J, *et al*. Anticancer effects of asiatic acid against doxorubicin-resistant breast cancer cells via an AMPK-dependent pathway *in vitro*. *Phytomedicine*. 2021;92:153737.

doi: 10.1016/j.phymed.2021.153737

32. Samuel MS, Ravikumar M, John J A, *et al*. A review on green synthesis of nanoparticles and their diverse biomedical and environmental applications. *Catalysts*. 2022;12(5):459.

doi: 10.3390/catal12050459

33. Jiang Z, Li L, Huang H, He W, Ming W. Progress in laser ablation and biological synthesis processes: "Top-Down" and "Bottom-Up" approaches for the green synthesis of Au/Ag nanoparticles. *Int J Mol Sci*. 2022;23(23):14658.

doi: 10.3390/ijms232314658

34. Patwekar M, Sehar N, Patwekar F, *et al*. Novel immune checkpoint targets: A promising therapy for cancer treatments. *Int Immunopharmacol*. 2024;126:111186.

doi: 10.1016/j.intimp.2023.111186

35. Shabani L, Kasaee SR, Chelliapan S, *et al*. An investigation into green synthesis of Ru template gold nanoparticles and the *in vitro* photothermal effect on the MCF-7 human breast cancer cell line. *Appl Phys A*. 2023;129(8):564.

doi: 10.1007/s00339-023-06832-6

36. Lopes J, Lopes D, Pereira-Silva M, *et.al* Macrophage cell membrane-cloaked nanoplatforms for biomedical applications. *Small Methods*. 2022;6(8):2200289.

doi: 10.1002/smtd.202200289

37. Sukardima, Ervina M. The recent use of *Swietenia mahagoni* (L.) Jacq. as antidiabetes type 2 phytomedicine: A systematic review. *Heliyon*. 2020;6(3):e03536.

doi: 10.1016/j.heliyon.2020.e03536

38. Radheshyam JB, Tripathi S, Singh R, *et al*. Recent studies on phytomedicine used in diabetic disorder. *J Pharm Pharmacol*. 2022;10:159-172.

doi: 10.17265/2328-2150/2022.05.002

39. Deng W, Wang H, Wu B, Zhang X. Selenium-layered nanoparticles serving for oral delivery of phytomedicines with hypoglycemic activity to synergistically potentiate the antidiabetic effect. *Acta Pharm Sin B*. 2019;9(1):74-86.

doi: 10.1016/j.apsb.2018.09.009

40. Govindan N, Vairaprakasam K, Chinnasamy C, Sivalingam T, Mohammed MK. Green synthesis of Zn-doped *Catharanthus roseus* nanoparticles for enhanced anti-diabetic activity. *Mater Adv*. 2020;1(9):3460-3465.

doi: 10.1039/D0MA00698J

41. Nagaraja S, Ahmed SS, Bharathi DR, *et al*. Green synthesis and characterization of silver nanoparticles of *Psidium guajava* leaf extract and evaluation for its antidiabetic activity. *Molecules*. 2022;27(14):4336.

doi: 10.3390/molecules27144336

42. Jobie FN, Ranjbar M, Moghaddam AH, Kiani M. Green synthesis of zinc oxide nanoparticles using *Amygdalus scoparia* Spach stem bark extract and their applications as an alternative antimicrobial, anticancer, and anti-diabetic agent. *Adv Powder Technol*. 2021;32(6):2043-2052.

doi: 10.1016/j.apt.2021.04.014

43. Hamza RZ, Al-Salmi FA, El-Shenawy NS. Zinc oxide nanoparticles with green tea extract complex in the pancreas of rats against monosodium glutamate toxicity. *J Basic Clin Physiol Pharmacol*. 2020;32(5):979-985.

doi: 10.1515/jbcpp-2020-0164

44. Sidorowicz A, Fais G, Casula M, *et al*. Nanoparticles from microalgae and their biomedical applications. *Mar Drugs*. 2023;21(6):352.

doi: 10.3390/md21060352

45. Yosri N, Khalifa SA, Guo Z, Xu B, Zou X, El-Seedi HR. Marine organisms: Pioneer natural sources of polysaccharides/proteins for green synthesis of nanoparticles and their potential applications. *Int J Biol Macromol*. 2021;193:1767-1798.

doi: 10.1016/j.ijbiomac.2021.10.229

46. Venkatesan J, Anil S, Kim SK, Shim MS. Seaweed polysaccharide-based nanoparticles: Preparation and applications for drug delivery. *Polymers*. 2016;8(2):30.

doi: 10.3390/polym8020030

47. Rai PK, Kumar V, Lee S, *et al*. Nanoparticle-plant interaction: Implications in energy, environment, and agriculture. *Environ Int*. 2018;119:1-9.

doi: 10.1016/j.envint.2018.06.012

48. Sharma G, Pandey S, Ghatak S, Watal G, Rai PK. Potential of spectroscopic techniques in the characterization of "green nanomaterials". In: *Nanomaterials in Plants, Algae, and Microorganisms*. United States: Academic Press; 2018. p. 59-77.

doi: 10.1016/B978-0-12-811487-2.00003-7

49. Khandker SS, Shakil MS, Hossen MS. Gold nanoparticles; potential nanotheranostic agent in breast cancer: A comprehensive review with systematic search strategy. *Curr Drug Metab*. 2020;21(8):579-598.

doi: 10.1016/B978-0-12-811487-2.00003-7

50. Mei W, Wu Q. Applications of metal nanoparticles in medicine/metal nanoparticles as anticancer agents. In: *Metal Nanoparticles: Synthesis and Applications in Pharmaceutical Sciences*. Germany: WILEY-VCH Verlag GmbH & Co.; 2018. p. 169-90.

51. Cheeseman S, Christofferson AJ, Kariuki R, *et al*. Antimicrobial metal nanomaterials: From passive to stimuli-activated applications. *Adv Sci*. 2020;7(10):1902913.

doi: 10.1002/advs.201902913

52. Dey AD, Bigham A, Esmaeili Y, *et al*. Dendrimers as nanoscale vectors: Unlocking the bars of cancer therapy. *Semin Cancer Biol*. 2022;86:396-419.

doi: 10.1016/j.semcancer.2022.06.003

53. Ragni R, Cicco S, Vona D, Leone G, Farinola GM. Biosilica from diatoms microalgae: Smart materials from bio-medicine to photonics. *J Mater Res*. 2017;32(2):279-291.

doi: 10.1557/jmr.2016.459

54. Sprynskyy M, Pomastowski P, Hornowska M, Król A, Rafińska K, Buszewski B. Naturally organic functionalized 3D biosilica from diatom microalgae. *Mater Des*. 2017; 132:22-29.

doi: 10.1016/j.matdes.2017.06.044

55. Rea I, De Stefano L. Special issue on new frontiers in diatom nanotechnology. *Appl Sci*. 2022;12(20):10332.

doi: 10.3390/app122010332

56. Bayu A, Yoshida A, Guan G. Hierarchical nanoporous silica-based materials from marine diatoms. In: *Handbook of Greener Synthesis of Nanomaterials and Compounds*. Amsterdam: Elsevier; 2021. p. 307-328.

doi: 10.1016/B978-0-12-822446-5.00014-9

57. Ali DM, Divya C, Gunasekaran M, Thajuddin N. Biosynthesis and characterization of silicon-germanium oxide nanocomposite by diatom. *Dig J Nanomater Biostruct*. 2011;6:117-120.

58. Yaseen M, Humayun M, Khan A, *et al*. Preparation, functionalization, modification, and applications of nanostructured gold: A critical review. *Energies*. 2021; 14(5):1278.

doi: 10.3390/en14051278

59. Singh S, Singh P, Mishra N, *et al*. Advanced drug delivery systems in breast cancer. In: *Advanced Drug Delivery Systems in the Management of Cancer*. United States: Academic Press; 2021. p. 107-126.

doi: 10.1016/B978-0-323-85503-7.00028-6

60. Hemdan BA, Hassan GK, Abou Hammad AB, El Nahrawy AM. *Industrial Perspective of Microbial Application of Nanoparticles Synthesis. Microbial Nanotechnology: Green Synthesis and Applications*. Berlin: Springer; 2021. p. 155-190.

doi: 10.1007/978-981-16-1923-6_9

61. Zhang F, Li Z, Duan Y, *et al*. Gastrointestinal tract drug delivery using algae motors embedded in a degradable capsule. *Sci Robot*. 2022;7(70):eabo4160.

doi: 10.1126/scirobotics.abo4160

62. Jo MJ, Bae SJ, Son BW, Kim CY, Kim GD. 3, 4-dihydroxyphenyl acetic acid and (+)-epoxydon isolated from marine algae-derived microorganisms induce down regulation of epidermal growth factor activated mitogenic signaling cascade in Hela cells. *Cancer Cell Int*. 2013;13(1):1-9.

doi: 10.1186/1475-2867-13-49

63. Shera SS, Banik RM. Algal nanoparticles: Synthesis and characterization. In: *Bioprospecting Algae for Nanosized Materials*. Cham: Springer International Publishing; 2022. p. 25-69.

doi: 10.1007/978-3-030-81557-8_2

64. Tsolakis N, Goldsmith AT, Aivazidou E, Kumar M. Microalgae-based circular supply chain configurations using Industry 4.0 technologies for pharmaceuticals. *J Clean Prod*. 2023;395:136397.

doi: 10.1016/j.jclepro.2023.136397

65. Srivastava N, Srivastava M, Singh R, *et al*. Co-fermentation of residual algal biomass and glucose under the influence of Fe3O4 nanoparticles to enhance biohydrogen production under dark mode. *Bioresour Technol*. 2021;342:126034.

doi: 10.1016/j.biortech.2021.126034

66. Mariano S, Panzarini E, Inverno MD, Voulvoulis N, Dini L. Toxicity, bioaccumulation and biotransformation of glucose-capped silver nanoparticles in green microalgae *Chlorella vulgaris*. *Nanomaterials*. 2020;10(7):1377.

doi: 10.3390/nano10071377

67. Sahayaraj K, Rajesh S, Rathi JA, Kumar V. Green preparation of seaweed-based silver nano-liquid for cotton pathogenic fungi management. *IET Nanobiotechnol*. 2019;13(2):219-225.

doi: 10.1049/iet-nbt.2018.5007

68. Neumann U, Derwenskus F, Flaiz Flister V, Schmid-Staiger U, Hirth T, Bischoff SC. Fucoxanthin, a carotenoid derived from *Phaeodactylum tricornutum* exerts antiproliferative and

antioxidant activities *in vitro*. *Antioxidants*. 2019;8(6):183.

doi: 10.3390/antiox8060183

69. Scholtz J, Van der Colff J, Steenekamp J, Stieger N, Hamman J. More good news about polymeric plant-and algae-derived biomaterials in drug delivery systems. *Curr Drug Targets*. 2014;15(5):486-501.

doi: 10.2174/1389450113149990175

70. Ho TC, Chang CC, Chan HP, *et al*. Hydrogels: Properties and applications in biomedicine. *Molecules*. 2022;27(9):2902.

doi: 10.3390/molecules27092902

71. Thomas D, O'Brien T, Pandit A. Toward customized extracellular niche engineering: progress in cell-entrapment technologies. *Adv Mater*. 2018;30(1):1703948.

doi: 10.1002/adma.201703948

72. Pangestuti R, Kim SK. Biological activities and health benefit effects of natural pigments derived from marine algae. *J Funct Foods*. 2011;3(4):255-266.

doi: 10.1016/j.jff.2011.07.001

73. Kim SK, Pangestuti R. Biological activities and potential health benefits of fucoxanthin derived from marine brown algae. *Adv Food Nutr Res*. 2011;64:111-128.

doi: 10.1016/B978-0-12-387669-0.00009-0

74. Menaa F, Wijesinghe U, Thiripuranathar G, *et al*. Marine algae-derived bioactive compounds: A new wave of nanodrugs? *Mar Drugs*. 2021;19(9):484.

doi: 10.3390/md19090484

75. Pereira L, Valado A. Algae-derived natural products in diabetes and its complications-current advances and future prospects. *Life*. 2023;13(9):1831.

doi: 10.3390/life13091831

76. Jain C, Ansarullah, Bilekova S, Lickert H. Targeting pancreatic β cells for diabetes treatment. *Nat Metab*. 2022;4(9):1097-1108.

doi: 10.1038/s42255-022-00618-5

77. Kaneto H, Kajimoto Y, Miyagawa JI, *et al*. Beneficial effects of antioxidants in diabetes: Possible protection of pancreatic beta-cells against glucose toxicity. *Diabetes*. 1999;48(12):2398-2406.

doi: 10.2337/diabetes.48.12.2398

78. Quazi A, Patwekar M, Patwekar F, *et al*. *In vitro* alpha-amylase enzyme assay of hydroalcoholic polyherbal extract: Proof of concept for the development of polyherbal teabag formulation for the treatment of diabetes. *Evid Based Complement Alternat Med*. 2022;2022:1577957.

doi: 10.1155/2022/1577957

79. Patwekar M, Patwekar F, Mezni A, *et al*. Assessment of antioxidative and alpha-amylase potential of polyherbal extract. *Evid Based Complement Alternat Med*. 2022;2022:7153526.

doi: 10.1155/2022/7153526

80. Kaur A, Kaur G, Rai MP. Algae cultivation for biomedical applications: Current scenario and future direction. In: *Algal Biotechnology*. Netherlands: Elsevier; 2022. p. 283-303.

doi: 10.1016/B978-0-323-90476-6.00009-1

81. Lobine D, Rengasamy KR, Mahomoodally MF. Functional foods and bioactive ingredients harnessed from the ocean: Current status and future perspectives. *Crit Rev Food Sci Nutr*. 2022;62(21):5794-5823.

doi: 10.1080/10408398.2021.1893643

82. Shinde MU, Patwekar M, Patwekar F, *et al*. Nanomaterials: A potential hope for life sciences from bench to bedside. *J Nanomater*. 2022;2022:1-3.

doi: 10.1155/2022/5968131

83. Kalasariya HS, Patel AK, Suthar RJ, Pereira L. *Exploring the Skin Cosmetic Benefits of Phenolic Compounds and Pigments from Marine Macroalgae: A Novel Green Approach for Sustainable Beauty Solutions*. Available from: https://www.preprints.org/manuscript/202307.0739 [Last accessed on 2025 Jan 21].

84. Cotas J, Pacheco D, Gonçalves AM, Silva P, Carvalho LG, Pereira L. Seaweeds' nutraceutical and biomedical potential in cancer therapy: A concise review. *J Cancer Metastasis Treat*. 2021;7:13.

doi: 10.20517/2394-4722.2020.134

85. Patwekar M, Patwekar F, Medikeri A, *et al*. Mechanistic insights on anticancer drugs with specific biological targets and signalling pathways. *Explor Med*. 2023;4(5):637-663.

doi: 10.37349/emed.2023.00166

86. Zia KM, Zuber M, Ali M, editors. Algae Based Polymers, Blends, and Composites: Chemistry, Biotechnology and Materials Science. Amsterdam: Elsevier; 2017.

87. Singh PK, Fillat MF, Kumar A, editors. *Cyanobacterial Lifestyle and its Applications in Biotechnology*. United States: Academic Press; 2021.

88. Siddiqui SA, Pahmeyer MJ, Mehdizadeh M, Nagdalian AA, Oboturova NP, Taha A. Consumer behavior and industry implications. In: *The Age of Clean Label Foods*. Cham: Springer International Publishing; 2022. p. 209-247.

doi: 10.1007/978-3-030-96698-0_7

89. Ahmed SR, Cardoso AG, Kumar S, Ortega GA, Srinivasan S, Rajabzadeh AR. *7 Nanozymes in Biosensing. Nanozymes: Advances and Applications*. Boca Raton: CRC Press; 2021. p. 115.

90. Madamsetty VS, Mohammadinejad R, Uzieliene I, *et al*. Dexamethasone: Insights into pharmacological aspects, therapeutic mechanisms, and delivery systems. *ACS*

Biomater Sci Eng. 2022;8(5):1763-1790.

doi: 10.1021/acsbiomaterials.2c00026

91. Samavati SS, Kashanian S, Derakhshankhah H, Rabiei M. Nanoparticle application in diabetes drug delivery. *J Nanoparticle Res*. 2022;24(9):178.

doi: 10.1007/s11051-022-05547-8

92. Mohammad G, Mishra VK, Pandey HP. Antioxidant properties of some nanoparticle may enhance wound healing in T2DM patient. *Digest J Nanomater Biostruct*. 2008;3(4):159-162.

93. Fu LH, Qi C, Lin J, Huang P. Catalytic chemistry of glucose oxidase in cancer diagnosis and treatment. *Chem Soc Rev*. 2018;47(17):6454-6472.

doi: 10.1039/C7CS00891K

94. Li C, Wang J, Wang Y, *et al*. Recent progress in drug delivery. *Acta Pharm Sin B*. 2019;9(6):1145-1162.

doi: 10.1016/j.apsb.2019.08.003

95. Patra JK, Das G, Fraceto LF, *et al*. Nano based drug delivery systems: Recent developments and future prospects. *J Nanobiotechnol*. 2018;16(1):1-33.

doi: 10.1186/s12951-018-0392-8

96. Li Z, Wang Y, Liu J, Rawding P, Bu J, Hong S, Hu Q. Chemically and biologically engineered bacteria-based delivery systems for emerging diagnosis and advanced therapy. *Adv Mater*. 2021;33(38):2102580.

doi: 10.1002/adma.202102580

97. Yao J, Yang M, Duan Y. Chemistry, biology, and medicine of fluorescent nanomaterials and related systems: New insights into biosensing, bioimaging, genomics, diagnostics, and therapy. *Chem Rev*. 2014;114(12):6130-6178.

doi: 10.1021/cr200359p

98. Wu F, Liu J. Decorated bacteria and the application in drug delivery. *Adv Drug Deliv Rev*. 2022;2022:114443.

doi: 10.1016/j.addr.2022.114443

99. Xie J, Lee S, Chen X. Nanoparticle-based theranostic agents. *Adv Drug Deliv Rev*. 2010;62(11):1064-1079.

doi: 10.1016/j.addr.2010.07.009

100. Luther DC, Huang R, Jeon T, *et al*. Delivery of drugs, proteins, and nucleic acids using inorganic nanoparticles. *Adv Drug Deliv Rev*. 2020;156:188-213.

doi: 10.1016/j.addr.2020.06.020

101. Thakuria A, Kataria B, Gupta D. Nanoparticle-based methodologies for targeted drug delivery-an insight. *J Nanoparticle Res*. 2021;23:1-30.

doi: 10.1007/s11051-021-05190-9

ACCSCIENCE PUBLISHING

Global Translational Medicine

PERSPECTIVE ARTICLE

Patient-oriented and clinical considerations supporting the single-incision subepithelial connective tissue harvest

Han S. Kim[1], Denise M. Cacho[1], Alan R. George[1], Joseph K. Retrum[2], Carsen R. McDaniel[3], Adam R. Lincicum[1], Kimberly Ann Inouye[1], Brian W. Stancoven[1], and Thomas M. Johnson[1]*

[1]Department of Periodontics, Army Postgraduate Dental School, Postgraduate Dental College, Uniformed Services University, Fort Eisenhower, Augusta, Georgia, United States of America

[2]Department of Periodontics, United States Army Dental Activity, Fort Riley, Kansas, United States of America

[3]Department of Periodontics, Army Postgraduate Dental School, Postgraduate Dental College, Uniformed Services University, Fort Bliss, El Paso, Texas, United States of America

(This article belongs to the *Special Issue: Soft and Hard Tissues Reconstruction in Dentistry*)

Abstract

The subepithelial connective tissue graft (SCTG) has become the gold standard for treating gingival recession. In addition, SCTG is a reliable technique for augmenting the dimensions of attached gingiva and peri-implant mucosa, thereby supporting periodontal and peri-implant health and stability. Various autogenous soft-tissue harvesting techniques have been developed for use in periodontal plastic surgery, each with its own set of advantages and limitations. Over the past 5 years, updated reviews of human palatal anatomy have influenced clinical decision-making regarding SCTG harvesting, expanding the safety zone for palatal SCTG procedures. New histological and molecular findings have provided insights into the underlying mechanisms that may explain the observed differences in clinical outcomes based on the harvesting method and graft type. The purpose of this paper is to recommend a preferred SCTG harvesting technique applicable to most cases and to identify specific clinical scenarios where available evidence may support the use of alternative methods.

Keywords: Clinical protocols; Esthetics; Palate; Hard; Patient satisfaction; Tissue transplantation; Treatment outcome

***Corresponding author:**
Thomas M. Johnson
(thomas.m.johnson34.mil@health.mil)

Citation: Kim HS, Cacho DM, George AR, *et al*. Patient-oriented and clinical considerations supporting the single-incision subepithelial connective tissue harvest. *Global Transl Med*. 2025:4(1):35-46.
doi: 10.36922/gtm.4860

Received: September 15, 2024

1st revised: November 10, 2024

2nd revised: November 23, 2024

Accepted: November 25, 2024

Published online: December 16, 2024

1. Introduction

Compared to alternative treatment methods, subepithelial connective tissue graft (SCTG)-based procedures are known to achieve complete root coverage most frequently, offer the highest average root coverage percentage, and provide the most favorable temporal stability of results.[1-3] However, both patients and clinicians must make concessions to attain this level of clinical predictability. Autologous soft-tissue harvesting has been associated with postoperative complications such as prolonged bleeding, neurosensory dysfunction, flap necrosis, and discomfort, particularly when the operator

lacks experience.[4-7] In addition, the emergence of multiple harvesting techniques – each with its own advantages and disadvantages – has increased the complexity of treatment planning in periodontal plastic surgery.

Following the introduction of SCTG for root coverage, multiple authors identified the area of the palate between the mesial of the first molar and the distal of the canine as the optimal anatomic location for SCTG harvests.[8-11] Within this limited zone, SCTGs were typically sufficient for addressing isolated defects or two adjacent sites exhibiting gingival recession.[7] More recently, Tavelli *et al.*,[6,12] using an updated review of palatal anatomy literature, defined an evidence-based safety zone for palatal tissue harvesting. Newly identified anatomic details – such as the mean distances between the greater palatine artery and the maxillary posterior teeth – have expanded the safe harvesting zone to include the second molar area, provided that the apicocoronal dimension of the safety zone (10.9 mm in the second molar area) is respected.[12] This expanded safety zone permits SCTG harvests with greater mesiodistal width, allowing clinicians to address multiple adjacent recession defects over a wider span. Moreover, graft-splitting techniques can, in some cases, double the mesiodistal dimension of the SCTG, substantially increasing the number of defects treatable in a single procedure.[13]

Although evidence on this topic is limited, variations in graft composition, patient outcomes, and complication risks have been observed across different SCTG harvesting methods.[4,6,7] Therefore, practitioners who are familiar with all available harvesting methods are better equipped to tailor treatment to the specific needs of each patient and site. The purpose of this paper is to propose a preferred SCTG harvesting technique applicable to most root coverage and gingival augmentation cases, and to identify clinical scenarios in which alternative approaches may be more appropriate.

2. Methods

Due to terminological heterogeneity among authors, it is necessary to define the terms used in this paper. For the purposes of this article, an SCTG refers to autogenous connective tissue removed from the hard palate or maxillary tuberosity area for gingival/mucosal augmentation or root coverage.[14] The epithelial layer is either not harvested or removed secondarily before graft implantation. A de-epithelialized gingival graft (DGG) is a specific type of SCTG, harvested as a traditional free gingival graft (FGG).[15] However, unlike an FGG, the preparation of a DGG involves removing the epithelium extraorally or intraorally using a scalpel or other instrument.

This article summarizes the available methods for harvesting SCTGs, comparing the advantages and disadvantages of each technique. In addition, author preferences for SCTG harvesting methods in specific clinical situations are described. To identify relevant articles on SCTG harvesting, a literature search was conducted in May of 2024 using the PubMed database. The search strategy included the following terms: "subepithelial connective tissue graft" OR "connective tissue graft" OR "autologous soft tissue graft" OR "free soft-tissue autograft" OR "de-epithelialized gingival graft" OR "free gingival graft," AND "harvest technique" OR "harvest." The bibliographies of identified articles were manually reviewed to identify additional publications, and this search strategy was applied recursively. Articles describing SCTG harvesting methods and comparing the clinical performance of various graft types were included in the study. No restrictions were placed on the study design. The identified articles were critically appraised.

3. SCTG harvesting techniques

Although minor intracategory variations exist, an operator harvesting an SCTG for root coverage or gingival/mucosal augmentation generally has four options: a single-incision technique (SIT),[9,16] a multiple-incision technique (MIT),[17,18] a DGG technique,[15] or an SCTG harvest from the maxillary tuberosity SCTG (tSCTG).[19]

3.1. SIT

The SIT involves making a single horizontal incision through which the underlying connective tissue is harvested (Figures 1 and 2).[9,16] The incision is oriented orthogonally to the surface of the palatal mucosa, approximately 2 – 3 mm apical to the gingival margin. Depending on the required graft dimensions, the horizontal incision may extend from the canine to the second molar area.[6,12] However, the safely obtainable apicocoronal graft dimension narrows from posterior to anterior: 8 mm in the molar and second premolar areas, 7.6 mm in the first premolar area, and 5 mm in the canine area.[12]

In inexperienced surgeons, the risk of overthinning the superficial tissue or perforating the palatal mucosa may increase as the scalpel is advanced apically during sharp dissection. This risk of primary flap laceration can be minimized by performing the harvest in a stepwise manner (Table 1). When the intended primary flap thickness is 1.5 – 2 mm, grafts harvested using the SIT are predominantly composed of tissue originating deep to the lamina propria.[20-22] Substantial interpatient variability exists in both the composition of the submucosa and the overall thickness of palatal soft tissue.[20-22] Consequently, the clinical quality of the graft depends in part on the

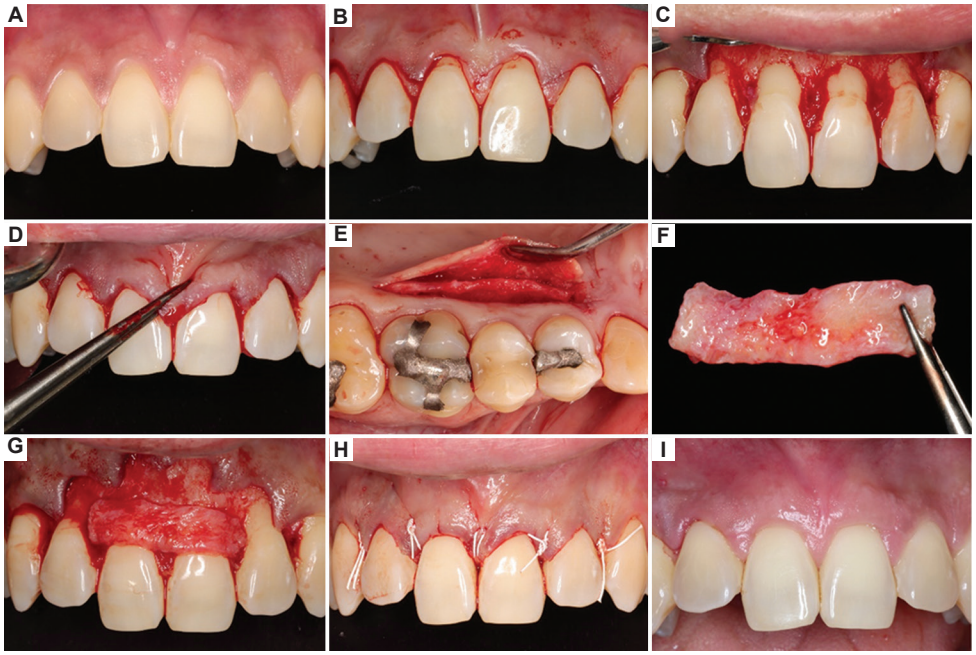

Figure 1. Single-incision SCTG harvest for root coverage at the maxillary central incisors. (A) Baseline clinical appearance, with recession defects measuring 1.5 mm at tooth #8 and 2 mm at tooth #9. (B) Initial incisions; no vertical incisions were used. (C) Facial mucoperiosteal flap reflection, with a spit-full-split flap design employed. (D) Coronal advancement of the flap. (E) SCTG harvest site before graft retrieval. (F) SCTG harvested. (G) Graft in position and stabilized before closure. (H) Wound closure. (I) Post-operative appearance at 3 months.
Abbreviation: SCTG: Subepithelial connective tissue graft.

relative proportions of fibrous, adipose, and glandular tissue present.

Several authors suggest that the SIT promotes early donor site healing and enhances patient-centered outcomes, although supporting evidence remains limited.[9,16,23] Compared to traditional techniques, the SIT involves less disruption of the blood supply to the primary flap, as vertical incisions are avoided. Moreover, the SIT may reduce flap movement during early healing and increase clot stability in the void created by graft removal. Therefore, the claim that single-incision harvests promote donor-site healing is plausible. Further research comparing clinical and patient-reported outcomes following different harvesting methods may identify a superior evidence-based technique. Given the limited research available, the SIT offers potential advantages in wound healing and patient comfort and is applicable in many root coverage and gingival/mucosal augmentation procedures. Thus, the SIT may be the preferred harvesting method when feasible.

3.2. MIT

One or two vertical incisions may be added to the horizontal incision at SCTG donor sites, with or without retention of an epithelial band at the coronal aspect of the graft (Figures 3-5).[17,18] When two vertical incisions are used, the technique is commonly referred to as the "trap-door" approach.[23] Alternatively, the operator may place a single vertical incision at one boundary of the harvest site and extend the horizontal incision mesially or distally to ensure adequate access for graft harvesting. In his landmark article on SCTG harvesting, Dr. Alan Edel described two methods for performing trap-door harvests. In Method 1, the operator first establishes a partial-thickness palatal pedicle flap and then harvests the underlying connective tissue.[17] Method 2 involves extending the horizontal and vertical incisions to the bone, reflecting a full-thickness palatal pedicle, and thinning the flap to remove the SCTG.[17]

The use of multiple incisions for SCTG harvesting offers several advantages. Clinicians harvesting an SCTG for the first time may face a steep learning curve. While many new practitioners enter periodontics training with some experience in mucoperiosteal flaps, few have experience harvesting palatal tissue, which is a substantially different clinical skill. In addition, periodontists in training are well aware of the complications associated with autologous soft-tissue harvesting. As a result, this procedure may induce anxiety in both the patient and the operator. Initially, inexperienced clinicians may struggle to establish a palatal flap of appropriate thickness. If the primary partial-thickness access flap is too thin, necrosis may occur; conversely, excessive flap thickness may result in an SCTG of unfavorable quality and thickness. Trap-door harvests –

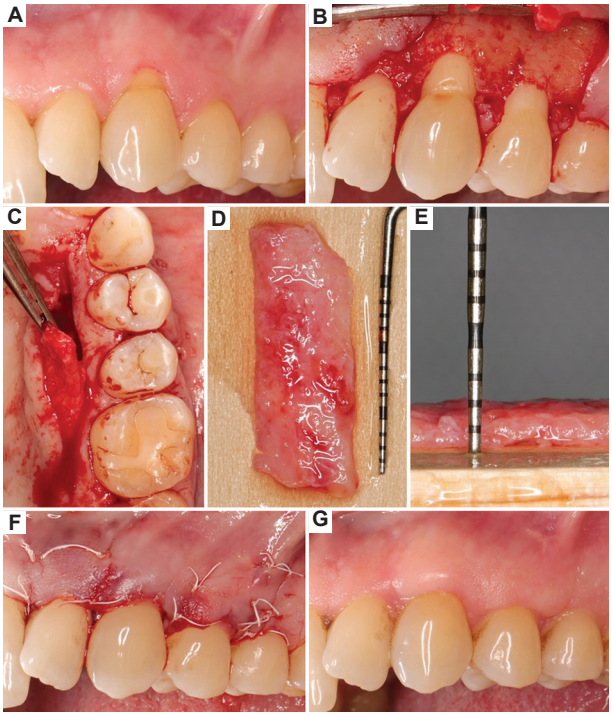

Figure 2. Single-incision SCTG harvest for root coverage at the maxillary left canine and first premolar. (A) Baseline clinical appearance. (B) Facial mucoperiosteal flap reflection (split-full-split flap design). A vertical incision was placed at the mesiobuccal line angle of tooth #13. (C) Single-incision harvest. (D) SCTG removed. (E) Graft thickness was approximately 2 mm. (F) Wound closure. (G) Post-operative appearance at 2 months. Abbreviation: SCTG: Subepithelial connective tissue graft.

particularly those utilizing Method 2 – allow the clinician to assess the full thickness of the palatal soft tissue before dividing it between the flap and the graft. When a primary flap is established before the SCTG harvest (Method 1), the operator can more easily monitor flap thickness during sharp dissection. By contrast, an SIT makes gauging flap thickness more challenging. In addition, an MIT provides clear anterior and posterior limits for the harvest site, allowing the clinician to tailor the SCTG to the dimensions of the recipient site. Given that postoperative discomfort has been shown to correlate with various measures of donor site size,[4,5,15] the ability to limit the harvest site dimensions is particularly beneficial when treating an isolated recession defect.

Intuitively, the use of vertical incisions in SCTG harvesting may lead to less favorable donor site healing and possibly increased patient discomfort. Initial evidence appears to support this assumption.[9,16,23] Compared to the SIT, the MIT may require more suturing, the use of a protective palatal stent, and the application of hemostatic materials or agents.[9] As a result, vertical incisions may also extend the duration of the procedure.

Table 1. A stepwise approach to single-incision subepithelial connective tissue graft harvesting

Step	Description
1	Identify the start and end points of the horizontal incision based on anatomic limitations and the dimensions of the required graft.
2	Connect the start and end points with an incision oriented orthogonally to the surface of the palatal mucosa, extending to the bone.
3	Reorient the scalpel to create a split-thickness incision in the palatal tissue. Use the surface of the palatal mucosa and the long axes of the maxillary teeth as anatomic landmarks. Establish a primary flap thickness of approximately 1.5 mm.
4	Continue sharp dissection until the apicocoronal dimension of the flap reaches 4 mm.
5	To reduce the risk of primary flap laceration, change the scalpel angle by approximately 10°, directing the tip toward the maxilla. Increase the depth of the sharp dissection until the intended graft width is reached, respecting the apicocoronal safety zone limitations.
6	Make vertical incisions and an apical horizontal incision to the bone, outlining the graft.
7	Begin the graft harvest by reflecting the periosteum at the coronal aspect of the graft.
8	Complete the harvest using sharp dissection on the deep aspect of the graft or by continuing to reflect the periosteum until the apical incision is reached.

3.3. DGG technique

An SCTG harvesting method that differs fundamentally from the SIT and MIT involves removing the epithelium from a traditional FGG using a scalpel, bur, or laser, either before or after graft harvest (Figure 6).[15,24,25] Zucchelli *et al.*[15] referred to this graft type as a DGG. Given that DGG harvests involve the removal of superficial palatal tissue, the graft composition differs from that of an SCTG harvested using an MIT or SIT. The soft tissue of the hard palate, from superficial to deep, consists of masticatory mucosa (an orthokeratinized oral epithelium together with the subjacent lamina propria), the submucosa, and the periosteum.[26] The submucosa contains blood vessels, nerves, adipose tissue, glandular tissue, and loose connective tissue. Adjacent to the maxillary teeth and in the midpalatal raphe, the submucosa is minimal or absent.[26] In these areas, the periosteum is separated from the lamina propria by dense connective tissue of variable thickness.[26] On average, the thicknesses of the epithelium and lamina propria are 0.4 mm and 0.9 – 2.0 mm, respectively.[20,27] Thus, a typical FGG measuring 2 mm in thickness includes an epithelial layer <0.5 mm, most or all of lamina propria thickness, and minimal submucosal tissue.[20,27] Because the papillary layer of the lamina propria

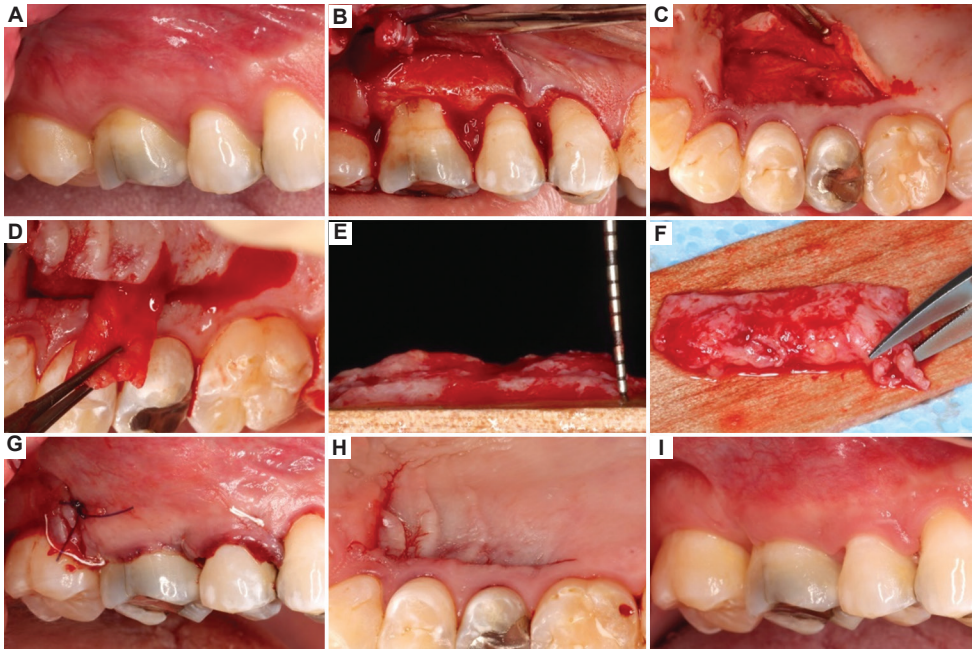

Figure 3. Two-incision SCTG graft harvest for root coverage at the maxillary right first molar. (A) Baseline clinical appearance. (B) Buccal mucoperiosteal flap reflection. A vertical incision was placed at the mesiobuccal line angle of tooth #2. (C) Donor site after preparation of the primary flap. (D) SCTG harvested. (E) Initial graft thickness was irregular, partly due to the presence of yellowish adipose tissue within the graft. (F) The graft was thinned to achieve a uniform thickness of approximately 2 mm. (G) Wound closure. (H) Donor site at the completion of the procedure. (I) Post-operative appearance at 2 months.
Abbreviation: SCTG: Subepithelial connective tissue graft.

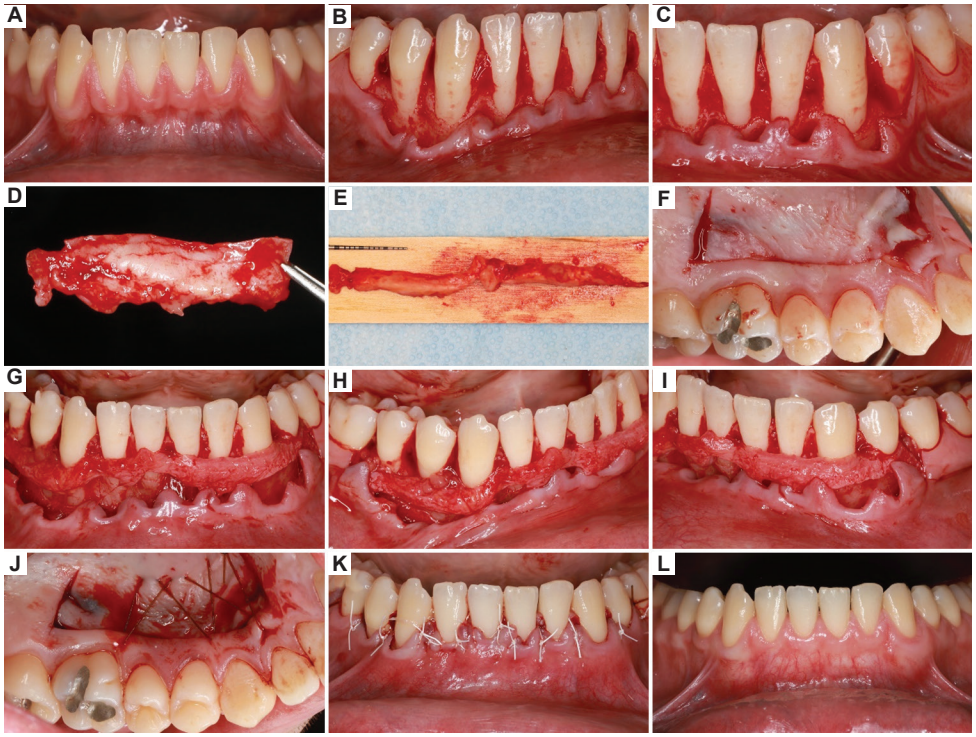

Figure 4. Three-incision SCTG harvest with graft splitting for root coverage from tooth #21 – tooth #29. (A) Baseline clinical appearance. (B, C) Facial mucoperiosteal flap reflection (split-full-split flap design). Vertical incisions were placed at the mesiobuccal line angles of teeth #20 and 30. (D) SCTG harvested. (E) After splitting, the graft measured 62 mm. (F) Donor site after graft removal. (G) SCTG positioned at the cementoenamel junctions. (H, I) Distal aspects of the SCTG. (J) Donor site at the completion of the procedure. (K) Wound closure. (L) Post-operative appearance at 6 months.
Abbreviation: SCTG: Subepithelial connective tissue graft.

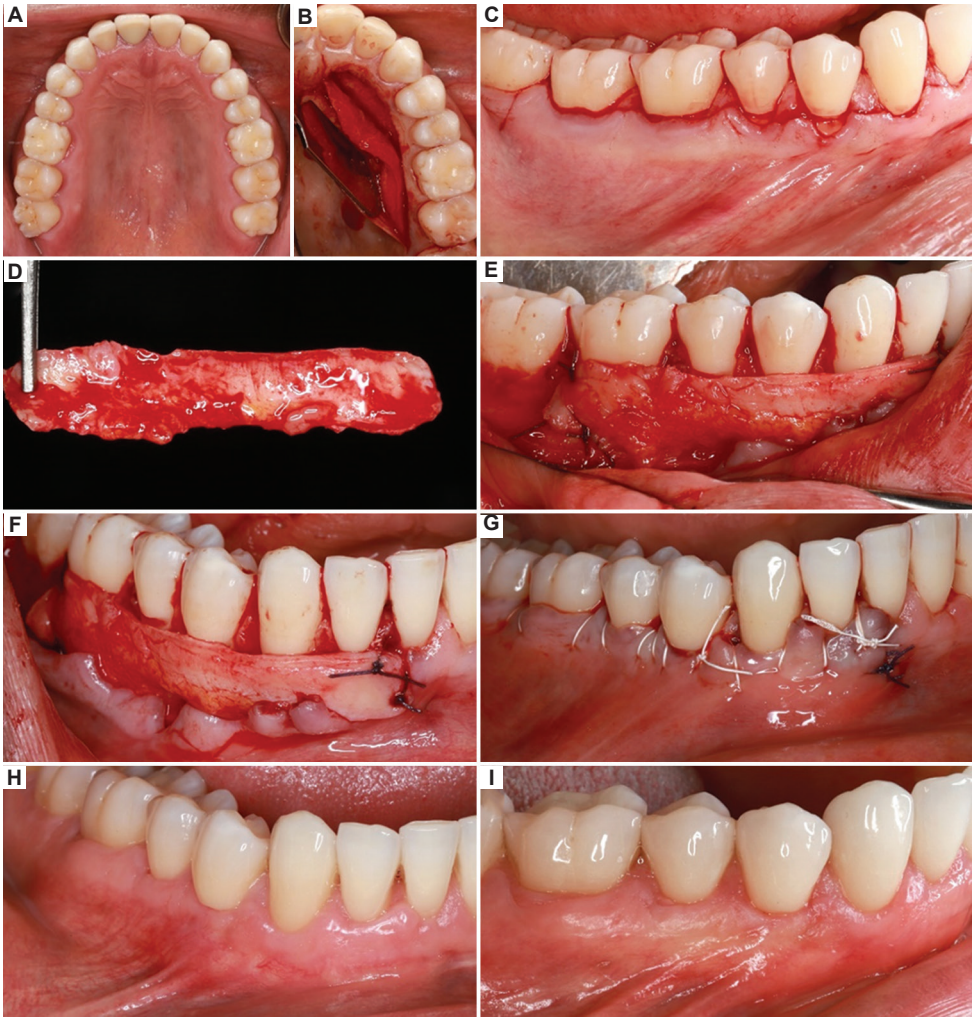

Figure 5. Two-incision SCTG harvest for root coverage at teeth #26 through #30. (A) Baseline clinical appearance of the hard palate. The patient exhibited an unusually large, ovoid maxillary arch form. (B) SCTG harvested using a two-incision technique. (C) Incision design. A vertical incision was placed at the mesiobuccal line angle of tooth #32. (D) SCTG harvested. Dimensions were approximately 8 × 42 mm. (E, F) Graft stabilized in position. (G) Wound closure. (H, I) Post-operative appearance at 10 months.
Abbreviation: SCTG: Subepithelial connective tissue graft.

interdigitates with the epithelial pegs, complete removal of the epithelium is difficult without sacrificing a portion of the reticular layer. In contrast, assuming a primary access flap thickness of approximately 1.5 mm, an SCTG 2 mm in thickness obtained through SIT or MIT may consist predominantly of tissue derived from the submucosa, with little contribution from the lamina propria and no epithelial cells.[20,27] Indeed, a cadaver study demonstrated that palatal SCTGs harvested using a partial-thickness flap (MIT or SIT) include a higher proportion of adipose and glandular tissue compared with DGGs.[20]

The higher proportion of fibrous tissue found in DGGs may or may not translate into differences in clinical outcomes between the two graft types, with mixed results reported. A systematic review and meta-analysis found that 1-year mean root coverage (MRC) percentages for DGG and SCTG were 94% and 89%, respectively.[28] The use of DGG also resulted in superior probing depth reduction and gains in clinical attachment and keratinized tissue width.[28] However, this analysis included only 10 studies, and intergroup differences in clinical parameters were all within 1 mm.[28] In contrast to the findings of this systematic review, Bakhishov *et al.*[29] did not identify graft type (DGG vs. SCTG) as a statistically significant predictor of MRC percentage. Zangrando *et al.*[30] compared clinical and patient-reported outcomes following root coverage procedures using DGG or SCTG harvested using a double-blade scalpel (DBS). No statistically significant differences in clinical parameters were identified; however, the DBS group experienced significantly more discomfort compared

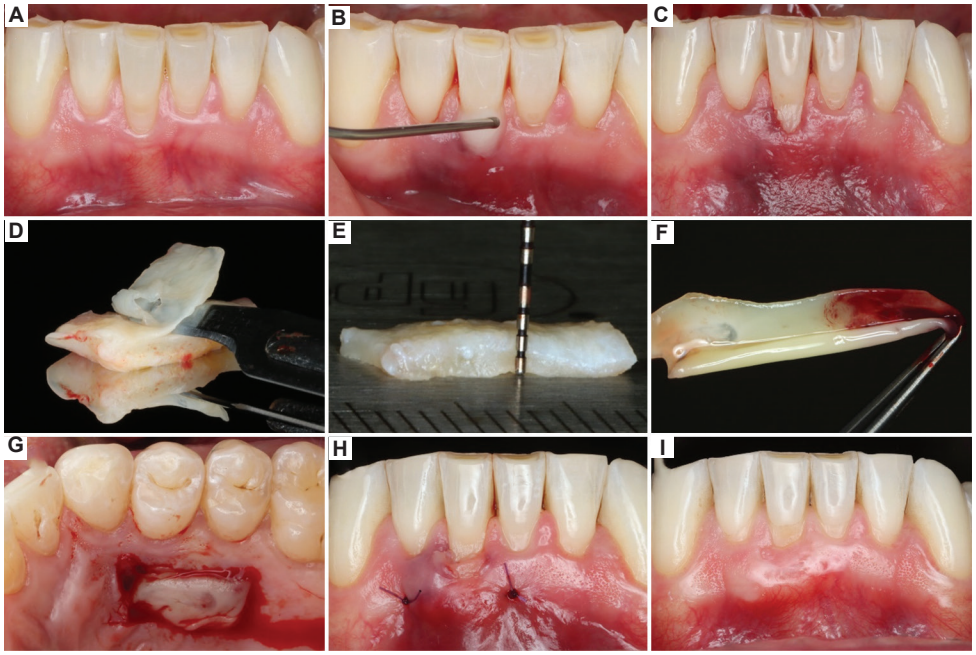

Figure 6. DGG for root coverage at the mandibular right central incisor. (A) Baseline clinical appearance. (B) Root surface modification with 24% ethylenediaminetetraacetic acid. (C) Raetzke pouch prepared. (D) DGG harvested. The epithelium was removed with a scalpel. (E) DGG after epithelium removal, thinned to approximately 2 mm in thickness. (F) PRF membrane used to improve healing and patient comfort at the donor site. (G) PRF membrane sutured in place at the donor site. (H) Graft stabilized, wound closed. (I) Post-operative appearance at 2 months.
Abbreviations: DGG: De-epithelialized gingival graft; PRF: Platelet-rich fibrin.

to the DGG group.[30] Other investigators completed a split-mouth study comparing outcomes of coronally advanced flaps with DGG or SCTG.[31] The authors found no statistically significant difference in MRC.[31] However, complete root coverage was significantly more frequent in the SCTG group, whereas gingival thickness was significantly greater in the DGG group.[31] In addition, post-operative pain and analgesic consumption were significantly higher in patients who received a DGG.[31] Zucchelli *et al.*[15] found no difference in patient discomfort between DGG and trap-door SCTG harvest sites. However, the grafts used in this study were small, and the DGG harvest sites were covered with absorbable collagen membranes.[15] DGG harvest sites heal by secondary intention and are susceptible to topical irritation during the early postoperative period. Thus, most authors have observed greater discomfort in DGG/FGG versus SIT/MIT harvest sites.[4,5,31]

Late complications of SCTG procedures include the presence of a persistent pasty white or yellowish discharge and the development of a gingival "cul-de-sac" or cyst-like lesion, both of which are thought to relate to epithelial inclusions.[2,32-35] Cytologic analysis has shown that the discharge is consistent with degenerating normal epithelial cells.[34] Such discharge has occurred at postoperative timepoints ranging from 2 to 15 months and at sites receiving palatal grafts harvested using various methods.[32] The cellular discharge can be released into the oral cavity through a small "cul-de-sac" opening or expressed through the epithelium.[32] It has been speculated that epithelial remnants within the graft may increase the risk of these complications.[32] Harris[36] reported epithelial remnants in 24 of 30 SCTGs (80%) harvested using a DBS technique, despite attempts to remove the epithelial bands. Romano *et al.*[37] performed a histological assessment of 16 DGGs after 2 months of healing. Epithelial inclusions were found at two recipient sites (12.5%).[37] One site exhibited a cyst lined by stratified squamous epithelium, and at the other site, small islands of stratified squamous epithelium were integrated within the connective tissue.[37] Whether grafts harvested using a split-thickness technique (SIT or MIT) without an epithelial band are less likely to produce an epithelium-related late complication remains unestablished.

3.4. SCTG harvested from the maxillary tuberosity

As an alternative to palatal tissue, clinicians may choose to harvest soft tissue from the maxillary tuberosity area. tSCTG harvests are typically performed using a distal wedge or a gingivectomy (DGG) approach, although the dimensions of the grafts that can be obtained generally limit tSCTG applications to isolated recipient sites (Figure 7).[38] The lamina propria of the masticatory mucosa in this region is denser and less vascular than that of the

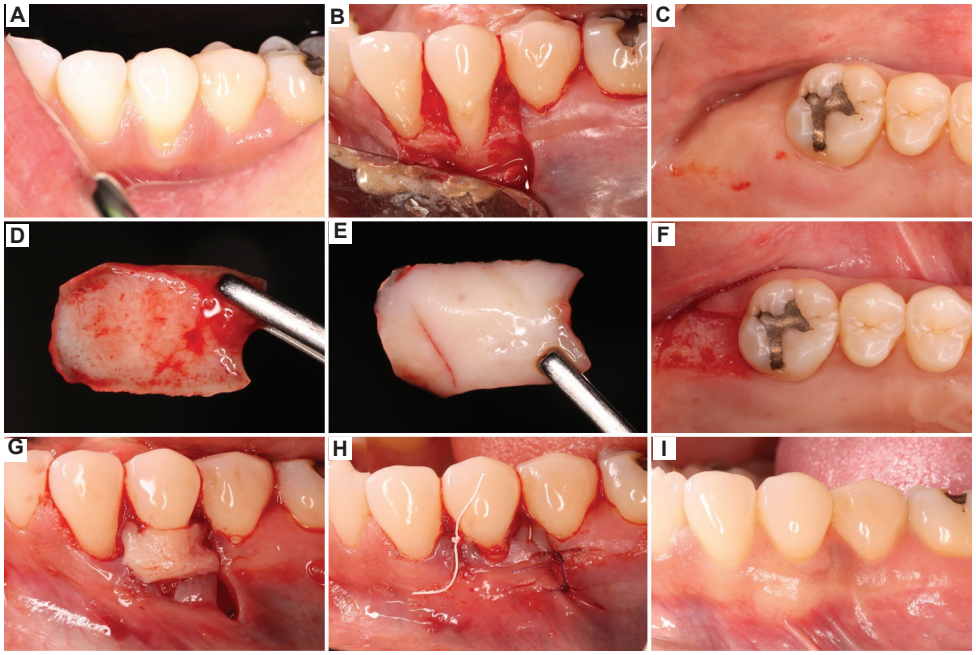

Figure 7. DGG harvested from the maxillary right tuberosity area for root coverage at the mandibular left first premolar. (A) Baseline clinical appearance. Tooth #20 exhibited a buccal gingival recession defect measuring 2.5 mm in depth. (B) Buccal mucoperiosteal flap (split-full-split flap design). (C) Maxillary right tuberosity area before graft harvest. (D, E) Deep and superficial surfaces of the graft, respectively. The epithelium was removed with a scalpel. (F) Donor site after harvest. (G) DGG stabilized with interproximal sutures. (H) Wound closure. (I) Post-operative appearance at 3 months. Abbreviation: DGG: De-epithelialized gingival graft.

palate lamina propria,[39] and the ratio of lamina propria to submucosa is higher in tSCTG relative to palatal SCTGs.[40] In the tuberosity area, fibrous tissue predominates in the zone between the lamina propria and the periosteum, with submucosa typically accounting for <5% of tSCTG composition.[40] In contrast, submucosal tissue may comprise more than a quarter of the structure of palatal SCTGs.[40]

In addition to these structural differences, tSCTG and palatal SCTGs appear to differ in gene expression patterns and clinical performance. Lysyl hydroxylase (LH) catalyzes the hydroxylation of lysine residues in collagen molecules, a process critical for collagen maturation, fibril formation, and cross-linking.[39,41] Overexpression of LH has been associated with fibrosis and defective fibrillogenesis.[39,41] Dellavia *et al.*[39] compared the expression levels of collagen type I (COL-I), collagen type III, lysyl hydroxylase 2b (LH2b), and matrix metalloproteinases-1 and -2 (MMP-1, MMP-2) in cell cultures derived from tuberosity and palatal fibroblasts. The ratio of LH2b to COL-I mRNA (LH2b/COL-I) was 4 times higher in cell cultures derived from tuberosity compared to palatal fibroblasts.[39] Consistent with these results, immunohistochemical analyses conducted by another group of investigators found higher levels of LH2 and MMP-2 in tSCTGs compared to palatal SCTGs.[40] Based on these studies, an emerging hypothesis posits that collagen in the tuberosity area may be comparatively resistant to MMP-mediated degradation.[19] This mechanism may explain the clinical observations that sites treated with tSCTGs tend to exhibit collagen accumulation, fibrosis, and compromised esthetics.[19,39,41] Oral epithelial cells at tSCTG and palatal SCTG harvest sites also exhibit distinct cytokeratin expression patterns.[40] Whether the differential expression of specific cytokeratin types indicates that tSCTGs more strongly induce keratinization remains unknown. However, several clinical and patient-oriented advantages have been associated with soft tissue harvests from the maxillary tuberosity. Limited evidence suggests that harvesting soft tissue from the tuberosity results in faster donor site healing, less discomfort, reduced analgesic consumption, and greater tissue thickness gain compared to the use of palatal SCTGs.[19,38,40,42]

4. Discussion

The objectives of this article were to review commonly applied SCTG harvesting methods, propose a preferred technique applicable in most circumstances, and identify specific clinical scenarios in which alternative harvesting techniques may be superior. Popular biomaterials, such as acellular dermal matrix and xenogeneic collagen matrix, along with emerging alternatives like living cellular constructs, are available for patients who wish to avoid

the discomfort and potential morbidity associated with palatal donor sites.[43] The present paper is relevant for both practitioners and patients seeking to optimize clinical outcomes and ensure the stability of results through the selection of autogenous tissue for root coverage and gingival/mucosal augmentation procedures.

The choice of the SCTG harvest technique is a critical clinical decision. The selected method may influence the clinical behavior of the graft, donor-site morbidity, patient-oriented outcomes, and long-term stability. The main complications associated with SCTG harvesting are donor-site hemorrhage and excessive pain.[1,4-7] Primary flap laceration can occur at both the SIT and MIT harvest sites; surgical trauma or overthinning of the primary flap may result in necrosis and potentially, exposure of the underlying bone.[6] Post-operative infections and donor-site neurosensory changes are rare but have been reported.[6,44,45] Most studies comparing patient-reported outcomes following SCTG harvesting focus primarily on post-operative discomfort and analgesic consumption.[7,46,47] Zuhr *et al.*[48] have noted that further research is needed to clarify differences among graft types with regard to recipient-site esthetics, volume stability, and other patient-centric concerns. Given the important unanswered questions related to this gold-standard procedure, expert opinion and operator preference remain relevant factors in the decision-making process when selecting an SCTG harvesting technique.[48]

In recent years, the defined safety zone for harvesting palatal SCTGs has expanded considerably, due to updated investigations into human palatal anatomy.[12] However, it is important to note that research related to SCTG harvesting is still far from comprehensive. Only a few studies have compared SCTGs obtained from deep palatal tissue, tSCTGs, and DGGs at the mRNA and protein levels.[39-41] Attempts to correlate existing molecular data with the observed clinical performance of the various graft types remain largely speculative.[19,39-41]

Nevertheless, an argument can be made that the SIT represents the presumptive technique of choice, based on limited data suggesting that this method may expedite healing, offer a superior patient experience, and minimize the risk of late complications.[9,16,23] The use of a tSCTG may reduce patient discomfort in cases involving isolated recipient sites.[19,38,40,42] However, the SIT allows the clinician to minimize donor-site morbidity when applying an SCTG across a wide mesiodistal span. In some cases, graft splitting may reduce donor-site dimensions, thereby enhancing patient-reported outcomes.[13] In addition, when esthetic concerns are paramount, SIT palatal harvests avoid the potential fibrosis associated with tSCTG placement. When a portion of the graft remains exposed after surgery, differences in esthetic outcomes achievable using deep palatal tissue, DGG, and tSCTG have not been clarified through controlled clinical research.

Grafts harvested using the SIT and MIT are obtained from the same anatomical location and are expected to exhibit no significant differences in structure, composition, or clinical performance. However, the SIT is generally preferred due to potential differences in patient-reported outcomes[9,16,23] Nevertheless, clinicians new to palatal tissue harvesting may initially find the MIT easier to perform. Moreover, the presence of a transpalatal arch wire or other fixed appliance may necessitate the use of MIT.

Although there is a clear rationale for preferring the SIT in most situations, the advantages of alternative methods warrant consideration in specific clinical scenarios. For instance, a tSCTG may be favored at an isolated site where tissue thickness is particularly important, and esthetics are not the primary concern. A tSCTG is an excellent choice for augmenting peri-implant mucosa and masking slight alveolar ridge deficiencies at isolated dental implant sites, particularly those outside the esthetic zone. Importantly, the clinician's ability to harvest a tSCTG depends on the patient's anatomy. Some individuals – especially those with retained maxillary third molars – may not be suitable candidates for this graft type. Similarly, patients with a shallow palatal vault or thin palatal tissue may not be ideal candidates for palatal SCTG harvesting through either SIT or MIT. In these cases, a DGG may be a superior option. Due to its higher content of fibrous and lower content of adipose and glandular tissue, the DGG typically offers better clinical handling and is easier to suture. Nevertheless, DGGs are associated with an increased risk of epithelial inclusion, which can lead to late complications.[32-36] In addition, patient discomfort is known to correlate with the size of the DGG.[4,5,15] Thus, larger DGGs may increase the risk of an unpleasant patient experience. While some studies suggest that the high clinical quality of DGGs may result in slightly superior clinical outcomes, further research is needed to confirm this hypothesis.[28-31]

It is important to acknowledge the limitations of this article. Few randomized controlled clinical trials (RCTs) comparing clinical and patient-reported outcomes of the various SCTG harvesting methods are available for analysis. Moreover, no RCT has included all four of the harvesting techniques described in this paper. The available studies are subjected to several concerns, including a high risk of bias. Common sources of bias include ambiguity in subject randomization and the potential for assessors to be aware of the interventions received by the study participants. As a result, the present commentary relies heavily on uncontrolled clinical research, comparative histologic

analyses, case reports, and expert opinion from key figures in the field of periodontology.

5. Conclusion

It is striking that significant gaps in knowledge still exist regarding the SCTG – a well-established and reliable method for gingival/mucosal augmentation, and the recognized gold standard for root coverage. Periodontists have yet to fully understand the differences among SCTG types at the clinical, ultrastructural, and molecular levels. However, the available evidence suggests that the SIT is generally preferred, as it may optimize both clinical and patient-oriented outcomes in most situations. The attributes of alternative graft types, such as tSCTGs and DGGs, may offer significant advantages in specific clinical scenarios. Initial studies comparing gene expression and protein distribution among various graft types are consistent with observed differences in clinical performance. Recent advances in our understanding of human palatal anatomy have substantially expanded the safety zone for palatal SCTG harvesting, allowing a broader mesiodistal span to be addressed in a single procedure. tSCTGs, DGGs, and SCTGs obtained from deep palatal tissue are structurally distinct, exhibit unique clinical limitations, and have potential to produce different treatment outcomes. Future studies, particularly those utilizing modern laboratory techniques, will help elucidate the biological basis for these graft-related differences. In addition, further controlled clinical research is needed to validate indications for each graft type.

Acknowledgments

None.

Funding

The research was entirely funded by the Defense Health Agency (United States), with no extramural funding provided to the authors.

Conflict of interest

The authors declare that they have no competing interests.

Author contributions

Conceptualization: Thomas M. Johnson

Methodology: Han S. Kim, Denise M. Cacho, Alan R. George, Joseph R. Retrum, Carsen R. McDaniel

Writing – original draft: Han S. Kim, Denise M. Cacho, Alan R. George, Joseph R. Retrum, Carsen R. McDaniel, Thomas M. Johnson

Writing – review & editing: Brian W. Stancoven, Kimberly Ann Inouye, Adam R. Lincicum

Ethics approval and consent to participate

Not applicable.

Consent for publication

Not applicable.

Availability of data

Not applicable.

References

1. Chambrone L, Ortega MA, Sukekava F, *et al*. Root coverage procedures for treating single and multiple recession-type defects: An updated Cochrane systematic review. *J Periodontol*. 2019;90(12):1399-1422.

   doi: 10.1002/JPER.19-0079

2. Chambrone L, Tatakis DN. Periodontal soft tissue root coverage procedures: A systematic review from the AAP regeneration workshop. *J Periodontol*. 2015;86(Suppl):S8-S51.

   doi: 10.1902/jop.2015.130674.

3. Cairo F, Nieri M, Pagliaro U. Efficacy of periodontal plastic surgery procedures in the treatment of localized facial gingival recessions. A systematic review. *J Clin Periodontol*. 2014;41(Suppl 15):S44-S62.

   doi: 10.1111/jcpe.12182

4. Wessel JR, Tatakis, DN. Patient outcomes following subepithelial connective tissue graft and free gingival graft procedures. *J Periodontol*. 2008;79(3):425-430.

   doi: 10.1902/jop.2008.070325

5. Berridge JP, Johnson TM, Cheng AW, Swenson DT, Miller PD Jr. Focus on epithelialized palatal grafts. Part 3: Methods to enhance patient comfort at palatal donor sites. *Clin Adv Periodontics*. 2019;9(4):177-184.

   doi: 10.1002/cap.10066

6. Tavelli L, Barootchi S, Stefanini M, Zucchelli G, Giannobile WV, Wang HL. Wound healing dynamics, morbidity, and complications of palatal soft-tissue harvesting. *Periodontol 2000*. 2023;92(1):90-119.

   doi: 10.1111/prd.12466

7. Tavelli L, Barootchi S, Di Gianfilippo R, *et al*. Patient experience of autogenous soft tissue grafting has an implication for future treatment: A 10- to 15-year cross-sectional study. *J Periodontol*. 2021;92(5):637-647.

   doi: 10.1002/JPER.20-0350

8. Harris RJ. The connective tissue and partial thickness double pedicle graft: A predictable method of obtaining root coverage. *J Periodontol*. 1992;63(5):477-486.

   doi: 10.1902/jop.1992.63.5.477

9. Hürzeler MB, Weng D. A single-incision technique to harvest subepithelial connective tissue grafts from the palate. *Int J Periodontics Restorative Dent*. 1999;19(3):279-287.

10. Studer SP, Allen EP, Rees TC, Kouba A. The thickness of masticatory mucosa in the human hard palate and tuberosity as potential donor sites for ridge augmentation procedures. *J Periodontol*. 1997;68(2):145-151.

    doi: 10.1902/jop.1997.68.2.145

11. Monnet-Corti V, Santini A, Glise JM, *et al*. Connective tissue graft for gingival recession treatment: Assessment of the maximum graft dimensions at the palatal vault as a donor site. *J Periodontol*. 2006;77(5):899-902.

    doi: 10.1902/jop.2006.050047

12. Tavelli L, Barootchi S, Ravidà A, Oh TJ, Wang HL. What is the safety zone for palatal soft tissue graft harvesting based on the locations of the greater palatine artery and foramen? A systematic review. *J Oral Maxillofac Surg*. 2019;77(2):271e1-271e6.

    doi: 10.1016/j.joms.2018.10.002

13. Martin-Cabezas R, Deschamps-Lenhardt S, Huck O. Optimization of connective tissue graft length by graft splitting: A case series. *Clin Adv Periodontics*. 2021;11(3):165-170.

    doi: 10.1002/cap.10175

14. Glossary of Periodontal Terms. *American Academy of Periodontology*; 2017. Available from: https://members.perio.org/libraries/glossary?ssopc=1 [Last accessed on 2024 Nov 18].

15. Zucchelli G, Mele M, Stefanini M, *et al*. Patient morbidity and root coverage outcome after subepithelial connective tissue and de-epithelialized grafts: A comparative randomized-controlled clinical trial. *J Clin Periodontol*. 2010;37(8):728-738.

    doi: 10.1111/j.1600-051X.2010.01550.x

16. Lorenzana ER, Allen EP. The single-incision palatal harvest technique: A strategy for esthetics and patient comfort. *Int J Periodontics Restorative Dent*. 2000;20(3):297-305.

17. Edel A. Clinical evaluation of free connective tissue grafts used to increase the width of keratinised gingiva. *J Clin Periodontol*. 1974;1(4):185-196.

    doi: 10.1111/j.1600-051x.1974.tb01257.x

18. Langer B, Langer L. Subepithelial connective tissue graft technique for root coverage. *J Periodontol*. 1985;56(12):715-720.

    doi: 10.1902/jop.1985.56.12.715

19. Tavelli L, Barootchi S, Greenwell H, Wang HL. Is a soft tissue graft harvested from the maxillary tuberosity the approach of choice in an isolated site? *J Periodontol*. 2019;90(8):821-825.

    doi: 10.1002/JPER.18-0615

20. Bertl K, Pifl M, Hirtler L, *et al*. Relative composition of fibrous connective and fatty/glandular tissue in connective tissue grafts depends on the harvesting technique but not the donor site of the hard palate. *J Periodontol*. 2015;86(12):1331-1339.

    doi: 10.1902/jop.2015.150346

21. Zucchelli G, Tavelli L, McGuire MK, *et al*. Autogenous soft tissue grafting for periodontal and peri-implant plastic surgical reconstruction. *J Periodontol*. 2020;91(1):9-16.

    doi: 10.1002/JPER.19-0350

22. Wara-aswapati N, Pitiphat W, Chandrapho N, Rattanayatikul C, Karimbux N. Thickness of palatal masticatory mucosa associated with age. *J Periodontol*. 2001;72(10):1407-1412.

    doi: 10.1902/jop.2001.72.10.1407

23. Fickl S, Fischer KR, Jockel-Schneider Y, Stappert CF, Schlagenhauf U, Kebschull M. Early wound healing and patient morbidity after single-incision vs. trap-door graft harvesting from the palate--a clinical study. *Clin Oral Investig*. 2014;18(9):2213-2219.

    doi: 10.1007/s00784-014-1204-7

24. Grzech-Leśniak K, Matys J, Jurczyszyn K, *et al*. Histological and thermometric examination of soft tissue de-epithelialization using digitally controlled Er: YAG laser handpiece: An *ex vivo* study. *Photomed Laser Surg*. 2018;36(6):313-319.

    doi: 10.1089/pho.2017.4413

25. Marques de Mattos P, Papalexiou V, Tramontina VA, *et al*. Evaluation of 2 techniques of epithelial removal in subepithelial connective tissue graft surgery: A comparative histological study. *J Periodontal Implant Sci*. 2019;50(1):2-13.

    doi: 10.5051/jpis.2020.50.1.2

26. Cohen MS, Shorr N. Eyelid reconstruction with hard palate mucosa grafts. *Ophthalmic Plast Reconstr Surg*. 1992;8(3):183-195.

    doi: 10.1097/00002341-199209000-00005

27. Soehren SE, Allen AL, Cutright DE, Seibert JS. Clinical and histologic studies of donor tissues utilized for free grafts of masticatory mucosa. *J Periodontol*. 1973;44(12):727-741.

    doi: 10.1902/jop.1973.44.12.727

28. Tavelli L, Ravidà A, Lin GH, Del Amo FS, Tattan M, Wang HL. Comparison between subepithelial connective tissue graft and de-epithelialized gingival graft: A systematic review and a meta-analysis. *J Int Acad Periodontol*. 2019;21(2):82-96.

29. Bakhishov H, Isler SC, Bozyel B, Yıldırım B, Tekindal MA, Ozdemir B. De-epithelialized gingival graft versus subepithelial connective tissue graft in the treatment of multiple adjacent gingival recessions using the tunnel technique: 1-year results of a randomized clinical trial. *J Clin Periodontol*. 2021;48(7):970-983.

    doi: 10.1111/jcpe.13452

30. Zangrando MSR, Eustachio RR, De Rezende MLR, Sant'ana ACP, Damante CA, Greghi SLA. Clinical and patient-centered outcomes using two types of subepithelial connective tissue grafts: A split-mouth randomized clinical trial. *J Periodontol*. 2021;92(6):814-822.

doi: 10.1002/JPER.19-0646

31. Beymouri A, Yaghobee S, Khorsand A, Safi Y. Comparison of morbidity at the donor site and clinical efficacy at the recipient site between two different connective tissue graft harvesting techniques from the palate: A randomized clinical trial. *J Adv Periodontol Implant Dent*. 2023;15(2):108-116.

doi: 10.34172/japid.2023.016

32. Cardoso MV, Lara VS, Sant'Ana ACP, Damante CA, Zangrando MSR. Late complications after root coverage with two types of subepithelial connective tissue grafts, clinical and histopathological evaluation: A prospective cohort study. *J Clin Periodontol*. 2021;48(3):431-440.

doi: 10.1111/jcpe.13413

33. Breault LG, Billman MA, Lewis DM. Report of a gingival "surgical cyst" developing secondarily to a subepithelial connective tissue graft. *J Periodontol*. 1997;68(4):392-395.

doi: 10.1902/jop.1997.68.4.392

34. Parashis AO, Tatakis DN. Subepithelial connective tissue graft for root coverage: A case report of an unusual late complication of epithelial origin. *J Periodontol*. 2007;78(10):2051-2056.

doi: 10.1902/jop.2007.070099

35. Wang YS, Bissonnette C, Brett C, McNamara KK, Tatakis DN. Multiple epithelial origin complications following subepithelial connective tissue graft for root coverage. *Clin Adv Periodontics*. 2021;11(3):140-144.

doi: 10.1002/cap.10146

36. Harris RJ. Histologic evaluation of connective tissue grafts in humans. *Int J Periodontics Restorative Dent*. 2003;23(6):575-583.

37. Romano F, Perotto S, Cricenti L, Gotti S, Aimetti M. Epithelial inclusions following a bilaminar root coverage procedure with a subepithelial connective tissue graft: A histologic and clinical study. *Int J Periodontics Restorative Dent*. 2017;37(5):e245-e252.

doi: 10.11607/prd.3189

38. Jung UW, Um YJ, Choi SH. Histologic observation of soft tissue acquired from maxillary tuberosity area for root coverage. *J Periodontol*. 2008;79(5):934-940.

doi: 10.1902/jop.2008.070445

39. Dellavia C, Ricci G, Pettinari L, Allievi C, Grizzi F, Gagliano N. Human palatal and tuberosity mucosa as donor sites for ridge augmentation. *Int J Periodontics Restorative Dent*. 2014;34(2):179-186.

doi: 10.11607/prd.1929

40. Sanz-Martín I, Rojo E, Maldonado E, Stroppa G, Nart J, Sanz M. Structural and histological differences between connective tissue grafts harvested from the lateral palatal mucosa or from the tuberosity area. *Clin Oral Investig*. 2019;23(2):957-964.

doi: 10.1007/s00784-018-2516-9

41. Pornprasertsuk S, Duarte WR, Mochida Y, Yamauchi M. Overexpression of lysyl hydroxylase-2b leads to defective collagen fibrillogenesis and matrix mineralization. *J Bone Miner Res*. 2005;20(1):81-87.

doi: 10.1359/JBMR.041026

42. Amin PN, Bissada NF, Ricchetti PA, Silva APB, Demko CA. Tuberosity versus palatal donor sites for soft tissue grafting: A split-mouth clinical study. *Quintessence Int*. 2018;49(7):589-598.

doi: 10.3290/j.qi.a40510

43. Barootchi S, Tavelli L, Zucchelli G, Giannobile WV, Wang HL. Gingival phenotype modification therapies on natural teeth: A network meta-analysis. *J Periodontol*. 2020;91(11):1386-1399.

doi: 10.1002/JPER.19-0715

44. Harris RJ, Miller R, Miller LH, Harris C. Complications with surgical procedures utilizing connective tissue grafts: A follow-up of 500 consecutively treated cases. *Int J Periodontics Restorative Dent*. 2005;25(5):449-459.

45. Buff LR, Bürklin T, Eickholz P, Mönting JS, Ratka-Krüger P. Does harvesting connective tissue grafts from the palate cause persistent sensory dysfunction? A pilot study. *Quintessence Int*. 2009;40(6):479-89.

46. Malpartida-Carrillo V, Tinedo-Lopez PL, Guerrero ME, Huamani-Echaccaya JL, Özcan M, Rösing CK. Outcome measurements following palatal soft tissue graft harvesting: A review. *J Clin Exp Dent*. 2021;13(5):e527-e535.

doi: 10.4317/jced.57625

47. Basma HS, Saleh MHA, Abou-Arraj RV, *et al*. Patient-reported outcomes of palatal donor site healing using four different wound dressing modalities following free epithelialized mucosal grafts: A four-arm randomized controlled clinical trial. *J Periodontol*. 2023;94(1):88-97.

doi: 10.1002/JPER.22-0172

48. Zuhr O, Bäumer D, Hürzeler M. The addition of soft tissue replacement grafts in plastic periodontal and implant surgery: Critical elements in design and execution. *J Clin Periodontol*. 2014;41(Suppl 15):S123-S142.

doi: 10.1111/jcpe.12185

ACCSCIENCE PUBLISHING

Global Translational Medicine

PERSPECTIVE ARTICLE

State-of-the-art perspective: Advances in incretin-based therapy targeting progression of diabetes and cardiovascular-kidney-metabolic syndrome

Samar A. Nasser[1], Anuhya V. Pulapaka[2], Shaveta Gupta[2], and Keith C. Ferdinand[2]*

[1]Department of Clinical Research and Leadership, School of Medicine and Health Sciences, The George Washington University, Washington, D.C., United States of America

[2]Department of Medicine, Tulane University School of Medicine, New Orleans, Louisiana, United States of America

(This article belongs to the *Special Issue: Convergence of Cardiorenal Metabolic Disease: From Epigenetics to End Stage*)

Abstract

The incretin system is targeted in the treatment of type 2 diabetes mellitus (T2DM) and cardiovascular-kidney-metabolic (CKM) conditions. Increasingly, incretin hormones (i.e., gut peptides that enhance glucose-stimulated insulin secretion) reduce blood glucose levels, consequently alleviating CKM syndrome. Specifically, glucagon-like peptide 1 (GLP-1) demonstrated glucose-lowering effects, delayed gastric emptying, decreased glucagon secretion, and weight loss. An investigational medication, retatrutide, interacts as a tri-agonist with glucose-dependent insulinotropic polypeptide (GIP), GLP-1, and the glucagon receptor. Contemporary data indicate that early intervention, targeting not only the GLP-1 receptor but also the GIP and glucagon receptors, are forthcoming therapeutics affecting T2DM in earlier phases and CKM outcomes, demonstrating the advances in tri-agonists versus only GLP-1. Notably, endogenous levels of gut incretin hormones shift as pre-diabetes progresses to diabetes or regresses to normoglycemia. The present perspective provides a review of incretin therapy and its prospects in hindering the progression of T2DM and CKM syndrome.

Keywords: Pre-diabetes; Type 2 diabetes; Cardiovascular-kidney-metabolic syndrome; Incretin mimetics; Obesity

***Corresponding author:**
Keith C. Ferdinand
(kferdina@tulane.edu)

Citation: Nasser SA, Pulapaka AV, Gupta S, Ferdinand KC. State-of-the-art perspective: Advances in incretin-based therapy targeting progression of diabetes and cardiovascular-kidney-metabolic syndrome. *Global Transl Med*. 2025:4(1):47-55. doi: 10.36922/gtm.4405

Received: August 1, 2024

1st revised: September 4, 2024

2nd revised: September 18, 2024

Accepted: October 8, 2024

Published online: December 31, 2024

1. Introduction

Incretin-based therapies have revolutionized the treatment of type 2 diabetes mellitus (T2DM) and cardiovascular-kidney-metabolic (CKM) conditions. These therapies target the incretin system, which involves gut peptides that enhance glucose-stimulated insulin secretion, thereby reducing blood glucose levels and alleviating CKM syndrome.[20,21] Glucagon-like peptide-1 (GLP-1) has emerged as a key player in this therapeutic approach. GLP-1 receptor agonists demonstrate multiple beneficial

effects, including glucose-lowering effects, delayed gastric emptying, decreased glucagon secretion, and weight loss.[26-29] These culminating effects make GLP-1 receptor agonists powerful tools for controlling blood glucose and improving CKM syndrome.

Notably, endogenous levels of gut incretin hormones shift as prediabetes progresses to diabetes or regresses to normoglycemia.[23] This dynamic nature of incretin hormone levels underscores the potential benefits of early intervention with incretin-based therapies. Recently, multi-agonist approaches have been developed, particularly the combination of GLP-1, glucose-dependent insulinotropic polypeptide (GIP), and glucagon receptor activation.[34] This tri-agonist approach, exemplified by investigational medications like retatrutide, aims to provide enhanced therapeutic benefits compared to GLP-1 receptor agonists alone. Early clinical data suggest that these tri-agonists may offer superior efficacy in weight reduction and glycemic control compared to selective GLP-1 receptor agonists.[35] Contemporary research indicates that early intervention with incretin-based therapies may be crucial in hindering the progression of T2DM and CKM syndrome. Targeting not only the GLP-1 receptor but also the GIP and glucagon receptors in earlier phases of the disease could potentially lead to better outcomes.

As the development of incretin-based therapies continue to evolve, additional research has been focused upon optimizing the balance between GLP-1, GIP, and glucagon receptor activation, developing long-acting formulations for improved patient compliance, and investigating potential applications beyond T2DM, such as in neurodegenerative optic disease and metabolic dysfunction-associated steatohepatitis.[21,41] Thus, incretin-based therapies offer a promising approach to targeting the progression of diabetes and CKM syndrome, with potential benefits extending beyond glycemic control to address the broader spectrum of metabolic disorders.

2. Impact of pre-diabetes and diabetes in the United States

In 2021, diabetes was the eighth leading cause of mortality in the United States (U.S.), with 103,294 death certificates documenting diabetes as the underlying cause of death (crude rate: 31.1/100,000 people).[1] Among the U.S. population in 2021, the crude estimate for diabetes was 38.4 million people across all ages (11.6% of the U.S. population).[1] Furthermore, in 2022, the total direct and indirect estimated costs of diagnosed diabetes in the U.S. was $413 billion.[2] Besides diabetes being a leading cause of mortality globally, it is also a leading cause of disability worldwide, accounting for 26.8%.[3] Based upon the National Diabetes Statistics Report from the Centers for Disease Control and Prevention, an estimated 97.6 million adults aged 18 years or older had pre-diabetes (38.0% of the adult U.S. population) in 2021. Moreover, 27.2 million people aged 65 years or older (48.8%) had pre-diabetes.[1] These data demonstrate the significant public health impact of the potential progression of those with pre-diabetes to overt diabetes.

A new American Heart Association (AHA) presidential advisory identified the strong connections between cardiovascular disease (CVD), kidney disease, type 2 diabetes mellitus (T2DM), and obesity, defining cardiovascular-kidney-metabolic (CKM) syndrome.[4] As the pre-cursor to diabetes, pre-diabetes is the earlier phase of the toxic CKM cascade of diabetes. Pre-diabetes is clinically diagnosed with glycated hemoglobin (hemoglobin A1C) or dysglycemia levels.[5] According to the American Diabetes Association, pre-diabetes can be defined by the following:[5]

(i) Hemoglobin A1C: 5.7 – 6.4%
(ii) Fasting blood glucose: 100 – 125 mg/dL
(iii) Oral glucose tolerance test 2-h blood glucose: 140 – 199 mg/dL

The pathophysiology of pre-diabetes involves dysglycemia with increased insulin production and overstimulation of pancreatic β-cells, with diminished insulin receptor response over time. Consequently, if pre-diabetes is unabated, insulin resistance, insulin hypersecretion, and progression of pancreatic β-cell function decline will occur, resulting in T2DM. Ultimately, if left untreated, inflammatory responses stimulate both micro- (i.e., retina, kidney, and nerves) and macrovascular complications (i.e., cardiovascular [CV] system). The AHA recently developed an inclusive equation, Predicting Risk of Cardiovascular Disease Events (PREVENT), with clinical variables of obesity, diabetes, kidney disease, and social risk, thereby supporting a multicomponent concept for effectively and equitably enhancing CKM population health.[6] The PREVENT equation facilitates both 10- and 30-year risk estimates among adults at 30 – 79 years of age for total CVD and includes the estimated glomerular filtration rate as a predictor while adjusting for competing risk of non-CVD death. Ndumele *et al.*[4] provided a synopsis of new strategies and research aimed at improving CKM syndrome, focusing on CKM variables and their relation to where, when, and how to implement and disseminate the vast array of cardioprotective therapies for CKM. Recently, meta-analyses demonstrated that pre-diabetes is associated with the risk of mortality, diabetes-related complications, and CV comorbidities,[7] representing a continuum of risk for diabetes and eventual CKM.[5,8]

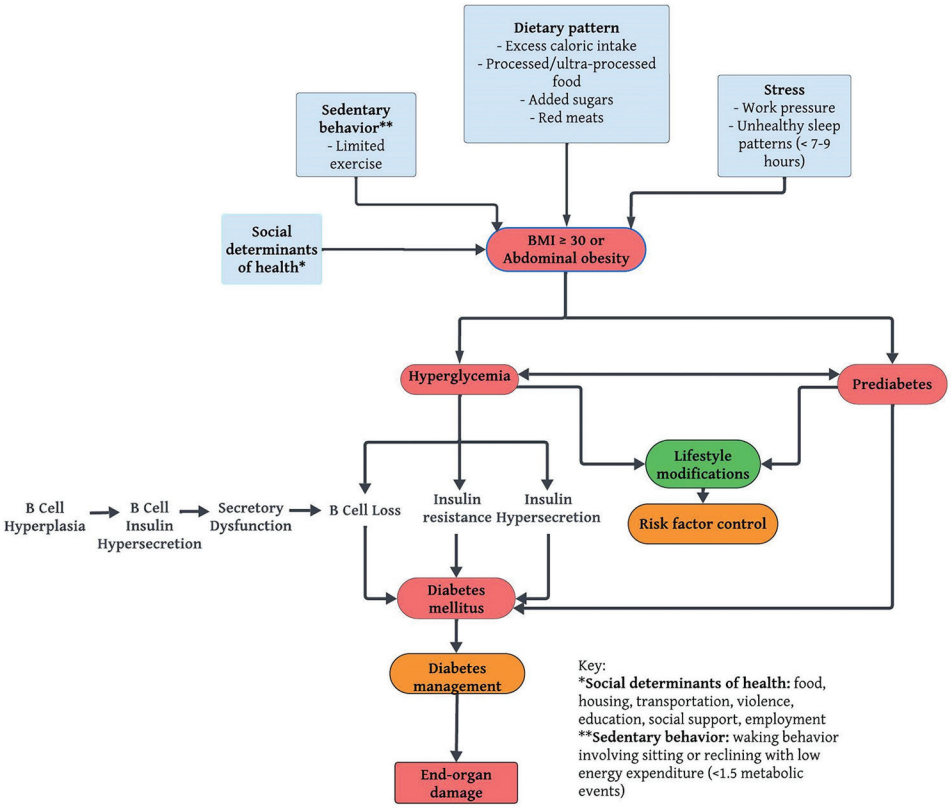

Figure 1. Progression of risk factors to diabetes mellitus and corresponding outcomes. Adapted from[10,16,17,18]

3. Addressing pre-diabetes, diabetes, and associated obesity

Of those who experience intermediate hyperglycemia or pre-diabetes, almost all of them will progress to T2DM.[9] Notably, there has been a striking increase in diabetes, rising from only 1% five decades ago to nearly 10% today.[10] Insulin resistance and genetic abnormalities are not independently responsible for this dramatic increase in diabetes. Conversely, obesity has been characteristically centered at the core of the crisis, with overweight and obesity noted as the most common risk factors associated with the development of T2DM.[10,11] As a major risk factor leading to the development of T2DM, obesity can lead to β-cell loss and dysfunction.[8] Biondi and colleagues[8] outlined the natural history of β-cell failure in obesity-induced T2DM, separating into successive steps beginning with β-cell compensatory hyperplasia and insulin hypersecretion, to insulin secretory dysfunction, and finally, loss of β-cell mass (Figure 1). Aligned with the chronic obesity-induced pathophysiologic changes leading to diabetes, at least a 5% weight reduction may result in a reversal of metabolic abnormalities and with additional weight loss, the potential to discontinue diabetic medications.[12]

Table 1. Mechanisms of incretin-based therapy in dysglycemia

Agent	Mechanism
GLP-1 receptor agonist	Binds to GLP-1 receptors on pancreatic B-cells, stimulating insulin, inhibiting glucagon release, slowing gastric emptying, and promoting satiety to improve blood glucose control
Dual GIP/GLP-1 receptor agonist	Binds to GLP-1 receptors (see above) and GIP receptors on pancreatic B-cells, enhancing insulin secretion, inhibiting glucagon release, and improving insulin sensitivity to regulate blood glucose levels
GIP-1/GLP-1/ glucagon receptor triagonist (retatrutide*)	GIP-1/GLP-1 agonist mechanism is similar to the above; glucagon receptor activation stimulates lipolysis, increases energy expenditure, prevents hypoglycemia, and balances glucose control effects when combined with GLP-1 and GIP agonists

Note: *Retatrutide is currently under investigation. Adapted from Jakubowska *et al.*[20]
Abbreviations: GLP: Glucagon-like peptide; GIP: Glucose-dependent insulinotropic polypeptide.

The cornerstone of pre-diabetes management is through lifestyle modification, with a focus on significant weight loss. A weight loss reduction of 5 – 7% has been demonstrated to be effective, typically achieved through a low-fat diet combined with an exercise regimen of about

30 min/day.[13] Therefore, proper management of pre-diabetes with specific lifestyle modifications is effective in preventing diabetes, thereby reducing the risk of CVD. Accordingly, the U.S. National Diabetes Prevention Program (DPP) integrates moderate weight loss (5 – 7%) through a healthy diet and physical activity over the course of a year for those with increased risk of diabetes or diagnosed with pre-diabetes.[13] The DPP is an evidence-based program that demonstrated a significant reduction in risk of developing T2DM by 58% (71% for people over 60 years old) after losing 5 – 7% of their body weight with healthier eating and 150 min of physical activity per week.[14] Moreover, surgical interventions (i.e., bariatric surgery) demonstrated beneficial outcomes, including improved glycemic control and weight reduction, in the treatment of pre-diabetes and T2DM.[15]

Although difficult to instill and maintain, lifestyle interventions, including diet and exercise, are considered first-line cornerstone treatments. As exemplified by the long-term follow-up of the original DPP study, the DPP outcomes study evaluates the effects of the interventions on diabetes complications, (i.e., retinopathy, microangiopathy, CVD). Accordingly, although the lifestyle group participants started off with the most weight loss (mean of 7 kg after 1 year), they gradually regained most of the weight.[5] Therefore, the need for medical therapy, in addition to lifestyle interventions, should be instilled and maintained as part of a toolbox of interventions. Pre-diabetes can be managed with two medications, metformin and acarbose; however, these are contraindicated among patients with renal disease.[15] A compounding challenge of pre-diabetes is its predominantly asymptomatic nature, which acts as a "silent incubator" for impending morbidity. As pre-diabetes develops into T2DM, medications also contribute significantly to controlling the toxic effects of hyperglycemia. Despite these evidence-based treatment options, tackling pre-diabetes is not fully targeted as a method to prevent the negative impacts of T2DM. Examining the mechanism of action and potential early targets of the newer incretin mimetics may expose the underutilization of these mechanisms to slow or potentially halt the progression of overt diabetes (Table 1). Given the abundant data conferring pre-diabetes as an increased risk for progression to T2DM and CKM syndrome, treatment should focus on preventing the progression to T2DM.[19]

Encouragingly, Glucagon-like peptide-1 (GLP-1) receptor agonists demonstrate a reduction in liver fat and consequently improve liver enzyme levels, thereby paving a treatment avenue for metabolic dysfunction-associated steatotic liver disease or the more advanced form, metabolic dysfunction-associated steatohepatitis (MASH), for which there is no Food and Drug Administration-approved treatment at this time.[21] Ongoing phase 3 trials aim to provide data that may support the development of effective pharmacotherapies for patients with MASH.[21] Accordingly, efocipegtrutide (HM15211), long-acting glucagon, Glucose-dependent insulinotropic polypeptide (GIP), and GLP-1 triple full agonist, is currently in the pipeline and undergoing a phase 2 randomized, multicenter 52-week study among patients with biopsy-confirmed non-alcoholic steatohepatitis.[22]

4. Targeting incretin response

Among healthy individuals, oral glucose stimulates greater insulin secretory responses than intravenous glucose, despite equivalent glucose levels. Food breakdown in the gut promotes the release of incretins (i.e., GIP and GLP-1), which enhance insulin release. Notably, this physiologic response (also known as the "incretin effect") in T2DM is markedly decreased or absent. The malfunction may be linked to the dysfunction of β-cells or a specific defect within the GIP signaling pathway.[23] Thus, a depressed incretin effect of GIP leads to an increase in post-prandial glucose levels, potentially worsening glycemic control. In contrast, GLP-1 is much less impaired than GIP in the setting of T2DM. The CKM outcomes of GLP-1 secondary to its glucose-lowering effects include a reduction in A1C (~0.8 – 1.6%), body weight (~1 – 3 kg), blood pressure, and lipids.[24,25]

In 2024, the landmark "Evaluate Renal Function with Semaglutide Once Weekly" trial reported findings of the first kidney outcomes trial evaluating the GLP-1 receptor agonist semaglutide.[26] Compared to those who received a placebo, participants with T2DM and chronic kidney disease who received semaglutide demonstrated a 24% risk reduction of the composite primary endpoint, including kidney outcomes and mortality secondary to CV and kidney causes.[26] Secondary endpoints include significant enhancements with semaglutide, slower estimated glomerular filtration rate slope, a decrease in major CV events (18%), and a reduced risk of all-cause death (20%). Notably, the reduction in kidney outcomes with semaglutide was consistent in participants with/without baseline sodium-glucose cotransporter-2 inhibitor (SGLT2i) use. A recent meta-analysis and systematic review of randomized controlled trials (RCTs) validated the long-term efficacy and safety of semaglutide compared to placebo in overweight/obese adults without diabetes. The once-weekly semaglutide dose was associated with decreased body weight and demonstrated beneficial effects on CV risk factors (i.e., body mass index, waist circumference, blood pressure), with limited mild-to-moderate gastrointestinal (GI) side effects.[27]

Since exogenous GLP-1 stimulates insulin, suppresses glucagon, and decreases plasma glucose concentrations

in both fasting and post-prandial states, the development of selective GLP-1 receptor agonists and co-agonists (i.e., stimulation of GIP and GLP-1 receptors) are the imminent therapeutic focus for early intervention of diabetes. Furthermore, in June 2024, a 1.8 mg liraglutide injection became the first generic GLP-1 approved in the U.S. for the treatment of T2DM.[28]

An example of the synergistic effects of GIP and GLP-1 includes the medication tirzepatide, which is an innovative treatment for T2DM classified as a dual agonist. Tirzepatide increases post-prandial insulin secretion, while concurrently inhibiting glucagon secretion. Moreover, tirzepatide enhances satiety through central (hypothalamus) and peripheral (slowing of gastric emptying) action, resulting in substantially improved glycemic control and weight reduction in T2DM.[29] Notably, tirzepatide has demonstrated a greater degree of engagement for the GIP receptor than the GLP-1 receptor, corroborating an imbalanced mechanism of action.[30] This supports its classification as an imbalanced dual GIP and GLP-1 receptor agonist. *Post hoc* analysis from the "Study of Tirzepatide in Participants with Type 2 Diabetes Not Controlled with Diet and Exercise Alone" (SURPASS) program indicated beneficial effects of tirzepatide with improvement in A1c, body weight, and cardiometabolic markers. These benefits were observed in participants with early-onset T2DM (<40 years of age), who, despite their younger age, demonstrated higher glycemic levels and lower metabolic health at baseline.[31] Recently, Malhotra *et al.*[32] completed a 52-week phase 3, double-blind RCT to evaluate the efficacy and safety of tirzepatide for the treatment of moderate to severe obstructive sleep apnea (OSA) in obese people. Of the 469 participants that were randomized 1:1 to receive tirzepatide or placebo, tirzepatide reduced moderate-to-severe OSA severity by up to 62.8%, which translates to 30 fewer events restricting or blocking a person's airflow per hour of sleep. In addition to reducing the hypoxic burden, tirzepatide also reduced body weight, high-sensitivity C-reactive protein concentration, and systolic blood pressure and enhanced sleep-related patient-reported outcomes.[32] Currently, tirzepatide is being investigated with dulaglutide to evaluate the CV protective outcomes in the "Effect of Tirzepatide Versus Dulaglutide on Major Adverse Cardiovascular Events" (SURPASS-CVOT) study in patients with T2DM (ClinicalTrials.gov: NCT04255433).[33]

In addition, a novel incretin mimetic under investigation is retatrutide, a GLP-1/GIP/glucagon receptor tri-agonist. Jastreboff *et al.*[34] completed a phase 2 RCT in 338 obese adults with retatrutide versus placebo over 48 weeks. At the maximum dosage of retatrutide (12 mg) and after 48 weeks, the average weight loss was 24.2% with a weight reduction of up to 30% from the baseline weight among 25% of participants. Notably, the weight reductions were accompanied by several encouraging CKM outcomes, including improved glycemic control among both fasting glucose and Hemoglobin A1C (HbA1c), decreased waist circumference, lower systolic and diastolic blood pressures, and lower lipid levels. The side effects and safety profile were similar to GIP/GLP-1 receptor co-agonists, with mild-to-moderate GI effects, which mostly occurred during dose escalations.[34] Importantly, the documented weight loss is the most significant through a pharmacological agent, and the mechanism of action is secondary to the GIP/GLP-1 receptor co-agonism complemented by the glucagon receptor activation and augmentation of energy intake.[35]

5. Potential side effects of incretin agonists in overweight and obesity

Although incretin agonists provide multiple beneficial impacts on CKM, including significant weight reduction of ~15 – 24% in adults with overweight and obesity, there is a concern for potential sarcopenia. Several trials have reported that about 25 – 40% of the weight loss was composed of fat-free mass (FFM)/lean body mass; however, obese people have greater amounts of FFM and skeletal muscle mass (SMM) than the lean population. The SMM is higher in obese people than in lean individuals, but the percentage of the SMM (compared to total body mass) is lower.

Intentional weight loss leads to a greater decrease in body fat than FFM or SMM, thus improving the ratio of FFM/SMM to fat mass and the quality of the remaining muscle.[31,36] Recent reports have demonstrated that appropriate counseling to mitigate this potential side effect includes maintaining a balanced diet rich in protein, ensuring adequate hydration, and engaging in regular physical activity with resistance training.[37,38] While achieving fat loss, Locatelli *et al.*[38] further proposed that resistance training should be integrated as an adjunct to incretin therapy to optimize changes in body composition, leading to the preservation of lean body mass. Although there is concern that significant weight loss induced by incretin mimetics can cause physical frailty or sarcopenia, there is currently no data to support this claim.[39]

In regards to the adverse effects of GLP-1 receptor agonists, GI effects are the most prevalent; however, these effects are dependent on agent potency and dose. The side effects include various upper GI (i.e., nausea, vomiting) and lower GI (i.e., diarrhea, constipation) symptoms. However, slower dose titration reduced these effects, and thus, the overall safety profile remains strong.[40] According

to an observational retrospective matched cohort study, semaglutide was associated with an increased risk of non-arteritic anterior ischemic optic neuropathy,[41] and future studies to assess causality were proposed. Well-designed trials powered for microvascular outcomes are warranted to clarify associations between incretin therapies and microvascular diseases.

Previous meta-analyses of RCTs suggested an association between the use of GLP-1 receptor agonists and retinopathy in patients with T2DM. However, conflicting results from additional studies challenge these findings.[42] According to a recent systematic review and meta-analysis of RCTs comparing the effect of SGLT-2i, GLP-1 receptor agonists, and dipeptidyl peptidase-4 inhibitors (DPP-4i) on the risk of diabetic retinopathy in patients with T2DM, Malyszczak and colleagues[42] highlighted the challenges in concluding that these newer antidiabetic drugs differ substantially in their effect on diabetic retinopathy complications. Currently, the data advises caution with the use of DPP-4 inhibitors and semaglutide, especially among patients with underlying retinopathy.

Given the innovative therapeutics being developed and studied for T2DM and obesity, the data support the implementation of these medications in clinical studies to potentially treat pre-diabetes and obesity early on as a preventative measure to halt the progression to overt T2DM. With the increasing prevalence of these co-morbidities and the frequent association of obesity with CKM syndrome, the effective weight loss and HbA1c reduction achieved with incretin mimetics may also benefit patients with pre-diabetes, offering cardioprotective and hepatic steatosis-reducing properties. Although the early results are encouraging, the mechanisms of action of incretin hormones on various organs and systems remain inconclusive.

Overall, incretin mimetics offer many positive effects to negate the progression of diabetes. Besides the glucose-lowering properties of incretin mimetic, both the reduction of appetite and food intake result in weight loss, thereby proposing a feasible mechanism of action for diabetes prevention. Although incretins' efficacy for weight loss and improvement in quality-of-life has been documented, there is a gap in evidence among patients with and without diabetes demonstrating a reduction in the risk of CVD in the intervention phase or during chronic follow-up care.[20,43,44]

6. Conclusion

Although both therapeutic and lifestyle interventions have demonstrated the benefit of reducing the incidence of T2DM, there remains a gap in understanding the impact of incretin mimetics in reducing CKM risk in pre-diabetic patients post-intervention. In addition, although lifestyle modification should be the cornerstone of therapy, innovative incretin therapeutics may have a significant impact, given the concurrent weight loss outcomes as well.

Incretin mimetics simulate the incretin hormone function to return blood glucose levels to the euglycemic range. More recently, a study demonstrated how endogenous levels of gut incretin hormones change as pre-diabetes advances to diabetes or regresses to normoglycemia.[45] Based on contemporary data, evidence indicates that early intervention, targeting not only the GLP-1 receptor but also the GIP and glucagon receptors, is imminent. Now is the time to implement and disseminate these therapeutics to tackle T2DM in its earlier phases, ensuring physiologic β-cell function and promoting weight reduction. Furthermore, these are therapeutic targets that could potentially be implemented in patients diagnosed with pre-diabetes to hinder the progression to T2DM. Most recently, the emerging benefits of GLP-1 receptor agonists, beyond glucose control, have reportedly impacted not only CKM conditions but OSA as well.[46] Shifting from sedentary habits and overnutrition to increased physical activity and reduced nutrient intake leads to weight loss, subsequent euglycemia, and improvements in CKM outcomes. Future research directions should focus on how incretin mimetics affect individualized responses to treatment of obesity and CKM syndrome by evaluating their interactions with endocrine cells, the nervous system, genetic makeup, and the composition and intake of nutrients.

Acknowledgments

None.

Funding

None.

Conflict of interest

The authors declare no conflicts of interest.

Author contributions

Conceptualization: Samar A. Nasser and Keith C. Ferdinand
Writing – original draft: Samar A. Nasser
Writing – review & editing: All authors

Ethics approval and consent to participate

Not applicable.

Consent for publication

Not applicable.

Availability of data

Not applicable.

References

1. Centers for Disease Control. *National Diabetes Statistics Report*; 2024. Available from: https://www.cdc.gov/diabetes/php/data-research/index.html#:~:text=prevalence%20of%20prediabetes%20among%20adults,in%202021%20(table%204) [Last accessed on 2024 Jun 07].
2. Parker ED, Lin J, Mahoney T, *et al*. Economic costs of diabetes in the U.S. in 2022. *Diabetes Care*. 2024;47(1):26-43.
   doi: 10.2337/dci23-0085
3. Lu Y, Wang W, Liu J, Xie M, Liu Q, Li S. Vascular complications of diabetes: A narrative review. *Medicine (Baltimore)*. 2023;102(40):e35285.
   doi: 10.1097/MD.0000000000035285
4. Ndumele CE, Rangaswami J, Chow SL, *et al*. American Heart Association. Cardiovascular-kidney-metabolic health: A presidential advisory from the American heart association. *Circulation*. 2023;148:1606-1635.
   doi: 10.1161/CIR.0000000000001184
5. American Diabetes Association Professional Practice Committee. 2. Diagnosis and classification of diabetes: Standards of care in diabetes-2024. *Diabetes Care*. 2024;47(Suppl 1):S20-42.
   doi: 10.2337/dc24-S002
6. Khan SS, Matsushita K, Sang Y, *et al*. Chronic kidney disease prognosis consortium and the American heart association cardiovascular-kidney-metabolic science advisory group. development and validation of the American Heart Association's PREVENT equations. *Circulation*. 2024;149(6):430-449.
   doi: 10.1161/CIRCULATIONAHA.123.067626
7. Schlesinger S, Neuenschwander M, Barbaresko J, *et al*. Prediabetes and risk of mortality, diabetes-related complications and comorbidities: Umbrella review of meta-analyses of prospective studies. *Diabetologia*. 2022;65:275-285.
   doi: 10.1007/s00125-021-05592-3
8. Biondi G, Marrano N, Borrelli A, *et al*. Adipose tissue secretion pattern influences β-Cell wellness in the transition from obesity to type 2 diabetes. *Int J Mol Sci*. 2022;23(10):5522.
   doi: 10.3390/ijms23105522
9. Al-Omar HA, Czech M, Quang Nam T, *et al*. Cost saving analysis of prediabetes intervention modalities in comparison with inaction using Markov state transition model-A multiregional case study. *J Diabetes*. 2024;16(5):e13553.
   doi: 10.1111/1753-0407.13553
10. Chockalingam A, Natarajan P, Dorairajan S, Khan U. Early recognition of overweight hyperglycaemia may improve clinical outcomes in type 2 diabetes. *touchREV Endocrinol*. 2023;19(1):33-37.
    doi: 10.17925/EE.2023.19.1.33
11. Lizarzaburu-Robles JC, Herman WH, Garro-Mendiola A, Galdón Sanz-Pastor A, Lorenzo O. Prediabetes and cardiometabolic risk: The need for improved diagnostic strategies and treatment to prevent diabetes and cardiovascular disease. *Biomedicines*. 2024;12(2):363.
    doi: 10.3390/biomedicines12020363
12. Ko JH, Kim TN. Type 2 diabetes remission with significant weight loss: Definition and evidence-based interventions. *J Obes Metab Syndr*. 2022;31(2):123-133.
    doi: 10.7570/jomes22001
13. Tuomilehto J, Uusitupa M, Gregg EW, Lindström J. Type 2 diabetes prevention programs-from proof-of-concept trials to national intervention and beyond. *J Clin Med*. 2023;12:1876.
    doi: 10.3390/jcm12051876
14. National Diabetes Prevention Program Website. Available from: https://coveragetoolkit.org/about-national-dpp/ndpp-overview [Last accessed on 2024 Jun 20].
15. Braga T, Kraemer-Aguiar LG, Docherty NG, Le Roux CW. Treating prediabetes: Why and how should we do it? *Minerva Med*. 2019;110(1):52-61.
    doi: 10.23736/S0026-4806.18.05897-4
16. Morris AA, Masoudi FA, Abdullah AR, *et al*. 2024 ACC/AHA key data elements and definitions for social determinants of health in cardiology: A report of the American college of cardiology/American heart association joint committee on clinical data standards. *Circ Cardiovasc Qual Outcomes*. 2024;17(10):e000133.
    doi: 10.1161/HCQ.0000000000000133
17. American Heart Association. *How to Get Healthy Sleep Fact Sheet*. Available from: https://www.heart.org/en/-/media/healthy-living-files/le8-fact-sheets/le8_how_to_get_healthy_sleep.pdf?sc_lang=en [Last accessed on 2024 Dec 12].
18. Nguyen S, Bellettiere J, Anuskiewicz B, *et al*. Prospective associations of accelerometer-measured machine-learned sedentary behavior with death among older women: The OPACH study. *J Am Heart Assoc*. 2024;13(5):e031156.
    doi: 10.1161/JAHA.123.031156
19. Samson SL, Vellanki P, Blonde L, *et al*. American association of clinical endocrinology consensus statement: Comprehensive type 2 diabetes management algorithm-2023 update. *Endocr Pract*. 2023;29(5):305-340.

20. Jakubowska A, Roux CW, Viljoen A. The road towards triple agonists: Glucagon-like peptide 1, glucose-dependent insulinotropic polypeptide and glucagon receptor-an update. *Endocrinol Metab* (*Seoul*). 2024;39(1):12-22.

doi: 10.3803/EnM.2024.1942

21. Loomba R, Hartman ML, Lawitz EJ, *et al*. Tirzepatide for metabolic dysfunction-associated steatohepatitis with liver fibrosis. *N Engl J Med*. 2024;391:299-310.

doi: 10.1056/NEJMoa2401943

22. Abdelmalek MF, Suzuki A, Sanchez W, *et al*. A phase 2, adaptive randomized, double-blind, placebo-controlled, multicenter, 52-week study of HM15211 in patients with biopsy-confirmed non-alcoholic steatohepatitis-study design and rationale of HM-TRIA-201 study. *Contemp Clin Trials*. 2023;130:107176.

doi: 10.1016/j.cct.2023.107176

23. Nauck MA, Müller TD. Incretin hormones and type 2 diabetes. *Diabetologia*. 2023;66(10):1780-1795.

doi: 10.1007/s00125-023-05956-x

24. Nauck MA, Quast DR, Wefers J, Meier JJ. GLP-1 receptor agonists in the treatment of type 2 diabetes-state-of-the-art. *Mol Metab*. 2021;46:101102.

doi: 10.1016/j.molmet.2020.101102

25. Tschöp M, Nogueiras R, Ahrén B. Gut hormone-based pharmacology: Novel formulations and future possibilities for metabolic disease therapy. *Diabetologia*. 2023;66(10):1796-1808.

doi: 10.1007/s00125-023-05929-0

26. Mann JFE, Rossing P, Bakris G, *et al*. Effects of semaglutide with and without concomitant SGLT2 inhibitor use in participants with type 2 diabetes and chronic kidney disease in the flow trial. *Nat Med*. 2024;30:2849-2856.

doi: 10.1038/s41591-024-03133-0

27. Moiz A, Levett JY, Filion KB, Peri K, Reynier P, Eisenberg MJ. Long-term efficacy and safety of once-weekly semaglutide for weight loss in patients without diabetes: A systematic review and meta-analysis of randomized controlled trials. *Am J Cardiol*. 2024;222:121-130.

doi: 10.1016/j.amjcard.2024.04.041

28. Teva Launches Generic Formulation of Liraglutide in US. Available from: https://www.pharmacytimes.com/view/teva-launches-generic-formulation-of-liraglutide-in-us [Last accessed on 2024 Jun 28].

29. Scheen AJ. Dual GIP/GLP-1 receptor agonists: New advances for treating type-2 diabetes. *Ann Endocrinol* (*Paris*). 2023;84(2):316-321.

doi: 10.1016/j.ando.2022.12.423

30. Willard FS, Douros JD, Gabe MB, *et al*. Tirzepatide is an imbalanced and biased dual GIP and GLP-1 receptor agonist. *JCI Insight*. 2020;5(17):e140532.

doi: 10.1172/jci.insight.140532

31. Zeitler P, Galindo RJ, Davies MJ, *et al*. Early-onset type 2 diabetes and tirzepatide treatment: A post hoc analysis from the SURPASS clinical trial program. *Diabetes Care*. 2024;47(6):1056-1064.

doi: 10.2337/dc23-2356

32. Malhotra A, Bednarik J, Chakladar S, *et al*. Tirzepatide for the treatment of obstructive sleep apnea: Rationale, design, and sample baseline characteristics of the SURMOUNT-OSA phase 3 trial. *Contemp Clin Trials*. 2024;141:107516.

doi: 10.1016/j.cct.2024.107516

33. ClinicalTrials.gov Identifier: NCT04255433. *A Study of Tirzepatide (LY3298176) Compared with Dulaglutide on Major Cardiovascular Events in Participants with Type 2 Diabetes (SURPASS-CVOT)*. Available from: https://clinicaltrials.gov/study/nct04255433 [Last accessed on 2024 Jun 10].

34. Jastreboff AM, Kaplan LM, Frias JP, *et al*. Triple-hormone-receptor agonist retatrutide for obesity: A phase 2 trial. *N Engl J Med*. 2023;389:514-526.

doi: 10.1056/NEJMoa2301972

35. Rosenstock J, Frias J, Jastreboff AM, *et al*. Retatrutide, a GIP, GLP-1 and glucagon receptor agonist, for people with type 2 diabetes: A randomised, double-blind, placebo and active-controlled, parallel-group, phase 2 trial conducted in the USA. *Lancet*. 2023;402(10401):529-544.

doi: 10.1016/S0140-6736(23)01053-X

36. Jensen TL, Brønden A, Karstoft K, Sonne DP, Christensen MB. The body weight reducing effects of tirzepatide in people with and without type 2 diabetes: A review on efficacy and adverse effects. *Patient Prefer Adherence*. 2024;18:373-382.

doi: 10.2147/PPA.S419304

37. Melson E, Ashraf U, Papamargaritis D, Davies MJ. What is the pipeline for future medications for obesity? *Int J Obes* (*Lond*). 2024.

doi:10.1038/s41366-024-01473-y

38. Locatelli JC, Costa JG, Haynes A, *et al*. Incretin-based weight loss pharmacotherapy: Can resistance exercise optimize changes in body composition? *Diabetes Care*. 2024:dci230100.

doi: 10.2337/dci23-0100

39. Conte C, Hall KD, Klein S. Is weight loss-induced muscle mass loss clinically relevant? *JAMA*. 2024;332(1):9-10.

doi: 10.1001/jama.2024.6586

40. Pillai P, Modarressi T. *GLP1RAs in Clinical Practice: Therapeutic Advances and Safety Perspectives; 2024. American College of Cardiology*. Available from: https://www.acc.org/

latest-in-cardiology/articles/2024/04/15/11/19/glp1ras-in-clinical-practice [Last accessed on 2024 Nov 02].

41. Hathaway JT, Shah MP, Hathaway DB, *et al.* Risk of nonarteritic anterior ischemic optic neuropathy in patients prescribed semaglutide. *JAMA Ophthalmol*. 2024:e242296.

doi: 10.1001/jamaophthalmol.2024.2296

42. Małyszczak A, Przeździecka-Dołyk J, Szydełko-Paśko U, Misiuk-Hojło M. Novel antidiabetic drugs and the risk of diabetic retinopathy: A systematic review and meta-analysis of randomized controlled trials. *J Clin Med*. 2024; 13(6):1797.

doi: 10.3390/jcm13061797

43. Xu D, Nair A, Sigston C, *et al*. Potential roles of glucagon-like peptide 1 receptor agonists (GLP-1 RAs) in nondiabetic populations. *Cardiovasc Ther.* 2022:6820377.

doi: 10.1155/2022/6820377

44. Farr OM, Mantzoros CS. Treating prediabetes in the obese: Are GLP-1 analogues the answer? *Lancet*. 2017;389: 1371-1372.

doi: 10.1016/S0140-6736(17)30315-X

45. Hoffmann C, Schwarz PE, Mantzoros CS, *et al.* Circulating levels of gastrointestinal hormones in prediabetes reversing to normoglycemia or progressing to diabetes in a year-A cross-sectional and prospective analysis. *Diabetes Res Clin Pract*. 2023;199:110636.

doi: 10.1016/j.diabres.2023.110636

46. Le KDR, Le K, Foo F. The impact of glucagon-like peptide 1 receptor agonists on obstructive sleep apnoea: A scoping review. *Pharmacy* (*Basel*). 2024;12(1):11.

doi: 10.3390/pharmacy12010011

ACCSCIENCE PUBLISHING

Global Translational Medicine

PERSPECTIVE ARTICLE

Overestimation of the cardiovascular consequences of low-dose radiation exposures

Sergei V. Jargin*

Department of Public Health, Peoples' Friendship University (RUDN), Moscow, Russia

Abstract

This study focuses on radioactive contamination in the Urals, where the consequences were more severe in the long term than those after the Chernobyl accident. The difference is that the latter was a technogenic catastrophe, while the former was radioactive contamination tolerated for 70 years, with several accidents in between. In earlier publications by Russian researchers, no cancer frequency elevation was reported after exposures of <0.5 Sv or generally in the populations exposed to low doses. Later, the same scientists started to claim similar relative risks for cancer and other diseases among exposed people in the Urals and atomic bomb survivors in Japan. Apparently, there was an ideological shift in 2005 – 2007. Trimming of statistics was not unusual in the former Soviet Union. Potential motives included stirring antinuclear protests in other countries and the strangulation of nuclear energy aimed at boosting fossil fuel prices.

Keywords: Techa river; East Urals Radioactive trace; Ionizing radiation; Cerebrovascular diseases; Cardiovascular diseases

***Corresponding author:**
Sergei V. Jargin
(sjargin@mail.ru)

Citation: Jargin SV. Overestimation of the cardiovascular consequences of low-dose radiation exposures. *Global Transl Med*. 2025:4(1):56-66. doi: 10.36922/gtm.7229

Received: December 10, 2024

Revised: January 14, 2025

Accepted: February 17, 2025

Published online: March 18, 2025

1. Introduction

At times of international tensions, scientists must preserve objectivity. Potential conflicts of interest should be discussed. For many years, certain environmentalists and grassroots groups have acted in accordance with the interests of companies and governments selling petroleum and natural gas.[1,2] The most evident example is this tendency with regard to ionizing radiation, where the overestimation of the medical and environmental side effects of atomic energy contributes to its strangulation,[3] supporting appeals to dismantle nuclear power plants (NPPs). Fueled by the Chernobyl accident in 1986, environmentalist movements mobilized political forces, which made nuclear energy untenable in some countries.[4] The use of nuclear energy for electricity production is on the agenda today due to the increasing energy needs of humankind. Of note, health risks and environmental damage are maximal for coal and oil, lower for gas, and much lower for atomic energy, the cleanest, safest, and practically inexhaustible energy resource.[3,5]

This perspective article focuses on radioactive contamination in the Urals, where the consequences have been more severe in the long run than those after the Chernobyl accident. The Chernobyl disaster has been discussed previously.[1,2] The Mayak Production Association (MPA) was the first plutonium production site in the former Soviet Union (SU), built in 1948. The dumping of radioactive materials into the Techa River, the 1957 Kyshtym accident, and dispersion by winds from the open repository Lake

Karachai in 1967 led to resident exposures. The East Urals radioactive trace (EURT) cohort includes people exposed following the Kyshtym accident. The difference between the contaminations in the Urals and Chernobyl is that the latter was a technogenic catastrophe; however, the former was radioactive contamination tolerated for 70 years, with several accidents in between. For inside observers, the party leadership prepared an end to the communist regime since the mid-1980s at the latest to privatize state property, which was accomplished in the early 1990s. The most efficient tools to destabilize the Soviet society were as follows:

(A) Shortage of consumer goods (the word "deficit" is used in Russian). The situation was somewhat better in Moscow and certain Soviet republics in 1986 – 1990. This was also a disguised inflation: salaries and prices in state-owned shops were kept stable; however, shops were empty, while prices at markets were much higher. This is explained by market economics. Shops would never be empty if prices were set by supply and demand. Waiting hours in queues is a cost.

(B) The Chernobyl accident contributed to the destabilization; however, it would be speculation to claim that there was an intention. At least, negligence and disregard for written instructions were among the causes of the disaster.[6-8] The number of control rods in the reactor was only half the minimum required for safe operation.[9] An emergency power system had been shut off, which is forbidden during online operation.[10] Purportedly, this was done to conduct an experiment.[9,11] The weightiest argument against NPPs is that they are potential targets in an armed conflict, with radiation-related environmental consequences. Therefore, military threats are arguments against the use of nuclear power for electricity production, thus boosting fossil fuel prices. The Chernobyl accident was exploited for the same purpose.[3]

(C) The anti-alcohol campaign (1985 – 1989), which ended in failure, contributed to crime and the use of alcohol surrogates and narcotic drugs. After the campaign, drunkenness, which anesthetized the population during the privatization of state property, increased.

2. Dose–response relationships

In earlier publications by Russian researchers, cancer frequency did not increase in cohorts with average exposures <0.5 Sv or among MPA employees in general.[12-17] The absolute risk of leukemia per 1 Gy and 10000 man-years was 3.5-fold smaller in the Techa River cohort than in atomic bomb survivors of Hiroshima and Nagasaki. This was reasonably explained by the higher efficiency of acute exposure than chronic ones. Later, the same scientists started to claim similar risks for cancer and other diseases in the Techa River, MPA, and EURT cohorts as well as atomic bomb survivors.[18-20] Analogously, an earlier study found a reduction in cancer mortality in the EURT cohort compared with the general population.[15] A review confirmed the same level of both cancer and all-cause mortality in the EURT cohort and control.[13] In a later report on the same cohort, the authors avoided direct comparisons but fitted the data into a linear model. The configuration of the dose–response curves shown in this paper is inconclusive; nonetheless, the authors claimed a high cancer risk in the EURT cohort.[21] An unofficial directive was apparently behind this ideological shift noticed in 2005 – 2007 (Table 1). Trimming of statistics has been unusual in the former SU.[22] Potential motives have been discussed previously: financing, international help after the Chernobyl accident, publication pressure, stirring antinuclear protests in other countries, and the strangulation of atomic energy aimed at boosting fossil fuel prices. Some papers about radioactive contaminations in the former SU have common features: large volume, plentiful details, and mathematical computations but no clear insight into medical consequences. Cancer-related aspects of the problem have been reviewed previously.[1,2] Cardiovascular and cerebrovascular diseases (CeVD) and their supposed associations with low-dose low-rate radiation exposure are discussed below.

3. Natural radiation background and Dose and Dose-rate Effectiveness Factor (DDREF)

Enhanced risks of cardiovascular diseases were claimed for the Chernobyl, MPA, Techa River, and EURT populations, where the average doses were comparable with those from the natural radiation background. In many densely populated areas in the world, the dose rates from the natural background are 10 – 100-fold higher than the global average (2.4 mSv/year) with no health risks reliably proven.[35] The doses have been protracted over decades: studied MPA workers were first employed in 1948 – 1982. For example, the mean dose of gamma radiation was 0.54 Gy in men and 0.44 Gy among women in the MPA cohort study, where the incidence of arteriosclerosis in the lower limbs correlated with the radiation dose.[32] The average doses in the Techa River cohort were 34 – 35 mGy, whereas the follow-up was since the 1950s[33]; thus, the dose rates were compatible with those from the natural background in some populated areas. Apparently, the Techa River cohort data do not possess sufficient statistical power to determine the dose–response shape. The authors acknowledged that the risks for doses ≤0.1 Gy may be smaller than those calculated based on the linear model.[36]

Table 1. Chronologically ordered studies of exposed populations in the Urals with special reference to cardiovascular and cerebrovascular conditions

Year of publication	Studied population (s)	Main findings and conclusions	References
1990	EURT	Average dose~0.5 Sv. No increase in radiation-related diseases	Buldakov *et al.*[14]
1991	Review	At annual doses of 150 mSv and accumulated doses of 250 mSv, life expectancy did not shorten. The effects of low doses cannot be detected by epidemiology. Unfavorable effects are overestimated. The favorable effects of low doses are "undoubted."	Buldakov[23]
1991	EURT	No significant increase in morbidity and chromosomal abnormalities	Krestinina *et al.*[24]
1994	EURT evacuees	No significant changes in mortality	Kostyuchenko and Krestinina[15]
1995	Radiochemical industry	10 – 1000 mGy (92.4% <500 mGy); incorporation of Plutonium-^{239}: 70 – 7620 Bq (86% <1480 Bq). No frequency increase in ischemic heart disease (IHD). From the literature: myocardial changes with function decline develop after acute exposures to 20 – 50 Gy.	Dudchenko and Okladnikova[25]
2002	MPA	For lung cancer induction, an effect was demonstrated for high external gamma-ray doses (>2.0 Gy) plus high 239Pu intake. Results indicate that cancer risks at low doses are generally overestimated.	Tokarskaya *et al.*[17]
2000	MPA	No radiation-induced conditions were found. The overall morbidity was designated as low.	Okladnikova *et al.*[16]
2004	Review	EURT: The overall and cancer morbidity rates were not different from the general population. Techa River cohort: absolute risk of leukemia 3.5 times lower than among atomic bomb survivors in Japan.	Akleev *et al.*[13]
2005	Personnel in contact with highly enriched uranium	External doses of 0.58 – 2.02 mSv/year. Average airborne radioactivity at workplaces is up to 0.74 Bq/m^3, occasionally up to 5.9 (permitted 1.0 Bq/m^3). No increase in potentially radiogenic non-cancer morbidity.	Sumina *et al.*[26]
2007	Personnel of nuclear reactors since 1948	The first signs of early (age<45 years) cerebral atherosclerosis appeared after exposures to high doses (accumulated 4.3 Gy; annual >2.5 Gy). The mortality structure was the same as in the general population. Chronic external exposure to gamma rays within permitted limits did not cause radiation-induced abnormalities.	Okladnikova *et al.*[27]
2008	Techa River cohort	Average dose, 0.04 Gy; maximal, 0.47 Gy. Significant dose–response relationship for breast cancer	Ostroumova *et al.*[20]
2010	Techa River cohort	Radiation-related cancer risk "not less" than that among atomic bomb survivors in Japan	Akleev and Krestinina[18]
2012	Occupationally exposed workers	The risk of death from IHD was significantly higher in workers with absorbed doses to the liver >0.025 Gy from internal alpha radiation.	Azizova *et al.*[28]
2012	MPA	The incidence of CeVD was significantly higher in workers chronically exposed to external gamma rays at ≥1.0 Gy. Significantly increased CeVD incidence with internal liver exposure to plutonium alpha radiation. Higher risks than among atomic bomb survivors in Japan.	Moseeva *et al.*[29]
2014	MPA	Morbidity of aortic atherosclerosis significantly increased at external doses ≥0.5 Gy (all subjects) and internal doses ≥0.025 Gy (females only)	Azizova *et al.*[30]
2015	MPA	Significant upward trends in CeVD with increasing total absorbed dose from external gamma and internal alpha radiations	Azizova *et al.*[31]
2016	MPA	Significant association of lower extremity arterial disease incidence with the total dose from external gamma rays	Azizova *et al.*[32]
2019	EURT and Techa River cohorts	Increase in mortality from all circulatory diseases, including IHD	Krestinina *et al.*[33]
2023	MPA	Significantly increased IHD mortality per unit of external gamma-ray exposure (0.005 – 0.050 Gy/year).	Azizova *et al.*[34]

Abbreviations: CeVD: Cerebrovascular diseases; DDREF: Dose and dose-rate effectiveness factor; ERR: Excess relative risk; EURT: East Urals radioactive trace; ICRP: International Commission on Radiological Protection; IHD: Ischemic heart disease; MPA: Mayak Production Association; SU: Soviet Union; UNSCEAR: United Nations Scientific Committee on the Effects of Atomic Radiation.

In particular, the uncertain and biased data are unsuitable for the computations of the DDREF. Earlier Russian publications stressed the higher biological efficiency of acute exposures to chronic and fractionated ones[12]; later, the same scientists reiterated that the International Commission on Radiological Protection underestimates cancer risks from chronic exposures and recommended the use of DDREF = 1.0, meaning acute and chronic exposures are equally efficient.[37] This recommendation is obviously unreasonable for dose rates compatible with those from the natural radiation background. DDREF has been discussed in more detail previously.[1,38]

4. Cardiovascular and cerebrovascular conditions

In earlier reports, an incidence increase in cardiovascular diseases and CeVD, if found in MPA, Techa River, and EURT populations, was not accompanied by a mortality increase.[28,31,39] This can be reasonably explained by the greater diagnostic effectiveness in people with higher doses, with the registration of mild and questionable cases. However, a recent paper utilizing the MPA cohort reported an increase in the excess relative risk (ERR/Gy) of mortality due to ischemic heart disease for the dose range of 5 – 50 mGy/year.[34] Our preceding comments, although not cited, might have been taken into account by the authors. Moreover, the recent review by Koterov *et al.*[40] was influenced by our comments cited by Koterov[41] and commented.[42] However, trying to shift responsibility for biased information onto foreign experts can be illustrated by the following quote from the English abstract: "In most sources, 2005 – 2021 (publications by M.P. Little with co-workers, and others) reveals an ideological bias toward the effects of low doses of radiation… In selected M.P. Little and co-authors sources for reviews and meta-analyses observed both absurd ERR values per 1 Gy and incorrect recalculations of the risk estimated in the originals at 0.1 Gy."[40] Relevant papers co-authored by Professor Little[43,44] used the data provided by coworkers from the former SU. In this connection, the author agreed that "Russian national mortality data are likely to be particularly unreliable, with major variations in disease coding practices across the country [references], and should therefore probably not be used for epidemiologic analysis, in particular for the Russian worker studies considered here [references]."[45] Koterov[41] used mistranslations of quotes with a change of meaning in his Russian-language writings, as commented previously.[42]

The recent review noted the "diagnosis (by a physician knowing the patient's history) could vary with dose" and the "inter-study variation in unmeasured confounders or effect modifiers."[44] Mild and borderline conditions must be more often diagnosed in people with higher doses due to the more thorough examinations and patients' attention to their health. "The markedly elevated mortality and morbidity rates of circulatory disease in the Russian population compared with other developed countries"[43] has been explained by unsubstantiated conclusions in unclear cases, both post- and ante-mortem. At least in the former SU, the lower the diagnostic quality, the higher the fraction of cardiovascular diseases among all causes of death. The same is also true for deceased patients not undergoing autopsy, where cardiovascular diseases are often recorded as causes of death in questionable cases.[46]

A recent study based on the MPA cohort analyzed 9469 CeVD cases including 2078 strokes. The following statements appear contradictory: "CeVD incidence was found to be significantly associated with cumulative radiation dose" and "No significant associations of either stroke or its types with cumulative gamma-ray dose of external exposure or alpha-particle dose of internal exposure were found."[47] Expectedly, with more arterial occlusions and stenoses, there would be more strokes. An apparent explanation for the discrepancy is the dose-dependent diagnostic quality and a larger screening effect in patients with higher doses. At that time, mild and borderline conditions would be recorded more frequently. On the contrary, strokes are usually diagnosed based on distinct morphological and/or clinical criteria, with false positivity being less probable. Moreover, "The estimates of the CeVD incidence risk significantly decreased with the increasing duration of employment for the entire cohort ($p < 0.001$)." "In addition, a significant decrease in CeVD diseases incidence risk with increasing attained age was observed in both males and females."[47] The incidence of CeVD increases with age; therefore, the above quotes are compatible with a protective effect of radiation, that is, hormesis. Azizova *et al.*[47] did not mention radiation hormesis nor other above-cited papers. In our opinion, the authors should have discussed harmful CeVD (strokes) and concluded the lack of increase in strokes following the low-dose, low-rate exposures. In fact, this is common knowledge. By including relatively harmless and less reliably diagnosed conditions, they were able to conclude that low-dose radiation increases the frequency of CeVD.

The greater CeVD risk at higher doses in women than in men[47] agrees with the known tendency that women in Russia care more than men about their health and are generally given more attention by medical personnel. Hence, in the world's highest sex gaps in life expectancy, countries of the former SU lead the list.[48] Accordingly, the diagnostics in women must be, on average, more efficient

and more reliable than that in men. This notion does not contradict the higher relative risk in some low-dose male groups, as indicated in Tables 1.[47] CeVD is more frequent in men, among other reasons, due to alcohol abuse and cigarette smoking. Some mild conditions may be overdiagnosed because these conditions are expected. For example, the author encountered descriptions of age- and hypertension-related changes of retinal vessels in a medical record of a middle-aged man after a dispensarization (yearly workplace examination), where his eye grounds had not been inspected. As for post-mortem supposedly age-related changes (aortal, coronary, cerebral, or basilar atherosclerosis), they have habitually been written without sufficient evidence in autopsy reports and death certificates.[46] In higher-dose groups, the diagnostics would be more reliable, resulting in a more pronounced screening effect in women but less frequent unsubstantiated recordings in men.

In the MPA cohort, the incidence of circulatory diseases was found to be higher in members who received gamma-ray doses of >0.1 Gy than those exposed to lower doses.[49,50] The ERR/Gy of CeVD in MPA employees was claimed to be even higher than that among atomic bomb survivors in Japan,[49,51] where dose-dependent selection could have taken place, as in other epidemiological studies. Some data assessments of life span studies of atomic bomb survivors are compatible with hormesis.[52-55] For cancers, a dose–response association was detected among survivors who received doses ≤0.5 Sv but not <0.2 Sv.[55-57] For example, the data about renal cancer in men indicated hormesis: U-shaped dose–response curves with negative ERR estimates at low-to-moderate doses, whereas those in women did not. These findings could have been observed by chance.[54] A preceding article by the same researchers also showed different shapes of the dose–response curves for men and women.[58] When studies based on the same cohort revealed different dose–response curves, reliability should be doubted. Other studies found no significant risks for kidney cancer from low doses.[59-61] To reliably evaluate dose–effect relationships at low doses, epidemiological data have too many uncertainties. Thus, large-scale animal experiments would be more informative.

5. Cancer-related research: An example

This perspective article is about cardiovascular diseases; however, one insightful example from the oncology field should be provided at the end. A significantly increased risk of non-melanoma skin cancer was reported in MPA workers exposed to radiation at doses ≥2.0 Sv accumulated over prolonged periods.[51] In comparison, the non-melanoma skin cancer dataset among Japanese atomic bomb survivors indicated a threshold of approximately 1.0 Sv for acute exposure.[62] However, observation bias appears to be probable in the study.[51] The workers and some medical personnel knew the individual work histories, from which accumulated doses could be approximately inferred, potentially influencing diagnostic thoroughness. The skin doses were unknown. The participants were exposed mainly to gamma rays, which have a relatively high penetration distance in tissues so that the absorbed doses within the skin must have been relatively low. Accordingly, the premalignant skin lesions and actinic keratoses were "very rare" in the study cohort.[51] Radiation exposure is associated with premalignant epidermal changes; in particular, actinic keratosis may be caused by X-ray and radiotherapy.[63,64] Therefore, a cause–effect relationship between radiation and skin tumors in the study[51] is improbable.

6. Confounding factors and bias: About motives

Considering the above, the following claims by the same scientists, being unfounded and/or excessively generalized, create a biased impression of the risks associated with low-dose low-rate radiation exposures. The statements cited below, not specifying dose levels, does not apply to the cohorts under discussion (EURT, MPA, and Techa River) and to low doses in general. The claims exemplified below, reiterated in numerous papers, demonstrate that the risks have been intentionally exaggerated. An unofficial directive was behind this ideological bias. Trimming of statistics has been not unusual in the former SU.[22] Here, follow the examples:

> "It was shown that ionizing radiation is one of the promoters of the development of atherosclerosis."[65]
>
> "It is concluded that this study provides evidence for an association of lower extremity arterial disease incidence with dose from external gamma-rays."[32]
>
> "This study provides *strong evidence* [emphasis added] of ischemic heart disease (IHD) incidence and mortality association with external gamma-ray exposure and some evidence of IHD incidence and mortality association with internal alpha-radiation exposure."[66]
>
> "A significant increasing trend in circulatory diseases mortality with increasing dose from internal alpha-radiation to the liver was observed."[67]
>
> "Significant associations were observed between doses from external gamma-rays and IHD and CVD incidence and also between internal doses from alpha-radiation and IHD mortality and CVD incidence."[68]
>
> "Findings are that aortal atherosclerosis prevalence was higher in males and females underwent external gamma-irradiation of total dose over 0.5 Gy, in males

and females underwent internal alpha-irradiation from incorporated plutonium of total absorbed radiation dose in liver over 0.025 Gy."[30]

"There was a significantly increasing trend (ERR/Gy) of the IHD mortality with the total absorbed dose to liver from internal alpha-radiation due to incorporated plutonium."[28]

"The incidence data point to higher risk estimates (in MPA workers) compared to those from the Japanese A-bomb survivors."[29]

"The categorical analyses showed that CeVD incidence was significantly higher among workers with total absorbed external gamma-ray doses *>0.1 Gy* [emphasis added] compared to those exposed to lower doses and that CeVD incidence was also significantly higher among workers with total absorbed internal alpha-particle doses to the liver from incorporated plutonium >0.01 Gy compared to those exposed to lower doses."[49]

The risk estimates by Azizova *et al.*[69] were significantly higher than those in other studies.[70] In the MPA cohort, the incidence of circulatory diseases was reported to be higher in members who received gamma-ray doses of >0.1 Gy than in people exposed to lower doses.[49,50] Cause–effect relationships are improbable at such a low dose, taking into account the dose comparisons below. The United Nations Scientific Committee on the Effects of Atomic Radiation[71] (UNSCEAR 2006) could not conclude causality between exposures below 1 – 2 Gy and cardiovascular diseases. The level 1 – 2 Gy is an underestimation resulting from the screening effect, selection, self-selection, other biases, and confounding factors in epidemiological studies. Approximately 10 years ago, during the author's visit at the Medical Radiological Research Center in Obninsk, Russia, Victor Ivanov emphasized his leading role in the UNSCEAR Reports. Political and economic interests sometimes overweigh scientific objectivity, which is perceivable from certain documents issued by esteemed international organizations such as UNSCEAR. As mentioned above, the Chernobyl accident has been exploited to strangulate the worldwide development of the atomic industry.[3] At present, there are no alternatives to nuclear power; in the long run, non-renewable fossil fuels will probably become increasingly expensive, contributing to uncontrolled population growth in oil-producing countries and poverty in the rest of the world.

7. Discussion

Dose levels associated with cardiac derangements in animal experiments and humans following radiotherapy have been much higher than the average doses in the cohorts discussed above.[72-75] Results of animal experiments are generally compatible with hormesis, that is, favorable effects within a certain low-dose range, possibly except in genetically modified cancer-prone animals. In some experimental and epidemiological studies, low doses turned out to be protective against cardiovascular diseases.[72] Existing evidence in favor of hormesis is considerable.[76-80] This implies that epidemiological data partly disagree with the experiments. The cause thereof may be bias in some epidemiological research on low-dose exposures to ionizing radiation, that is, inter-study differences in quality and reliability.[1,81]

In humans who received radiotherapy, myocardial fibrosis developed at doses ≥30 Gy. An increased risk of coronary disease following radiotherapy has been registered after exposures to 7.6 – 18.4 Gy,[74] which is still much higher than the mean doses in the cohorts discussed above. Unrealistic cardiovascular risks at low-dose exposures call into question the cancer risks reported by the same researchers. Finally, the quality of dose estimation is crucial for studies of radiation risks. Recall bias should be mentioned in this connection: patients with cancer and individuals with other diseases tend to recollect all circumstances related to radiation better than healthy controls.[82]

Summarizing the above and previously published arguments,[1,2] the detrimental effects of anthropogenic radiation would approach zero as the dose rate decreases to levels comparable to natural background radiation. Moreover, the dose–effect relationship may exhibit an inverse correlation within a certain range, consistent with the convey of hormesis. Obviously, hormesis cannot be used in radiation safety regulations if consistent experimental evidence has not been obtained in large-scale animal experiments using different species. Even thereafter, precautions would be necessary as hormetic stimuli may act without a threshold on pre-damaged or atrophic tissues or synergistically with known or unknown noxious agents. DNA damage and repair are normally in a dynamic equilibrium. Accordingly, there may be an optimal exposure level, as it is for many other environmental agents, such as visible and ultraviolet light, various chemical elements and compounds, as well as products of water radiolysis.[83] Moreover, evolutionary adaptation to a changing environmental factor would lag behind its current value and correspond to some average from the past. Natural background radiation has been decreasing during the time of life's existence on Earth.[84] The character of the dose–response relationship at the dose close to the natural radiation background can be predicted based on general considerations. Many carcinogenic factors exist. The lower the level of environmental radioactivity,

the less the contribution of radioactive contamination compared with the natural radioactive background and other carcinogens. The relationship between dose and effect may become inversely related according to the concept of hormesis. A corresponding graph, plotted based on experimental data, with a sagging of the dose–effect curve below the background cancer risk within the dose range of 0.1 – 700 mGy, is depicted in the review.[85] The dose–effect relationships after low-dose exposures should be clarified in lifelong animal experiments with known doses and dose rates. Animal studies can provide reliable information; however, dose reconstructions in human populations are often inaccurate and, as discussed above, partly comparable with doses from the natural radiation background. In this direction, further studies on the relative biological effectiveness of radiation in different animal species[86] would better quantify the radiosensitivity of the species, thus enabling more precise extrapolations to humans.

Nuclear power has returned to the agenda due to concerns about increasing global energy demand, declining fossil fuel reserves, and climate changes. NPPs emit virtually no greenhouse gases in comparison with coal, oil, or gas.[5] Hopefully, nuclear fission will be replaced in the future by fusion, which is intrinsically safer. Fusion offers a potential source of clean power generation with an abundant supply of raw materials.[87] More international trust and cooperation would enable the construction of NPPs in optimally suitable places, notwithstanding national borders, considering all sociopolitical, geographic, and geologic factors.

The optimal approach for radiation protection is to determine the threshold dose for carcinogenic effects and establish regulations to ensure that doses are kept well below the threshold,[52] as low as reasonably achievable, considering economic and societal factors. To determine threshold doses, large-scale animal experiments using different species are the most reliable tool. In the author's opinion, the current safety norms are exceedingly restrictive. Increasing limits must be accompanied by measures guaranteeing their observance. Strictly observed realistic safety regulations would bring more benefit for public health than excessive restrictions that would be violated in countries that disregard international law. Excessive restrictions are harmful to the economy.

8. Conclusions

This perspective article focuses on radioactive contamination in the Urals, where the consequences were more severe in the long term than those after the Chernobyl accident. Recent publications claiming cardiovascular risks after low-dose, low-rate exposures and recommending more stringent standards of radiological protection are discussed in detail here. Such recommendations for dose rates compatible with the natural radiation background are non-sensical. Concerns were raised about ideological changes in the Russian professional literature in 2005–2007, sometimes accompanied by the manipulation of statistical data and overemphasis on the risk from low-dose exposures to ionizing radiation. Considering the history of statistical manipulation in the former SU,[22] further clarifications are necessary. Furthermore, the article points out that some conclusions about the health risks associated with low-dose, low-dose-rate radiation are not sufficiently substantiated. Although associations with cardiovascular and CeVD are suggested, data may not be sufficient to confirm causal relationships at low doses. Thus, further epidemiological studies and large-scale animal experiments are required. The article mentions the possibility that low-dose radiation could have beneficial health effects (hormesis effect). This topic must be carefully discussed to reach conclusions based on solid evidence. Thus far, the causal relationships at the low-dose level remain unclear. The quality of diagnosis may affect the results. Specifically, the potential for overdiagnosis, that is, excessively diagnosed mild conditions in exposed individuals, may distort the findings, necessitating a re-evaluation. Some studies have reported a link between radiation exposure and cardiovascular diseases; however, their risk estimates appear higher than those in other studies, raising doubts about reliability. Selection, self-selection, and ideological bias should be considered when evaluating data reliability. Discussions of radiation risks, including those from the Chernobyl disaster and contaminations in the Urals, may be influenced by political and economic interests related to the development of the nuclear power industry. This article stresses that the Russian literature overemphasizes the risks associated with low-dose radiation, which requires thorough investigations based on solid scientific evidence. In this regard, more long-term and rigorous studies are necessary.

In summary, studies of human populations exposed to low-dose, low-rate ionizing radiation, though important, will unlikely add much reliable information on the dose–effect relationships, hormesis, and DDREF. Factors such as screening effect, selection, self-selection, and ideological biases will contribute to the emergence of new reports on enhanced risks associated with a moderate increase in the radiation background, which would not establish causality. Reliable results can be derived from lifelong animal experiments. The lifespan is a sensitive endpoint that can measure the net harm or potential benefit (within a certain range according to the concept of hormesis) from low-dose exposures.

Acknowledgments

None.

Funding

None.

Conflict of interest

The author declares that he has no competing interests.

Author contributions

This is a single-authored article.

Ethics approval and consent to participate

Not applicable.

Consent for publication

Not applicable.

Availability of data

Not applicable.

Further disclosure

The paper has been deposited onto a preprint server: Jargin SV. Overestimation of cardiovascular consequences of low-dose radiation exposures. Preprints 2023, 2023061344. https://doi.org/10.20944/preprints202306.1344.v1

References

1. Jargin SV. *The Overestimation of Medical Consequences of Low-dose Exposure to Ionizing Radiation*. 2nd ed. United Kingdom: Cambridge Scholars Publishing; 2023.
2. Jargin SV. Overestimation of cardiovascular and ophthalmological consequences of low-dose radiation. *J Ocular Biol*. 2024;8(1):1.

   doi: 10.13188/2334-2838.1000033
3. Jaworowski Z. Observations on the chernobyl disaster and LNT. *Dose Response*. 2010;8(2):148-171.

   doi: 10.2203/dose-response.09-029.Jaworowski
4. Rüdig W. *Anti-nuclear Movements: A World Survey of Opposition to Nuclear Energy.* Harlow: Longman Current Affairs; 1990.
5. Markandya A, Wilkinson P. Electricity generation and health. *Lancet*. 2007;370:979-990.

   doi: 10.1016/s0140-6736(07)61253-7
6. Beliaev IA. *Chernobyl. Vahta Smerti [Chernobyl. Death Shift]*. Moscow: IzdAT; 2006.
7. Mould RF. *Chernobyl Record. The Definitive history of Chernobyl Catastrophe*. United States: Institute of Physics, CRC Publishers; 2000.
8. Semenov AN. *Chernobyl'. Desjat' Let Spustja: Neizbezhnost' Ili Sluchajnost'*? [*Chernobyl. Ten Years Later: Inevitability or Coincidence*?] Moscow: Energoatomizdat; 1995.
9. Smith JT, Beresford NA, editors. Introduction. In: *Chernobyl-Catastrophe and Consequences*. Berlin: Springer; 2005. p. 1-34.
10. Ludewig B, Eidemüller D. *The Nuclear Dream: The Hidden World of Atomic Energy*. Berlin: DOM; 2020.
11. Medvedev G. *The Truth about Chernobyl*. United Kingdom: Tauris; 1991.
12. Akleyev AV, Kossenko MM, Krestinina LY, *et al. Zdorov'e Naseleniia, Prozhivajushhego Na Radioaktivno Zagriaznennyh Territoriiah Ural'skogo Regiona [Health Status of Population Exposed to Environmental Contamination in the Southern Urals*]. Moscow: Radekon; 2001.
13. Akleev AV, Preston D, Krestinina LI. Medical and biological consequences of human's chronic exposure to radiation. *Med Tr Prom Ekol*. 2004;3:30-36.
14. Buldakov LA, Demin SN, Kosenko MM, *et al.* The medical sequelae of the radiation accident in the Southern Urals in 1957. *Med Radiol (Mosk*). 1990;35(12):11-15.
15. Kostyuchenko VA, Krestinina LYu. Long-term irradiation effects in the population evacuated from the east-Urals radioactive trace area. *Sci Total Environ*. 1994;142(1-2): 119-125.

   doi: 10.1016/0048-9697(94)90080-9
16. Okladnikova ND, Pesternikova VS, Azizova TV, *et al.* Health status among the staff at the nuclear waste processing plant. *Med Tr Prom Ekol*. 2000;6:10-14.
17. Tokarskaya ZB, Scott BR, Zhuntova GV, *et al.* Interaction of radiation and smoking in lung cancer induction among workers at the Mayak nuclear enterprise. *Health Phys*. 2002;83(6):833-846.

   doi: 10.1097/00004032-200212000-00011
18. Akleev AV, Krestinina LI. Carcinogenic risk in residents of the Techa riverside villages. *Vestn Ross Akad Med Nauk*. 2010;6:34-39.
19. Krestinina LY, Davis FG, Schonfeld S, *et al.* Leukaemia incidence in the Techa river cohort: 1953-2007. *Br J Cancer*. 2013;109(11):2886-2893.

   doi: 10.1038/bjc.2013.614
20. Ostroumova E, Preston DL, Ron E, *et al.* Breast cancer incidence following low-dose rate environmental exposure: Techa river cohort, 1956-2004. *Br J Cancer*. 2008;99(11):1940-1945.

   doi: 10.1038/sj.bjc.6604775
21. Akleyev AV, Krestinina LY, Degteva MO, Tolstykh EI. Consequences of the radiation accident at the Mayak

production association in 1957 (the "Kyshtym Accident"). *J Radiol Prot*. 2017;37(3):R19-R42.

doi: 10.1088/1361-6498/aa7f8d

22. Jargin SV. *Misconduct in Medical Research and Practice. Ethical Issues in the 21st Century.* United States: Nova Science Publishers; 2020.

doi: 10.52305/GIEZ3244

23. Buldakov LA. Radiobiology and radiation hygiene. *Radiobiologiia*. 1991;31(4):527-536.

24. Krestinina LIu, Kosenko MM, Kostiuchenko VA. Lethal developmental defects in the offspring of a population living in a territory with traces of radioactivity. *Med Radiol* (*Mosk*). 1991;36(6):30-32.

25. Dudchenko NN, Okladnikova ND. Ischemic heart disease in workers of radiochemical industry chronically exposed to radiation dosage less than MPEL. *Med Tr Prom Ekol*. 1995;6:7-10.

26. Sumina MV, Azizova TV, Pesternikova VS, Beliaeva ZD, Tel"nov VI, Lobanov BG. Some health parameters in personnel contacting highly enriched uranium. *Med Tr Prom Ekol*. 2005;11:24-30.

27. Okladnikova ND, Sumina MV, Pesternikova VS, Azizova TV, Ia Kabasheva N. Long-term consequences of external gamma-radiation according to the results of the observation of the personnel of the first atomic power plant in the country. *Klin Med* (*Mosk*). 2007;85(10):21-26.

28. Azizova TV, Moseeva MB, Grigor'eva ES, *et al.* Mortality risk of cardiovascular diseases for occupationally exposed workers. *Radiats Biol Radioecol*. 2012;52(2):158-166.

29. Moseeva MB, Azizova TV, Muirhed CR, *et al.* Risk of cerebrovascular disease incidence in the cohort of Mayak production association workers first employed during 1948-1958. *Radiats Biol Radioecol*. 2012;52(2):149-157.

30. Azizova TV, Kuznetsova KV, Bannikova MV, *et al.* Prevalence of aortal atherosclerosis in workers underwent occupational irradiation. *Med Tr Prom Ekol*. 2014;11:1-6.

31. Azizova TV, Haylock R, Moseeva MB, Bannikova MV, Grigoryeva ES. Cerebrovascular diseases incidence and mortality in an extended Mayak worker cohort 1948-1982. *Med Radiol Radiaton Safety* (*Moscow*). 2015;60(4):43-61.

32. Azizova TV, Bannikova MV, Grigorieva ES, *et al.* Risk of lower extremity arterial disease in a cohort of workers occupationally exposed to ionizing radiation over a prolonged period. *Radiat Environ Biophys*. 2016;55:147-159.

doi: 10.1007/s00411-016-0645-6

33. Krestinina LY, Silkin SS, Degteva MO, Akleyev AV. Risk analysis of the mortality from the diseases of the circulatory system in the Ural cohort of emergency-irradiated population for the years 1950-2015. *Radiation Hygiene*. 2019;12(1):52-61.

doi: 10.21514/1998-426x-2019-12-1-52-61

34. Azizova TV, Grigoryeva ES, Hamada N. Dose rate effect on mortality from ischemic heart disease in the cohort of Russian Mayak Production Association workers. *Sci Rep.* 2023;13(1):1926.

doi: 10.1038/s41598-023-28954-w

35. Sacks B, Meyerson G, Siegel JA. Epidemiology without biology: False paradigms, unfounded assumptions, and specious statistics in radiation science. *Biol Theory*. 2016;11:69-101.

doi: 10.1007/s13752-016-0244-4

36. Schonfeld SJ, Krestinina LY, Epifanova S, *et al.* Solid cancer mortality in the Techa River cohort (1950-2007). *Radiat Res*. 2013;179(2):183-189.

doi: 10.1667/RR2932.1

37. Akleyev AV Degteva MO, Krestinina LY. Overall results and prospects of the cancer risk assessment in the Urals population affected by chronic low dose-rate exposure. *Radiation Med Protect*. 2022;3(4):159-166.

doi: 10.1016/j.radmp.2022.08.002

38. Jargin SV. On the dose and dose rate effectiveness factor (DDREF). *Radiats Biol Radioecol.* 2017;57(3):308-314.

doi: 10.7868/S0869803117030080

39. Soloviev VY, Krasnyuk VI. On possible mistakes in the estimation of radiation risk non-cancer effects in Mayak plant workers. *Med Radiol Radiaton Safety* (*Moscow*). 2018;63(6):83-84.

doi: 10.12737/article_5c0bdefea14005.22956834

40. Koterov AN, Ushenkovaa LN, Wainson AA, *et al.* Excess relative risk of mortality from diseases of the circulation system after irradiation. Report 1. Overview of reviews and meta-analysis declared effects of low doses. *Radiats Biol Radioecol.* 2023;63(1):3-33.

doi: 10.31857/S0869803123010095

41. Koterov AN. To the letter to the editor of S.V. Jargin "On RET/PTC rearrangements in thyroid carcinoma after the chernobyl accident". *Med Radiol Radiaton Safety* (*Moscow*). 2017;62(2):53-64.

doi: 10.12737/article_58f0b9573ddc88.95867893

42. Jargin SV. Comment on the article: Koterov AN, Wainson AA. Radiation hormesis and epidemiology of carcinogenesis: "Never the twain shall meet". *Med Radiol Radiation Saf.* 66(2):36-52.

43. Little MP, Azizova TV, Hamada N. Low and moderate-dose non-cancer effects of ionizing radiation in directly exposed individuals, especially circulatory and ocular diseases: A review of the epidemiology. *Int J Radiat Biol.* 2021;97: 782-803.

doi: 10.1080/09553002.2021.1876955

44. Little MP, Azizova TV, Richardson DB, *et al.* Ionising radiation and cardiovascular disease: Systematic review and meta-analysis. *BMJ*. 2023;380:e072924.

doi: 10.1136/bmj-2022-072924

45. Little MP. Radiation and circulatory disease. *Mutat Res*. 2016;770(Pt B):299-318.

doi: 10.1016/j.mrrev.2016.07.008

46. Jargin SV. Cardiovascular mortality trends in Russia: possible mechanisms. *Nat Rev Cardiol*. 2015;12(12):740.

doi: 10.1038/nrcardio.2015.166

47. Azizova TV, Moseeva MB, Grigoryeva ES, Hamada N. Incidence risks for cerebrovascular diseases and types of stroke in a cohort of Mayak PA workers. *Radiat Environ Biophys*. 2022;61(1):5-16.

doi: 10.1007/s00411-022-00966-6

48. Wikipedia. *List of Countries by Life Expectancy. Gender gap. World Bank Group Data for 2020*. Available from: https://en.wikipedia.org/wiki/list_of_countries_by_life_expectancy [Last accessed on 2024 Dec 09].

49. Azizova TV, Haylock RG, Moseeva MB, Bannikova MV, Grigoryeva ES. Cerebrovascular diseases incidence and mortality in an extended Mayak Worker Cohort 1948-1982. *Radiat Res.* 2014;182:529-544.

doi: 10.1667/RR13680.1

50. Simonetto C, Schöllnberger H, Azizova TV, Grigoryeva ES, Pikulina MV, Eidemüller M. Cerebrovascular diseases in workers at Mayak PA: The difference in radiation risk between incidence and mortality. *PLoS One.* 2015;10:e0125904.

doi: 10.1371/journal.pone.0125904

51. Azizova TV, Bannikova MV, Grigoryeva ES, Rybkina VL. Risk of malignant skin neoplasms in a cohort of workers occupationally exposed to ionizing radiation at low dose rates. *PLoS One*. 2018;13:e0205060.

doi: 10.1371/journal.pone.0205060

52. Doss M. Future of radiation protection regulations. *Health Phys*. 2016;110:274-275.

doi: 10.1097/HP.0000000000000381

53. Luckey TD. Atomic bomb health benefits. *Dose Response*. 2008;6:369-382.

doi: 10.2203/dose-response.08-009.Luckey

54. Grant EJ, Yamamura M, Brenner AV, *et al.* Radiation risks for the incidence of kidney, bladder and other urinary tract cancers: 1958-2009. *Radiat Res*. 2021;195:140-148.

doi: 10.1667/RADE-20-00158.1

55. Little MP, Muirhead CR. Evidence for curvilinearity in the cancer incidence dose-response in the Japanese atomic bomb survivors. *Int J Radiat Biol*. 1996;70:83-94.

doi: 10.1080/095530096145364

56. Little MP, Muirhead CR. Curvature in the cancer mortality dose response in Japanese atomic bomb survivors: Absence of evidence of threshold. *Int J Radiat Biol.* 1998;74:471-480.

doi: 10.1080/095530098141348

57. Heidenreich WF, Paretzke H, Jacob P. No evidence for increased tumour rates below 200 mSv in the atomic bomb survivors data. *Radiat Environ Biophys*. 1997;36:205-207.

doi: 10.1007/s004110050073

58. Grant EJ, Brenner A, Sugiyama H, *et al.* Solid Cancer Incidence among the Life Span Study of Atomic Bomb Survivors: 1958-2009. *Radiat Res.* 2017;187(5):513-537.

doi: 10.1667/RR14492.1

59. Boice JD, Cohen SS, Mumma MT, *et al.* Mortality among U.S. military participants at eight aboveground nuclear weapons test series. *Int J Radiat Biol*. 2022;98(4):679-700.

doi: 10.1080/09553002.2020.1787543

60. Haylock RGE, Gillies M, Hunter N, Zhang W, Phillipson M. Cancer mortality and incidence following external occupational radiation exposure: An update of the 3rd analysis of the UK national registry for radiation workers. *Br J Cancer*. 2018;119(5):631-637.

doi: 10.1038/s41416-018-0184-9

61. Richardson DB, Cardis E, Daniels RD, *et al.* Site-specific solid cancer mortality after exposure to ionizing radiation: A Cohort Study of Workers (INWORKS). *Epidemiology*. 2018;29(1):31-40.

doi: 10.1097/EDE.0000000000000761

62. Little MP, Charles MW. The risk of non-melanoma skin cancer incidence in the Japanese atomic bomb survivors. *Int J Radiat Biol*. 1997;71(5):589-602.

doi: 10.1080/095530097143923

63. Gawkrodger DJ. Occupational skin cancers. *Occup Med* (*Lond*). 2004;54(7):458-463.

doi: 10.1093/occmed/kqh098

64. Schmitt JV, Miot HA. Actinic keratosis: A clinical and epidemiological revision. *An Bras Dermatol.* 2012;87(3):425-434.

doi: 10.1590/s0365-05962012000300012

65. Rybkina VL, Azizova TV. The influence of the ionizing radiation on the development of atherosclerosis. *Radiats Biol Radioecol*. 2016;56(1):44-55.

66. Azizova TV, Grigoryeva ES, Haylock RG, Pikulina MV, Moseeva MB. Ischaemic heart disease incidence and mortality in an extended cohort of Mayak workers first employed in 1948-1982. *Br J Radiol.* 2015;88(1054):20150169.

doi: 10.1259/bjr.20150169

67. Azizova TV, Grigorieva ES, Hunter N, Pikulina MV, Moseeva MB. Risk of mortality from circulatory diseases in Mayak workers cohort following occupational radiation exposure. *J Radiol Prot*. 2015;35(3):517-538.

doi: 10.1088/0952-4746/35/3/517

68. Moseeva MB, Azizova TV, Grigoryeva ES, Haylock R. Risks of circulatory diseases among Mayak PA workers with radiation doses estimated using the improved Mayak Worker Dosimetry System 2008. *Radiat Environ Biophys.* 2014;53:469-477.

doi: 10.1007/s00411-014-0517-x

69. Azizova TV, Muirhead CR, Moseeva MB, *et al.* Cerebrovascular diseases in nuclear workers first employed at the Mayak PA in 1948-1972. *Radiat Environ Biophys*. 2011;50(4):539-552.

doi: 10.1007/s00411-011-0377-6

70. Ruehm W, Breckow J, Dietze G, *et al.* Dose limits for occupational exposure to ionising radiation and genotoxic carcinogens: A German perspective. *Radiat Environ Biophys*. 2020;59(1):9-27.

doi: 10.1007/s00411-019-00817-x

71. UNSCEAR 2006 Report. *Efects of Ionizing Radiation. Annex B. Epidemiological Evaluation of Cardiovascular Disease and other Non-Cancer Diseases Following Radiation Exposure*. United Nations; 2006.

72. Authors on behalf of ICRP, Stewart FA, Akleyev AV, *et al.* ICRP publication 118: ICRP statement on tissue reactions and early and late effects of radiation in normal tissues and organs - threshold doses for tissue reactions in a radiation protection context. *Ann ICRP.* 2012;41(1-2):1-322.

doi: 10.1016/j.icrp.2012.02.001

73. Boerma M, Sridharan V, Mao XW, *et al.* Effects of ionizing radiation on the heart. *Mutat Res Rev Mutat Res*. 2016;770(Pt B):319-327.

doi: 10.1016/j.mrrev.2016.07.003

74. Puukila S, Lemon JA, Lees SJ, Tai TC, Boreham DR, Khaper N. Impact of ionizing radiation on the cardiovascular system: A review. *Radiat Res.* 2017;188(4.2):539-546.

doi: 10.1667/RR14864.1

75. Schultz-Hector S. Radiation-induced heart disease: Review of experimental data on dose response and pathogenesis. *Int J Radiat Biol*. 1992;61:149-160.

doi: 10.1080/09553009214550761

76. Baldwin J, Grantham V. Radiation hormesis: Historical and current perspectives. *J Nucl Med Technol*. 2015;43(4):242-246.

doi: 10.2967/jnmt.115.166074

77. Calabrese EJ. Linear non-threshold (LNT) fails numerous toxicological stress tests: Implications for continued policy use. *Chem Biol Interact.* 2022;365:110064.

doi: 10.1016/j.cbi.2022.110064

78. Doss M. Linear no-threshold model vs. radiation hormesis. *Dose Response*. 2013;11:480-497.

doi: 10.2203/dose-response.13-005.Doss

79. Scott BR. It's time for a new low-dose-radiation risk assessment paradigm-one that acknowledges hormesis. *Dose Response*. 2008;6:333-351.

doi: 10.2203/dose-response.07-005.Scott

80. Shibamoto Y, Nakamura H. Overview of biological, epidemiological, and clinical evidence of radiation hormesis. *Int J Mol Sci.* 2018;19:2387.

doi: 10.3390/ijms19082387

81. Little MP, Tawn EJ, Tzoulaki I, *et al.* Review and metaanalysis of epidemiological associations between low/moderate doses of ionising radiation and circulatory disease risks, and their possible mechanisms. *Radiat Environ Biophys*. 2010;49:139-53.

doi: 10.1007/s00411-009-0250-z

82. Jorgensen TJ. Dental x-rays and risk of meningioma. *Cancer*. 2013;119(2):463.

doi: 10.1002/cncr.27710

83. Kaludercic N, Deshwal S, Di Lisa F. Reactive oxygen species and redox compartmentalization. *Front Physiol.* 2014;5:285.

doi: 10.3389/fphys.2014.00285

84. Karam PA, Leslie SA. Calculations of background beta-gamma radiation dose through geologic time. *Health Phys.* 1999;77(6):662-667.

doi: 10.1097/00004032-199912000-00010

85. Mitchel RE. The dose window for radiation-induced protective adaptive responses. *Dose Response.* 2009;8:192-208.

doi: 10.2203/dose-response.09-039.Mitchel.

86. Higley KA, Kocher DC, Real AG, Chambers DB. Relative biological effectiveness and radiation weighting factors in the context of animals and plants. *Ann ICRP.* 2012;41:233-245.

doi: 10.1016/j.icrp.2012.06.014

87. Duffy DM. Fusion power: A challenge for materials science. *Philos Trans A Math Phys Eng Sci.* 2010;368(1923):3315-28.

doi: 10.1098/rsta.2010.0060

ACCSCIENCE PUBLISHING

Global Translational Medicine

ORIGINAL RESEARCH ARTICLE

Optimization of gelatin-based cell carriers for tooth-germ organoids

Anisha Jackson, Cemile Bektas, and Yong Mao*

Laboratory for Biomaterials Research, Department of Chemistry and Chemical Biology, Rutgers University, Piscataway, New Jersey, United States of America

(This article belongs to the *Special Issue: Soft and Hard Tissues Reconstruction in Dentistry*)

Abstract

Tooth loss is a widespread condition that significantly impacts quality of life, and effective functional treatments remain limited. Research in regenerative technologies is advancing toward solutions that are functional, customizable, and biologically integrative. Tooth-germ organoids – three-dimensional constructs cultured *in vitro* – hold promise for developing functional dental tissues. Hydrogel microparticles, selected for their structural support, resemblance to the natural extracellular matrix, and moldability, serve as carriers and scaffolds for organoid culture. Methacrylate gelatin microspheres (GelMA MS) have previously been identified as suitable scaffolds for dental organoids, as they support the composition of multiple cell types necessary for forming functional dental tissue. However, producing GelMA MS at a scale sufficient for tooth-organoid research is time-consuming and suffers from limited reproducibility. This study aims to develop alternative gelatin-based carriers with simpler, more reproducible fabrication processes that provide equal or enhanced support for tooth-germ organoid formation. Two alternative carriers – gelatin microspheres (Gel MS) and micronized photo-crosslinked GelMA microparticles (GelMA MP) – were evaluated in comparison to GelMA MS and GelMA hydrogel. Both Gel MS and GelMA MP were found to be more cost-effective, easier to produce, and more reproducible than GelMA MS. To assess their effectiveness as cell carriers, the growth and osteogenic differentiation of human dental pulp stem cells (hDPSCs) were directly compared across all carriers. Results showed that hDPSCs demonstrated significant proliferation and formed organoid-like clusters on both Gel MS and GelMA MP, similar to GelMA MS. Cell viability was higher on GelMA MS, GelMA MP, and Gel MS than in GelMA hydrogel, a commonly used cell carrier. Among the four cell carriers, Gel MS provided the best support for the growth and osteogenic differentiation of hDPSCs. This study identifies viable alternatives to GelMA MS and highlights the superior performance of Gel MS as a cell carrier, advancing tooth-germ organoid research and developing potential therapeutic applications.

Keywords: Gelatin microspheres; Methacrylate gelatin; Microparticles; Tooth; Organoids; Stem cells; Cell-carriers

***Corresponding author:**
Yong Mao
(maoy@dls.rutgers.edu)

Citation: Jackson A, Bektas C, Mao Y. Optimization of gelatin-based cell carriers for tooth-germ organoids. *Global Transl Med.* 2025:4(1):67-79.
doi: 10.36922/gtm.5897

Received: November 13, 2024

1st revised: December 11, 2024

2nd revised: December 24, 2024

Accepted: December 25, 2024

Published online: January 16, 2025

1. Introduction

Dental interventions can partially restore tooth functionality, but the ultimate goal of dental repair is the regeneration of natural teeth and associated dental tissues.[1] Among

the various stem cells used in tooth regeneration research, dental pulp stem cells (DPSCs) are considered an optimal choice due to their self-renewal capabilities and potential for multilineage differentiation.[2,3] DPSCs, derived from the pulp within the pulp chamber, play a crucial role in replenishing odontoblasts, contributing to dentin repair, and maintaining postnatal tooth homeostasis and repair.[2,4,5]

Recent advancements have highlighted tooth organoids – three-dimensional constructs containing multiple cell types, including DPSCs and dental epithelial cells – as a promising approach for tooth regeneration.[6-8] Unlike traditional two-dimensional cell cultures, organoids mimic the *in vivo* environment by providing a three-dimensional structure that supports complex cellular and structural interactions essential for growth and differentiation.[9] The three-dimensional nature of organoids allows the presence of structural properties and chemical signals that promote accurate cell differentiation, making them a powerful model for studying cellular behaviors outside of animal models.[9] Through cell-cell interactions, organoids support self-assembly, wherein cells drive scaffold aggregation to form organoids, and self-organization, in which cellular interactions organize different cell types to mimic natural tissue structure, providing a functional representation of *in vivo* tissues (Figure 1E).[10-12] Fine-tuning the scaffolding material is critical to successfully cultivating organoids that accurately replicate the structure and function of natural dental tissues.

Hydrogels (HG), biomaterials that mimic the natural cellular environment, are widely used in biomedical applications due to their crosslinked hydrophilic polymer networks, which allow them to retain large amounts of water within their three-dimensional networks.[13-15] Gelatin, derived from collagen (the most abundant protein in the extracellular matrix), interacts with cells and forms HG upon crosslinking. Methacrylate gelatin (GelMA), a derivative of gelatin modified with methacrylate anhydride, is photo-crosslinkable, allowing live cell encapsulation and crosslinking within GelMA HG.[16] Due to their biocompatibility and tunability, gelatin-based HG is frequently used in regenerative medicine, including tooth regeneration. Studies have shown that GelMA microspheres (GelMA MS) can be loaded with human DPSCs (hDPSCs) and injected into diseased dental pulp to support regeneration.[5] In addition, GelMA MS have been shown to support the growth of hDPSCs and human dental epithelial cells (hDECs) into organoid-like structures. Co-culturing organoids formed from hDECs and hDPSCs resulted in fused organoids with cell-cell interactions occurring between different cell types, closely resembling the natural tissue environment.[7] These results indicate the ability of GelMA MS as a scaffolding material for the formation of tooth organoids.

While GelMA MS is promising for tooth organoid development, larger-scale studies, and pre-clinical animal models are needed to validate their efficacy. Producing GelMA MS in high quantities requires a scalable and reproducible method.[7] The current production process is labor-intensive, involving high-speed mixing, temperature control, nitrogen purging, heat crosslinking, and extensive washing steps, resulting in microspheres of variable sizes and shapes that hinder reproducibility and scalability. Therefore, a simpler and more consistent production method is desired.

Given the photo-crosslinkable nature of GelMA, encapsulating single or multiple cell types within a three-dimensional HG is achievable. However, while encapsulated cells in GelMA HG remain viable, limited nutrient and waste diffusion can reduce cell viability and functionality compared to cells cultured on HG surfaces.[17,18] To increase surface area, photo-crosslinked GelMA HG can be micronized into GelMA microparticles (GelMA MP), which are easier to produce than GelMA MS. However, to evaluate the effectiveness of GelMA MP as a cell carrier, its ability to support cell growth and differentiation must be directly compared to that of GelMA MS.

Gelatin can also form microspheres (Gel MS), which have been shown to support human mesenchymal stem cell growth and functionality.[18,19] The production process of Gel MS is simpler and more reproducible, allowing easy sorting by size.[18]

In this study, we generated three types of gelatin-based HG microparticles and compared hDPSCs cultured on these carriers to cells encapsulated in GelMA HG. We evaluated hDPSC growth and osteogenic differentiation across the different carriers. Similar to GelMA MS, both GelMA MP and Gel MS supported the formation of organoid-like structures. Among the four carriers, Gel MS was most effective at supporting cell growth and differentiation, highlighting its potential as a superior scaffold for tooth organoid formation.

2. Materials and methods

2.1. Synthesis of methacrylated gelatin

The synthesis and characterization of GelMA were previously described.[7] The one-pot GelMA synthesis approach[20] provides several notable benefits over conventional methods, such as reduced reaction and purification times, improved batch-to-batch uniformity, and increased process control. Briefly, type A gelatin from porcine skin (300 bloom, Sigma Aldrich, United States) was

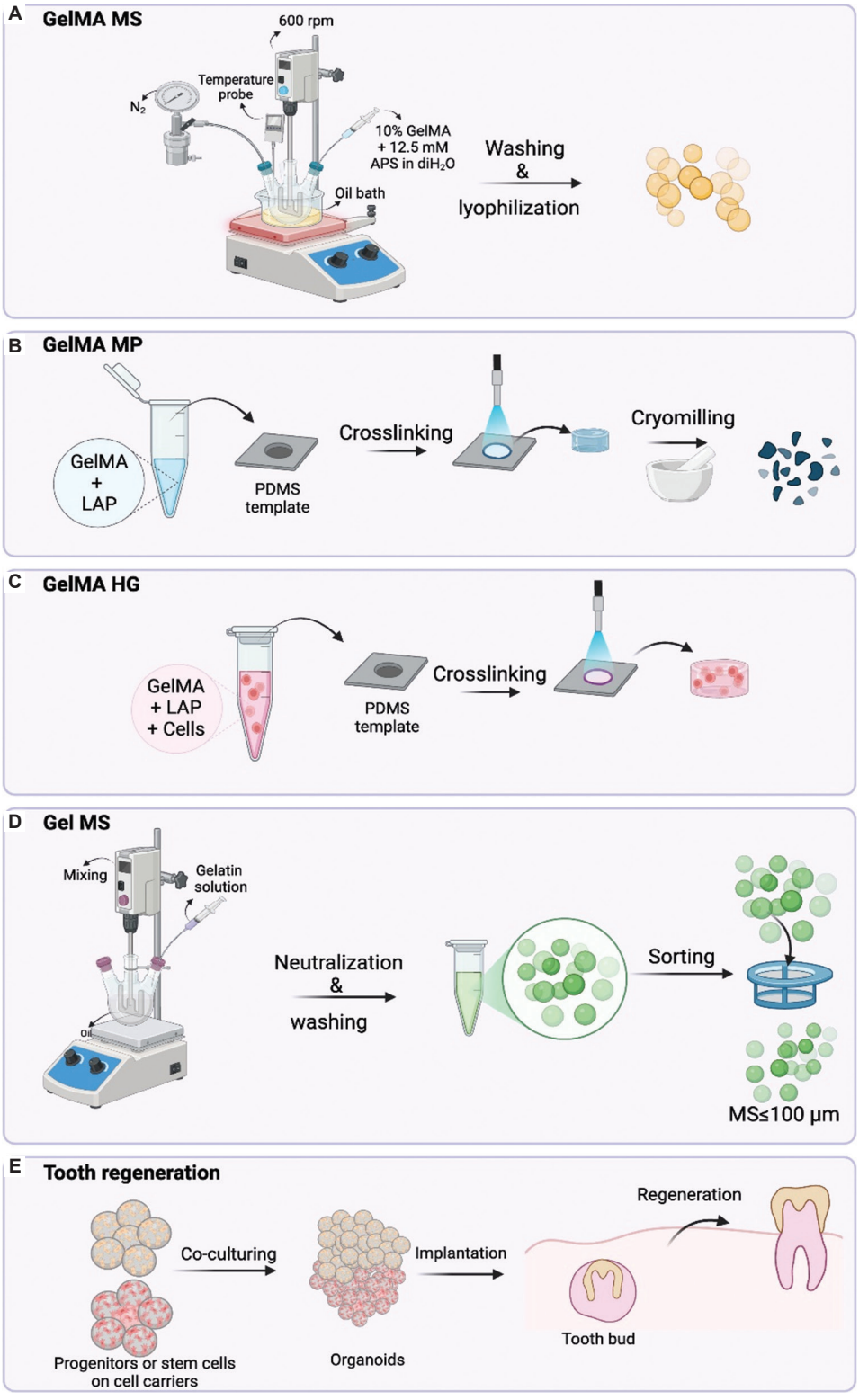

Figure 1. Schematic illustration of the fabrication processes for various cell carriers and the application of dental organoids. Key steps in the fabrication of methacrylate gelatin (GelMA) microspheres (MS) (A), GelMA microparticles (MP) (B), GelMA hydrogels (HG) (C), and Gel MS (D) are shown. The use of organoids in tooth regeneration is highlighted (E). Progenitor cells, including dental pulp stem cells (bottom) and dental epithelial cells (top), are shown. Implantation may be performed in the mandible.

Abbreviations: APS: Ammonium persulfate; diH_2O: Deionized water; LAP: Lithium phenyl-2,4,6-trimethylbenzoylphosphinate; N_2: Nitrogen gas; PDMS: Polydimethylsiloxane; rpm: Revolutions per minute.

dissolved at 10% w/v in 100 mL of 0.25 M, pH 9.4 carbonate-bicarbonate buffer (Sigma Aldrich, United States) at 55°C. The pH of the solution was adjusted to 9.4, and 0.938 mL methacrylic anhydride (Sigma Aldrich, United States) was added slowly under continuous magnetic stirring at 500 revolutions per minute (rpm) to achieve a targeted 100% degree of substitution. The reaction was continued for 1 h at 55°C and was stopped by lowering the pH to 7.4. After filtration, the solution was dialyzed for 2 days and lyophilized for use in subsequent experiments.

2.2. Preparation of methacrylated gelatin microspheres

Methacrylated gelatin microspheres were prepared as previously described.[7] Briefly, lyophilized GelMA was fully dissolved at 10% w/w in 5 mL of deionized water (diH_2O) at 37°C. Separately, 75 mL of mineral oil (Sigma Aldrich, United States) was heated to 37°C in a two-neck, 250-mL round-bottomed flask. To this, 1 mL of Tween 20 (Thermo Fisher Scientific, United States) was added and stirred at 600 rpm for 5 min. The 10% GelMA solution was mixed with 14 mg (12.5 mM) ammonium persulfate (Sigma Aldrich, United States) and added dropwise to the oil phase. The oil-water emulsion was stirred at 400 rpm for 5 min, and nitrogen gas was bubbled through the emulsion for 20 min at 45°C to purge oxygen. Under continuous stirring, the temperature was increased to 100°C for 40 min to allow for crosslinking.

After the reaction, the mixture was centrifuged at 2,500 rpm at 4°C to collect the GelMA MS pellet. The pellet was washed extensively with distilled water (diH_2O; including one overnight wash to remove residual surfactant), followed by 50%, 70%, and 100% acetone washes to remove oil residuals. Following the acetone washes, the GelMA MS was washed three times in diH_2O with a 15-min mixing before centrifugation to remove residual acetone (Figure 1A). The entire process took approximately 2 days. Finally, the pellet was lyophilized and stored at 4°C if not used immediately. The average size of rehydrated GelMA MS was determined by measuring the microsphere sizes using an optical light microscope (Echo Revolve, United States) and FIJI software (National Institute of Health [NIH ImageJ2 version:2.14.0/1.54f, USA).

2.3. Preparation of methacrylated gelatin microparticles

To prepare GelMA MP, a 10% (w/v) GelMA solution (10 mL) was prepared. A 1% stock solution of the photoinitiator lithium phenyl-2,4,6-trimethylbenzoylphosphinate (LAP, Sigma Aldrich, United States) was added to the GelMA solution to achieve a final concentration of 0.05% (w/v). The mixture was transferred to a polydimethylsiloxane (PDMS)-coated 6-well plate. Light crosslinking (405 nm; Sovol, China) was performed at 20 mW/cm^2 for 2 min at a distance of 13 cm from the top of each well, followed by flipping the gelled discs and repeating the light crosslinking on the opposite side of the GelMA HG discs. The solidified GelMA HG was cut into approximately 3 mm × 3 mm pieces and frozen at -80°C or in liquid nitrogen. Once frozen, the GelMA pieces were transferred to a pre-chilled pestle and mortar and ground into fine particles by repeated grinding motions (Figure 1B). This process took about 1 h. The particles were collected and lyophilized. The average size of rehydrated GelMA MP was determined by measuring the longest side of irregular shaped microparticles using an optical light microscope (Echo Revolve) and FIJI software (NIH ImageJ2).

2.4. Preparation of methacrylate gelatin hydrogel-containing cells

Methacrylate gelatin hydrogels are widely used as cell carriers.[21,22] In this study, GelMA HG-containing cells were used as the control. Briefly, 15 µL of 10 mg/mL LAP and 85 µL of culture media were added to 200 µL of 15% w/v GelMA solution containing 1.5 × 10^6 hDPSCs. After thorough mixing, 30 µL of this mixture (with a final GelMA concentration of 10%) was transferred to a PDMS mold (6 mm in diameter) and crosslinked for 40 s using a 405 nm light source (Sovol, China). The gelled GelMA HG discs contained 3 mg of GelMA (dry weight) per disc and 1.5 × 10^5 cells per disc. The GelMA HG discs were rinsed with PBS and cultured in a 48-well cell-repellent plate (Greiner Bio-One, Austria) in a cell culture medium. The entire process of preparing GelMA HG with cells took approximately 30 min (Figure 1C).

2.5. Preparation of gelatin microspheres

Gelatin microspheres were synthesized using a modified water-in-oil polymerization method as described previously.[18] Briefly, two grams of porcine type A gelatin was dissolved in 10 mL of distilled water at 55°C to create a clear solution. The gelatin solution was then added dropwise to pre-heated olive oil (Ward's Science, United States) at 40°C, under constant stirring at 500 rpm. The water-in-oil emulsion was mixed for 30 min at 40°C, then immediately cooled to 4°C. To crosslink, 20 mL of chilled acetone containing 200 µL of 25% glutaraldehyde was added slowly using a syringe, tubing, and an 18 G needle. After fixing at 4°C for 1 h, the oil and acetone phases were removed. The Gel MS pellets were washed with acetone, followed by centrifugation at 3,400 rpm at 4°C for 5 min. After three washes with acetone, 20 mL of 10 mM glycine was added to the Gel MS to neutralize residual

glutaraldehyde. After glycine treatment, the Gel MS was washed three times with diH_2O. The Gel MS mixture was passed through a 100 μm cell strainer (Corning Inc., United States) (Figure 1D). This process typically takes approximately 8 h. The filtered Gel MS (≤100 μm) was then lyophilized and stored at 4°C until use.

2.6. Culture of hDPSCs

The hDPSCs were kindly provided by Dr. Pamela Yelick and Dr. Weibo Zhang from Tufts University.[7] Cells (passages 5 – 9) were cultured in minimum essential medium (MEM)-alpha (HyClone, United States) supplemented with 10% fetal bovine serum (CPS Serum, United States) and 25 μg/mL of gentamicin (Sigma-Aldrich, USA) in tissue culture-treated polystyrene plates (CELLTREAT, United States). Cells were sub-cultured when they reached 80% confluence, if not immediately used for experiments.

2.7. hDPSC seeding on different gelatin-based cell carriers

Three milligrams of lyophilized GelMA MS, GelMA HP, or GelMS were sterilized under ultraviolet light for 30 min (n=4 for each group). After sterilization, the samples were transferred to sterile Eppendorf tubes. Each tube was filled with 1 mL of MEM-alpha complete medium and centrifuged at room temperature for 1 – 2 h to facilitate rehydration. After rehydration, the medium was removed from each tube.

hDPSCs were trypsinized and collected after reaching 80% confluence. One hundred μL of 1.5×10^6/mL hDPSC suspension (1.5×10^5 cells/sample) was added to each tube. The cells were mixed with the cell carriers using pipette tips and incubated in the tubes in a tissue culture incubator for 30 min, with gentle mixing every 10 min. Following the initial cell seeding, 200 μL of complete medium was added to each tube. The mixed cells and carriers were then transferred to the wells of a 48-well cell-repellent plate and cultured statically overnight. After 48 h, the culture was continued with gentle shaking (200 rpm) on a BT4500 CO_2 Orbi-Shaker (Benchmark Scientific, United States) in the tissue culture incubator. The medium was changed every 3 days.

2.8. Viable cell staining with calcein acetoxymethyl ester

After 10 days of culture, cells on/in the carriers were stained with the live dye calcein, following the manufacturer's instructions. Briefly, the samples were treated with calcein acetoxymethyl ester (AM; 1 μM in growth medium) (Corning Inc., United States) for 30 min in the cell culture incubator. After staining, the samples were washed with PBS and visualized using a fluorescence microscope (Echo Revolve, United States).

2.9. Cell viability monitoring using a metabolic activity assay

Cell viability on/in the cell carriers was assessed using the alamarBlue assay (Bio-Rad Laboratories, United States). After 10 days of culture, 0.3 mL of alamarBlue solution (complete growth medium + 10% alamarBlue reagent) was added to each well and incubated at 37°C for 30 min. After incubation, 0.1 mL of the supernatant was transferred to a 96-well plate, and fluorescence intensity was measured using a multimode microplate reader (Spark®, Tecan Life Sciences, Switzerland) at excitation/emission wavelengths of 540 nm/590 nm. The fluorescent intensity was reported in arbitrary units.

2.10. Deoxyribonucleic acid quantification

Cells were released from aggregates or HG by enzymatic digestion with 0.5 mg/mL collagenase in PBS for 2 h in a 37°C incubator shaking at 200 rpm. After digestion, samples were treated with a cell lysis buffer (Cell Signaling Technology, United States) containing 0.5% sodium dodecyl sulfate (Fisher Scientific, United States). The released deoxyribonucleic acid (DNA) from cells cultured on/in cell carriers was quantified using the Helixyte Green dsDNA Assay Kit (AAT Bioquest, Pleasanton, CA, USA) following the manufacturer's protocol.

2.11. Osteogenic differentiation of hDPSCs on/in various cell carriers

After hDPSCs were cultured on GelMA MS, GelMA HP, Gel MS, or in GelMA HG for 10 days, one set of samples underwent osteogenic differentiation. Osteogenic medium (growth medium containing 10% fetal bovine serum, supplemented with 20 mM β-glycerophosphate, 50 μg/mL ascorbic acid, and 100 nM dexamethasone; Sigma-Aldrich, United States) was added to each well at a volume of 0.4 mL/well.[23] A control set was cultured in growth medium for the same duration. The induction or growth medium was changed every 3 days for a total of 10 days.

2.12. Staining and quantification of osteogenic differentiation

To evaluate osteogenic differentiation of hDPSCs on/in different carriers, samples were stained with 0.2 mL/well of alizarin red solution (EMD Millipore Corp., United States) for 5 min after 10 days of induction. Alizarin red stains the calcium deposits formed during osteogenic differentiation of stem cells. The stained samples were washed in excess water and examined under a light microscope. Color (red, green, blue [RGB]) images were captured using an Echo Revolve Microscope (Echo Revolve, United States) with a 10× objective. To quantify the intensity of red staining in each image, at least 15 images from each group were

analyzed using the NIH ImageJ software. The RGB_Measure.java plugin java file was used to measure the red channel intensity of each sample. Data were then analyzed using GraphPad Prism version 10.3.1 (United States).

2.13. Statistical analysis

For each experiment, biological repeats ($n \geq 3$) were used, and data are presented as mean ± standard deviation. One-way ANOVA with Tukey's multiple comparisons test was performed to determine statistical significance, using GraphPad Prism version 10.3.1. Differences were considered significant at a $P < 0.05$.

3. Results and discussion

3.1. Fabrication and characterization of gelatin-based cell carriers

To explore additional cell carrier options for culturing hDPSCs, four configurations of gelatin-based HG materials were prepared.

3.1.1. Methacrylate gelatin microspheres

Methacrylate gelatin microspheres were produced using a water-in-oil emulsion method, followed by ammonium persulfate-initiated thermal crosslinking.[7] This process involves multiple high-temperature steps (e.g., 100°C) and requires the use of surfactants, nitrogen purging, and extensive washing (Figure 1A). It typically takes about 2 days to obtain a clean batch ready for lyophilization. The labor-intensive, multi-step nature of this method contributes to significant batch-to-batch variability, presenting challenges for scaling up the process. The hydrated GelMA MS, which was measured to range from 50 to 250 µm with an average size of 134.75 ± 69.2 µm, was used in this study (Figure 2A and E). This wide size range further underscores the challenges in producing large, uniform batches of GelMA MS, which could hinder the scalability required for larger studies. The characterization of these GelMA MS has been reported in our previous study.[7] Once lyophilized, GelMA MS remain shelf-stable when stored at 4°C, allowing for off-the-shelf use.

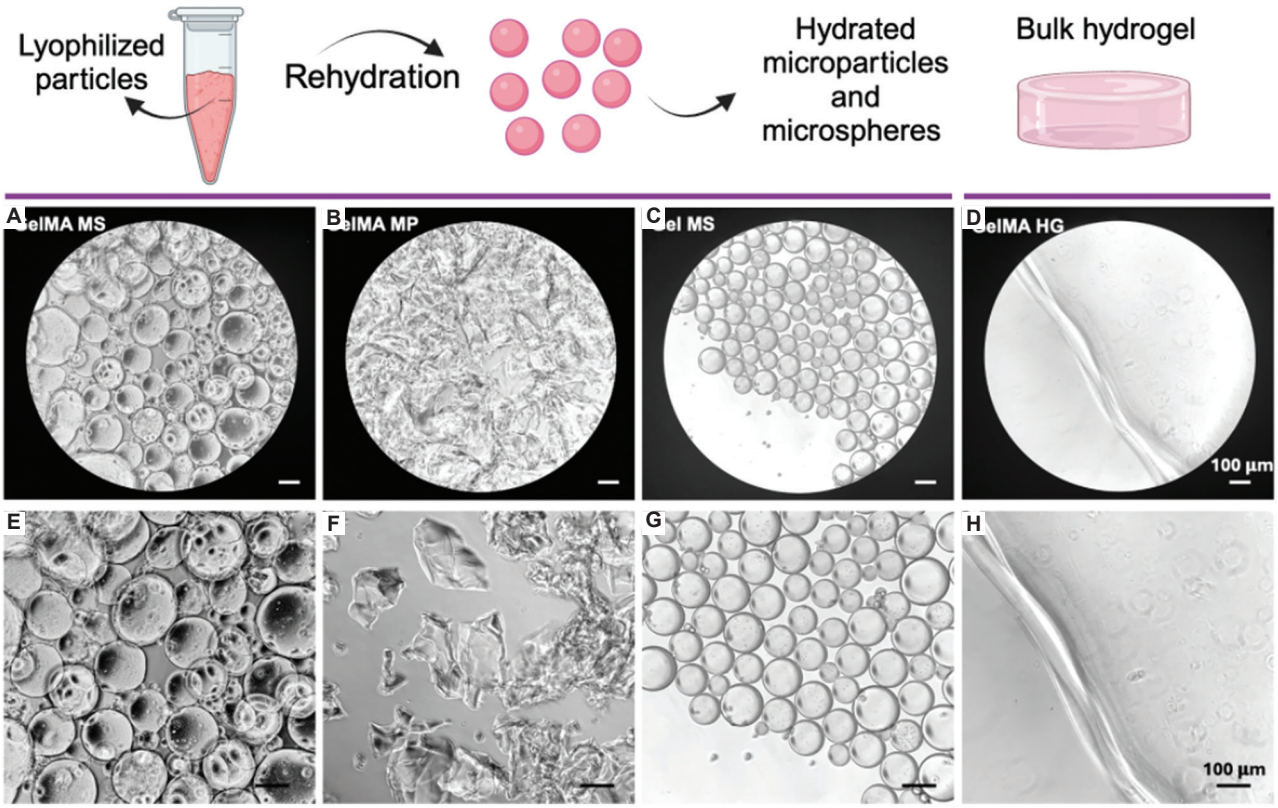

Figure 2. Morphologies of various gelatin-based carriers. Lyophilized cell carriers were rehydrated in cell culture medium for 1 h. Representative phase-contrast images of rehydrated methacrylate gelatin (GelMA) microspheres (MS) (A and E), GelMA microparticles (MP) (B and F), and gelatin microspheres (Gel MS; C and G) were captured using a light microscope. Crosslinked GelMA hydrogel (GelMA HG) without cells are shown in D and H. Scale bar = 100 µm; Magnification power for A–D=100×; Magnification power for E–H = 170×.

3.1.2. Methacrylate gelatin microparticles

Photocrosslinking offers a simple and reproducible approach for preparing GelMA HG.[24] To increase the surface area, the crosslinked GelMA HG was frozen at −80°C or in liquid nitrogen, then micronized using a mortar and pestle (Figure 1B). Mechanical fragmentation is a widely adopted technique due to its simplicity and efficiency in producing hydrogel microparticles (HMPs). This method facilitates the rapid generation of substantial quantities of MP in a single, streamlined procedure.[25] In this study, the process yielded MP with a heterogeneous range of sizes and shapes, completed in approximately 1 h. The average size (measured along the longitude axis) was 147.83 ± 54.02 μm (Figure 2B and F). Lyophilized GelMA MP remains stable when stored at 4°C and can be used off-the-shelf.

3.1.3. Methacrylate gelatin hydrogels

Encapsulating cells in photocrosslinked GelMA HG is a commonly used method for cell delivery due to its ease of size and shape determination and the low cytotoxicity of photocrossslinking on cells.[21,22] In this study, hDPSCs were mixed with a solubilized GelMA solution and encapsulated within the GelMA HG matrix using LAP-initiated photocrosslinking (Figure 1C). The encapsulation process took approximately 30 min post-cell preparation. GelMA HG without cells appeared transparent and smooth (Figure 2D and H). The GelMA HG with embedded cells demonstrated a uniform distribution throughout both the surface and interior of the construct, as expected. HG dimensions can be easily adjusted by modifying the mold and gel volume; in this study, a 6 mm diameter and 1 mm thickness were used. Encapsulated hDPSCs in GelMA HG served as the reference for comparison with other cell carriers.

3.1.4. Gelatin microspheres

In this configuration, gelatin (rather than GelMA) was used as the starting material. Gel MS were formed using the water-in-oil emulsion technique, followed by glutaraldehyde-mediated crosslinking and subsequent washing, filtration, and lyophilization for long-term storage. The gentle processing conditions allow for the integration of proteins, drug compounds, or cells during the fabrication of HMPs.[26,27] Microsphere sizes were selected by passing them through cell strainers with the desired pore sizes[18] (Figure 1D). Preparation of Gel MS typically takes approximately 8 h, including glutaraldehyde neutralization and multiple washes. The average size of the Gel MS used in this study was 109.47 ± 19.15 μm (Figure 2C and G). Previous studies have shown that this size is most efficient for supporting cell growth, as opposed to larger sizes of Gel MS.[18] Once lyophilized, Gel MS remains stable at 4°C and is suitable for off-the-shelf use.

As shown in Figure 2, GelMA MS and Gel MS displayed relatively uniform spherical shapes, while GelMA MP exhibited a range of sizes and shapes. In addition, the surfaces of the GelMS, GelMA MP, and GelMA HG appeared smooth (Figure 2), while the surface of the GelMA MS showed notable surface topography, likely resulting from the harsh processing conditions at high temperatures and extended washing steps. The key characteristics of each cell carrier are summarized in Table 1.

3.2. Evaluation of hDPSC growth on/in various cell carriers

To assess the ability of different carriers to support hDPSC growth, GelMA MS, GelMA MP, and Gel MS were rehydrated using equal dry weights, while GelMA HG was prepared with an equivalent weight of GelMA powder. Equal numbers of hDPSCs were then seeded onto each carrier or encapsulated within GelMA HG. After 10 days of culture, cell-laden GelMA MS, GelMA MP, and Gel MS carriers formed aggregates (Figure 3A[v–vii]), whereas the corresponding cell-free controls remained separate (Figure 3A[ix–xi]), consistent with previous studies conducted using only GelMA MS.[7] Viable cells on each carrier were visualized by calcein AM staining, where green fluorescence indicated cell viability (Figure 3A). Fluorescent intensity was strongest on Gel MS (Figure 3A[iii]) and particularly prominent on the surfaces of GelMA MS and GelMA MP (Figure 3A[i and ii]). In GelMA HG, higher cell viability was observed on the HG surface than within the matrix (Figure 3A[iv]).

Table 1. Key characteristics of the gelatin-based cell carriers used in this study

Cell carrier	Average size (μm)	Shapes	Crosslinking	Processing time	Batch variability
GelMA MS	134.8±69.2	Spheres	Thermal	2 days	Medium
GelMA MP	147.8±54.0	Irregular	Photo	1 h	Minimal
Gel MS	109.5±19.1	Spheres	Glutaraldehyde	8 h	Minimal
GelMA HG	6×1[a]	Disc	Photo	0.5 h	Minimal

Note: [a]Average size is reported in diameter × thickness in mm.
Abbreviations: GelMA HG: Methacrylate gelatin hydrogel; GelMA MP: Methacrylate gelatin microparticles; GelMA MS: Methacrylate gelatin microspheres; Gel MS: Gelatin microspheres.

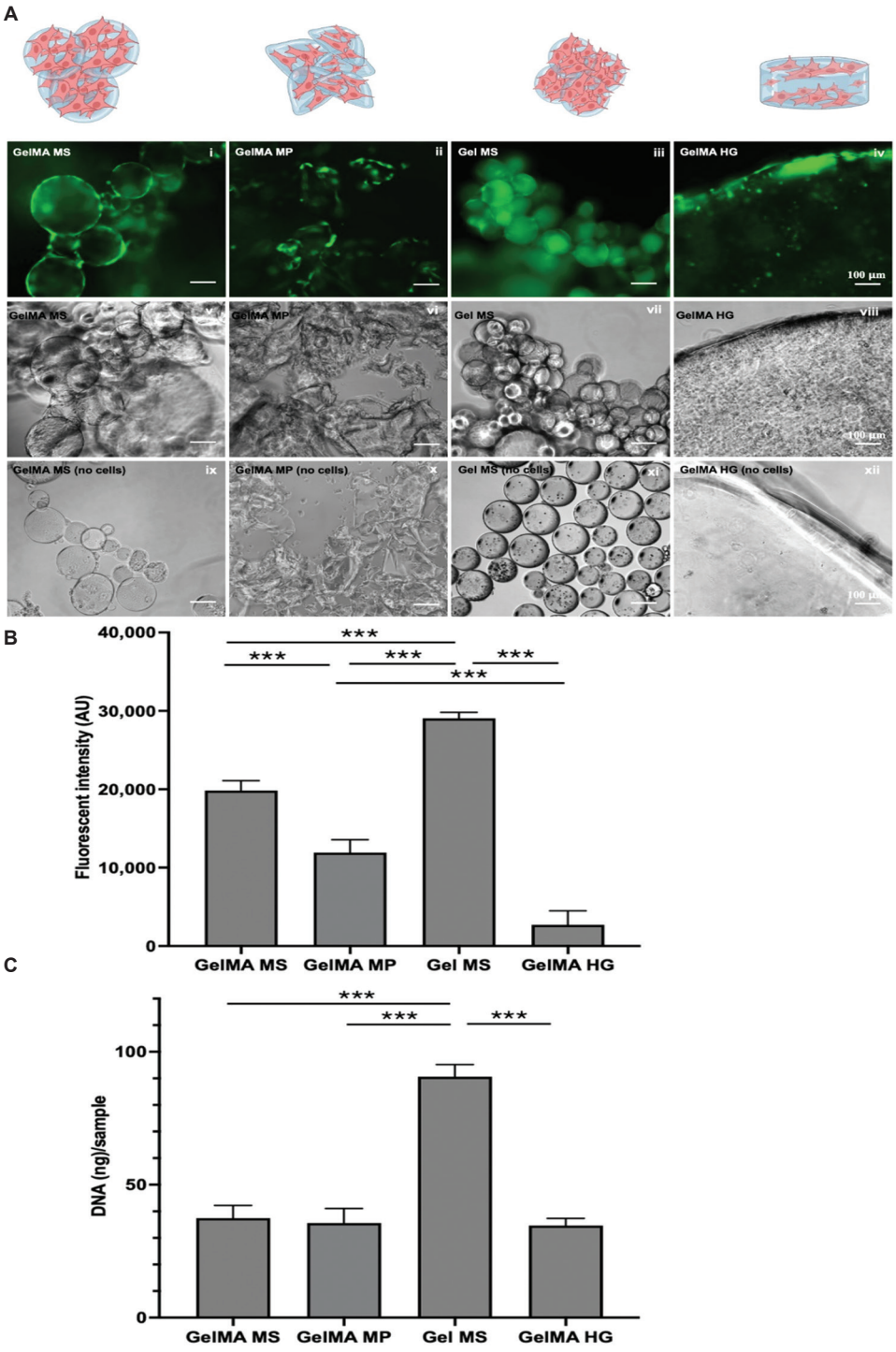

Figure 3. Viability of cells on/in different cell carriers. Cells were cultured on or in different carriers for 10 days. The samples were stained with calcein acetoxymethyl ester. (A) Representative fluorescent images (upper row of A) and phase-contrast images (middle row of A) are shown. The carriers without cells (lower row of A) showed no aggregation. Scale bar = 100 μm; magnification power = 100×. (B) The metabolic activity of cells on/in the carriers was measured using the alamarBlue assay. (C) Deoxyribonucleic acid (DNA) released from each sample after the dissolution of aggregates or hydrogel was quantified using the Helixyte DNA assay. Data are presented as mean ± standard deviation ($n = 4$; $^{***}P < 0.005$).
Abbreviations: AU: Arbitrary units; GelMA HG: Methacrylate gelatin hydrogel; GelMA MP: Methacrylate gelatin microparticles; GelMA MS: Methacrylate gelatin microspheres; Gel MS: Gelatin microspheres.

GelMA HG possesses a crosslinked structure that forms a bulk HG, which may hinder effective nutrient and waste exchange between embedded cells and their surrounding environment.[28] In contrast, cells in GelMA MS and Gel MS exhibited an elongated morphology and spanned between microparticles (Figure 3A[i, iii, v, vii]), whereas cells in GelMA HG and maintained a non-elongated morphology (Figure 3A[iv and viii]). This cellular arrangement promotes aggregation, suggesting enhanced cell-cell contact and communication compared to GelMA HG, where cells were only elongated on the HG surface and remained rounded within the bulk HG. Studies have shown that cell-cell communication is important for the viability and functionality of hDPSCs in tooth organoid formation.[29] Furthermore, the observed 3D structure and cell spreading likely enhance both cell-cell and cell-scaffold mechanical interactions, which are essential for maintaining stem cell viability.[30]

Cell viability was further quantified using the alamarBlue assay to assess metabolic activity (Figure 3B). Notably, cells on Gel MS exhibited significantly higher metabolic activity than those on GelMA MS or GelMA MP. Between GelMA MS and GelMA MP, which share the same material composition, GelMA MS supported significantly higher viability. Although GelMA MP is expected to provide more surface area than spherical GelMA MS, the lower metabolic activity observed suggests that factors such as surface curvature may influence cell adhesion, proliferation, or metabolism beyond surface area alone. Among all four carriers, GelMA HG showed the lowest cell viability.

Since the alamarBlue assay may not accurately reflect cell counts due to reagent permeability limitations in aggregates or HG,[28] DNA quantification was conducted as an additional measure.[28] After treating the samples with type I collagenase to dissolve aggregates or the HG, released DNA was measured using the Helixyte DNA assay (Figure 3C). Consistent with the metabolic activity results, Gel MS supported the highest cell growth based on DNA content. Interestingly, DNA quantities on GelMA MS, GelMA MP, and in GelMA HG were similar. The similar DNA levels between GelMA MS and GelMA MP indicated comparable cell numbers on these two carriers. This result may highlight the differential effects that size, crosslinking methods, and geometries have in promoting cell viability. Although the reason for the higher metabolic activity of cells in GelMA MS compared to GelMA MP (Figure 3B) remains unclear, Calcein AM staining revealed elongated cells on the surfaces of GelMA MS (Figure 3A[i]), whereas staining on GelMA MP appeared punctuated and discrete (Figure 3A[ii]). Increased cell spreading is known to raise metabolic rates,[31] which may contribute to the higher metabolic activity on GelMA MS. Factors such as size distribution, porosity, and surface topography likely influence the rate and effectiveness of nutrient exchange within the constructs, as well as the available surface area for cell adhesion and growth.[32,33] These characteristics may differ between carriers due to their respective fabrication methods and crosslinking agents.[34]

Cell viability in GelMA HG may be underestimated due to limited reagent permeability in and out of the HG in the metabolic assay (Figure 3B). Conversely, DNA measured from dissolved GelMA HG might include DNA from dead cells trapped in the HG, potentially overestimating cell numbers. Although neither assay provides a definitive measure of cell growth on GelMA-based carriers, both consistently showed that Gel MS supported the highest hDPSC growth, which was consistent with phase image observations (Figure 3A[v-viii]).

3.3. Osteogenic differentiation of hDPSCs on/within different cell carriers

To support tooth regeneration, hDPSCs in organoid cultures undergo lineage-specific differentiation.[7,35] Osteogenic and odontogenic differentiation are commonly used to assess the differentiation potential of hDPSCs in tooth tissue applications, as these cell types share similarities, and hDPSCs have been shown to be capable of differentiating into both lineages.[36] To assess the osteogenic differentiation potential of hDPSCs on/in various carriers, cell aggregates were cultured in osteogenic medium for 10 days. These organoid-like aggregates, both with and without osteogenic induction, were then stained with alizarin red solution (Figure 4). Alizarin red stains calcium deposited by osteogenically differentiated cells. Osteogenically-induced samples (Figure 4A, upper panel) displayed significantly stronger red staining compared to uninduced samples (Figure 4A, lower panel), with the exception of GelMA HG. Interestingly, GelMA HG without cells also showed strong staining (Figure 4A), indicating possible non-specific dye binding or inefficient dye elution from GelMA HG despite extensive washing steps.

In aggregates, intense red staining was localized to areas where cells aggregated between particles (Figure 4A[i–iii]), while in GelMA HG, staining was more pronounced on the surface where elongated cells were located (Figure 4A[iv]). This pattern aligns with viability assays, which indicated higher viability of cells grown on GelMS MS, GelMS MP, and Gel MS throughout organoid-like structures, compared to the lower viability of hDPSCs encapsulated in GelMA HG. These findings suggest that cell-cell interactions and elongation facilitated differentiation, as these phenomena

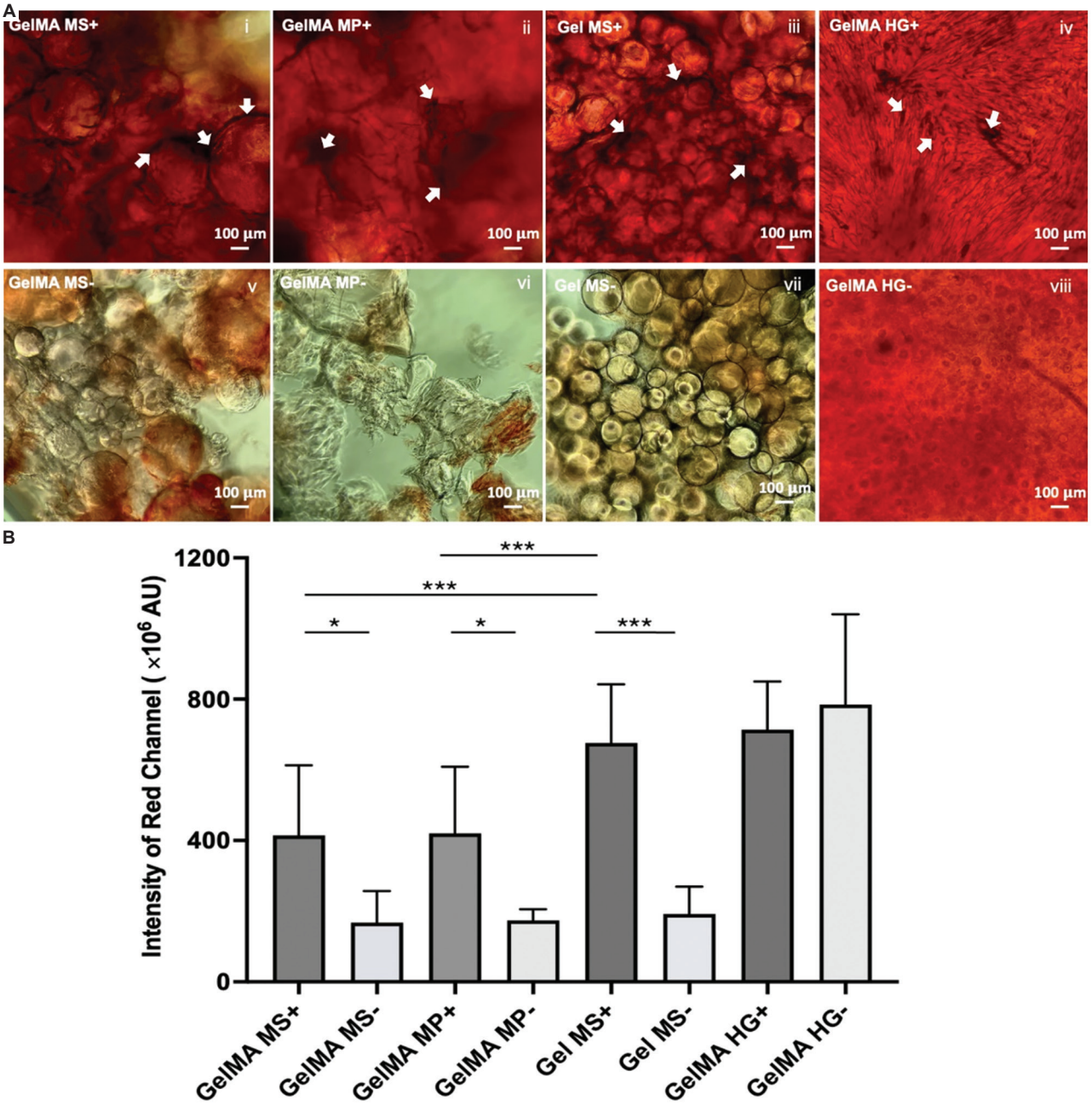

Figure 4. Osteogenic induction of human dental pulp stem cells (hDPSCs) on/in different carriers. hDPSCs cultured on/in different carriers for 10 days, followed by incubation in osteogenic induction medium (upper row) or growth medium (lower row) for an additional 10 days. Samples were stained with alizarin red solution and subjected to extensive washes. (A) Representative images of GelMA MS (i and v), GelMA MP (ii and vi), Gel MS (iii and vii), and GelMA HG (iv and viii) are shown. Representative calcium deposits are indicated by white arrows. Scale bar=100 µm; magnification power = 100×. (B) Staining was semi-quantitatively measured using ImageJ. Data are presented as mean ± SD ($n > 15$; $^{*}P < 0.05$, $^{***}P < 0.005$).
Abbreviations: AU: Arbitrary units; GelMA HG: Methacrylate gelatin hydrogel; GelMA MP: Methacrylate gelatin microparticles; GelMA MS: Methacrylate gelatin microspheres; Gel MS: Gelatin microspheres.

predominantly occurred between the particles. Increased cell-cell communication and cell density have been shown to promote osteogenic differentiation of hDPSC.[37] The distribution of calcium deposits throughout the constructs in GelMA MS, GelMA MP, and Gel MS may offer advantages in tooth organoid generation compared to the surface-limited deposits observed in GelMS HG, potentially leading to improved distribution of deposited

material and structural properties in tooth-germ organoids. This property is crucial, as material distribution during differentiation directly influences tooth germ development.[38] Staining intensity was semi-quantitatively analyzed using ImageJ software, examining over five images per sample (>15 images per group) to assess levels of osteogenic differentiation (Figure 4B). Across all groups except GelMA HG, cells subjected to osteogenic induction showed significantly stronger staining compared to those in growth medium (+ versus -). Notably, induced cells on Gel MS (Gel MS+) exhibited stronger staining compared to those on GelMA MS or GelMA MP. The higher cell density on Gel MS may contribute to these observed differences in intensity. In addition, factors such as sphere diameter, curvature, and size distribution have been shown to influence the osteogenic differentiation of stem cells.[39] Substrate stiffness is also known to affect the osteogenic differentiation of stem cells, as reported in several studies.[40-42] The Gel MS, GelMA MP, GelMA MS, and GelMA HG synthesized in this study have not been characterized for mechanical properties such as stiffness, which may differ due to the various crosslinking methods used.[43] Exploring the role of these features in cell differentiation on cell carriers could provide valuable insights into their impact on hDPSC differentiation and their potential as scaffolds.

The mechanisms underlying the differential effects of various cell carriers on hDPSCs require further investigation. Once these mechanisms are fully understood, it will be possible to develop cell carriers with optimized features that facilitate tooth-germ organoid formation and harness the advantages of multiple attributes. Using a combination of heterogeneous cell carriers to maximize the benefits of diverse features could also be a viable approach. Future studies will assess contributing factors such as base materials (gelatin versus GelMA) and particle sizes. In addition, to determine whether these *in vitro* observations are translatable to *in vivo* conditions and whether these organoids can support tooth regeneration, pre-clinical studies will be essential.

Our results suggest that Gel MS not only provides superior support for cell growth but also promotes osteogenic differentiation in organoid-like aggregates of hDPSCs. Among the four cell carriers tested, Gel MS stands out as a promising candidate for dental organoid formation. Notably, GelMA MS and GelMA MP showed similar capabilities in supporting cell growth and differentiation. However, given that the production of GelMA MP is simpler, more reproducible, and scalable than that of GelMA MS, GelMA MP may serve as a practical alternative. Importantly, the photocrosslinking of GelMA MP does not compromise protein integrity, making it suitable for the incorporation of growth factors, immune modulators, or cytokines.[22] This dual-functionality carrier holds promise for applications in other tissue regeneration contexts as well.

4. Conclusion

Tooth organoids hold great promise for supporting tooth regeneration, creating a demand for cell carriers that are not only biocompatible and effective but also scalable for clinical applications. In this study, we compared four different gelatin-based cell carriers to evaluate their ability to support the growth and differentiation of hDPSCs. Our results demonstrate that Gel MS, produced through a reproducible and scalable process, most effectively supported cell growth and osteogenic differentiation of hDPSCs compared to GelMA-based carriers (GelMA MS and GelMA MP). While further research is needed to elucidate the mechanisms underlying the differential effects of these carriers, Gel MS has emerged as a strong candidate for tooth organoid generation. Moving forward, pre-clinical studies using Gel MS will be crucial to determine its effectiveness *in vivo* and its potential to support tooth regeneration in clinical settings.

Acknowledgments

The authors would like to express their gratitude to Dr. Pamela Yelick and Dr. Weibo Zhang at Tufts University for providing hDPSCs. The authors also thank Dr. Derya Ozhava, Peter Winkler, and Krishi Patel for their technical assistance. Anisha Jackson acknowledges the support of the Aresty Research Center at Rutgers University. All illustrations in this report were created using Biorender software.

Funding

None.

Conflict of interest

The authors declare that they have no competing interests.

Author contributions

Conceptualization: All authors
Methodology: All authors
Investigation: Anisha Jackson, Yong Mao
Visualization: All authors
Writing – original draft: Anisha Jackson, Yong Mao
Writing – review & editing: All authors

Ethics approval and consent to participate

Not applicable.

Consent for publication

Not applicable.

Availability of data

All data and materials are available upon request from the corresponding author. The data are not publicly available due to ongoing research that involves part of the data.

References

1. Zhang W, Yelick PC. Tooth repair and regeneration: Potential of dental stem cells. *Trends Mol Med*. 2021;27(5):501-511.

   doi: 10.1016/j.molmed.2021.02.005

2. Gronthos S, Mankani M, Brahim J, Robey PG, Shi S. Postnatal human dental pulp stem cells (DPSCs) *in vitro* and *in vivo*. *Proc Natl Acad Sci U S A*. 2000;97(25):13625-13630.

   doi: 10.1073/pnas.240309797

3. Zhang W, Saxena S, Fakhrzadeh A, *et al*. Use of human dental pulp and endothelial cell seeded tyrosine-derived polycarbonate scaffolds for robust *in vivo* alveolar jaw bone regeneration. *Front Bioeng Biotechnol*. 2020;8:796.

   doi: 10.3389/fbioe.2020.00796

4. Zhang W, Abukawa H, Troulis MJ, Kaban LB, Vacanti JP, Yelick PC. Tissue engineered hybrid tooth-bone constructs. *Methods*. 2009;47(2):122-128.

   doi: 10.1016/j.ymeth.2008.09.004

5. Zheng L, Liu Y, Jiang L, *et al*. Injectable decellularized dental pulp matrix-functionalized hydrogel microspheres for endodontic regeneration. *Acta Biomater*. 2023;156:37-48.

   doi: 10.1016/j.actbio.2022.11.047

6. Farshbaf A, Mottaghi M, Mohammadi M, *et al*. Regenerative application of oral and maxillofacial 3D organoids based on dental pulp stem cell. *Tissue Cell*. 2024;89:102451.

   doi: 10.1016/j.tice.2024.102451

7. Kilic Bektas C, Zhang W, Mao Y, Wu X, Kohn J, Yelick PC. Self-assembled hydrogel microparticle-based tooth-germ organoids. *Bioengineering* (*Basel*). 2022;9(5):215.

   doi: 10.3390/bioengineering9050215

8. Sloan AJ, Smith AJ. Stem cells and the dental pulp: Potential roles in dentine regeneration and repair. *Oral Dis*. 2007;13(2):151-157.

   doi: 10.1111/j.1601-0825.2006.01346.x

9. Lehmann R, Lee CM, Shugart EC, *et al*. Human organoids: A new dimension in cell biology. *Mol Biol Cell*. 2019;30(10):1129-1137.

   doi: 10.1091/mbc.E19-03-0135

10. Misteli T. The concept of self-organization in cellular architecture. *J Cell Biol*. 2001;155(2):181-185.

    doi: 10.1083/jcb.200108110

11. Kim J, Koo BK, Knoblich JA. Human organoids: Model systems for human biology and medicine. *Nat Rev Mol Cell Biol*. 2020;21(10):571-584.

    doi: 10.1038/s41580-020-0259-3

12. Cacciamali A, Villa R, Dotti S. 3D cell cultures: Evolution of an ancient tool for new applications. *Front Physiol*. 2022;13:836480.

    doi: 10.3389/fphys.2022.836480

13. Revete A, Aparicio A, Cisterna BA, *et al*. Advancements in the use of hydrogels for regenerative medicine: Properties and biomedical applications. *Int J Biomater*. 2022;2022:3606765.

    doi: 10.1155/2022/3606765

14. Bektas C, Mao Y. Hydrogel microparticles for bone regeneration. *Gels*. 2023;10(1):28.

    doi: 10.3390/gels10010028

15. Ahmed EM. Hydrogel: Preparation, characterization, and applications: A review. *J Adv Res*. 2015;6(2):105-121.

    doi: 10.1016/j.jare.2013.07.006

16. Kilic Bektas C, Hasirci V. Mimicking corneal stroma using keratocyte-loaded photopolymerizable methacrylated gelatin hydrogels. *J Tissue Eng Regen Med*. 2018;12(4):e1899-e1910.

    doi: 10.1002/term.2621

17. Carpentier N, Ye SC, Delemarre MD, *et al*. Gelatin-based hybrid hydrogels as matrices for organoid culture. *Biomacromolecules*. 2024;25(2):590-604.

    doi: 10.1021/acs.biomac.2c01496

18. Ozhava D, Bektas C, Lee K, Jackson A, Mao Y. Human mesenchymal stem cells on size-sorted gelatin hydrogel microparticles show enhanced *in vitro* wound healing activities. *Gels*. 2024;10(2):97.

    doi: 10.3390/gels10020097

19. Kong YQ, Li D, Wang LJ, Adhikari B. Preparation of gelatin microparticles using water-in-water (W/W) emulsification technique. *J Food Eng*. 2011;103(1):9-13.

    doi: 10.1016/j.jfoodeng.2010.09.012

20. Zhu M, Wang Y, Ferracci G, Zheng J, Cho NJ, Lee BH. Gelatin methacryloyl and its hydrogels with an exceptional degree of controllability and batch-to-batch consistency. *Sci Rep*. 2019;9(1):6863.

    doi: 10.1038/s41598-019-42186-x

21. Nichol JW, Koshy ST, Bae H, Hwang CM, Yamanlar S, Khademhosseini A. Cell-laden microengineered gelatin methacrylate hydrogels. *Biomaterials*. 2010;31(21):5536-5544.

    doi: 10.1016/j.biomaterials.2010.03.064

22. Bupphathong S, Quiroz C, Huang W, Chung PF, Tao HY, Lin CH. Gelatin methacrylate hydrogel for tissue engineering applications-a review on material modifications. *Pharmaceuticals* (*Basel*). 2022;15(2):171.

    doi: 10.3390/ph15020171

23. Martinez-Ibanez M, Murthy NS, Mao Y, *et al*. Enhancement of plasma protein adsorption and osteogenesis of hMSCs by functionalized siloxane coatings for titanium implants. *J Biomed Mater Res B Appl Biomater*. 2018;106(3):1138-1147.

doi: 10.1002/jbm.b.33889

24. Ma H, Peng Y, Zhang S, Zhang Y, Min P. Effects and progress of photo-crosslinking hydrogels in wound healing improvement. *Gels*. 2022;8(10):609.

doi: 10.3390/gels8100609

25. Daly AC, Riley L, Segura T, Burdick JA. Hydrogel microparticles for biomedical applications. *Nat Rev Mater*. 2020;5(1):20-43.

doi: 10.1038/s41578-019-0148-6

26. Contessi Negrini N, Lipreri MV, Tanzi MC, Fare S. *In vitro* cell delivery by gelatin microspheres prepared in water-in-oil emulsion. *J Mater Sci Mater Med*. 2020;31(3):26.

doi: 10.1007/s10856-020-6363-2

27. Tang XY, Wang ZM, Meng HC, *et al*. Robust W/O/W emulsion stabilized by genipin-cross-linked sugar beet pectin-bovine serum albumin nanoparticles: Co-encapsulation of betanin and curcumin. *J Agric Food Chem*. 2021;69(4):1318-1328.

doi: 10.1021/acs.jafc.0c05212

28. Bonnier F, Keating ME, Wrobel TP, *et al*. Cell viability assessment using the Alamar blue assay: A comparison of 2D and 3D cell culture models. *Toxicol In Vitro*. 2015;29(1):124-131.

doi: 10.1016/j.tiv.2014.09.014

29. Zhou H, Li X, Yin Y, *et al*. The proangiogenic effects of extracellular vesicles secreted by dental pulp stem cells derived from periodontally compromised teeth. *Stem Cell Res Ther*. 2020;11(1):110.

doi: 10.1186/s13287-020-01614-w

30. Schultz KM, Kyburz KA, Anseth KS. Measuring dynamic cell-material interactions and remodeling during 3D human mesenchymal stem cell migration in hydrogels. *Proc Natl Acad Sci U S A*. 2015;112(29):E3757-E3764.

doi: 10.1073/pnas.1511304112

31. Xie W, Wei X, Kang H, *et al*. Static and dynamic: Evolving biomaterial mechanical properties to control cellular mechanotransduction. *Adv Sci* (*Weinh*). 2023;10(9):e2204594.

doi: 10.1002/advs.202204594

32. Kim TK, Yoon JJ, Lee DS, Park TG. Gas foamed open porous biodegradable polymeric microspheres. *Biomaterials*. 2006;27(2):152-159.

doi: 10.1016/j.biomaterials.2005.05.081

33. Wang YJ, Shi XT, Ren L, Wang CM, Wang DA. Porous poly (lactic-co-glycolide) microsphere sintered scaffolds for tissue repair applications. *Mat Sci Eng C*. 2009;29(8):2502-2507.

doi: 10.1016/j.msec.2009.07.018

34. Amoyav B, Benny O. Microfluidic based fabrication and characterization of highly porous polymeric microspheres. *Polymers* (*Basel*). 2019;11(3):419.

doi: 10.3390/polym11030419

35. Awais S, Balouch SS, Riaz N, Choudhery MS. Human dental pulp stem cells exhibit osteogenic differentiation potential. *Open Life Sci*. 2020;15:229-236.

doi: 10.1515/biol-2020-0023

36. Son YB, Kang YH, Lee HJ, *et al*. Evaluation of odonto/osteogenic differentiation potential from different regions derived dental tissue stem cells and effect of 17beta-estradiol on efficiency. *BMC Oral Health*. 2021;21(1):15.

doi: 10.1186/s12903-020-01366-2

37. Noda S, Kawashima N, Yamamoto M, *et al*. Effect of cell culture density on dental pulp-derived mesenchymal stem cells with reference to osteogenic differentiation. *Sci Rep*. 2019;9(1):5430.

doi: 10.1038/s41598-019-41741-w

38. Spagnuolo G, De Luca I, Iaculli F, *et al*. Regeneration of dentin-pulp complex: Effect of calcium-based materials on hDPSCs differentiation and gene expression. *Dent Mater*. 2023;39(5):485-491.

doi: 10.1016/j.dental.2023.03.017

39. Werner M, Blanquer SB, Haimi SP, *et al*. Surface curvature differentially regulates stem cell migration and differentiation via altered attachment morphology and nuclear deformation. *Adv Sci* (*Weinh*). 2017;4(2):1600347.

doi: 10.1002/advs.201600347

40. Xu JJ, Sun MY, Tan Y, *et al*. Effect of matrix stiffness on the proliferation and differentiation of umbilical cord mesenchymal stem cells. *Differentiation*. 2017;96:30-39.

doi: 10.1016/j.diff.2017.07.001

41. Na J, Yang ZJ, Shi QS, *et al*. Extracellular matrix stiffness as an energy metabolism regulator drives osteogenic differentiation in mesenchymal stem cells. *Bioact Mater*. 2024;35:549-563.

doi: 10.1016/j.bioactmat.2024.02.003

42. Sun MY, Chi GF, Li PD, *et al*. Effects of matrix stiffness on the morphology, adhesion, proliferation and osteogenic differentiation of mesenchymal stem cells. *Int J Med Sci*. 2018;15(3):257-268.

doi: 10.7150/ijms.21620

43. Walejewska E, Melchels FPW, Paradiso A, *et al*. Tuning physical properties of GelMA hydrogels through microarchitecture for engineering osteoid tissue. *Biomacromolecules*. 2023;25(1):188-199.

doi: 10.1021/acs.biomac.3c00909

ACCSCIENCE PUBLISHING

Global Translational Medicine

ORIGINAL RESEARCH ARTICLE

Morphological signs of neurodegenerative and inflammatory processes in the brain of rats on a high-calorie diet

Tatyana E. Kuznetsova, Tatyana A. Mityukova*, Anastasia A. Basalai, and Olga Y. Poluliakh

Department of Laboratory of Biomedical Technologies and Medical Rehabilitation, Institute of Physiology, National Academy of Sciences of Belarus, Minsk, Republic of Belarus

Abstract

Much attention has been focused on studying the effects of obesity, particularly on the central nervous system (CNS). This study investigated the histoarchitecture of the prefrontal cortex (PFC) and hippocampus as well as the behavioral characteristics in male and female Wistar rats with diet-induced visceral obesity. The influence of a high-calorie diet on male and female rats reveals sex-specific changes in glial cells and the peculiarities of neurodegenerative processes in the PFC and hippocampal regions. In the context of visceral obesity, signs of depression were observed in male rats, whereas female rats showed no such signs. These results confirm the sex-specific effect of visceral obesity on the CNS.

Keywords: High-calorie diet; Visceral obesity; Rats; Prefrontal cortex; Hippocampus; Signs of inflammation and neurodegeneration

***Corresponding author:**
Tatyana A. Mityukova
(mityukovat@gmail.com)

Citation: Kuznetsova TE, Mityukova TA, Basalai AA, Poluliakh OY. Morphological signs of neurodegenerative and inflammatory processes in the brain of rats on a high-calorie diet. *Global Transl Med*. 2025:4(1):80-89. doi: 10.36922/gtm.5000

Received: September 30, 2024

1st revised: November 21, 2024

2nd revised: December 6, 2024

3rd revised: December 30, 2024

Accepted: January 2, 2025

Published online: January 21, 2025

1. Introduction

Disorders of complex behavioral responses are usually associated with pathological processes involving the prefrontal cortex (PFC) and hippocampus. The PFC plays an important role in the formation of adaptive behavior. In both humans and animals, it is known to be involved in adaptation to changing environmental conditions, information processing and decision-making for survival in natural and social environments, and learning ability.[1,2] In addition, this brain region is implicated in the regulation of eating behavior in humans. High activity in the PFC is thought to facilitate conscious control over food intake and make healthy dietary choices. The hippocampus, on the other hand, is responsible for spatial orientation, learning, and memory.[3] Many studies support its important role in cognitive processes. Its high synaptic plasticity makes the hippocampus particularly sensitive to environmental influences, including lifestyle and nutrition. Hippocampal neurons are known to selectively transmit different types of information to targeted brain regions related to behavior. Moreover, the hippocampus interacts with subcortical areas and the PFC, playing a key role in executive functions. These interactions translate learning into behavior, and dysfunction of the hippocampus can lead not only to memory impairments but also to executive dysfunctions.[3]

The problem of obesity is now being considered not only in terms of its damage to somatic health but also its negative effects on psycho-emotional status, cognitive abilities, and behavior.[4] Experiments in rats have shown that long-term diet-induced obesity, initiated in prepubertal age, leads to depression and neuroinflammation. A review of the current literature generally confirms the link between obesity and depression in humans, although there are conflicting findings in some studies.[5]

Experimental studies in rats also show that high-fat or combined high-fat and sucrose diets cause cognitive impairments, particularly in reduced short-term and visuospatial memories.[6] Early obesity, before the onset of diabetes or metabolic syndrome, leads to cognitive impairment. This is due to changes in the PFC, including synapse loss, a reduction in dendritic spine density, altered expression of synaptic proteins, and structural changes in microglia. The results strongly suggest that obesity can be considered a contributing factor to dysfunction of the PFC.[7]

There is emerging evidence of a link between obesity and brain development during ontogenesis. For example, Laurent *et al.*[8] examined the relationship between body mass index (BMI), cortical thickness, and executive function in children. Among the 3190 children studied (mean age 10.0 years; 51.0% boys), those with a higher-than-normal BMI showed reduced cortical thickness. Hall *et al.*[9] suggested that the thickness of the inferior frontal gyrus and lateral orbitofrontal cortex may serve as predictors of body composition. The study concluded that PFC morphology is a reliable predictor of body composition in early adolescence and is associated with certain cognitive functions, while also being partially influenced by environmental factors.

Pathological changes in the state of the hippocampus in obesity in humans have been less studied, although associations have been made between the state of the hippocampus and several neuropathological processes.[3] However, there is evidence that a high-calorie diet (HCD) and physical inactivity, which promote obesity and diabetes, are risk factors for hippocampal neurodegeneration and cognitive impairment.[10] It has been suggested that diet-induced obesity may lead to impaired neuronal plasticity in the hippocampus, which in turn may contribute to cognitive decline, emotional disturbance, and hyperphagia. Adipose tissue regulates hippocampal function through the release of adipokines, which may directly or indirectly modulate both neural plasticity and neuroinflammation.[10] However, the potential mechanisms by which adipose tissue inflammation in obesity leads to neurodegeneration and neuroinflammation in the PFC and hippocampus remain poorly understood.

Changes in the cerebral cortex, which is responsible for the cognitive control of food intake, may either contribute to or result from obesity, further supporting the notion of impaired regulation of eating behavior.

The study aimed to investigate the histological characteristics of the PFC and hippocampus in male and female rats subjected to diet-induced visceral obesity.

2. Materials and methods

2.1. Animals and diets

The study was conducted on 2-month-old sexually mature male and female Wistar rats. These rats were bred in-house in a certified vivarium at the Institute of Physiology of the National Academy of Sciences of Belarus. They were kept under a 12/12 h light/dark cycle at a temperature of 22 ± 2°C and humidity of 60 – 65%. The male (n = 27) and female (n = 27) Wistar rats were randomly divided into two experimental groups: control and HCD. The control group, consisting of 13 male and 14 female rats, received the standard diet (StD), while the HCD group, comprising 14 male and 13 female rats, was given an HCD for 16 weeks.

The HCD consisted of StD supplemented with animal fats (lard) (45% of daily caloric content) and a 10% fructose solution (replacing water) *ad libitum*.[11] The caloric content of StD for each rat was 150 kcal/day (i.e., the normal diet at the vivarium of the Institute of Physiology of the National Academy of Sciences of Belarus). In contrast, the caloric content of HCD for each rat was 228 kcal/day.

This study was approved by the Bioethics Committee of the Institute of Physiology of the National Academy of Sciences of Belarus (protocols No:1 on January 22, 2021, and No:2 on February 2, 2022) and was conducted in accordance with the guidelines set forth by the European Convention for the Protection of Vertebrate Animals (ETS No. 123).

The rats were euthanized by decapitation under anesthesia induced with sodium thiopental. Female rats were euthanized during the diestrus phase of the estrous cycle, determined by the type of cells present in vaginal swabs.[12]

The body weight of the rats was measured using a weighing scale (Saturn ST-KS7230, China). After euthanasia, the visceral fat was collected and weighed on a laboratory weighing scale (Scout Pro, China). For male rats, the visceral fat mass included paranephral and epididymal fat deposits, while for female rats, it included paranephral and periovarian fat deposits. The mass coefficient (MC) of the visceral fat was calculated using the following formula:

$$MC = (\text{Visceral fat mass}/\text{Body weight}) \times 100\% \quad (I)$$

2.2. The Porsolt test

The Porsolt test (assessment of depression) was carried out at the final stage of the experiment (between 9:00 and 12:00, with the rats in a fasting state) and in females during the diestrus phase. Each rat was placed for 6 min in a vessel filled with water up to a 30 cm mark and maintained at a temperature of 24 – 25°C. The duration of the first act of active swimming, as well as the number and duration of "freezes" (absence of swimming movements), was recorded. A refusal to actively swim characterizes a state of "despair", which is considered a sign of depression.[13]

2.3. Morphological analysis

After the animals were sacrificed, the rat brain was isolated and placed on a cryostat block after deep freezing to eliminate artifacts. Unfixed brains were sectioned into frontal slices of 7 μm thickness using an HM525 Cryostat (MICROM International GmbH, Germany). The slice level was determined according to the stereotaxic atlas of the rat brain.[14] For light microscopy, the slices were stained with toluidine blue using the Nissl method. Micrographs and photomicrographs were captured using an Altami LUM-1 light microscope equipped with a digital camera (Altami LLC, Russia). Morphometric analysis of the digitized images was performed automatically using ImageJ software (National Institutes of Health, USA), utilizing tools from the "Analyze' menu, including the "Analyze Particles" and "Multi-Point Tool" options. Calibration of slice images in micrometers was performed using the built-in "Set Scale" function. Morphometric analysis of histological preparations was performed at ×400 magnification in 10 fields of view. In PFC preparations stained with the Nissl method, data were collected on the number of neurons per field of view, the mean neuron size (in μm^2), and the number of neurons with signs of destruction (ND). The total number of neurons and the number of neurons with signs of destruction per 1 mm^2 were determined in hippocampal preparations. The glial index (GI) was calculated as the ratio of the number of glial cells to the total number of neurons.

2.4. Statistical analysis

Statistical analysis was performed using Statistica 10.0 (Tibco, USA). Normality was assessed with the Shapiro–Wilk test. Parametric variables were expressed as mean ± standard deviation and analyzed with Student's *t*-test. The non-parametric variables were expressed as median and the 25th and 75th percentiles, and the variables were analyzed using the Mann–Whitney U-test. A $P < 0.05$ was considered statistically significant for all tests.

3. Results

3.1. Mass-metric parameters

As shown in Figure 1A and B, the body weight of rats in each experimental group increased progressively as the they matured from 2 to 6 months of age. By the end of the experiment, the body weight of rats of the same sex was comparable in all groups. However, in both sexes of rats receiving the HCD, there was a statistically significant increase in the mass (Figure 2A) and MC (Figure 2B) of visceral adipose tissue, indicating the development of diet-induced visceral obesity.

3.2. Morphological analysis of the PFC

In male rats on a StD, the histoarchitecture of the PFC was intact (Figure 3A). All six layers of neurons were visible. Most neurons were normochromic, with a centrally located nucleus and a distinct nucleolus. Mild changes were observed in a few individual neurons, mainly with disturbances in tinctorial properties. Blood vessels were unchanged. The GI, representing the ratio of the number of glial cells to the number of neurons, was 0.46 in the male control group (Figure 4D). Similarly, in female rats on StD, the histoarchitecture of the PFC remained intact (Figure 5A). All layers of neurons were identified. There were individual neurons with slight changes, mainly with disturbances of the tinctorial properties. Blood vessels were unchanged and the GI was 0.44 (Figure 4D).

The overall structure of PFC in the male rats remained intact after 16 weeks of being on a HCD (Figure 3B). All layers of neurons were identified. However, there was a tendency toward a reduction in neuron size and an increase in the number of neurons with moderate degenerative-dystrophic changes (Figure 4A-C). Hypochromic neurons and cells with disturbed tinctorial properties were found in the population of neurons. Individual destroyed neurons were identified, with glial elements accumulating around them in some areas, indicating neuronophagia (Figure 3B). The GI was statistically significantly increased, exceeding the control value by approximately 1.3 times ($P = 0.007$) (Figure 4D). In addition, perivascular edema was observed around the vessels of the microcirculatory channel.

In female rats on a HCD, the overall structure of the PFC remained undisturbed (Figure 5B). All neuronal layers were identified. Morphometric analysis revealed a significant increase in neuron size. However, the proportion (%) of neurons with degenerative-dystrophic changes was significantly higher compared to the control group (1.5-fold, $P = 0.018$) (Figure 4A-C). Hypochromic neurons and cells with disturbed tinctorial properties were found in the population of neurons, along with a few destroyed neurons

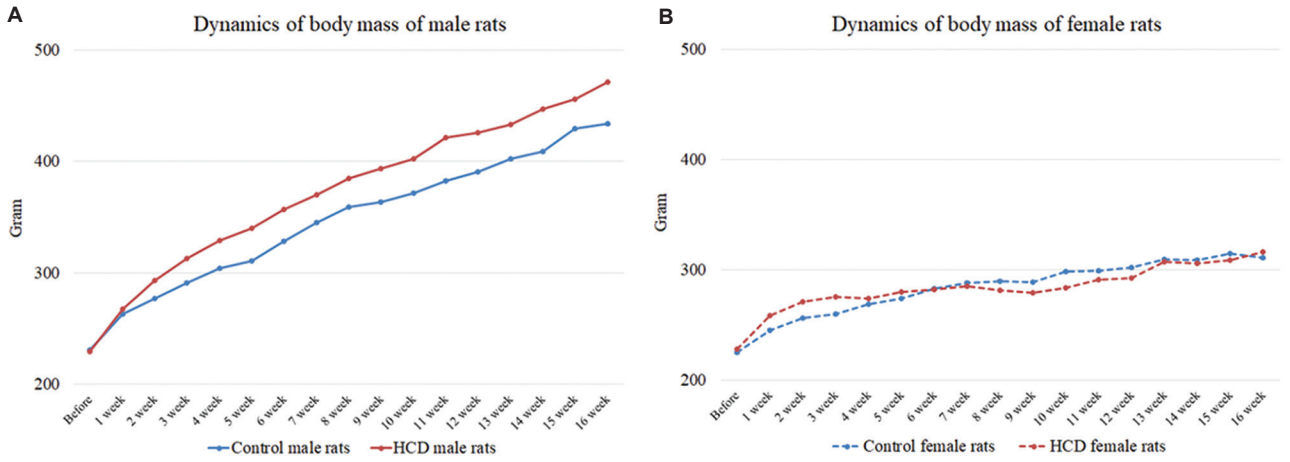

Figure 1. Body mass of the experimental animals during the experiment: (A) male and (B) female rats. Data are presented as mean.
Abbreviation: HCD: High-calorie diet.

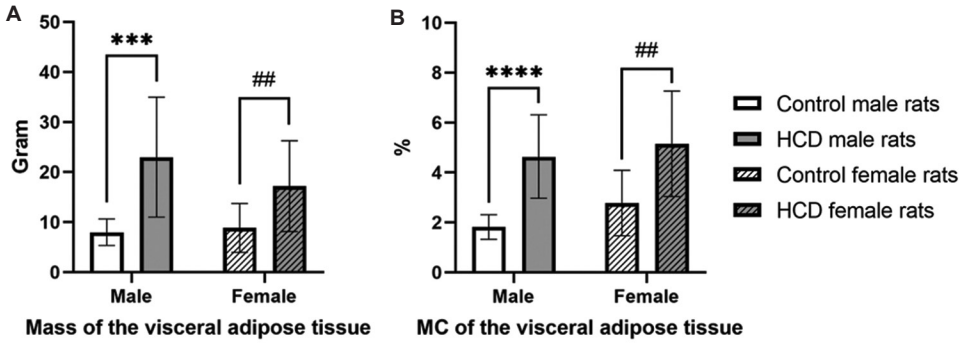

Figure 2. Mass-metric indices of the visceral adipose tissue of the experimental animals. (A) Mass and (B) MC of the visceral adipose tissue of male and female rats. Data are presented as mean ± standard deviation; statistically significant differences between the male HCD and male control groups at $^{***}P < 0.001$, $^{****}P < 0.0001$; statistically significant difference between the female HCD and female control groups at $^{\#\#}P < 0.01$.
Abbreviations: HCD: High-calorie diet; MC: Mass coefficient.

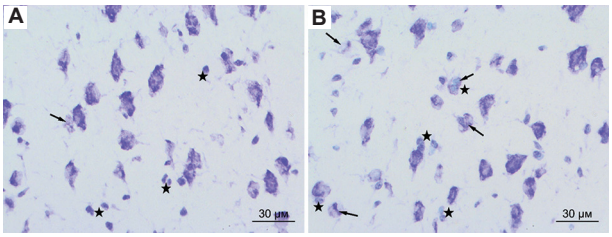

Figure 3. Histoarchitecture of the prefrontal cortex in male rats from the control (A) and HCD groups (B). Staining was performed with toluidine blue using the Nissl method. Magnification: ×400.
Symbols: ★ – Glial cells. ↑ – Neurons with destructive changes.
Abbreviation: HCD: High-calorie diet.

(Figure 5B). There was also a tendency toward an increased number of glial cells (Figure 4D). The increase in neuron size observed in parallel with the signs of neurodegeneration may be attributed to edema in the neurons.

Thus, an HCD induced neuroglial activation in the PFC of male rats, while female rats showed signs of neurodegeneration.

3.3. Morphological analysis of the hippocampus

In male rats on a StD, the cytoarchitectonics of the hippocampal fields remained intact (Figure 6A-D and Figure 7). Pyramidal neurons had a large rounded nucleus with one, two, or more distinct nuclei and a uniform distribution of Nissl substance. Only a few cells with chromatolysis or vacuoles in the cytoplasm were detected, and no signs of pericellular or perivascular edema were detected.

After 16 weeks on a high-calorie diet, the male rats exhibited an increase in the GI in the CA2 area (Figure 7F and Figure 8B), along with increased neuronal density and a decrease in the GI in the CA3 area (Figure 7G, I and Figure 8C). An increase in the number of neurons with destructive-dystrophic changes was observed in all hippocampal regions (Figure 7B, E, H, K and Figure 8A-D). Some disorganization of the pyramidal neuron layers was most pronounced in the CA4 area (Figure 8D).

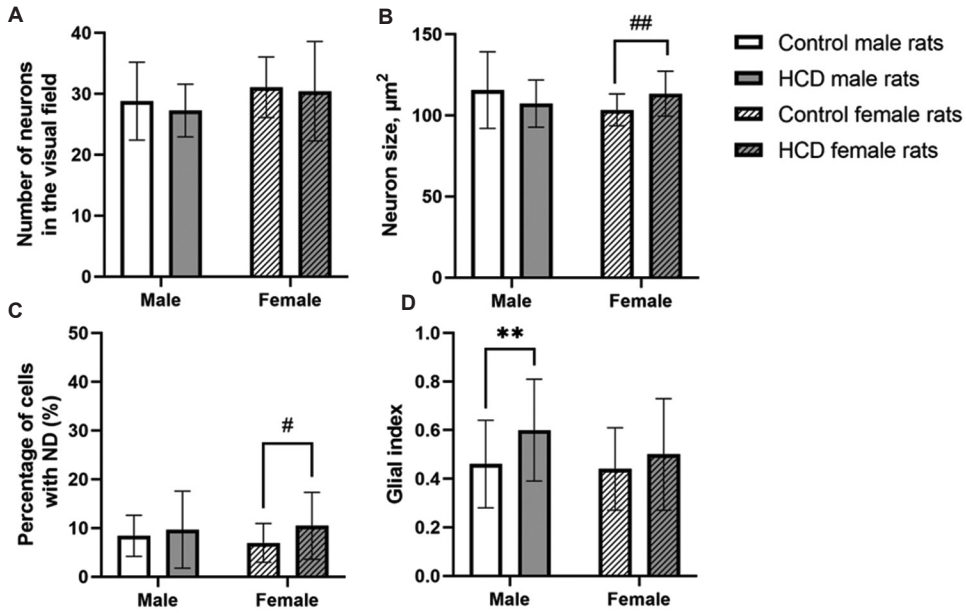

Figure 4. Morphometric indices of the prefrontal cortex of the experimental animals: (A) number of neurons in the visual field, (B) neuron size (μm²), (C) percentage of neurons (%) with signs of destruction (ND), (D) glial index. Data are presented as mean ± standard deviation; statistically significant differences between the male HCD and male control groups at $^{**}P < 0.01$; statistically significant differences between the female HCD and female control groups at $^{\#}P < 0.05$, $^{\#\#}P < 0.01$.
Abbreviations: HCD: High-calorie diet; ND: Neurons with signs of destruction.

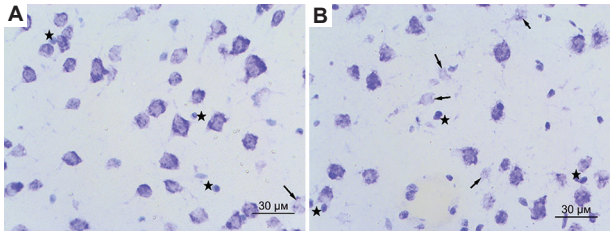

Figure 5. Histoarchitecture of the prefrontal cortex in female rats from the control (A) and HCD groups (B). Staining was performed with toluidine blue using Nissl method. Magnification: ×400.
Symbols: ★ – glial cells. ↑ – neurons with destructive changes.
Abbreviation: HCD: High-calorie diet.

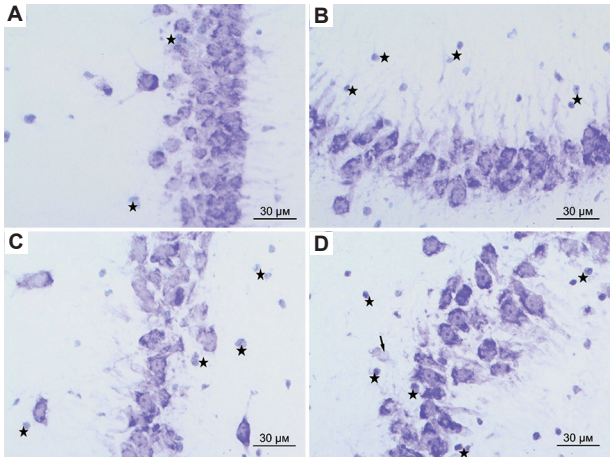

Figure 6. Histoarchitecture of the hippocampus of male rats from the control groups: (A) CA1, (B) CA2, (C) CA3, (D) CA4 areas. Staining was performed with toluidine blue using the Nissl method. Magnification: ×400.
Symbols: ★ – Glial cells. ↑ – Neurons with destructive changes.

In female rats on a StD, the cytoarchitectonics of the hippocampal fields remained undisturbed and generally corresponded to the physiological norm (Figure 7 and Figure 9A-D). Only a few cells with chromatolysis or vacuoles in the cytoplasm were detected, and no pericellular or perivascular edema was found.

An increase in neuronal density in the CA1 area of the hippocampus was observed in female rats on a HCD (Figure 7A). In contrast, a significant decrease in neuronal density was observed in other areas (Figure 7D, G, J). Destructive and dystrophic changes of neurons were observed in specific areas, including CA1, CA2, and CA4 (Figure 7B, E, K) without significant changes in the GI values (Figure 7C, F, L and Figure 10A, B, D). In addition, a decrease in the number of glial cells was observed in the CA3 area compared to the StD group (Figure 10C and Figure 7I).

A comparison of the effects of HCD on the hippocampal histoarchitecture in male and female rats showed some common features, such as increased neuronal density in specific areas of the hippocampus

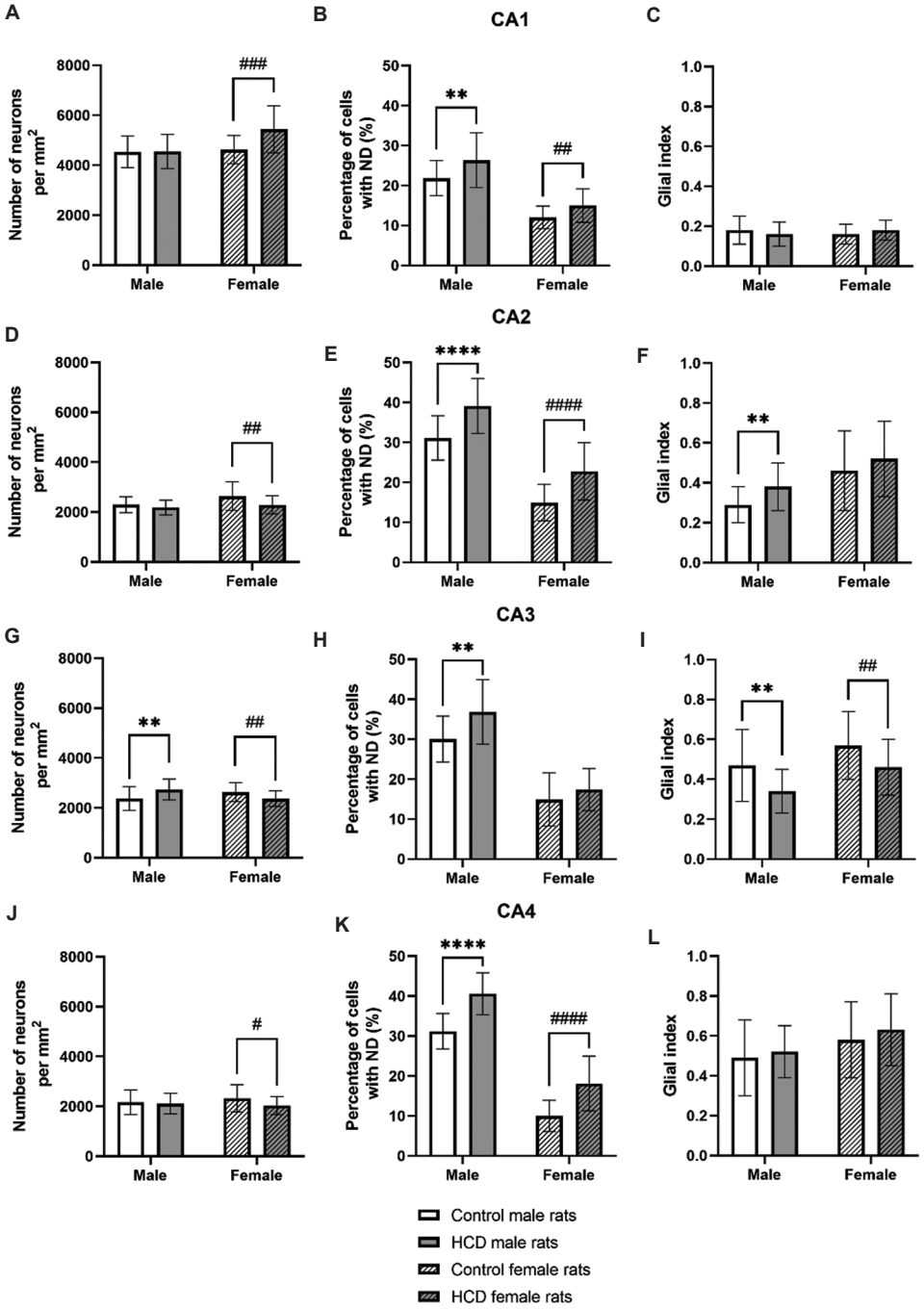

Figure 7. Morphometric indices of the hippocampus of the experimental animals: (A-C) CA1, (D-F) CA2, (G-I) CA3, (J-L) CA4 areas; (A, D, G, J) number of neurons per mm^2, (B, E, H, K) percentage of neurons (%) with signs of destruction (ND), (C, F, I, L) glial index. Data are presented as mean ± standard deviation; statistically significant differences between the male HCD and male control groups at $^{**}P < 0.01$, $^{***}P < 0.001$, $^{****}P < 0.0001$; statistically significant differences between the female HCD and female control groups at $^{\#}P < 0.05$, $^{\#\#}P < 0.01$, $^{\#\#\#}P < 0.001$, $^{\#\#\#\#}P < 0.0001$.
Abbreviations: HCD: High-calorie diet; ND: Neurons with signs of destruction.

(CA3 in males and CA1 in females). However, unlike males, females showed a decrease in neuronal density in areas CA2, CA3, and CA4. The presence of destructive-dystrophic changes in hippocampal neurons in HCD was comparable in both sexes. In males on a HCD, the number of glial cells increased in the CA2 area and decreased in the CA3 area, with the latter change also observed in females.

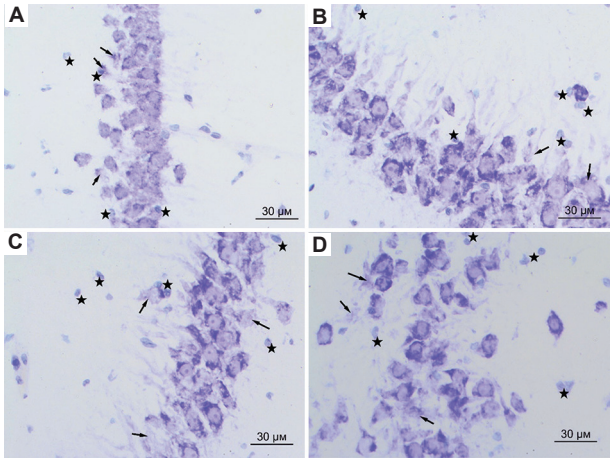

Figure 8. Histoarchitecture of the hippocampus of male rats from the HCD groups: (A) CA1, (B) CA2, (C) CA3, (D) CA4 areas. Staining was performed with toluidine blue using the Nissl method. Magnification: ×400.
Symbols: ★ – Glial cells. ↑ – Neurons with destructive changes.
Abbreviation: HCD: High-calorie diet.

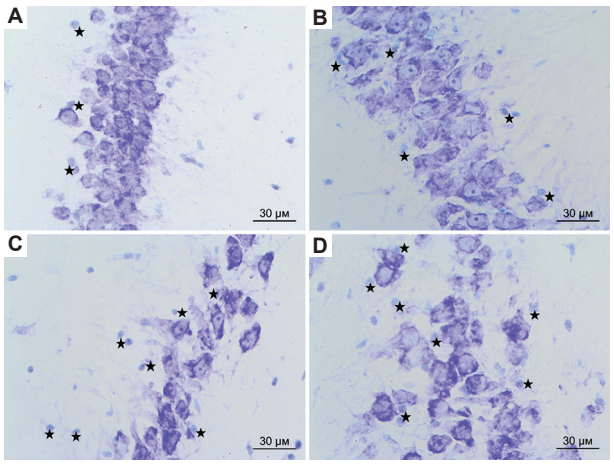

Figure 9. Histoarchitecture of the hippocampus of female rats from the control groups: (A) CA1, (B) CA2, (C) CA3, (D) CA4 areas. Staining was performed with toluidine blue using the Nissl method. Magnification: ×400.
Symbols: ★ – Glial cells.

3.4. Porsolt test results

Table 1 shows the results of the Porsolt test. The duration of the first act of swimming was almost identical in males and females on the StD. However, significant sex differences were found in the context of visceral obesity under the "unavoidable stress" condition. Male rats in the HCD group showed an approximately 2-fold reduction in the time of the first act of active swimming ($P < 0.05$), along with a 2-fold and 3.5-fold increase in the number and duration of freezing episodes, respectively, compared to the control group ($P < 0.05$ and $P < 0.01$, respectively). In contrast,

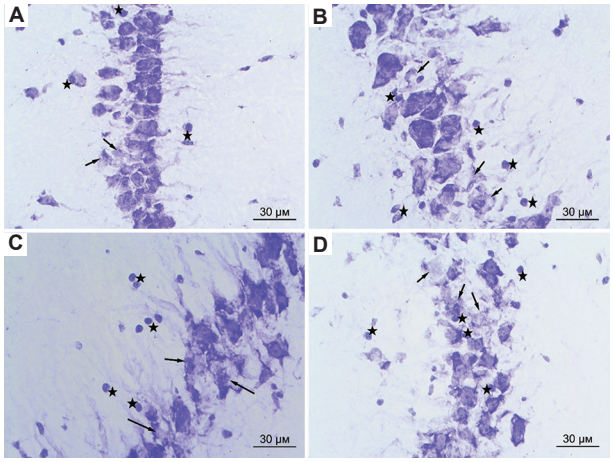

Figure 10. Histoarchitecture of the hippocampus of female rats from the HCD groups: (A) CA1, (B) CA2, (C) CA3, (D) CA4 areas. Staining was performed with toluidine blue using the Nissl method. Magnification: ×400.
Symbols: ★ – Glial cells. ↑ – Neurons with destructive changes.
Abbreviation: HCD: High-calorie diet.

female rats in the HCD group did not show statistically significant differences in behavior during the Porsolt test compared to the control group. These results suggest the development of depression in male rats with diet-induced obesity, whereas female rats were not similarly affected.

4. Discussion

To date, obesity has been associated with systemic inflammatory processes, and many authors have linked it to various neurodegenerative diseases.[15] It has been suggested that cognitive impairment in obesity may be due to microglial activation.[16] This hypothesis is supported by studies[17] investigating the effects of a HCD in mice, which found anxious behavior and behavioral despair associated with systemic inflammation and neuroinflammatory signs in the nucleus accumbens (NAc) of the forebrain. Similar data were obtained in another experimental study,[18] which investigated the effect of HCD on glial activation and neuroinflammation in the brains of mice. However, the role of inflammation in cognitive impairment has not been fully confirmed in several other studies.[7,19,20] For example, Bocarsly *et al.*[7] showed that obese rats exhibited deficits in cognitive tasks requiring involvement of the prefrontal and peripheral cortices. These cognitive deficits were accompanied by decreased dendritic root density and reduced expression of synaptic markers in both brain regions, along with altered microglial morphology in the PFC. However, the authors argue that these adverse changes occurred in the prefrontal and perirhinal cortices before the development of metabolic syndrome. Auer *et al.*[19] reported that a cafeteria diet in mice led to obesity and hyperglycemia, resulting in changes in central nervous

Table 1. Porsolt test indices of the experimental animals

Index	Male rats		Female rats	
	Control (*n*=13)	HCD (*n*=14)	Control (*n*=14)	HCD (*n*=13)
Time of the first swimming act (s)	258.00 (203.00, 320.00)	137.50 (85.00, 240.00)*	260.00 (226.00, 340.00)	265.00 (170.00, 360.00)
Number of freezing	6.00 (3.00, 11.00)	13.00 (9.00, 18.00)*	3.50 (2.00, 7.00)	8.00 (0.00, 13.00)
Freezing time (s)	10.00 (4.00, 13.00)	34.50 (13.00, 61.00)**	3.50 (2.00, 13.00)	8.00 (0.00, 21.00)

Notes: Data are presented as median (25th percentile; 75th percentile); statistically significant differences between the male HCD and male control groups at *P<0.05, **P<0.01.
Abbreviation: HCD: High-calorie diet.

system metabolites, such as decreased levels of glutamate and choline-containing compounds in the hippocampus. However, these effects were not associated with markers of central inflammation. The study by Guillemot-Legris *et al.*[20] in mice fed HCD showed that inflammatory processes were differentially manifested in different brain regions, potentially associated with astrocytes, but not microglial cells. In addition, evidence suggests that a HCD potentiates the formation of amyloid plaques in the brains of male and female APP/E4 mice, but not in APP/E3 mice.[21]

The analysis of literature data shows that many questions related to the mechanisms of obesity influence on metabolic and morpho-functional characteristics of neurons remain controversial. In our studies (using the Nissl staining method), pronounced glial activation was observed in the PFC of male rats with visceral obesity. However, this phenomenon was not observed in female rats, though significant neurodegenerative changes were found in their PFC. Our study of hippocampal morphology showed a variety of changes in different areas of this brain region, In males, signs of neurodegeneration were observed in all areas examined (CA1 – CA4), with glial activation occurring only in the CA2 area. In females, neurodegenerative changes were more selective, involving the CA1, CA2, and CA4 areas, while glial activation was absent.

The literature generally suggests that chronic inflammation of adipose tissue may induce neuroinflammation and hippocampal dysfunction, contributing to the development of cognitive deficits.[10] However, the search for mechanisms of the effect of obesity on hippocampal functional activity leads to equivocal findings. For example, it has been shown that high-density leptin receptors are expressed in several brain regions involved in higher cognitive functions, including the hippocampus. In addition, leptin has a cognitive stimulatory effect in the hippocampus, and leptin deficiency or insensitivity to leptin results in significant memory deficits.[22] In the context of obesity, several mechanisms of leptin resistance have been discussed, which may increase the risk of neurodegenerative diseases.[15] To date, molecular mechanisms linking obesity, diabetes, and neurodegenerative diseases have been actively investigated, and a link has been demonstrated in many studies. Our data provide direct evidence for the development of neurodegenerative processes in the PFC and hippocampus of rats on a HCD. However, glial activation in the brain areas studied does not always accompany visceral obesity.

In experiments on male mice, metabolic disturbances caused by long-term consumption of a high-fat diet were shown to increase neuronal oxidative stress and insulin resistance through suppression of the adiponectin receptor (AdipoR1).[23] The authors showed that a high-fat diet provokes microglial activation and neuroinflammation in the cortical and hippocampal regions of mice. However, suppression of AdipoR1 increased the amyloidogenic pathway both *in vivo* and *in vitro*. In summary, the authors concluded that excessive fat consumption has a significant impact on brain function, including an increase in cognitive impairment due to increased oxidative stress associated with obesity, insulin resistance, neuroinflammation, and suppression of AdipoR1 signaling in the brain.[23]

Our studies show that a HCD leads to depression-like behavior in male rats under conditions of "unavoidable stress" but has no significant effect on the behavioral strategy of female rats under the same conditions. Several published studies have noted that peripheral metabolic abnormalities in obesity are associated with different clinical health outcomes and may have sex differences. In one study,[24] a long-term high-fat diet for 16 weeks was shown to impair glucose metabolism in the brain. Behavioral tests of spatial memory, including the Morris water maze and Y-maze, showed that memory performance was impaired only in male rats on the high-fat diet. In addition, a significant decrease in glucose metabolism was observed in male rats, but not in female rats, on this diet. Analysis of genes related to glucose metabolism and Alzheimer's disease (AD) pathology in the hippocampus showed that the expression of glucose transporter 3 (GLUT3), insulin receptor substrate 2 (IRS2), and insulin-degrading enzyme (IDE) was significantly reduced in male

rats on the high-fat diet but not in females.[24] In a study by Li *et al.*,[25] investigating the effects of a maternal high-fat diet on offspring, male offspring showed significant metabolic abnormalities, whereas female offspring showed only a slight increase in body weight and did not develop the metabolic abnormalities observed in males. Carrillo *et al.*[26] studied the effects of estradiol during the early postnatal period on brain metabolic changes induced by overeating. Neonatal estradiol treatment restored body weight and subcutaneous fat to control levels in males fed a high-fat diet. In females, however, such exposure affected hypothalamic neuropeptides without changing body weight. The authors concluded that increasing estradiol levels during the neonatal period could induce different metabolic shifts in males and females, with estradiol preventing the adverse effects of overeating in males.[26] Based on our data, we hypothesize that female rats are more protected than males from psycho-emotional disorders, particularly depression, caused by obesity.

5. Conclusion

The comparison of the effects of a HCD on male and female rats reveals sex-specific changes in glial cells and peculiarities of neurodegenerative processes in the PFC. Comparable manifestations of neurodegenerative processes are observed in most hippocampal regions in both male and female rats. However, proinflammatory and neurodegenerative processes in the brain regions studied are associated with depression only in male rats, not in female rats.

Acknowledgments

None.

Funding

The work was supported by the State Program for Scientific Research (No.:4.1.1.5) of the National Academy of Sciences of Belarus.

Conflict of interest

The authors declare that they have no competing interests.

Author contributions

Conceptualization: Tatyana A. Mityukova
Formal analysis: Tatyana E. Kuznetsova, Anastasia A. Basalai, Olga Y. Poluliakh
Investigation: Tatyana E. Kuznetsova, Anastasia A. Basalai, Olga Y. Poluliakh
Methodology: Tatyana A. Mityukova, Tatyana E. Kuznetsova, Anastasia A. Basalai, Olga Y. Poluliakh
Writing – original draft: Tatyana A. Mityukova, Tatyana E. Kuznetsova
Writing – review & editing: Tatyana A. Mityukova, Tatyana E. Kuznetsova, Anastasia A. Basalai, Olga Y. Poluliakh

Ethics approval and consent to participate

This study was approved by the Bioethics Committee of the Institute of Physiology of the National Academy of Sciences of Belarus (protocols No.:1 on January 22, 2021, and No.:2 on February 2, 2022) and conducted in accordance with the guidelines set forth by the European Convention for the Protection of Vertebrate Animals (ETS No. 123).

Consent for publication

Not applicable.

Availability of data

The datasets used and/or analyzed during the present study are available from the Institute of Physiology of the National Academy of Sciences of Belarus, upon reasonable and justifiable request in accordance with the rules and procedures of the Institute of Physiology of the National Academy of Sciences of Belarus (https://physiology.by/or biblio@fizio.bas-net.by).

References

1. Badre D, Kayser AS, D'Esposito M. Frontal cortex and the discovery of abstract action rules. *Neuron*. 2010;66(2):315-326.
   doi: 10.1016/j.neuron.2010.03.025
2. Yang Y, Raine A. Prefrontal structural and functional brain imaging findings in antisocial, violent, and psychopathic individuals: A meta-analysis. *Psychiatry Res*. 2009;174(2):81-88.
   doi: 10.1016/j.pscychresns.2009.03.012
3. Li Y, Shen M, Stockton ME, Zhao X. Hippocampal deficits in neurodevelopmental disorders. *Neurobiol Learn Mem*. 2019;165:106945.
   doi: 10.1016/j.nlm.2018.10.001
4. Giel KE, Hartmann A, Zeeck A, *et al*. Decreased emotional perception in obesity. *Eur Eat Disord Rev*. 2016;24(4):341-346.
   doi: 10.1002/erv.2444
5. Blasco BV, García-Jiménez J, Bodoano I, Gutiérrez-Rojas L. Obesity and depression: Its prevalence and influence as a prognostic factor: A systematic review. *Psychiatry Investig*. 2020;17(8):715-724.
   doi: 10.30773/pi.2020.0099
6. Mabrok HB, Ramadan AA, Hamed IM, Mohamed DA. Obesity as inducer of cognitive function decline via dysbiosis of gut microbiota in rats. *Brain Sci*. 2024;14(8):807.
   doi: 10.3390/brainsci14080807
7. Bocarsly ME, Fasolino M, Kane GA, *et al*. Obesity

diminishes synaptic markers, alters microglial morphology, and impairs cognitive function. *Proc Natl Acad Sci U S A*. 2015;112(51):15731-15736.

doi: 10.1073/pnas.1511593112

8. Laurent JS, Watts R, Adise S, *et al*. Associations among body mass index, cortical thickness, and executive function in children. *JAMA Pediatr*. 2020;174(2):170-177.

doi: 10.1001/jamapediatrics.2019.4708

9. Hall PA, Best JR, Beaton EA, Sakib MN, Danckert J. Morphology of the prefrontal cortex predicts body composition in early adolescence: Cognitive mediators and environmental moderators in the ABCD Study. *Soc Cogn Affect Neurosci*. 2023;18(1):nsab104.

doi: 10.1093/scan/nsab104

10. Lee TH, Yau SY. From obesity to hippocampal neurodegeneration: Pathogenesis and non-pharmacological interventions. *Int J Mol Sci*. 2020;22(1):201.

doi: 10.3390/ijms22010201

11. Gancheva S, Zhelyazkova-Savova M, Galunska B, Chervenkov T. Experimental models of metabolic syndrome in rats. *Scr Sci Med*. 2015;47(2):14-21.

doi: 10.14748/ssm.v47i2.1145

12. Marcondes FK, Bianchi FJ, Tanno AP. Determination of the estrous cycle phases of rats: Some helpful considerations. *Braz J Biol*. 2002;62(4A):609-614.

doi: 10.1590/s1519-69842002000400008

13. Castagne V, Moser P, Porsolt RD. Behavioral assessment of antidepressant activity in rodents. In: *Methods of Behavior Analysis in Neuroscience*. 2nd ed., Ch. 6. Boca Raton, FL: CRC Press, Taylor & Francis; 2009.

14. Paxinos Y, Watson C. *The Rat Brain in Stereotaxic Coordinates*. San Diego: Academic Press; 1998. p. 256.

15. Neto A, Fernandes A, Barateiro A. The complex relationship between obesity and neurodegenerative diseases: An updated review. *Front Cell Neurosci*. 2023;17:1294420.

doi: 10.3389/fncel.2023.1294420

16. Nguyen JC, Killcross AS, Jenkins TA. Obesity and cognitive decline: Role of inflammation and vascular changes. *Front Neurosci*. 2014;8:375.

doi: 10.3389/fnins.2014.00375

17. Décarie-Spain L, Sharma S, Hryhorczuk C, *et al.* Nucleus accumbens inflammation mediates anxiodepressive behavior and compulsive sucrose seeking elicited by saturated dietary fat. *Mol Metab*. 2018;10:1-13.

doi: 10.1016/j.molmet.2018.01.018

18. Dasuri K, Zhang L, Kim SO, Bruce-Keller AJ, Keller JN. Dietary and donepezil modulation of mTOR signaling and neuroinflammation in the brain. *Biochim Biophys Acta*. 2016;1862(2):274-283.

doi: 10.1016/j.bbadis.2015.11.002

19. Auer MK, Sack M, Lenz JN, *et al.* Effects of a high-caloric diet and physical exercise on brain metabolite levels: A combined proton MRS and histologic study. *J Cereb Blood Flow Metab*. 2015;35(4):554-564.

doi: 10.1038/jcbfm.2014.231

20. Guillemot-Legris O, Masquelier J, Everard A, Cani PD, Alhouayek M, Muccioli GG. High-fat diet feeding differentially affects the development of inflammation in the central nervous system. *J Neuroinflammation*. 2016;13(1):206.

doi: 10.1186/s12974-016-0666-8

21. Nam KN, Wolfe CM, Fitz NF, *et al.* Integrated approach reveals diet, APOE genotype and sex affect immune response in APP mice. *Biochim Biophys Acta Mol Basis Dis*. 2018;1864(1):152-161.

doi: 10.1016/j.bbadis.2017.10.018

22. McGregor G, Harvey J. Regulation of hippocampal synaptic function by the metabolic hormone, leptin: Implications for health and neurodegenerative disease. *Front Cell Neurosci*. 2018;12:340.

doi: 10.3389/fncel.2018.00340

23. Hahm JR, Jo MH, Ullah R, Kim MW, Kim MO. Metabolic stress alters antioxidant systems, suppresses the adiponectin receptor 1 and induces Alzheimer's like pathology in mice brain. *Cells*. 2020;9(1):249.

doi: 10.3390/cells9010249

24. Abedi A, Foroutan T, Shalmani LM, Dargahi L. Sex-specific effects of high-fat diet on rat brain glucose metabolism and early-onset dementia symptoms. *Mech Ageing Dev*. 2023;211:111795.

doi: 10.1016/j.mad.2023.111795

25. Li C, Xu JJ, Hu HT, *et al.* Amylin receptor insensitivity impairs hypothalamic POMC neuron differentiation in the male offspring of maternal high-fat diet-fed mice. *Mol Metab*. 2021;44:101135.

doi: 10.1016/j.molmet.2020.101135

26. Carrillo B, Collado P, Díaz F, Chowen JA, Pérez-Izquierdo MÁ, Pinos H. Physiological and brain alterations produced by high-fat diet in male and female rats can be modulated by increased levels of estradiol during critical periods of development. *Nutr Neurosci*. 2019;22(1):29-39.

doi: 10.1080/1028415X.2017.1349574

ACCSCIENCE PUBLISHING

Global Translational Medicine

ORIGINAL RESEARCH ARTICLE

Comparative evaluation of the therapeutic effects of *Schisandra chinensis* and *Schisandra sphenanthera* on vascular cognitive impairment and their drug-like compounds

Yucen Zou[1†], Bin Li[1†], Meiqi Wang[1], Xiaomeng Xie[2], Jianuo Zhang[1], Qi Xiao[1], Chunyan Yang[1], Jiushi Liu[1], Haitao Sun[1], Bengang Zhang[1], Pei Ma[1*], and Haitao Liu[1*]

[1]State Key Laboratory of Bioactive Substance and Function of Natural Medicines, Institute of Medicinal Plant Development, Chinese Academy of Medical Sciences, Peking Union Medical College, Beijing, China

Abstract

The fruits of *Schisandra chinensis* (SCF) and *Schisandra sphenanthera* (SSF) are traditional Chinese herbal medicines classified as medicinal and food homologous materials, known for their significant neuroprotective efficacy. However, the differences in their therapeutic effects and active components for the treatment of vascular cognitive impairment (VCI) remain unclear. This study aimed to elucidate the neuroprotective activities of SCF and SSF on VCI and investigate the compositional disparities between the two. The lipopolysaccharide-induced and oxygen-glucose deprivation/reoxygenation (OGD/R)-induced BV2 cell models were used to evaluate the protective effects of SCF and SSF against neuroinflammation and mitochondrial damage, respectively. The therapeutic effects were further validated using a bilateral common carotid artery stenosis mouse model. Compositional differences were analyzed using ultraperformance liquid chromatography-quadrupole time-of-flight mass spectrometry (UPLC-Q-TOF/MS), and drug-like properties of their constituents were assessed. *In vitro* experiments showed that SCF and SSF at concentrations of 6.4, 16, and 40 μg/mL reduced nitric oxide, tumor necrosis factor-alpha, and interleukin-6 levels in a dose-dependent manner. Notably, at the same concentrations, SCF significantly mitigated OGD/R-induced mitochondrial damage, whereas SSF showed no significant effect. Compared with SSF, SCF exhibited stronger anti-neuroinflammatory and antioxidant properties. *In vivo* experiments further demonstrated that SCF, administered at 400 mg/kg, was more effective in improving learning ability, spatial learning and memory, cerebral blood flow, and nerve fiber repair than SSF. Moreover, 71 and 64 compounds were identified in SCF and SSF, respectively, using UPLC-Q-TOF/MS. Drug-like property analysis of these compounds revealed that the superior therapeutic effects of SCF may be attributed to differences in biphenylcyclooctene-type lignans. Our data support the conclusion that SCF possesses significantly superior neuroprotective activity compared to SSF, providing a theoretical basis for its clinical application in VCI.

Keywords: *Schisandra chinensis*; *Schisandra sphenanthera*; Vascular cognitive impairment; Neuroinflammation; Mitochondrial damage; UPLC-Q-TOF/MS

†These authors contributed equally to this work.

***Corresponding authors:**
Haitao Liu
(htliu@implad.ac.cn)
Pei Ma
(pma@implad.ac.cn)

Citation: Zou Y, Li B, Wang M, *et al*. Comparative evaluation of the therapeutic effects of *Schisandra chinensis* and *Schisandra sphenanthera* on vascular cognitive impairment and their drug-like compounds. *Global Transl Med*. 2025:4(1):90-103.
doi: 10.36922/gtm.6879

Received: December 3, 2024

Accepted: December 19, 2024

Published online: February 14, 2025

[2]The National Clinical Research Center for Mental Disorders and Beijing Key Laboratory of Mental Disorders, Beijing Anding Hospital and Advanced Innovation Center for Human Brain Protection, Capital Medical University, Beijing, China

1. Introduction

Vascular cognitive impairment (VCI) refers to a clinical syndrome characterized by the impairment of at least one cognitive function domain, caused by cerebrovascular disease and its associated risk factors.[1] It encompasses a broad spectrum of cognitive disorders, ranging from mild cognitive impairment to dementia.[2] The prevalence of VCI increases rapidly with age, making it the second most prevalent type of cognitive deficit after Alzheimer's disease.[3] The primary symptoms of VCI, including attention deficits, memory loss, language impairment, executive dysfunction, and spatial cognitive decline, significantly impact patients' quality of life.[4] Although studies have shown that medications, such as donepezil can benefit VCI patients, their clinical efficacy remains contentious.[5] This underscores the imperative for developing safe and effective therapeutic agents for VCI.

Traditional Chinese medicine (TCM) has attracted growing attention owing to its efficacy in the prevention and treatment of VCI.[6] More importantly, TCM is recognized for its safety and effectiveness, especially in managing chronic conditions.[7] Wuweizi, a well-known TCM, has been used as a tonic and sedative agent for thousands of years.[8] Modern pharmacological studies have suggested that Wuweizi possesses a range of biological activities, such as neuroprotective, anti-inflammatory, antioxidative, and hepatoprotective properties.[9-12] Historically, Wuweizi is referred to as the ripe fruit of both *Schisandra chinensis* (SCF) and *Schisandra sphenanthera* (SSF). However, since the 2000 edition of Chinese Pharmacopoeia (ChP), SCF and SSF have been classified as distinct crude drugs with independent quality standards, despite similarities in their described efficacies in ChP.[13]

Dibenzocyclooctadiene lignans are the major bioactive components responsible for many of the pharmacological activities of SCF and SSF.[14,15] Compounds, such as schisandrol A-B, schisandrin A-C, and schisantherin A are present in both SCF and SSF, although their quantities differ, potentially contributing to both similar and distinct pharmacological effects.[13] Recent studies have highlighted the neuroprotective properties of SCF and its major constituents, particularly dibenzocyclooctadiene-type lignans, including schisandrin A, schisandrin B, schisandrin C, schisantherin A, schisandrin, schisandrol B, gomisin A, and gomisin N. These compounds have demonstrated protective effects against neurodegenerative and hypoxia-ischemia-related neural injuries, including stroke, Alzheimer's disease, and Parkinson's disease.[16-20] In contrast, research on SSF remains relatively limited. It is unclear whether SCF and SSF exhibit significant therapeutic effects against VCI. The differences in pharmacological efficacy and contributing constituents between SCF and SSF are also uncertain.

In this study, we evaluated the therapeutic differences between SCF and SSF in VCI using *in vivo* and *in vitro* models, characterized their chemical composition through ultraperformance liquid chromatography-quadrupole time-of-flight mass spectrometry (UPLC-Q-TOF/MS), and evaluated the drug-like properties of their components. The findings aim to provide valuable insights into the pharmacological difference of SCF and SSF against VCI and offer a reference for their clinical applications.

2. Materials and methods

2.1. Cell culture

BV2 cells were cultured in Dulbecco's Modified Eagle Medium (DMEM) supplemented with 10% fetal bovine serum (Gibco, USA). Cells at 80% – 90% confluence were used for experiments. For neuroinflammation modeling, BV2 cells were seeded into 96-well plates at a density of 3×10^5 cells/mL, pretreated with SCF or SSF (at concentrations of 0 – 40 μg/mL) for 2 h, and subsequently stimulated with lipopolysaccharide (LPS, 1 μg/mL, Sigma, Germany) for 24 h. For the oxygen and glucose deprivation/reperfusion (OGD/R) model, SCF- or SSF-pretreated cells were incubated in oxygen deprivation (94% N_2 + 5% CO_2 + 1% O_2) and glucose-free DMEM for 6 h, followed by normal incubation for an additional 6 h.

2.2. Cell viability assay

Cells were assessed using the Cell Counting Kit-8 (CCK8, Solarbio, China) according to the manufacturer's protocol. Cells were incubated with CCK8 solution (10% v/v) for 1.5 h. Absorbance was measured at 450 nm using a microplate reader (Spark, Tecan, Switzerland).

2.3. Griess and ELISA assay for inflammatory cytokines

After treatment, cell culture supernatants were collected and centrifuged. The levels of nitric oxide (NO) in cell supernatants were determined using commercial kits (Griess, Beyotime Biotechnology, China) according to the manufacturer's instructions, and absorbance was measured at 540 nm using a microplate reader (Spark,

Tecan, Switzerland). While, the concentrations of tumor necrosis factor-alpha (TNF-α) and interleukin-6 (IL-6) were measured using ELISA kits (Cat. no: 431304 [IL-6], Cat. no: 430915 [TNF-α], Biolegend, USA) according to the manufacturer' s protocol.

2.4. Measurement of mitochondrial membrane potential

The mitochondrial membrane potential was assessed using a JC-1 kit (Beyotime, China) under OGD/R conditions. Cells were incubated with JC-1 working buffer in the dark for 30 min, following the manufacturer's protocol. Fluorescence signals representing mitochondrial membrane potential levels were detected using a fluorescence microscope at excitation/emission wavelengths of 514/529 nm (for JC-1 monomers) and 585/590 nm (for JC-1 aggregates).

2.5. Animal models and treatment protocols

All animal experiments were approved by the Committee on Use and Care of Animals of the Institute of Medicinal Plant Development. A total of 50 10-week-old male C57BL/6J mice (weighing 24 – 29 g) were provided by Vital River Laboratory Animal Technology (China) and acclimated to laboratory conditions for 7 days. The mice were randomly divided into five groups (n = 10 per group):

(i) Control (CON): Sham operation with no treatment.
(ii) Model (MOD): Bilateral common carotid artery stenosis (BCAS) surgery with vehicle treatment (0.5% sodium carboxymethyl cellulose [CMC-Na]).
(iii) Positive control (POS): BCAS surgery with 20 mg/kg of nimodipine (Bayer, Germany)
(iv) SCF group: BCAS surgery with 400 mg/kg SCF extract.
(v) SSF group: BCAS surgery with 400 mg/kg of SSF extract.

Mice were anesthetized, and both common carotid arteries (CCAs) were exposed. BCAS was induced using microcoils (0.18 mm inner diameter; Sawane Spring Co, Japan) following established protocols.[21] The microcoil was first applied to the right CCA by rotating it around the artery and then to the left CCA after a 30-min interval. Sham-operated control mice underwent the same surgical procedure without the placement of microcoils. Seven days post-surgery, BCAS mice in different groups received daily intragastric administration of the corresponding drug treatments for 30 consecutive days, while the CON and MOD groups received 0.5% CMC-Na as vehicle controls.

2.6. Neurological severity score test

Neurological function was evaluated using the modified neurological severity score (mNSS) test[22] on days 7, 14, 21, and 28 post-BCAS. The mNSS is a composite assessment of motor function (muscle status, abnormal movements), sensory function (visual, tactile, and proprioceptive), and reflexes. Scores range from 0 (normal) to 18 (maximal deficit), with higher scores indicating greater neurological impairment.

2.7. Open field test

Behavioral activity was assessed on day 29 using the open field test. Mice were placed individually in the center of a 50 × 50 × 50 cm white box, and their total distance traveled (in mm) was recorded over 5 min using a video analysis system (v5.2.0.0, SuperMaze, China).

2.8. Novel object recognition test (NORT)

Cognitive abilities were evaluated using the NORT from days 30 to 33. During the first 3 days, mice acclimated daily to a 50 × 50 × 50 cm white box containing two identical red cylinders placed at opposite ends. Tests were conducted on the 4th day in two phases:

(i) Phase 1: Mice were allowed to explore two identical cylinders (F1 and F2) for 5 min. The exploration time for each object was recorded, and the relative preference index was calculated as

$$RPI(\%) = \frac{F1 - F2}{F1 + F2} \times 100 \quad \text{(I)}$$

(ii) Phase 2: After a 30-min rest period, one cylinder was replaced with a new green square of the same height. Mice were allowed to explore the new object (N) and the remaining cylinder (F) for 5 min. The exploration time was recorded, and the relative discrimination index was calculated as follows:

$$RDI(\%) = \frac{N - F}{N + F} \times 100 \quad \text{(II)}$$

Exploration behaviors were recorded and analyzed using SuperMaze software.

2.9. Morris water maze (MWM) test

Spatial learning deficits were assessed twice daily using an enhanced MWM test from days 33 to 37. A 1-m-diameter pool was placed in a room devoid of external orientation cues and divided into four quadrants with four fixed points using the SuperMaze system. An invisible, submerged platform was fixed in the northwest quadrant. Mice were randomly placed at one of the designated starting points and were allowed 1.5 min to locate the platform, with a 10-s stay permitted upon successful navigation. Mice unable to find the platform were passively placed on it for 10 s. On day 38, the platform was removed, and mice underwent a free swim test for 1.5 min to evaluate spatial reference memory. The time taken to reach the previous

platform location and other behavioral data were analyzed using SuperMaze software.

2.10. Full-field laser perfusion imaging

One hour after final administration, anesthetized mice were subjected to craniotomy for full-field laser perfusion imaging (FLPI) (FLPI2, Moor Instruments, United Kingdom). The FLPI system was configured to a low-resolution, high-speed imaging mode with a display rate of 25 Hz, a time constant of 1.0 s, and an exposure time of 20 ms. Every measurement lasted 1 min, generating six stabilized blood flow images with the camera positioned 10 cm above the brain.

2.11. Luxol fast blue (LFB) staining

On day 40, anesthetized mice received transcardial perfusion with saline followed by paraformaldehyde. Brains were post-fixed, embedded in paraffin, sectioned into 4-μm slices, and stained with 0.1% LFB, followed by 0.05% lithium carbonate. The sections were then sealed with a coverslip and examined under a light microscope. The severity of demyelination was scored as follows: 0: normal; 1: disarrangement of nerve fibers; 2: obvious vacuoles; and 3: injured and disappearance of myelinated fibers.

2.12. Immunohistochemistry staining

Paraffin sections underwent antigen retrieval, treatment with 3% H_2O_2, and blocking with 3% bovine serum albumin. Sections were incubated overnight at 4°C with a rabbit anti-myelin basic protein (MBP) antibody (1:1000; Cat. no. K002910P, Solarbio, China), followed by incubation with horseradish peroxidase-labeled anti-rabbit secondary antibody (1:200; Cat. no. PV-9000, Solarbio, China) and diaminobenzidine staining. The sections were counterstained with hematoxylin and examined under a light microscope. The degree of demyelination was semi-quantified using Image-Pro Plus software.

2.13. Ethanol extract preparation for SCF and SSF

SCF and SSF fruits were harvested from Huanren (Jilin province) and Shangluo (Shaanxi province), China, respectively, in September 2020. The samples were identified by Dr. Yaodong Qi (Institute of Medicinal Plant Development, Chinese Academy of Medical Sciences), and voucher specimens were stored in the authors' laboratory. The dried fruit (500 g) was powdered, extracted using gradient ethanol (1:10 v/v), and enriched to obtain an ethanol extract.

2.14. Chemical constituent analysis of SCF and SSF

SCF and SSF extracts were analyzed using ACQUITY UPLC coupled with a Xevo G2 QTOF detector (Waters Corporation, United States). Major constituents were separated using an ACQUITY UPLC BEH C_{18} column (2.1 × 100 mm, 1.7 μm) at a flow rate of 0.3 mL/min and a temperature of 23°C, with an injection volume of 2 μL. The elution gradient was performed using 0.1% formic acid water (A) and acetonitrile (B) as follows: 0 – 1 min, 5% – 30% B; 1 – 2 min, 30% – 40% B; 2 – 4 min, 40% – 52% B; 4 – 6 min, 52% – 60% B; 6 – 9 min, 60% – 62% B; 9 – 10 min, 62% B; 10 – 13 min, 62% – 66% B; 13 – 15 min, 66% – 70%. Mass weight was detected in centroid mode using an electrospray ionization source over a mass range of 50 – 1700 Da, with a scan time of 0.3 s. The MS detector was set with a capillary voltage of 3 kV, a sampling cone voltage of 40 V, a source temperature of 100°C, a desolvation temperature of 350°C, and collision energy of 6 kV. Data were collected using MassLynx 4.1 software and profiled using Progenesis QI 2.3 software, with assistance from a self-constructed *Schisandra* compound database.

2.15. Evaluation of drug-likeness

For compounds identified using UPLC-Q-TOF/MS, six physicochemical properties, including lipophilicity, size, polarity, solubility, saturation, and flexibility, were evaluated for bioavailability. Predictions of passive human gastrointestinal absorption (HIA), blood-brain barrier (BBB) permeability, and interactions with permeability glycoprotein (P-gp) for active efflux were conducted using the SwissADME web tool (http://www.swissadme.ch).

2.16. Statistical analysis

Raw data were presented as mean ± SEM. One-way ANOVA was used for multiple group comparisons in GraphPad Prism 8.0, followed by Fisher's least significant difference test for normally distributed data, or the Kruskal–Wallis *H*-test for non-normally distributed data. Statistical significance was set at $P < 0.05$ or $P < 0.01$.

3. Results

3.1. SCF exhibits stronger anti-neuroinflammatory activity than SSF in LPS-induced BV2 cells model

Microglial activation is a prominent feature following chronic cerebral hypoperfusion.[23] To evaluate and compare the anti-neuroinflammation effects of SCF and SSF, an LPS-induced BV2 cell model was established. A pilot study (data not shown) confirmed that SCF and SSF had no significant effects on BV2 cell viability at concentrations below 80 μg/mL. Based on preliminary experimental results, 40, 16, 6.4, and 2.56 μg/mL were selected for further study.

As shown in Figure 1, LPS stimulation significantly increased the production of NO, TNF-α, and IL-6 in BV2 cells compared to the control group. Treatment with

SCF or SSF (40 and 16 μg/mL) significantly reduced NO and TNF-α levels. Furthermore, IL-6 production was markedly suppressed in BV2 cells treated with SCF or SSF at the highest dose (40 μg/mL). Notably, the reduction in inflammatory markers was more pronounced in the SCF group than in the SSF group at the same dose.

3.2. SCF ameliorates OGD/R-induced mitochondrial damage in BV2 cells

Mitochondrial damage serves as an indicator of oxidative stress and is relevant to studies on antioxidant-induced mitochondrial damage models.[24] To examine the effects of SCF and SSF on mitochondrial integrity, an OGD/R-BV2 cells model was employed. As shown in Figure 2, OGD/R treatment significantly decreased both cell viability and mitochondrial membrane potential in BV2 cells. Treatment with SCF (40, 16, and 6.4 μg/mL) resulted in a dose-dependent restoration of these parameters, whereas SSF had no significant effect. These results suggest that SCF provides superior mitochondrial protection compared to SSF.

3.3. SCF is more efficacious than SSF in alleviating cognitive impairment in BCAS mice

The BCAS mouse model is widely used to study aspects of VCT. To determine whether SCF or SSF treatment alleviates

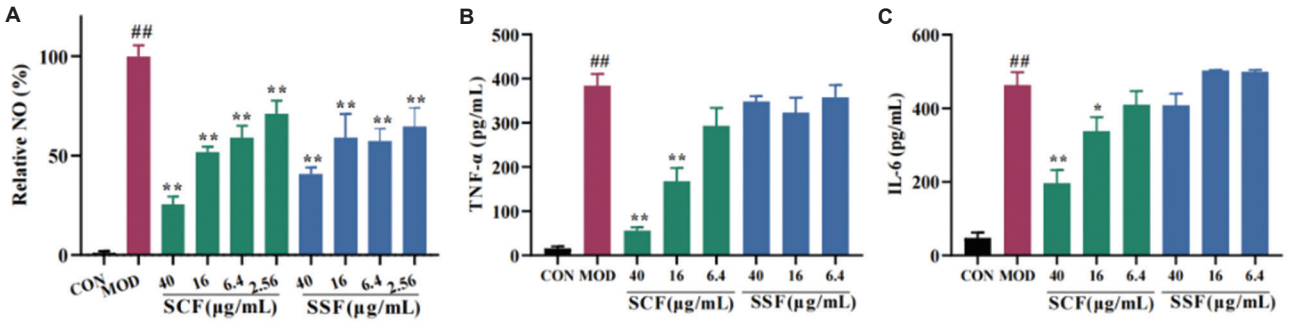

Figure 1. Comparative effects of SCF and SSF on neuroinflammation in LPS-induced BV2 cells. The production of (A) NO, (B) TNF-α, and (C) IL-6 was inhibited following SCF or SSF treatment. Data are presented as mean ± SEM (n = 3 per group). Notes: $^{*}P < 0.05$ and $^{**}P < 0.01$, compared with LPS-treated models (MOD); $^{\#}P < 0.05$ and $^{\#\#}P < 0.01$, compared with the control (CON).
Abbreviations: SCF: *Schisandra chinensis;* SSF: *Schisandra sphenanthera;* LPS: Lipopolysaccharide; NO: Nitric oxide; TNF-α: Tumor necrosis factor-alpha; IL-6: Interleukin-6.

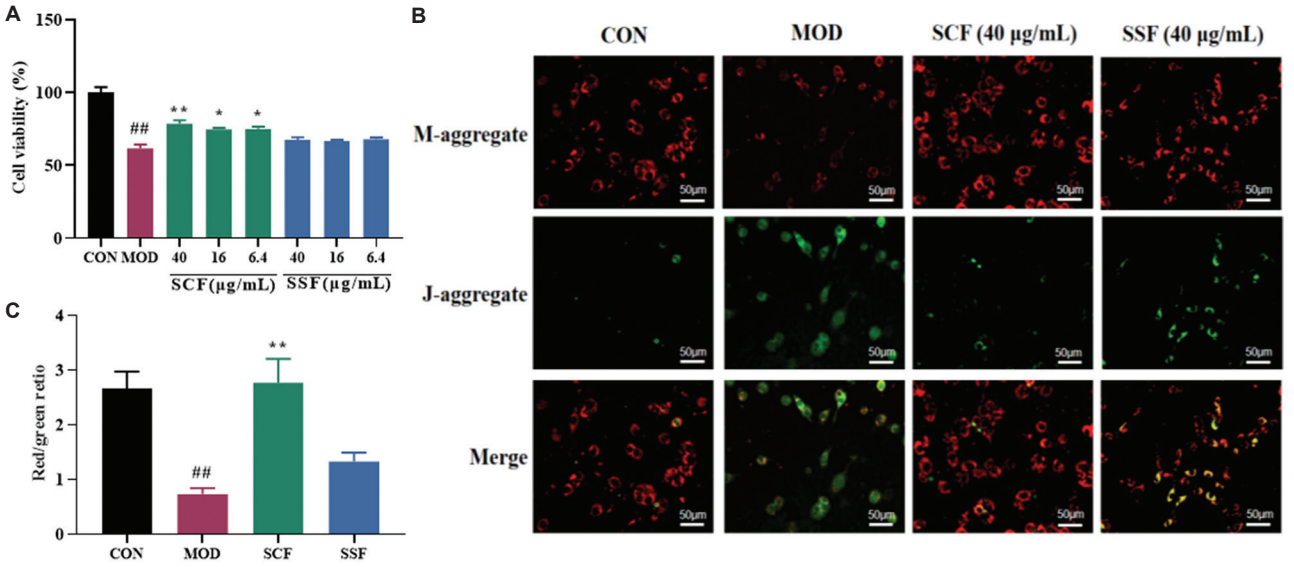

Figure 2. Comparative effects of SCF and SSF on cell viability and mitochondrial membrane potential in OGD/R-induced BV2 cells. (A) Cell viability. (B) Representative photomicrographs of JC-1 staining (Scale bars: 50 μm; magnification: 200×) and (C) corresponding quantification analysis. Data are presented as mean ± SEM (n = 3 per group). Notes: $^{*}P < 0.05$ and $^{**}P < 0.01$, compared with OGD/R-treated model (MOD); $^{\#}P < 0.05$ and $^{\#\#}P < 0.01$, compared with control (CON).
Abbreviations: SCF: *Schisandra chinensis;* SSF: *Schisandra sphenanthera.*

cognitive impairment, several behavioral experiments were conducted in BCAS mice. The mNSS revealed no significant limb-curl and tail-lift reflexes among all groups at 7, 14, 21, and 28 days post-operatively (Figure 3A), indicating normal neurological function and ensuring that cognitive impairment assessments were not confounded by motor deficits. Similarly, the open field test showed no significant differences in total distances traveled (Figure 3B), implying that BCAS surgery did not affect motor or optic nerve function.

Furthermore, during the NORT, no significant preference differences were observed for two old objects among groups during the training phase (Figure 3C). However, after BCAS surgery, mice exhibited reduced curiosity toward the new object, as indicated by a significantly decreased relative discrimination index in the MOD group compared to the CON group ($P < 0.05$) (Figure 3D). Notably, SCF (400 mg/kg) treatment significantly restored exploratory preference compared to the MOD group ($P < 0.05$), whereas SSF (400 mg/kg) showed a trend toward cognitive improvement without statistical significance ($P > 0.05$).

In the MWM test, baseline escape latency showed no significant difference among groups. However, BCAS mice exhibited a significant increase in escape latency on days 3 – 5 ($P < 0.01$, compared to control mice). SCF treatment significantly reduced the escape latency ($p<0.01$) (Figure 3E). During the spatial exploration test, BCAS mice in the MOD group exhibited a significantly decreased number of platform crossing ($P < 0.01$) (Figure 3F), a significantly decreased frequency of target quadrant crossing ($P < 0.01$) (Figure 3H), and less time spent in

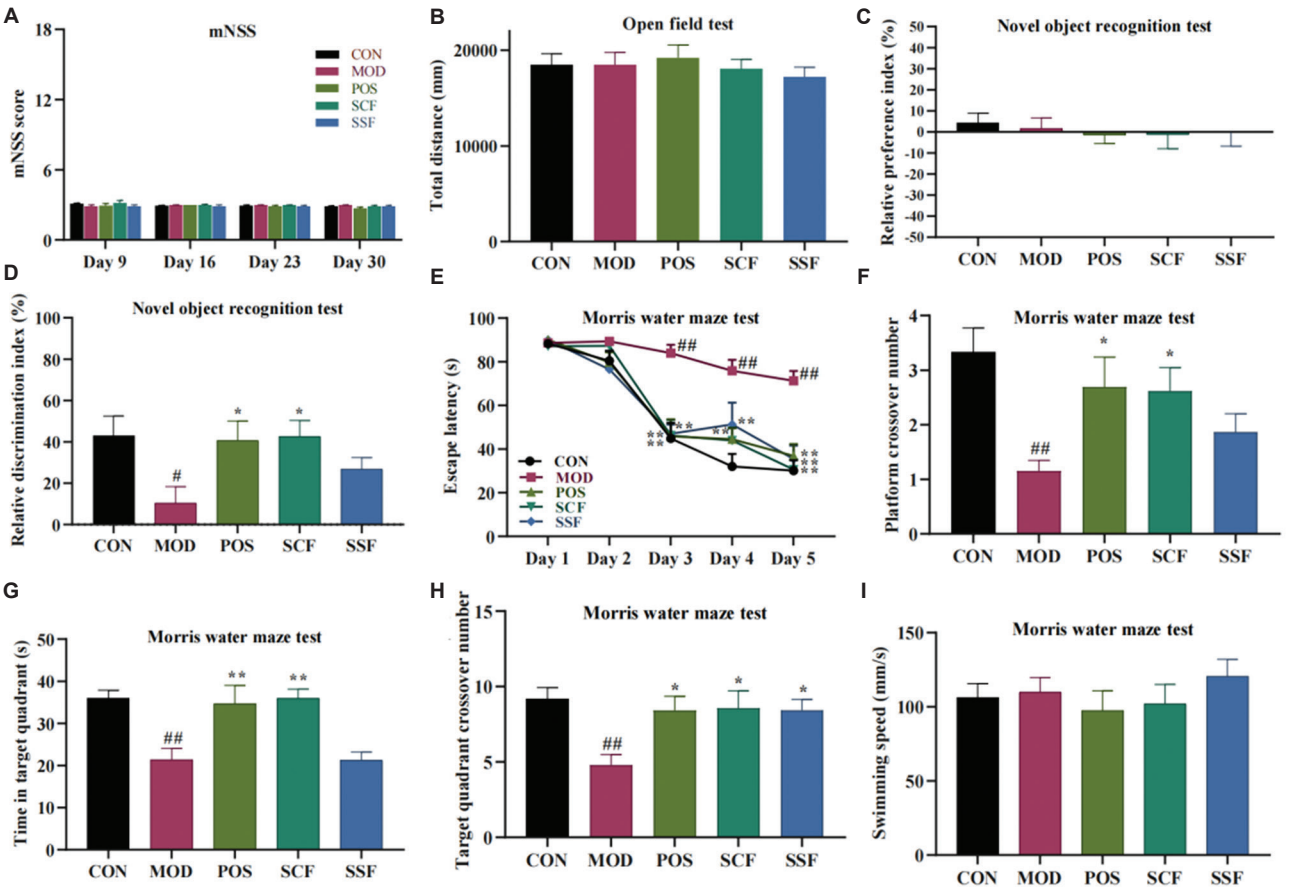

Figure 3. Effects of SCF and SSF on exploratory locomotor behavior and spatial learning memory following BCAS surgery. (A) mNSS at different time points. (B) Total distance traveled in the open field test on day 29 post-BCAS. (C) Relative preference index and (D) relative discrimination index in the novel object recognition test on day 32. (E) Escape latency in Morris water maze navigation test at different time points. (F-I) Frequency of platform crossings, time spent in the target quadrant, frequency of target quadrant crossings, and swimming speed in the Morris water maze probe test on day 38. Data are presented as mean ± SEM ($n = 8$ per group). Notes: $^{*}P < 0.05$ and $^{**}P < 0.01$, compared with the BCAS group (MOD); $^{\#}P < 0.05$ and $^{\#\#}P < 0.01$, compared with the control group (CON). POS: Positive control.
Abbreviations: SCF: *Schisandra chinensis;* SSF: *Schisandra sphenanthera;* BCAS: Bilateral common carotid artery stenosis; mNSS: Modified neurological severity score.

the target quadrant ($P < 0.01$) (Figure 3G). In contrast, SCF-treated mice demonstrated better spatial learning and memory ability than the MOD mice, as evidenced by a significantly increased frequency of platform crossing ($P < 0.05$), a higher frequency of target quadrant crossings ($P < 0.05$), and significantly more time spent in the target quadrant ($P < 0.01$). However, the cognitive improvement effects of SSF were less pronounced and not statistically significant ($P > 0.05$). In addition, no significant differences in swimming speed were observed among groups ($P > 0.05$) (Figure 3I). Overall, these behavioral assessments demonstrate that SCF treatment significantly ameliorates learning and memory deficits in BCAS mice.

3.4. SCF and SSF improves cerebral blood flow

As shown in Figure 4, cerebral blood flow was significantly reduced due to hypoperfusion induced by BCAS surgery ($P < 0.01$). In comparison to untreated BCAS mice, all drug-treated groups exhibited increased cerebral blood flow ($P < 0.01$), indicating that both SCF and SSF improved cerebral perfusion following BCAS surgery.

3.5. SCF is more efficacious than SSF in alleviating BCAS-induced white matter injury

In CON mice, LFB staining revealed a densely packed and well-organized myelin sheath. In contrast, MOD mice exhibited a disrupted myelin structure, characterized by a loose and disordered myelin sheath and the presence of white vacuoles in the corpus callosum (Cc, paramedian), fimbria of the hippocampus (Fi), ventral posteromedial thalamic nucleus (VPT), and caudate putamen (Cpu, striatum) ($P < 0.01$) (Figure 5). All drug-treated mice exhibited significantly preserved white matter integrity ($P < 0.05$ or $P < 0.01$). Notably, the SCF group showed a greater degree of preservation, with denser and more organized nerve fibers than the SSF group.

The MBP immunohistochemical staining results (Figure 6) were consistent with the LFB staining data. Compared with CON mice, the MOD mice exhibited significantly reduced and weaker MBP staining in the Cc, Fi, VPT, and Cpu ($P < 0.01$ or $P < 0.05$). SCF treatment significantly alleviated myelin degeneration in all four brain areas ($P < 0.01$ or $P < 0.05$), whereas SSF treatment exerted significant protective effects only in VPT and Cpu ($P < 0.01$)

3.6. Chemical characterization of SCF and SSF using UPLC-Q-TOF/MS

The chemical compositions of SCF and SSF were analyzed using UPLC-Q-TOF/MS (Figure 7). A total of 71 compounds were identified in SCF, including 56 lignans (42 diphenylcyclooctene lignans, 8 tetrahydrofuran

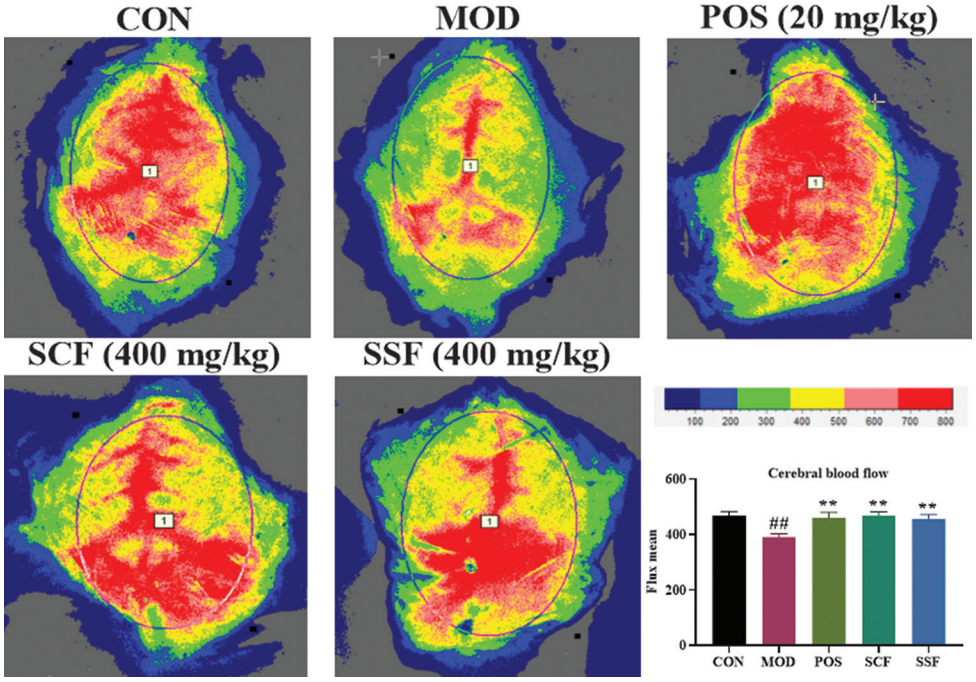

Figure 4. Representative images and related quantitative analysis for comparative effects of SCF and SSF on cerebral blood flow following BCAS surgery. The color bar (blue to red) indicates low to high flow velocity. Data are presented as mean ± SEM ($n = 8$ per group). Notes: $^{*}P < 0.05$ and $^{**}P < 0.01$, compared with the BCAS group (MOD); $^{\#}P < 0.05$ and $^{\#\#}P < 0.01$, compared with the control group (CON).
Abbreviations: POS: Positive control; SCF: *Schisandra chinensis;* SSF: *Schisandra sphenanthera;* BCAS: Bilateral common carotid artery stenosis.

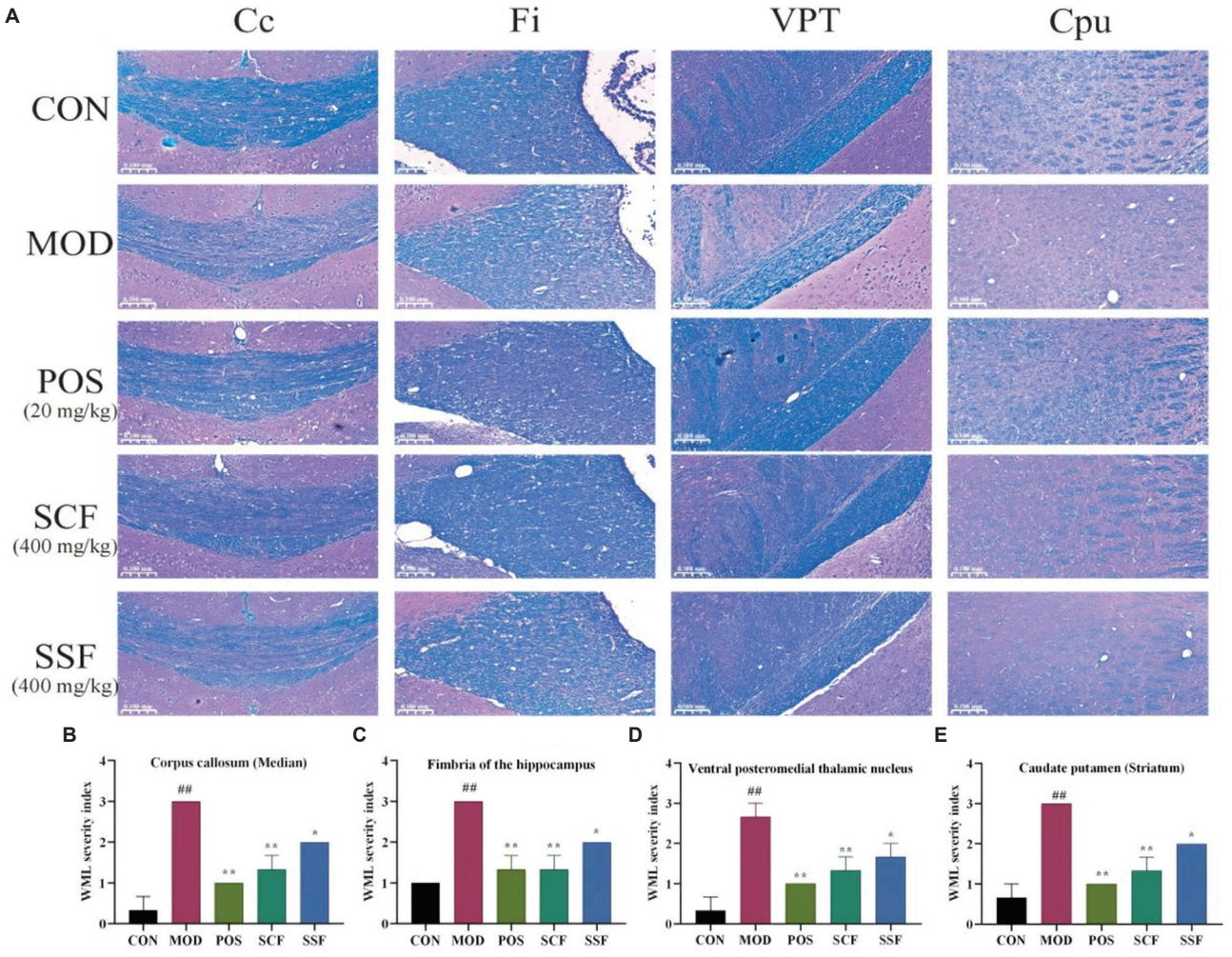

Figure 5. Comparative effects of SCF and SSF on white matter integrity following BCAS surgery. (A) LFB-stained images showing increased myelin rarefaction and white matter lesion formation in the Cc (paramedian), fimbria of the hippocampus (Fi), ventral posteromedial thalamic nucleus (VPT), and Cpu (striatum) of BCAS mice, with a visible protective effect in the SCF- and SSF- treated groups. All images were taken under identical exposures and conditions (Scale bar: 200 μm; magnification: 20×). (B-E) Quantification analysis of LFB-staining in Cc, Fi, VPT, and Cpu, respectively. Data are presented as mean ± SEM (n = 3 per group). Notes: $^{*}P < 0.05$ and $^{**}P < 0.01$, compared with the BCAS group (MOD); $^{\#}P < 0.05$ and $^{\#\#}P < 0.01$, compared with the control group (CON).

Abbreviations: POS: Positive control; SCF: *Schisandra chinensis;* SSF: *Schisandra sphenanthera;* BCAS: Bilateral common carotid artery stenosis; Cc: Corpus callosum; Cpu: Caudate putamen.

lignans, 4 furofurans, 2 lignan lactones), 10 carboxylic acids (5 eicosanoids, 5 carboxylic acids), 2 lactones, 2 sesterterpenoids, and 1 pyrrilium (Table S1). For SSF, a total of 63 compounds were identified, including 21 lignans (9 diphenylcyclooctene lignans, 4 dibenzylbutane lignans, 5 tetrahydrofuran lignans, 2 aryltetralin lignans, 1 furanoid lignan), 2 terpenoids (1 triterpenoid, 1 sesquiterpenoid), 1 lactone, 17 phenylpropanoids (16 phenylpropanoids, 1 flavonoid), 1 phenol, 16 alkaloids, 4 carboxylic acids, and 1 sulfoxide (Table S2). These results suggest that SCF and SSF exhibit distinct chemical compositions, which may contribute to different pharmacological effects.

3.7. Pharmacokinetic differences between compounds in SCF and SSF

Compounds with high bioavailability and drug-likeness properties are more likely to be absorbed.[25] Bioactive compounds with therapeutic effects are generally expected to exhibit passive HIA properties.[26] Therefore, we further conducted analysis of six physicochemical properties, HIA and BBB permeation, and interactions with P-gp in the identified compounds.

As shown in Figure 8, the predicted lipophilicity, size, polarity, solubility, flexibility, and saturation properties were evaluated for the identified compounds. A total of 64 compounds in SCF and 60 compounds in SSF were

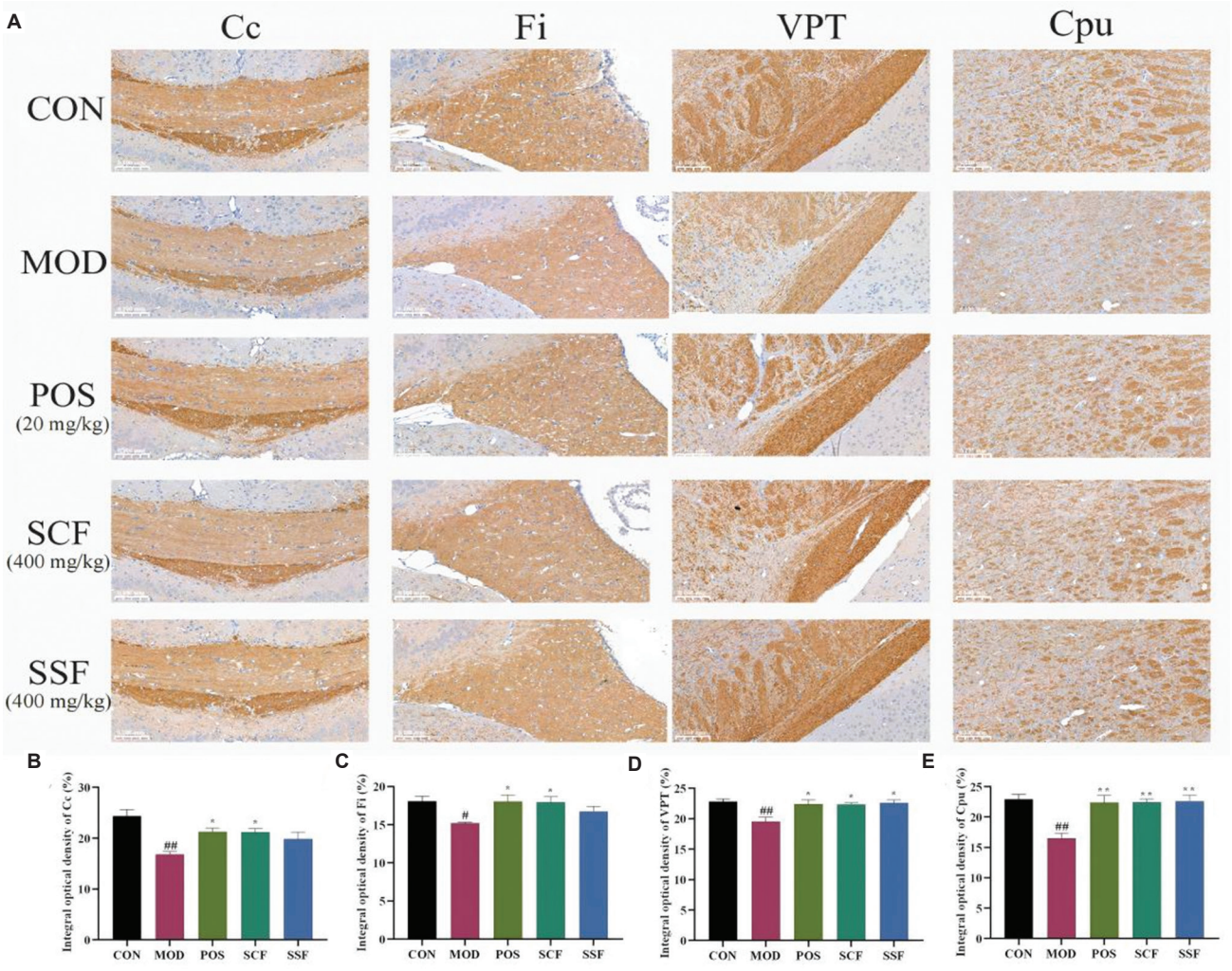

Figure 6. Comparative effects of SCF and SSF on myelin regeneration following BCAS surgery. (A) MBP immunoreactivity was reduced in the Cc, fimbria of the hippocampus (Fi), ventral posteromedial thalamic nucleus (VPT), and Cpu of BCAS mice. A trend of alleviation was observed in the positive control (POS), SCF-, and SSF-treated groups. All images were taken under identical exposures and conditions (Scale bar: 200 μm; magnification: 100×). (B-E) Quantification analysis of MBP in Cc, Fi, VPT, and Cpu, respectively. Data are presented as mean ± SEM (n = 3 per group). Notes: $^{*}P < 0.05$ and $^{**}P < 0.01$, compared with the BCAS group (MOD); $^{\#}P < 0.05$ and $^{\#\#}P < 0.01$, compared with the control group (CON).
Abbreviations: POS: Positive control; SCF: *Schisandra chinensis;* SSF: *Schisandra sphenanthera;* BCAS: Bilateral common carotid artery stenosis; Cc: Corpus callosum; Cpu: Caudate putamen; MBP: Myelin basic protein.

predicted to have HIA > 25% and bioavailability > 0.15. Among these highly absorbable compounds, lignans constituted a significant portion. Furthermore, P-gp interaction analysis revealed that:

(i) In SCF, 5 carboxylic acids and 2 lignans (1 furofuran lignan, 1 diphenylcyclooctene lignan) exhibited unacceptable P-gp interaction values.
(ii) In SSF, 1 phenylpropanoid and 2 carboxylic acids showed unacceptable P-gp interaction values.
(iii) None of the compounds in SCF and only 1 compound in SSF with poor passive gastrointestinal absorption were identified as P-gp substrates, indicating low potential for active transport.

These results indicate that lignans, particularly diphenylcyclooctene-type lignans, may be key contributors to the pharmacological differences between SCF and SSF in the treatment of VCI.

4. Discussion

VCI is a cognitive dysfunction syndrome characterized by neurodegeneration, memory impairment, and cognitive deficits, for which there is currently no effective treatment.[27] Considerable evidence indicates that neuroinflammation and oxidative stress are important factors contributing to the occurrence and development of VCI.[28,29] Neuroinflammation has been

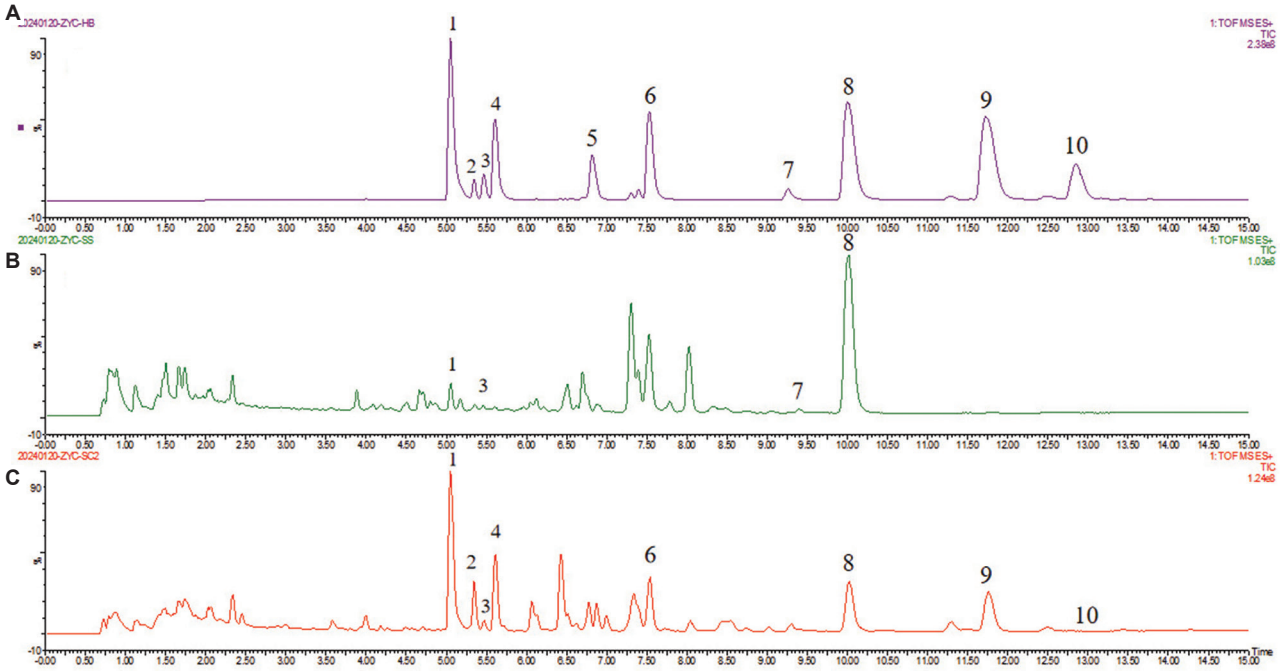

Figure 7. Total ions chromatogram of (A) standard compounds, (B) SSF, and (C) SCF in positive ion mode. Identified peaks: 1. schisandrin, 2. gomisin D, 3. gomisin J, 4. schisandrol B, 5. gomisin G, 6. schisantherin B, 7. anwulignan, 8. schisandrin A, 9. schisandrin B, 10. schisandrin C.
Abbreviations: SCF: *Schisandra chinensis;* SSF: *Schisandra sphenanthera.*

proven to contribute to the etiology of hypoxia-ischemia-induced neural injury.[30] Potential molecular mechanisms underlying VCI include inflammation and mitochondrial dysfunction.[31] Inflammatory cytokines, chemokines, and reactive oxygen and nitrogen species exacerbate neuronal damage and act as pivotal mediators of persistent neuronal injury.[32]

Previous studies have demonstrated that SCF and SSF exhibit a range of pharmacological activities, including neuroprotective, anti-inflammatory, antioxidative, and cardioprotective effects.[8,13] Notably, SCF has been shown to regulate inflammatory responses and inflammation-induced damage to cerebral vessels and brain tissue, thereby improving cerebral ischemia and neurological dysfunction.[33] Furthermore, SCF is capable of scavenging reactive oxygen species and mitigating oxidative stress-induced brain tissue damage, thereby alleviating symptoms associated with cerebral ischemia.[34]

Given the role of neuroinflammation and oxidative stress in VCI pathogenesis, we first investigated the effects of SCF and SSF in LPS- and OGD/R-induced BV2 cell models. Our data suggest that SCF exerts strong anti-neuroinflammatory and antioxidative effects in BV2 cells. Notably, SCF demonstrated significantly greater anti-neuroinflammatory and antioxidative capacity compared to SSF.

The ameliorative effects of SCF and SSF on VCI were further validated using a BCAS mouse model. This model is regarded as the most widely used experimental model for VCI,[35] as it reliably replicates both clinical and pathological features of the disease.[36] The BCAS model induces cognitive impairment, chronic hypoperfusion, and subsequent white matter damage.[21] Notably, BCAS mice do not develop cerebral infarctions and optic nerve damage but exhibit hippocampal neuronal death and atrophy, leading to learning and memory deficits.

As expected, SCF and SSF treatment significantly improved learning ability, spatial memory, and cerebral blood flow, and promoted nerve fiber repair. However, SCF was more effective than SSF in improving learning ability and spatial memory. Our results demonstrate that SCF exhibits superior efficacy in preventing white matter damage and cognitive decline, aligning with its traditional medicinal applications. However, there remains a lack of relevant research to elucidate the specific mechanisms underlying the pharmacological differences between SCF and SSF.

To address this issue, UPLC-Q-TOF/MS was used to comprehensively characterize and determine the chemical composition of SCF and SSF, as well as to evaluate the drug-like properties of their components. A total of 71 were identified in SCF, whereas 64 compounds were identified

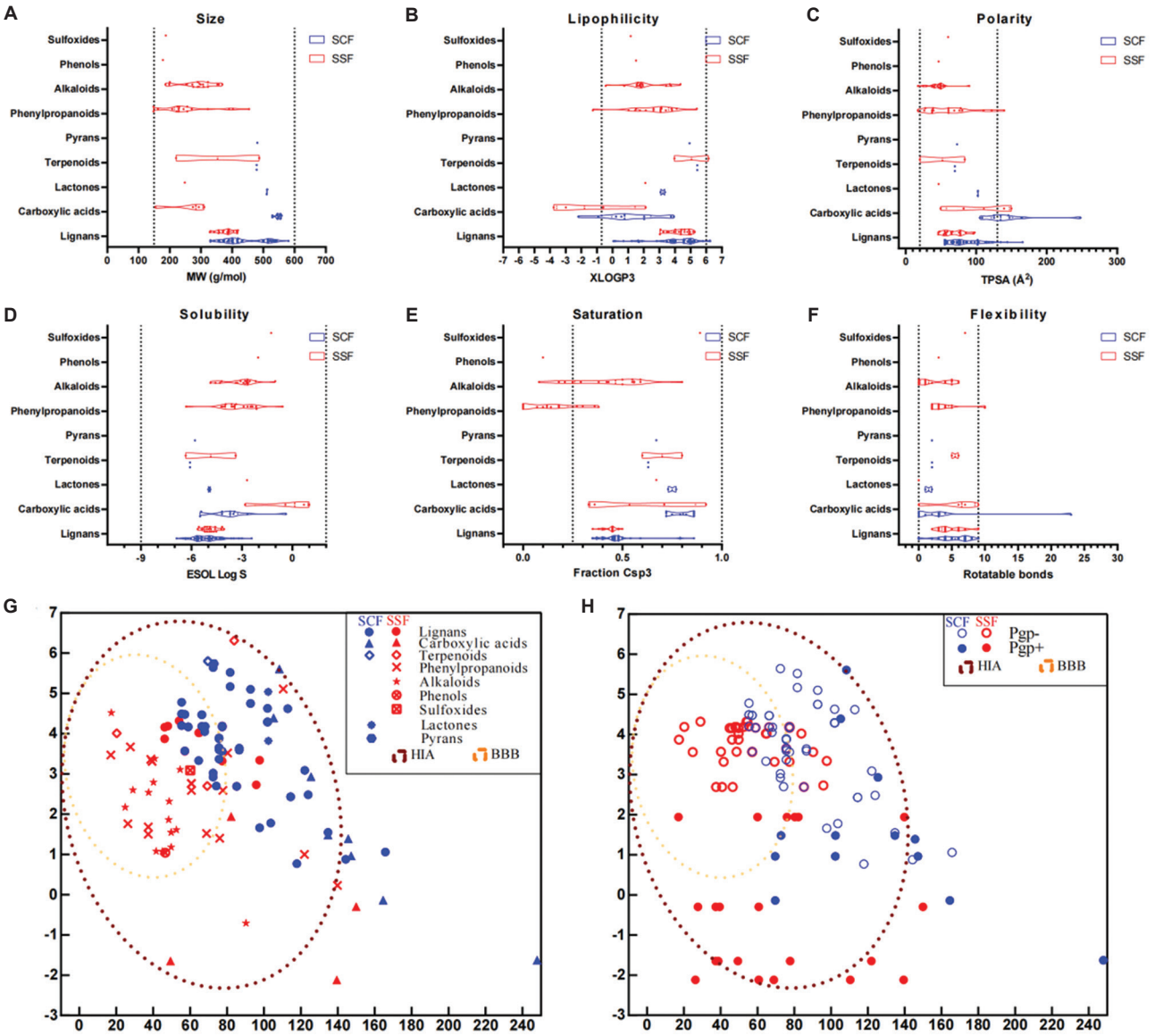

Figure 8. Drug-likeness properties and structures of identified compounds in SCF and SSF. (A-F) Six physicochemical properties for evaluating bioavailability (size, lipophilicity, polarity, solubility, saturation, and flexibility). Acceptable MW range: 150 – 600 g/moL; XLOGP3: −0.7 – 6.0; TPSA: 20 – 130 Å2; log S: −9 – 2; sp3 hybridized carbon atoms in the molecule: >0.25; number of rotatable bonds: <9. (G) Absorption, distribution, metabolism, and excretion (ADME) properties: Passive HIA and BBB permeation. (H) ADME properties: Interaction with P-gp substrates.
Abbreviations: SCF: *Schisandra chinensis;* SSF: *Schisandra sphenanthera;* MW: Molecular weight; TPSA: Topological polar surface area; HIA: Human intestinal absorption; P-gp: Permeability glycoprotein.

in SSF. SCF contained a higher number of lignans than SSF (56 vs. 16), while SSF contained more phenylpropanoids (16 vs. 0) and alkaloids (16 vs. 0).

Modern pharmacological research has demonstrated that lignans are the major bioactive constituents of SCF and SSF.[13] Particularly, dibenzocyclooctadiene lignans are regarded as the primary contributors to their pharmacological effects, which may account for their observed differences in efficacy.[13] Our data also include simulation results on compound permeability across the BBB. In SCF, the active compounds capable of effectively crossing the BBB predominantly belong to the biphenylcyclooctene lignan class, which encompasses schineolignin A, gomisin L_2, schisandrin, schisandrin A, schisandrin B, schisandrin C, schisanhenol, schisanchinin C, and schisandrol B. Notably, several of these lignans (schisandrin C, schisandrin A, schisandrin B, schisandrin, and schisandrol B) have been confirmed through comparison with standard samples and are relatively abundant in SCF.

In contrast, only schisandrin C was identified in SSF through comparison with standard samples and found to cross the BBB. The total lignin extracts of SCF have been demonstrated to possess robust anti-neuroinflammatory effects.[37] In addition, several studies have reported that schisandrin A, schisandrin B, schisandrin C, schisandrin, and schisandrol B – compounds isolated from SCF – can alleviate neuroinflammation *in vitro* and *in vivo* models, supporting their potential roles in the treatment of VCI.[19,38-41] Taken together, these findings suggest that the primary pharmacological effects of SCF likely stem from the specific compounds mentioned above.

5. Conclusion

The present study demonstrates that both SCF and SSF can effectively ameliorate VCI, at least in part, by enhancing anti-neuroinflammatory and antioxidative stress responses. However, SCF exhibits superior effects in improving cognitive impairment compared to SSF, likely due to its higher structural diversity of biphenylcyclooctene-type lignans. This study provides scientifically valuable data on the therapeutic differences between SCF and SSF in the treatment of VCI and offers insights relevant to clinical applications.

Acknowledgments

None.

Funding

This work was supported by the CAMS Innovation Fund for Medical Sciences (2023-I2M-QJ-013, 2021-I2M-1-031, 2023-I2M-2-006, and 2022-I2M-2-002), the Beijing Natural Science Foundation (No. Z220019), and National Natural Science Foundation of China (No. U23A20511, No. 82304708).

Conflict of interest

The authors declare that they have no known competing financial interests or personal relationships that could have appeared to influence the work reported in this paper.

Author contributions

Conceptualization: Pei Ma
Data curation: Yucen Zou, Bin Li, Meiqi Wang, Jianuo Zhang, Qi Xiao, Chunyan Yang
Formal analysis: Yucen Zou, Bin Li, Meiqi Wang, Xiaomeng Xie, Jianuo Zhang, Qi Xiao, Jiushi Liu
Investigation: Jiushi Liu
Methodology: Haitao Sun, Bengang Zhang
Writing – original draft: Yucen Zou, Bin Li, Pei Ma
Writing – review & editing: Haitao Liu

Ethics approval and consent to participate

BV2 cells were purchased from the Chinese Academy of Medical Sciences (Beijing, China). All animal experimental procedures in this study followed the Guide for the Care and Use of Laboratory Animals (National Institutes of Health), approved by the Experimental Animal Ethical Committee of the Institute of Medicinal Plant Development, Chinese Academy of Medical Sciences (SLXD-20230425013).

Consent for publication

Not applicable.

Availability of data

The data that support the findings of this study are available from the corresponding author upon reasonable request.

References

1. Wang Z, Han B, Qi J, Cao X, Gu H, Sun J. Chuanzhitongluo capsule improves cognitive impairment in mice with chronic cerebral poperfusion via the cholinergic anti-inflammatory pathway. *Exp Gerontol*. 2024;189:112407.

   doi: 10.1016/j.exger.2024.112407

2. Lou T, Wu H, Feng M, *et al*. Integration of metabolomics and transcriptomics reveals that da chuanxiong formula improves vascular cognitive impairment via Acsl4/Gpx4 mediated ferroptosis. *J Ethnopharmacol*. 2024;325:117868.

   doi: 10.1016/j.jep.2024.117868

3. Hao S, He Q, Yuan Y, Mu Q. The protective effects of Irbesartan in cognitive impairment in hypertension. *Aging* (*Albany NY*). 2024;16(6):5065-5076.

   doi: 10.18632/aging.205589

4. Li S, Xiao Z. Recent research progress on the use of transcranial magnetic stimulation in the treatment of vascular cognitive impairment. *Neuropsychiatr Dis Treat*. 2024;20:1235-1246.

   doi: 10.2147/ndt.S467357

5. Lu H, Zhang J, Liang Y, *et al*. Network topology and machine learning analyses reveal microstructural white matter changes underlying Chinese medicine Dengzhan Shengmai treatment on patients with vascular cognitive impairment. *Pharmacol Res*. 2020;156:104773.

   doi: 10.1016/j.phrs.2020.104773

6. Lv S, Wang Q, Zhang X, *et al*. Mechanisms of Multi-Omics and network pharmacology to explain traditional Chinese medicine for vascular cognitive impairment: A narrative review. *Phytomedicine*. 2024;123:155231.

   doi: 10.1016/j.phymed.2023.155231

7. Hu WH, Mak SH, Zheng ZY, *et al*. Shexiang Baoxin Pill, a traditional chinese herbal formula, rescues the cognitive

impairments in APP/PS1 transgenic mice. *Front Pharmacol*. 2020;11:1045.

doi: 10.3389/fphar.2020.01045

8. Sowndhararajan K, Deepa P, Kim M, Park SJ, Kim S. An overview of neuroprotective and cognitive enhancement properties of Lignans from *Schisandra chinensis*. *Biomed Pharmacother*. 2018;97:958-968.

doi: 10.1016/j.biopha.2017.10.145

9. Zhang M, Xu L, Yang H. *Schisandra chinensis* fructus and its active ingredients as promising resources for the treatment of neurological diseases. *Int J Mol Sci*. 2018;19(7):1970.

doi: 10.3390/ijms19071970

10. Rybnikár M, Malaník M, Smejkal K, *et al*. Dibenzocyclooctadiene Lignans from *Schisandra chinensis* with anti-inflammatory effects. *Int J Mol Sci*. 2024;25(6):3465.

doi: 10.3390/ijms25063465

11. Li B, Xiao Q, Zhang JN, *et al*. Exploring the active compounds and potential mechanism of the anti-nonalcoholic fatty liver disease activity of the fraction from *Schisandra chinensis* fruit extract based on multi-technology integrated network pharmacology. *J Ethnopharmacol*. 2023;301:115769.

doi: 10.1016/j.jep.2022.115769

12. Huang S, Zhang D, Li Y, *et al*. *Schisandra sphenanthera*: A comprehensive review of its botany, phytochemistry, pharmacology, and clinical applications. *Am J Chin Med*. 2021;49(7):1577-1622.

doi: 10.1142/s0192415x21500749

13. Yang K, Qiu J, Huang Z, *et al*. A comprehensive review of ethnopharmacology, phytochemistry, pharmacology, and pharmacokinetics of *Schisandra chinensis* (Turcz.) Baill. And *Schisandra sphenanthera* Rehd. et Wils. *J Ethnopharmacol*. 2022;284:114759.

doi: 10.1016/j.jep.2021.114759

14. Jafernik K, Motyka S, Calina D, Sharifi-Rad J, Szopa A. Comprehensive review of dibenzocyclooctadiene lignans from the *schisandra* genus: Anticancer potential, mechanistic insights and future prospects in oncology. *Chin Med*. 2024;19(1):17.

doi: 10.1186/s13020-024-00879-0

15. Liu SQ, Yang YP, Hussain N, *et al*. Dibenzocyclooctadiene Lignans from the Family *Schisandraceae*: A review of phytochemistry, structure-activity relationship, and hepatoprotective effects. *Pharmacol Res*. 2023;195:106872.

doi: 10.1016/j.phrs.2023.106872

16. Kim DH, Hung TM, Bae KH, *et al*. Gomisin a improves scopolamine-induced memory impairment in mice. *Eur J Pharmacol*. 2006;542(1):129-135.

doi: 10.1016/j.ejphar.2006.06.015

17. Li XL, Zhao X, Xu X, *et al*. Schisantherin a recovers Aβ-induced neurodegeneration with cognitive decline in mice. *Physiol Behav*. 2014;132:10-16.

doi: 10.1016/j.physbeh.2014.04.046

18. Xu MJ, Yan TX, Fan KY, *et al*. Polysaccharide of *Schisandra chinensis* fructus ameliorates cognitive decline in a mouse model of Alzheimer's disease. *J Ethnopharmacolo*. 2019;237:354-365.

doi: 10.1016/j.jep.2019.02.046

19. Hu D, Cao Y, He R, *et al*. Schizandrin, an antioxidant Lignan from *Schisandra chinensis*, ameliorates Aβ1-42-induced memory impairment in mice. *Oxid Med Cell Longev*. 2012;2012:721721.

doi: 10.1155/2012/721721

20. Zhao X, Liu CM, Xu MJ, Li XL, Bi KS, Jia Y. Total Lignans of *Schisandra chinensis* Ameliorates Aβ(1-42)-induced neurodegeneration with cognitive impairment in mice and primary mouse neuronal cells. *PLoS One*. 2016;11(4):e0152772.

doi: 10.1371/journal.pone.0152772

21. Shibata M, Ohtani R, Ihara M, Tomimoto H. White matter lesions and glial activation in a novel mouse model of chronic cerebral hypoperfusion. *Stroke*. 2004;35(11):2598-2603.

doi: 10.1161/01.Str.0000143725.19053.60

22. Zhang YL, Chopp M, Meng YL, *et al*. Effect of exosomes derived from multipluripotent mesenchyrnal stromal cells on functional recovery and neurovascular plasticity in rats after traumatic brain injury. *J Neurosurg*. 2015;122(4):856-867.

doi: 10.3171/2014.11.Jns14770

23. Wan YS, You Y, Ding QY, *et al*. Triptolide protects against white matter injury induced by chronic cerebral hypoperfusion in mice. *Acta Pharmacol Sin*. 2022;43(1):15-25.

doi: 10.1038/s41401-021-00637-0

24. Chen S, Li Q, Shi H, Li F, Duan Y, Guo, Q. New insights into the role of mitochondrial dynamics in oxidative stress-induced diseases. *Biomed Pharmacother*. 2024;178:117084.

doi: 10.1016/j.biopha.2024.117084

25. Ma P, Zhang R, Xu L, Liu H, Xiao P. The neuroprotective effects of coreopsis tinctoria and its mechanism: interpretation of network pharmacological and experimental data. *Front Pharmacol*. 2021;12:791288.

doi: 10.3389/fphar.2021.791288

26. Mendie LE, Hemalatha S. Bioactive compounds from nyctanthes arbor tristis linn as potential inhibitors of Janus Kinases (Jaks) involved in rheumatoid arthritis. *Appl Biochem Biotechnol*. 2023;195(1):314-330.

doi: 10.1007/s12010-022-04121-1

27. Yao JY, Yang YL, Chen WJ, Fan HY. Exploring the therapeutic potential of Qi Teng Mai Ning recipe in ischemic stroke and

vascular cognitive impairment. *Trad Med Res*. 2024;9:57.

28. Fu Z, Wang X, Fan Y, *et al*. Brozopine ameliorates cognitive impairment via upregulating Nrf2, antioxidation and anti-inflammation activities. *Front Pharmacol*. 2024;15:1428455.

    doi: 10.3389/fphar.2024.1428455

29. Cai H, Cai T, Zheng H, *et al*. The neuroprotective effects of danggui-shaoyao san on vascular cognitive impairment: Involvement of the role of the low-density lipoprotein receptor-related protein. *Rejuvenation Res*. 2020;23:420-433.

    doi: 10.1089/rej.2019.2182

30. Zheng V, Wong G. Neuroinflammation responses after subarachnoid hemorrhage: A review. *J Clin Neurosci*. 2017;42:7-11

    doi: 10.1016/j.jocn.2017.02.001

31. Kim T, Vemuganti R. Mechanisms of Parkinson's disease-related proteins in mediating secondary brain damage after cerebral ischemia. *J Cereb Blood Flow Metab*. 2017;37(6):1910-1926.

    doi: 10.1177/0271678x17694186

32. Ziemka-Nalecz M, Jaworska J, Zalewska T. Insights into the neuroinflammatory responses after neonatal hypoxia-ischemia. *J Neuropathol Exp Neurol*. 2017;76(8):644-654.

    doi: 10.1093/jnen/nlx046

33. Xiao ZH, Xiao W, Li GL. Research progress on the pharmacological action of Schisantherin A. *Evid Based Complement Alternat Med*. 2022;2022:6420865.

    doi: 10.1155/2022/6420865

34. Jung CH, Hong MH, Kim JH, *et al*. Protective effect of a Phenolie-rich fraction from *Schisandra chinensis* against H_2O_2-induced apoptosis in SH-SY5Y cells. *J Pharmacy Pharmacol*. 2007;59(3):455-462.

    doi: 10.1211/jpp.59.3.0016

35. Khan MB, Hoda MN, Vaibhav K, *et al*. Remote ischemic postconditioning: Harnessing endogenous protection in a murine model of vascular cognitive impairment. *Transl Stroke Res*. 2015;6(1):69-77.

    doi: 10.1007/s12975-014-0374-6

36. Hattori Y, Enmi JI, Iguchi S, *et al*. Substantial reduction of parenchymal cerebral blood flow in mice with bilateral common carotid artery stenosis. *Sci Rep*. 2016;6(1):32179.

    doi: 10.1038/srep32179

37. Wang JY, Zhang GL, Yang YF, *et al*. *Schisandra chinensis* Lignans exert antidepressant effects by promoting BV2 microglia polarization toward the M2 phenotype through the activation of the cannabinoid receptor type-2-signal transducer and activator of transcription 6 pathway. *J Agric Food Chem*. 2022;70(44):14157-14169.

    doi: 10.1021/acs.jafc.2c04565

38. Song FJ, Zeng KW, Liao LX, Yu Q, Tu PF, Wang XM. Schizandrin A inhibits microglia-mediated neuroninflammation through inhibiting TRAF6-NF-κB and JAK2-STAT3 signaling pathways. *PLoS One*. 2016;11(2):e0149991.

    doi: 10.1371/journal.pone.0149991

39. Zeng KW, Zhang T, Fu H, Liu GX, Wang XM. Schisandrin B exerts anti-neuroinflammatory activity by inhibiting the toll-like receptor 4-dependent MyD88/IKK/NF-κB signaling pathway in lipopolysaccharide-induced microglia. *Eur J Pharmacol*. 2012;692(1-3):29-37.

    doi: 10.1016/j.ejphar.2012.05.030

40. Chen S, Ding YH, Shi SS, Tu XK. Schisandrin B inhibits NLRP3 inflammasome pathway and attenuates early brain injury in rats of subarachnoid hemorrhage. *Chin J Integr Med*. 2022;28(7):594-602.

    doi: 10.1007/s11655-021-3348-z

41. Qun E, Tang M, Zhang X, *et al*. Protection of seven dibenzocyclooctadiene lignans from *schisandra chinensis* against serum and glucose deprivation injury in SH-SY5Y cells. *Cell Biol Int*. 2015;39(12):1418-1424.

    doi: 10.1002/cbin.10537

ACCSCIENCE PUBLISHING

Global Translational Medicine

ORIGINAL RESEARCH ARTICLE

Systemic and gastrointestinal amyloid A amyloidosis in rheumatoid arthritis: A post-mortem clinicopathologic study of 161 cases

Miklós Bély[1]* and Ágnes Apáthy[2]

[1]Department of Pathology, Hospital of the Order of the Brothers of Saint John of God, Budapest, Hungary

[2]Department of Rheumatology, St. Margaret Clinic, Budapest, Hungary

Abstract

Amyloidosis syndromes are characterized by the extracellular deposition of fibrillar proteins, with 22 systemic and 27 localized forms identified. Among these, amyloid A (AA) amyloidosis is a complication of chronic inflammatory diseases, particularly rheumatoid arthritis (RA), and can affect multiple organs, including the gastrointestinal (GI) tract. The study aimed to determine the prevalence and severity of systemic AA amyloidosis (sAAa) and GI AA amyloidosis (giAAa) in RA, evaluate their role in mortality, and clarify the diagnostic value of GI biopsy. A total of 161 randomly selected autopsy patients with RA were studied. In this study, the GI tract refers specifically to the stomach, small intestine, and large intestine. The presence and extent of sAAa and giAAa were assessed histologically; with AA deposition quantified using a semi-quantitative visual estimation scale ranging from 0 to 3. Demographic differences between patient cohorts were analyzed using the Student's (Welch) *t*-test. sAAa was identified in 34 (23.13%) of the 161 patients. Among these cases, tissue blocks containing one or more sections of the GI tract were available in 31 patients. In 29 of these cases, AA deposits were detected in branches of blood vessels and various tissue structures of the GI tract, while giAAa was histologically excluded in two patients with sAAa. sAAa and giAAa may develop in both sexes and can occur at any stage in the course of RA. These conditions represent progressive and cumulative processes, initially affecting only a few structures within various organs and expanding in the later stages of the disease. Although giAAa does not appear to be a life-threatening complication of RA, it emerges as an early pathological feature of significant clinical and diagnostic importance, particularly as an optimal biopsy site.

Keywords: Rheumatoid arthritis; Systemic amyloid A amyloidosis; Amyloid A amyloidosis of the gastrointestinal tract

***Corresponding author:**
Miklós Bély
(dr.bely.miklos@gmail.hu)

Citation: Bély M, Apáthy Á. Systemic and gastrointestinal amyloid A amyloidosis in rheumatoid arthritis: A post-mortem clinicopathologic study of 161 cases. *Global Transl Med*. 2025:4(1):104-125.
doi: 10.36922/gtm.5325

Received: October 21, 2024

Revised: January 12, 2025

Accepted: January 20, 2025

Published online: March 7, 2025

1. Introduction

Amyloidosis syndromes are systemic or localized disorders characterized by the extracellular deposition of chemically heterogeneous fibrillar proteins. To date, 49 distinct pre-cursor proteins have been identified in humans, with 22 proteins associated with systemic amyloidosis and 27 with localized forms.[1]

1.1. Nomenclature of amyloidosis

Amyloidosis syndromes are classified based on the composition of their fibrillar proteins.[1] For example:

- Amyloid A (AA) amyloidosis: Caused by deposits of AA protein, which is derived from serum AA, an acute-phase reactant produced by hepatocytes
- Amyloid light chain amyloidosis: Results from amyloid light chain deposits, which originate from immunoglobulin light chains (λ or κ) produced by B cells
- Amyloid heavy chain amyloidosis: Characterized by amyloid heavy chain (AH) deposits, derived from immunoglobulin heavy chains produced by B cells
- Amyloid transthyretin (ATTR) amyloidosis: Caused by ATTR deposits, which originate from either altered wild-type transthyretin (ATTRwt) or genetically determined mutant transthyretin variants (ATTRm), leading to ATTRwt amyloidosis or ATTRm amyloidosis
- Amyloid β_2-microglobulin amyloidosis: Results from deposits of amyloid β2-microglobulin, derived from β2-microglobulin, which is produced by lymphoid cells.

1.2. Histological characteristics of amyloid

All amyloid deposits exhibit eosinophilia, congophilia, and birefringence, displaying a characteristic apple-green color under polarized light. The presence of congophilia and birefringence remains the gold standard for the microscopic diagnosis of amyloid deposits.[2] While, our experience suggests that the intensity of birefringence may vary between adjacent amyloid deposits, even within the same slide.[3]

Cohen's statement[4(pp.649-650)] that "there are no laboratory abnormalities specific to or unique for amyloid" remains valid. Furthermore, "there is no one feature in the blood, urine, electrocardiogram, or X-ray that is specific for amyloidosis," and "the diagnosis should be based upon a biopsy using an appropriate staining procedure."

1.3. Underlying diseases associated with AA amyloidosis

Systemic (secondary or reactive) AA amyloidosis occurs in a wide spectrum of chronic inflammatory diseases,[5-7] such as:

- Chronic microbial infections: Tuberculosis,[8,9] leprosy,[10,11] fibrocystic lung diseases,[12,13] bronchiectasis,[9,14,15] lung abscess,[8] chronic osteomyelitis,[8,15] chronic xanthogranulomatous pyelonephritis,[16-18] chronic mesenteric lymphadenitis,[19] and decubitus ulcers.[9]
- Chronic reactive inflammatory diseases: Ankylosing spondylitis,[9,15] psoriatic arthritis,[8,15,20] and Reiter's syndrome.
- Autoimmune (inflammatory) diseases: Rheumatoid arthritis (RA),[3,9,15] juvenile chronic arthritis,[8,9,15] adult-onset Still's disease, systemic lupus erythematosus,[15] progressive systemic sclerosis,[21] Crohn's disease,[22] ulcerative colitis,[23] polymyositis [15], and polymyalgia rheumatica or giant cell arteritis.[24]
- Chronic cachectic diseases and malignancies: Renal cell carcinoma,[15,25,26] ovarian carcinoma,[27] hepatocellular adenoma,[28-30] bronchial carcinoma,[8,31] Hodgkin's lymphoma,[32,33] and cardiac (atrial) myxoma.[34]

1.4. Prevalence, signs, and symptoms of AA amyloidosis

Secondary or reactive AA amyloidosis accounts for approximately 45% of generalized amyloidosis cases.[35]

Signs and symptoms of amyloidosis vary depending on the affected organ. The most commonly involved organs include the gastrointestinal (GI) tract, pancreas, kidneys, heart, and liver, with the most extensive deposits typically occurring in the kidneys, heart, pancreas, GI tract, liver, and spleen.[3]

Renal involvement in AA amyloidosis often leads to massive amyloid deposition, resulting in nephrotic syndrome. This syndrome, similar to other causes of nephrotic syndrome, is characterized by impaired kidney function,[36] significant proteinuria, and hypoalbuminemia, which in turn leads to edema, particularly in the lower extremities.[37,38] Cardiac amyloidosis is associated with congestive heart failure and arrhythmias.[38]

GI amyloidosis, regardless of the specific amyloid type, commonly presents with symptoms such as abdominal pain, dysmotility (atony), malabsorption, diarrhea or constipation, and GI bleeding.[37,38] Hepatic involvement is frequently accompanied by hepatomegaly and, in some cases, portal hypertension and its associated complications.[38]

1.5. Literature review

The volume of literature dealing with amyloidosis is extensive, with more than 3,000 published articles. Many studies have explored the role of chronic inflammation, elevated serum AA, plasma levels of misfolded acute-phase proteins, and the involvement of serum amyloid P in amyloid fibril formation.[39,40] However, to the best of our knowledge, no studies have specifically examined the mechanistic understanding of amyloid deposition, the progression of amyloidosis, or the rate of amyloid accumulation from a histopathological perspective, apart from our previous publications.[41-43]

1.6. Objective

This study aims to determine the prevalence and severity of systemic AA amyloidosis (sAAa) in RA, assess the prevalence and extent of GI AA deposits (giAAa) in various tissue structures of the GI tract, and characterize the progression of AA deposition within the GI tract. In addition, this study seeks to evaluate the relationship between sAAa and giAAa, investigate the impact of sAAa and giAAa on mortality, and clarify the diagnostic value of GI biopsy in AA amyloidosis.

2. Methods

2.1. Patients (autopsy population)

At the National Institute of Rheumatology, 9,475 patients died between 1969 and 1992. Among them, 161 had RA and underwent autopsy.[3]

The clinical diagnosis of RA in these patients was established based on the criteria of the American College of Rheumatology.[44] The patient histories and clinical protocols were reviewed by co-author Ágnes Apáthy, a rheumatologist and neurologist. Autopsies and histopathological evaluations were conducted by Miklós Bély.

2.2. Methodology

In this study, the term "GI tract" refers specifically to the stomach, small intestine, and large intestine; other sections, such as the oral cavity, pharynx, and esophagus, were not evaluated separately.

The presence and extent of sAAa and giAAa were determined histologically through a detailed examination of eight organs (kidneys, heart, pancreas, GI tract, liver, lungs, skin, and brain).

AA deposition in various tissue structures of these organs was diagnosed histologically according to Romhányi's method,[45] utilizing a modified and more sensitive Congo red staining technique.[46] AA deposits were further identified in serial sections using immunohistochemical[47] and histochemical methods.[48-50]

2.3. Statistical analysis

The demographic characteristics of different patient cohorts were analyzed using the Student's (Welch) *t*-test to compare age, sex, disease onset, and disease duration at the time of death between patients with and without sAAa, as well as between patients with giAAa with mild (<0.8 deposits/patient) or severe (≥0.8/patient) AA deposits.[51]

The threshold value of 0.8 for classifying mild and severe cases was determined based on the Gauss distribution of AA deposition values. A significance level of $P < 0.05$ was considered statistically significant.

For comparisons between two datasets, the most stringent statistical criteria in Microsoft Excel were applied, using a two-tailed distribution (parameter="2") and assuming unequal variance (not homoscedastic, parameter="-3").

The mean age of patients varied within the observed minimum and maximum values, and the distribution of AA deposits followed a normal (Gaussian) distribution, characterized by a bell-shaped curve.

The correlation between sAAa and giAAa was assessed using Pearson's chi-squared (χ^2) test.[51]

3. Results

3.1. Demographics of patients with sAAa and/or giAAa

sAAa was identified in 34 (23.13%) of 161 patients with RA. Tissue blocks from at least one segment of the GI tract (stomach, small intestine, or large intestine) were available for 31 (91.18%) of these 34 patients.

In 29 of the 31 patients (93.55%) with available GI tissue, AA deposits were detected in branches of blood vessels of varying calibers and various tissue structures of the GI tract. In contrast, 2 (6.45%) of the 31 patients with sAAa did not exhibit histologically detectable AA deposits in the GI tract, and these cases were considered as latent-stage giAAa.

A strong positive correlation was observed between sAAa ($n = 34$) and giAAa ($n = 29$) ($c = 1.0$, $\chi^2 = 142.06$, $P < 0.000$). However, there was no significant difference between the average AA deposition in sAAa and giAAa ($P < 0.386$).

Table 1 summarizes the demographics, onset, and duration of disease for the total study population ($N = 161$), as well as for subgroups with sAAa ($n = 34$) and without sAAa ($n = 127$). In addition, it presents data for patients with giAAa ($n = 31$), categorized into latent ($n = 2$), mild ($n = 17$), and severe ($n = 12$) AA deposits in the GI tract.

A comparison of age, sex, RA onset, and disease duration at the time of death revealed no statistically significant differences in survival time, disease onset, or disease duration between patients with sAAa ($n = 34$) and the total study population ($n = 161$) ($P = 0.321$, $P = 0.376$, $P = 0.554$). No significant differences were observed between female patients ($P = 0.800$, $P = 0.631$, $P = 0.682$) and male patients ($P = 0.348$, $P = 0.565$, $P = 0.688$). Similarly, no statistically significant differences were found between patients with sAAa ($n = 34$) and those without sAAa

(n = 127) (P = 0.213, P = 0.262, P = 0.462), including within female (P = 0.745, P = 0.528, P = 0.593) and male subgroups (P = 0.297, P = 0.521, P = 0.662). Furthermore, comparisons between patients with sAAa (n = 34) and those with giAAa (n = 31) yielded no statistically significant differences (P = 0.811, P = 0.883, P = 0.867), including within female (P = 0.623, P = 0.820, P = 0.861) and male subgroups (P = 1.00, P = 1.00, P = 1.00).

No significant differences were observed in the mean age at death between patients with latent giAAa (n = 2) and those with mild giAAa (n = 17) (P = 0.364), latent giAAa (n = 2) and severe giAAa (n = 12) (P = 0.115), or mild giAAa (n = 17) and severe giAAa (n = 12) (P = 0.363). However, the mean age at death of female patients with latent giAAa (n = 2) was significantly higher than that of female patients with mild giAAa (n = 17) (69.00 years versus 67.69 years, P = 0.05). A statistically significant difference was also observed between the mean age at death of female patients with latent (n = 2) and those with severe giAAa (n = 12) (69.00 years versus 60.75 years, P = 0.048). Statistical significance was not calculated for male patients due to the presence of a zero divisor or limited data availability.

According to the results, amyloidosis developed in both sexes and at any stage during the course of the disease (Tables 1 and 2). The relationships (P values of correlation) between demographic characteristics, disease onset, and disease duration among RA patients (N = 161) with sAAa (n = 34 of 161) and without sAAa (n = 127 of 161), between patients with sAAa (n = 34) and those with giAAa (n = 31 of 34), as well as between patients with latent giAAa (n = 2 of 31) and mild (n = 17 of 31) or severe giAAa (n = 12 of 31), are summarized in Table 2.

3.2. Histological characteristics of sAAa and/or giAAa

AA deposits in the GI tract are demonstrated in Figures 1 and 2.

Table 1. Demographic and clinical characteristics of 161 autopsied RA patients with systemic and gastrointestinal amyloid A amyloidosis

Clinical and histological diagnosis	Number of autopsies	Age at death (Mean years±SD)	Age at onset of disease (Mean years±SD)	Disease duration (Mean years±SD)
RA patients (total)	161	65.32±12.99	50.83±17.02	14.43±10.55
Female	116	64.95±11.84	50.19±15.78	14.79±10.70
Male	45	66.27±15.67	52.57±20.15	13.46±10.22
With sAAa	34 (of 161)	62.41±15.82	47.61±18.33	15.58±9.51
Female	29	64.34±11.27	48.56±15.54	15.70±10.06
Male	5	51.20±31.51	41.25±34.72	14.75±5.12
Without sAAa	127 (of 161)	66.10±12.07	51.77±16.59	14.09±10.86
Female	87	65.15±12.08	50.79±15.92	14.49±10.97
Male	40	68.15±11.94	53.94±18.05	13.30±10.71
With giAAa[a]	31 (of 34)	63.32±14.77	48.29±16.68	16.00±9.66
Female	26	65.65±8.25	49.46±12.62	16.21±10.29
Male	5	51.20±31.51	41.25±34.72	14.75±5.12
With latent giAAa[b]	2 (of 31)	69.00±2.83	66.00±0.0	5.00±0.0
Female	2	69.00±2.83	66.00±0.0	5.00±0.0
Male	0	Not applicable	Not applicable	Not applicable
With mild giAAa	17 (of 31)	65.59±12.00	52.31±12.19	15.38±9.67
Female	16	67.69±8.58	53.31±12.19	15.38±9.67
Male	1	32.00	Not applicable	Not applicable
With severe giAAa	12 (of 31)	59.17±18.78	40.82±20.24	17.91±9.74
Female	8	60.75±6.65	40.57±8.92	19.71±11.60
Male	4	56.00±34.21	41.25±34.72	14.75±5.12

Notes: [a]Tissue blocks of the GI tract were not available in 3 of 34 patients with sAAa; [b]In 2 of 31 GI tract tissue blocks, amyloid A deposits were not detected histologically, and these were considered as latent-stage giAAa.
Abbreviations: giAAa: Gastrointestinal amyloid A amyloidosis; RA: Rheumatoid arthritis; sAAa: Systemic amyloid A amyloidosis; SD: Standard deviation; GI: Gastrointestinal.

Table 2. Statistical correlations (*P*-values) between female and male RA patients with sAAa and giAAa at different stages

Patient cohorts with RA	Age	Onset of RA	Duration of RA
RA patients (*n*=161) versus sAAa (*n*=34 of 161)	0.321	0.376	0.554
Female: *n*=116 of 161 versus *n*=29 of 34	0.800	0.631	0.682
Male: *n*=45 of 161 versus *n*=5 of 34	0.348	0.565	0.688
With sAAa (*n*=34 of 161) versus without sAAa (*n*=127 of 161)	0.213	0.262	0.462
Female: *n*=29 of 34 versus *n*=87 of 127	0.745	0.528	0.593
Male: *n*=5 of 34 versus *n*=40 of 127	0.297	0.521	0.662
With sAAa (*n*=34 of 161) versus with giAAa (*n*=31 of 34)	0.811	0.883	0.867
Female: *n*=29 of 34 versus *n*=26 of 31	0.623	0.820	0.861
Male: *n*=5 of 34 versus *n*=5 of 31	1.000	1.000	1.000
With latent[a] giAAa (*n*=2 of 31) versus with mild giAAa (*n*=17 of 31)	0.364	–	–
Female: *n*=2 of 2 versus *n*=0 of 17	0.676	–	–
Male: *n*=0 of 2 versus *n*=4 of 17	–	–	–
With latent* giAAa (*n*=2 of 31) versus with severe giAAa (*n*=12 of 31)	0.115	–	–
Female: *n*=2 of 2 versus *n*=8 of 12	0.050	–	–
Male: *n*=0 of 2 versus *n*=4 of 12	–	–	–
With mild giAAa (*n*=17of 31) versus with severe giAAa (*n*=12 of 31)	0.363	0.127	0.560–
Female: *n*=2 of 2 versus *n*=8 of 12	0.048	0.436	0.030
Male: *n*=0 of 2 versus *n*=4 of 12	–	–	–

Note: [a]Amyloid A deposits were not found (detected) in tissue blocks of the gastrointestinal tract of two patients with sAAa, which were considered as latent-stage giAAa.
Abbreviations: giAAa: Gastrointestinal amyloid A amyloidosis; RA: Rheumatoid arthritis; sAAa: Systemic amyloid A amyloidosis.

3.3. Immunohistochemical characteristics of sAAa and/or giAAa

AA deposits exhibit a positive reaction for anti-human AA components when subjected to immunohistochemical staining (Figure 3). The anti-human AA reaction is highly specific; however, minimal AA deposits may not be detected.

3.4. Histochemical characteristics of sAAa and/or giAAa

AA deposits associated with sAAa exhibit sensitivity to performate pre-treatment (1 s) and variable resistance to $KMnO_4$ oxidation, depending on the exposure time: (i) resistant for 30 sec – 1 min, (ii) resistant/sensitive for 3 – 5 min, and (iii) sensitive for 10 min. The histological and histochemical characteristics of sAAa and/or GI AA deposits are demonstrated using light and polarization microscopy in Figure 4.

3.5. Characteristics of sAAa

The accumulation of AA deposits in various organs followed a progressive and primarily linear trajectory, with an abrupt onset and an exponential increase in the terminal stage. Amyloid deposition most frequently affected the GI tract and pancreas, compared to other organs, while AA deposits were not observed in the brain. The most extensive deposits were found in the kidneys and heart (Table 3).

In 22 (64.71%) of 34 RA patients with sAAa, the average amount of AA deposits per patient was <0.8, which was classified as mild. In 12 (35.29%) of 34 patients, the AA deposit load was >0.8, classifying it as severe (Patients 23 – 34 in Table 3). Table 3 and Figures 5-7 summarize the quantitative differences in AA deposits across various organs (kidneys, heart, pancreas, GI tract, liver, lungs, skin, and brain) in 34 RA patients with sAAa.

The prevalence and amount of AA deposits in patients with sAAa followed a generally parallel trajectory (Table 3), aligning with the trend lines of incremental increase (Figure 5), except during the early and terminal stages of amyloid deposition. Figure 5 illustrates the prevalence and amount of AA deposits across eight organs in 34 RA patients with sAAa. In the early stage of sAAa, AA deposition started abruptly, while in the terminal stage, AA deposition accelerated again, resulting in an exponential increase in the growth curve. In some patients, moderate differences between the prevalence and severity of sAAa were observed, primarily due to the unavailability of tissue samples from certain organs.

The prevalence and amount of AA deposits in various organs of 34 RA patients with sAAa followed a generally

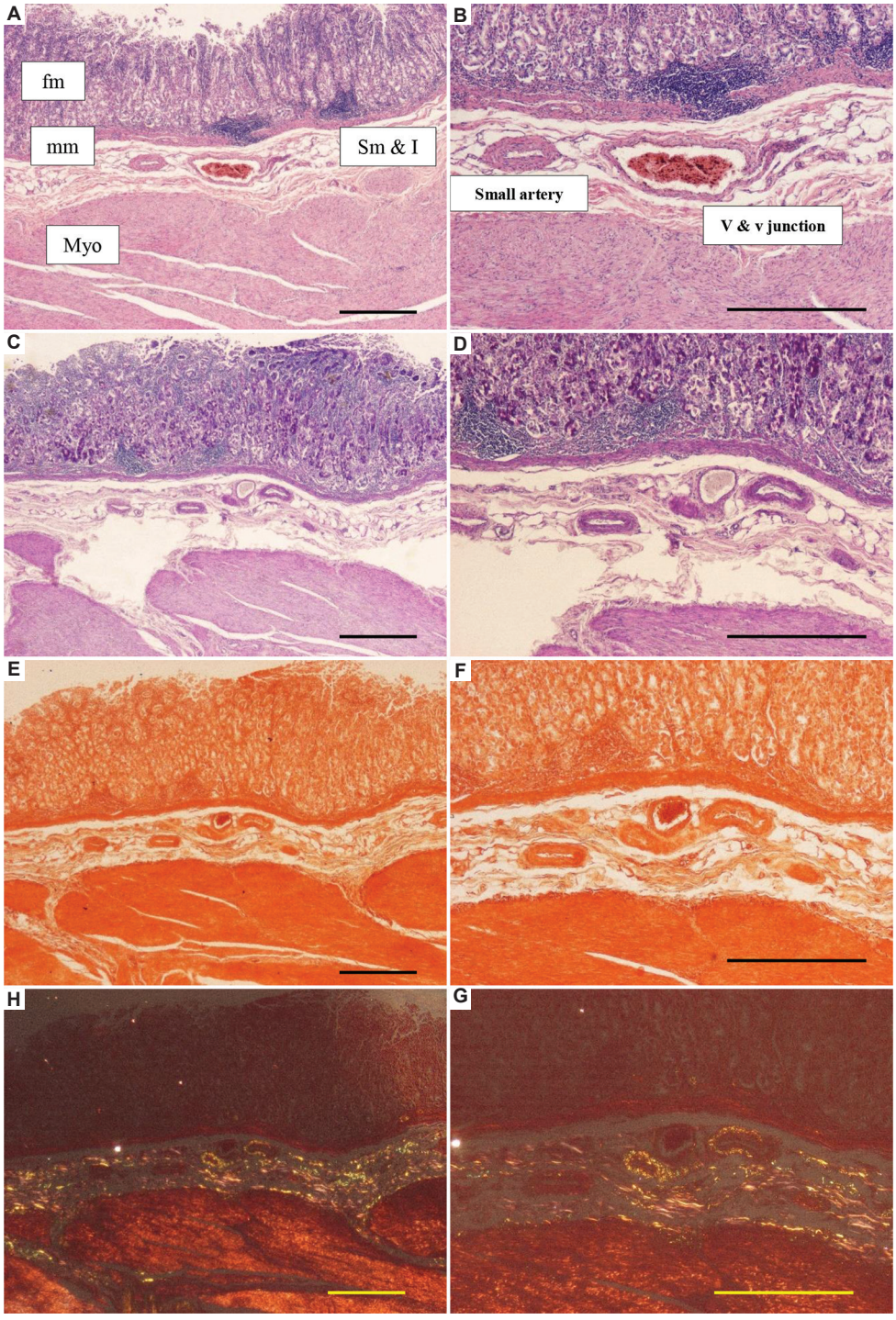

Figure 1. Rheumatoid arthritis, systemic secondary AA amyloidosis, gastrointestinal AA deposits with erosive gastritis. AA deposition is observed in the submucosa, within the walls of arterioles (a) and small arteries, as well as interstitial collagen fibers (I). Only minimal AA deposits are present within the walls of small veins (V), while the venule (v) remains unaffected. Hematoxylin and eosin: (A) Scale bar: 1000 μm, magnification: ×20; (B) Scale bar: 1000 μm, magnification: ×40. Periodic acid–Schiff stain: (C) Scale bar: 1000 μm, magnification: ×20; (D) Scale bar: 1000 μm, magnification: ×40; Congo red staining (without alcoholic differentiation, covered with gum Arabic): (E) Scale bar: 1000 μm, magnification: ×20; (F) Scale bar: 1000 μm, magnification: ×40; Congo red staining (without alcoholic differentiation, covered with gum Arabic, and viewed under polarized light): (G) Scale bar: 1000 μm, magnification: ×20; (H) Scale bar: 1000 μm, magnification: ×40.
Notes: fm: Gastric fundic mucosa; mm: muscularis mucosae; Myo: Muscularis propria; sm: Submucosa.
Abbreviation: AA: Amyloid A.

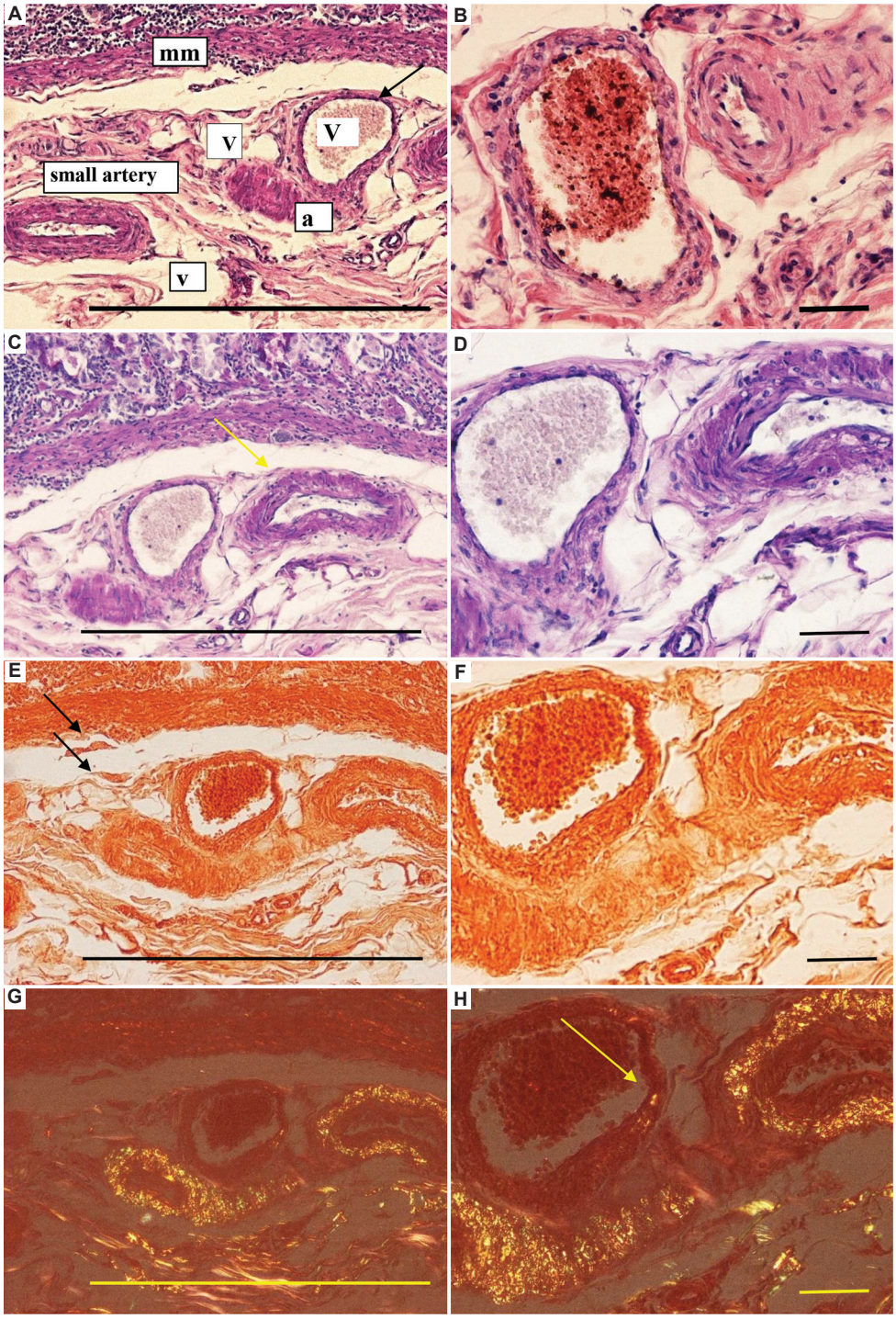

Figure 2. Rheumatoid arthritis, systemic secondary AA amyloidosis, and gastrointestinal AA deposits (same tissue sections shown in Figure 1). AA deposition is observed in the submucosa, within the walls of arterioles and small arteries, as well as interstitial collagen fibers. Only minimal deposits within the walls of small veins (yellow arrow), while the venules remain unaffected (black arrow). Hematoxylin and eosin: (A) Scale bar: 1000 μm, magnification: ×100; (B) Scale bar: 100 μm, magnification: ×200; Periodic acid–Schiff stain: (C) Scale bar: 1000 μm, magnification: ×100; (D) Scale bar: 100 μm, magnification: ×200; Congo red staining (without alcoholic differentiation, covered with gum Arabic): (E) Scale bar: 1000 μm, magnification: ×100; (F) Scale bar: 100 μm, magnification: ×200; Congo red staining (without alcoholic differentiation, covered with gum Arabic, and viewed under polarized light): (G) Scale bar: 1000 μm, magnification: ×100; (H) Scale bar: 100 μm, magnification: ×200.[52]
Abbreviations: a: Arteriole; A: Small artery; mm: Muscularis mucosae; Venule; V: Small vein; AA: Amyloid A.

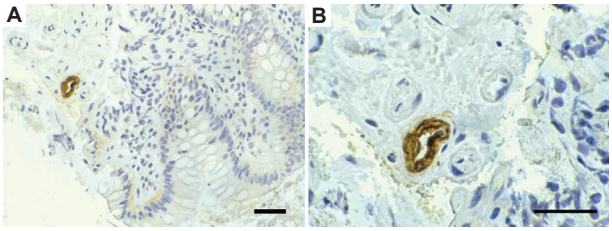

Figure 3. Immunohistochemical Staining of AA deposits using anti-human AA component. Anti-human AA component, dilution 1:100 (monoclonal antibody MO759, DAKO, Denmark], streptavidin-biotin-complex/horseradish peroxidase reaction: (A) scale bar: 100 μm, magnification: ×200; (B) scale bar: 100 μm, magnification: ×400.
Abbreviation: AA: Amyloid A.

parallel trend. Organs frequently affected by amyloid deposition exhibited extensive accumulation, whereas less frequently involved organs showed comparatively lower deposit levels. However, an inverse relationship was observed in the pancreas and GI tract (Table 3 and Figure 6). Figure 6 summarizes the quantitative differences in prevalence and amount of AA deposits across various organs in these 34 RA patients.

AA deposition in the kidneys, heart, pancreas, GI tract, liver, lungs, skin, and brain correlated with the average severity of sAAa. Figure 7 illustrates the distribution of AA deposition across these organs.

3.6. Characteristics of giAAa

The accumulation of AA deposits in the GI tract followed a progressive and generally linear trajectory, with an exponential increase in the terminal stage.

Among 31 RA patients with sAAa, AA deposition was absent in 2 patients (6.45%), representing a latent stage of GI amyloidosis (AA deposits = 0.00). In 17 (54.84%) of the 31 RA patients with giAAa, the average AA deposit level in the GI tract was <0.8, categorizing them as having mild involvement. In contrast, 12 (38.71%) of 31 patients had AA deposit levels >0.8, classifying them as severe (Patients 20 – 31 in Table 4). The difference in AA deposit levels between the mild (n = 17, <0.8) and severe (n = 12, >0.8) groups was statistically significant ($P < 0.000$).

Within the GI tract, AA deposition was most pronounced in the arterioles, small arteries, and interstitial collagen fibers, which are likely sites of early amyloid deposition. AA deposits were less frequent and of moderate severity in reticulin fibers (collagen III), medium-sized veins and arteries, small veins, and the basement membranes of GI glands, reflecting a more advanced stage of amyloid deposition. Rare and minimal AA deposits were observed in myocytes, venules, and nerves, indicating late-stage, pre-mortem (terminal) stage amyloidosis (see data under

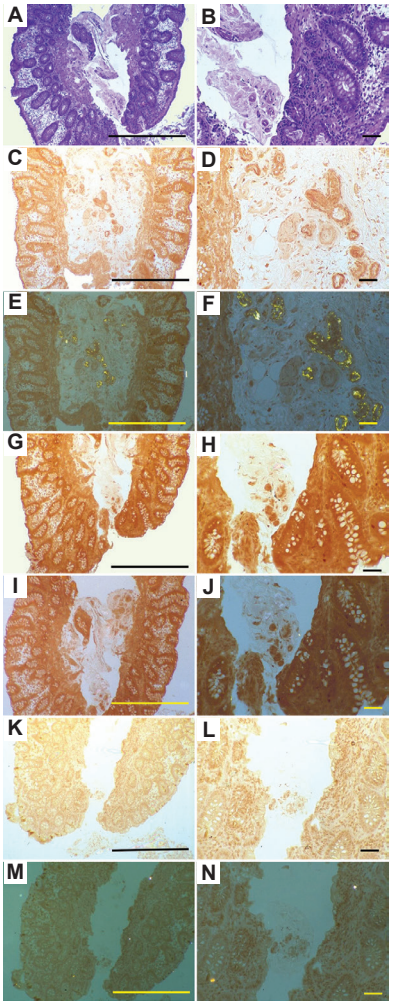

Figure 4. Cecum, rheumatoid arthritis, systemic secondary AA amyloidosis. AA deposits are observed within the walls of arterioles, while venules remain unaffected. Periodic acid–Schiff staining: (A) Scale bar: 1250 μm, magnification: ×50; (B) Scale bar: 125 μm, magnification ×125. Congo red staining (without alcoholic differentiation, covered with gum Arabic): (C) Scale bar: 1250 μm, magnification: ×50; (D) Scale bar: 125 μm, magnification ×125. Congo red staining (without alcoholic differentiation, covered with gum Arabic, viewed under polarized light): (E) Scale bar: 1250 μm, magnification: ×50; (F) Scale bar: 125 μm, magnification ×125. AA deposits exhibit birefringence under polarized light, appearing as characteristic apple-green birefringence. Congo red staining (without alcoholic differentiation, covered with gum Arabic): (G) Scale bar: 1250 μm, magnification: ×50; (H) Scale bar: 125 μm, magnification ×125. Performate pretreatment for 1 s and Congo red staining (without alcoholic differentiation, covered with gum Arabic, viewed under polarized light): (I) Scale bar: 1250 μm, magnification: ×50; (J) Scale bar: 125 μm, magnification ×125. After performate pretreatment (1 s), the staining intensity (congophilia) increases compared to Congo red staining without pretreatment. AA protein deposits are highly sensitive to performate pretreatment; birefringence disappears immediately, regardless of amyloid deposition quantity or disease stage. $KMnO_4$ oxidation (10 min) and Congo red staining (without alcoholic differentiation, covered with gum Arabic): (K) Scale bar: 1250 μm, magnification: ×50; (L) Scale bar: 125 μm, magnification ×125. $KMnO_4$ oxidation (10 min) and Congo red staining (without alcoholic differentiation, covered with gum Arabic, viewed under polarized light): (M) Scale bar: 1250 μm, magnification: ×50; (N) Scale bar: 125 μm, magnification ×125. AA protein deposits exhibit resistance to $KMnO_4$ oxidation (30 s – 1 min), resistance/sensitivity (3 – 5 min), and sensitivity (10 min).
Abbreviation: AA: Amyloid A.

Table 3. Prevalence and amount of amyloid A deposits in various organs of 34 rheumatoid arthritis patients with systemic amyloid A amyloidosis

Serial number	f/m	Pr. n[0]/y	Kidney	Heart	Pancreas	GI tract	Liver	Lung	Skin	Brain	Avg of sAAa/Pt	Count	Sum	Avg of sAAa/Pt	"0" *n*	"+" *n*	Prevalence in %	Severity (amount) in %	CoD	Cl+/Cl-
1	F	155/87	0.000	0.000	0.000	0.09	0.000	0.083	0	0	0.022	8	0.173	0.022	6	2	25.00	0.72	–	–
2	F	243/87	0.000	0.400	0.100	0.09	0.000	0.000	0	0	0.074	8	0.590	0.074	5	3	37.50	2.46	cAAa	–
3	F	76/79	0.250	0.000	ND	0.45	0.000	0.000	0	0	0.100	7	0.700	0.100	5	2	28.57	3.33	–	–
4	F	240/88	0.000	0.000	0.100	0.35	0.000	0.000	0.4	0	0.106	8	0.850	0.106	5	3	37.50	3.54	–	–
5	F	287/91	0.083	0.500	0.400	0.39	0.000	0.000	0	0	0.172	8	1.373	0.172	4	4	50.00	5.72	cAAa	–
6	F	226/85	0.417	0.600	0.200	0.52	0.111	0.167	0	0	0.252	8	2.015	0.252	2	6	75.00	8.40	–	–
7	F	183/92	0.667	0.000	0.500	0.27	0.111	0.000	ND	ND	0.258	6	1.548	0.258	2	4	66.67	8.60	–	–
8	F	266/78	0.333	0.500	ND	ND	0.111	0.167	ND	ND	0.278	4	1.111	0.278	0	4	100.00	9.26	–	–
9	F	306/90	0.750	0.800	0.400	ND	ND	0.000	0	0	0.325	6	1.950	0.325	3	3	50.00	10.83	rAAa-U	Cl+
10	F	430/80	0.417	0.400	0.400	0.61	0.111	0.167	0.6	0	0.338	8	2.705	0.338	1	7	87.50	11.27	cAAa	–
11	F	395/76	0.250	1.200	0.000	1.08	0.111	0.167	0	0	0.351	8	2.808	0.351	3	5	62.50	11.70	cAAa	–
12	F	80/80	0.750	0.400	ND	0.52	0.667	0.417	0	0	0.393	7	2.754	0.393	2	5	71.43	13.11	rAAa-U	Cl+
13	F	322/81	0.833	0.700	1.000	0.15	0.556	0.167	0	0	0.426	8	3.406	0.426	2	6	75.00	14.19	cAAa	–
14	F	162/78	0.083	1.100	0.550	1.18	0.111	0.000	ND	0	0.432	7	3.024	0.432	2	5	71.43	14.40	–	–
15	F	52/92	0.667	1.000	0.650	0.41	0.000	0.750	0	0	0.435	8	3.477	0.435	3	5	62.50	14.49	–	–
16	F	45/74	0.000	1.400	0.800	0.85	0.444	0.000	0	0	0.437	8	3.494	0.437	4	4	50.00	14.56	cAAa	–
17	M	342/86	0.750	1.100	0.300	0.85	0.333	0.250	0	0	0.448	8	3.583	0.448	2	6	75.00	14.93	rAAa-U	–
18	F	90/85	0.917	1.400	0.100	0	1.778	0.000	0	0	0.524	8	4.195	0.524	4	4	50.00	17.48	–	–
19	F	203/88	0.667	1.000	0.700	0.7	0.167	0.750	ND	0	0.569	7	3.984	0.569	1	6	85.71	18.97	rAAa-U	–
20	F	39/76	1.500	0.400	1.200	0.64	0.667	0.333	0	0	0.593	8	4.740	0.593	2	6	75.00	19.75	rAAa-U	–
21	F	245/88	1.000	1.500	1.100	0.76	0.556	0.250	ND	0	0.738	7	5.166	0.738	1	6	85.71	24.60	cAAa	–
22	M	232/74	1.833	1.300	0.600	0.45	1.000	0.333	0	ND	0.788	7	5.516	0.788	1	6	85.71	26.27	rAAa-U	Cl+
23	F	265/80	1.500	1.400	0.000	1.64	0.889	0.417	1	0	0.856	8	6.846	0.856	2	6	75.00	28.53	rAAa-U	Cl+
24	F	367/75	2.167	0.900	1.400	1.16	0.778	0.333	0.5	0	0.905	8	7.238	0.905	1	7	87.50	30.16	cAAa	–
25	F	73/87	1.417	1.600	1.300	1.06	1.111	0.833	0	0	0.915	8	7.321	0.915	2	6	75.00	30.50	rAAa-U	–
26	F	V/T	ND	1.300	ND	ND	1.111	0.417	ND	ND	0.943	3	2.828	0.943	0	3	100.00	31.42	rAAa-U	–
27	F	137/76	1.583	1.400	1.000	0.68	ND	0.917	0.2	ND	0.963	6	5.780	0.963	0	6	100.00	32.11	rAAa-U	–
28	M	43/85	1.083	1.000	1.350	1.34	1.222	1.167	ND	0	1.023	7	7.162	1.023	1	6	85.71	34.10	rAAa-U	–
29	F	174/88	1.917	1.000	1.800	0.65	0.889	0.917	ND	0	1.025	7	7.173	1.025	1	6	85.71	34.16	rAAa-U	–

(Cont'd...)

doi: 10.36922/gtm.5325

Table 3. ***(Continued)***

Serial number	f/m	Pr. n[0]/y	Kidney	Heart	Pancreas	GI tract	Liver	Lung	Skin	Brain	Avg of sAAa/Pt	Count	Sum	Avg of sAAa/Pt	"0" *n*	"+" *n*	Prevalence in %	Severity (amount) in %	CoD	Cl+/Cl-
30	F	237/70	2.250	ND	ND	0	1.222	0.917	ND	ND	1.097	4	4.389	1.097	1	3	75.00	36.58	rAAa-U	–
31	F	101/90	1.917	2.400	2.000	1.53	0.667	0.833	0.2	0	1.193	8	9.547	1.193	1	7	87.50	39.78	rAAa-U	–
32	F	255/83	2.083	1.600	1.650	1.42	2.000	0.917	0.5	0	1.271	8	10.17	1.271	1	7	87.50	42.38	rAAa-U	Cl+
33	M	53/87	2.667	2.300	1.900	1.83	1.000	1.167	0.8	ND	1.666	7	11.66	1.666	0	7	100.0	55.54	rAAa-U	Cl+
34	M	181/80	1.917	1.500	2.900	1.38	1.556	1.750	ND	ND	1.834	6	11.00	1.834	0	6	100.0	61.13	rAAa-U	Cl+
		Statistics																		
		Count	33	33	29	31	32	34	24	26	34	34	34	34	34	34	34	34	25	9
		Sum	32.67	32.10	24.40	23.05	19.28	14.59	4.20	0.00	21.75	ND	ND	21.75	ND	ND	ND	ND	–	–
		Avg	0.99	0.97	0.84	0.74	0.60	0.43	0.18	0.0	0.64	ND	ND	0.64	ND	ND	ND	ND	–	–
		SD	0.783	0.611	0.724	0.505	0.567	0.445	0.295	0.00	0.447	ND	ND	0.447	ND	ND	ND	ND	–	–
		"0"	4	4	3	2	6	9	16	26	0	ND	ND	0	ND	ND	ND	ND	–	–
		"+"	29	29	26	29	26	25	8	0	34	ND	ND	34	ND	ND	ND	ND	–	–
		Prev.%	87.879	87.879	89.655	93.548	81.250	73.529	33.333	0.000	100.000	ND	ND	100.00	ND	ND	ND	ND	–	–
		Sev. %	32.998	32.424	28.046	24.785	20.082	14.300	5.833	0.000	21.322	ND	ND	21.322	ND	ND	ND	ND	–	–

Notes: (i) Table 3 is organized based on increasing amounts of amyloid A (AA) deposits across eight organs (vertical: kidney, heart, pancreas, gastrointestinal [GI] tract, liver, lung, skin, brain) and increasing severity of AA deposits across 34 patients (horizontal: ordered by severity %/organ).

(ii) Definitions: Pr. n[0]/y: Protocol number/year; Prevalence/patient in % (Prev. %): Positive ("+") cases in % of "count"; Severity in % (Sev. %): "Avg" in % of maximum "3" value of severity; CoD: Cause of death; Cl+: Clinically recognized; Cl-: Clinically not recognized; f: Female; m: Male; ND: No data; Pt: Patient; SD: Standard deviation; "–": Died of other causes or were not diagnosed clinically; rAAa-U: Uremia due to massive AA deposition in the kidneys (rAAa) with consecutive renal insufficiency (*n*=17); cAAa: Lethal outcome exclusively caused by cardiac amyloidosis (*n*=3) (322/81, 430/80, 45/74); in additional 5 (243/87, 287/91, 395/76, 245/88, 367/75) of 31 patients, cardiac amyloidosis contributed to the death; sAAa led to death in 25 of 34 patients.

(iii) Lethal outcome of sAAa was diagnosed clinically in 9 of 25 patients.

(iv) AA deposits were not found in the brain.

(v) Gastrointestinal amyloidosis did not play a direct role in the mortality of rheumatoid arthritis patients.

doi: 10.36922/gtm.5325

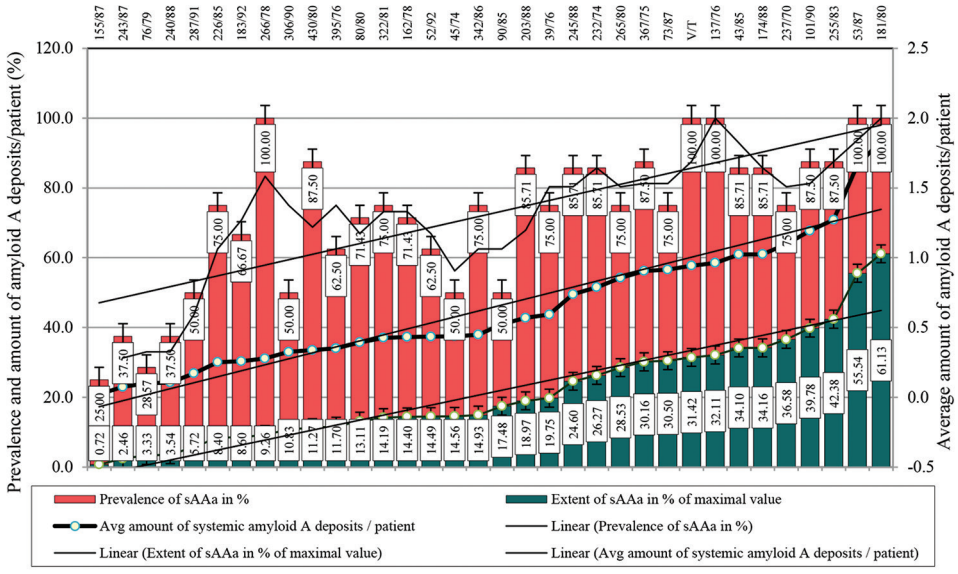

Figure 5. Prevalence and amount of AA deposits in 34 (21.12% of 161 rheumatoid arthritis cases) patients with systemic AA amyloidosis, arranged by increasing average AA deposition per patient. The prevalence and amount of AA deposits in the kidneys, heart, pancreas, gastrointestinal tract, liver, lungs, and skin followed a generally parallel trend. No AA deposits were detected in the brain. Missing tissue samples from some patients contributed to moderate discrepancies between the prevalence and amount of systemic AA deposits per patient (Table 3).
Abbreviation: AA: Amyloid A.

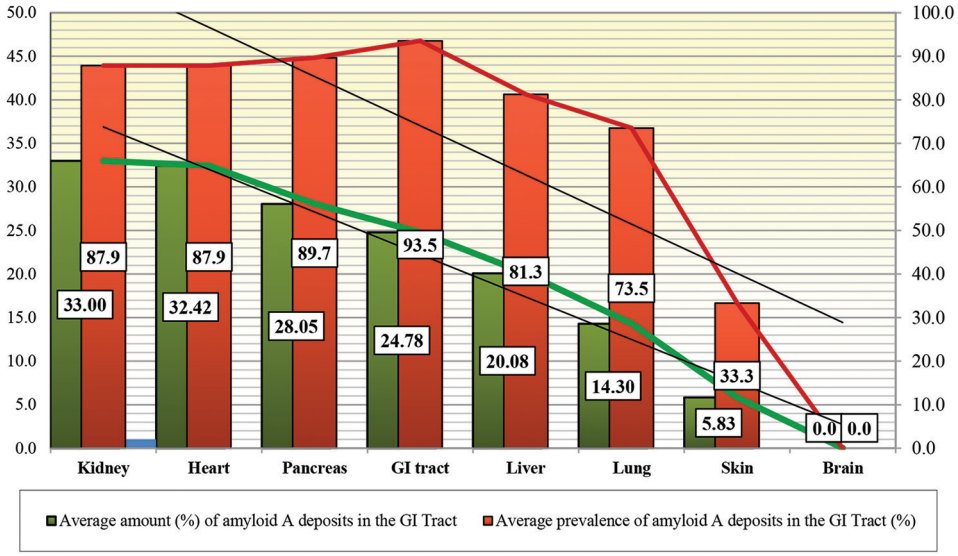

Figure 6. Prevalence and amount of amyloid A (AA) deposits across various organs in 34 RA patients with systemic AA amyloidosis. The average prevalence and amount of AA deposits across various organs of 34 RA patients followed a generally parallel trend, except for the pancreas and GI tract, where a minimal inverse relationship was observed (Table 3).
Abbreviations: AA: Amyloid A; GI: gastrointestinal; RA: Rheumatoid arthritis.

tissue classification variables ret, VV, AA, V, and BM in Table 4).

There was a statistically significant difference in AA deposit levels between early and advanced stages ($P < 0.000$), as well as between advanced and terminal stages ($P < 0.000$) of GI amyloidosis. A quantitative summary of AA deposits in different tissue structures of the GI tract of RA patients ($n = 31$) is presented in Table 4 and Figures 8-10.

In patients with mild and severe giAAa, AA deposition in the GI tract followed a linear growth trajectory after an initial latent stage. The progression of giAAa remained

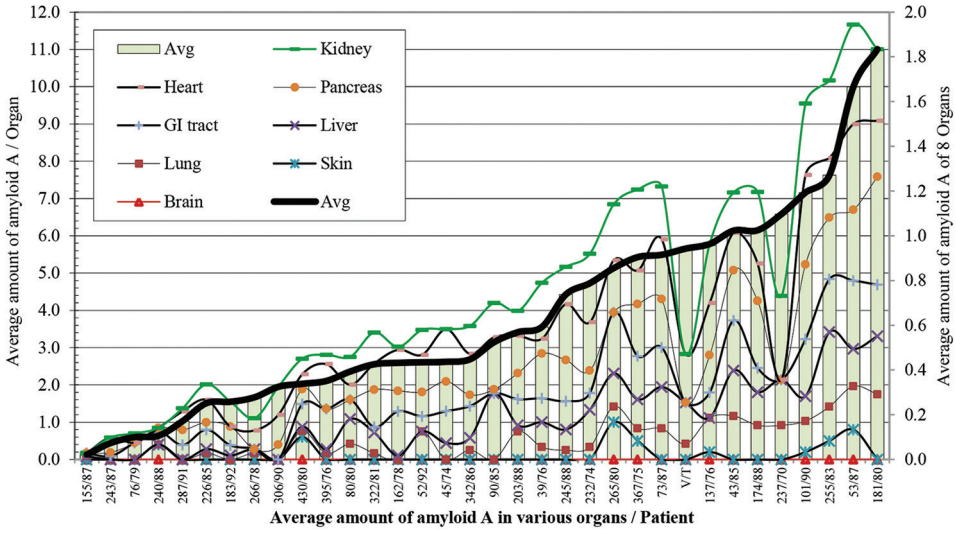

Figure 7. Quantitative differences in AA deposits in rheumatoid arthritis patients. AA deposition in the kidneys, heart, pancreas, GI tract, liver, lungs, skin, and brain is presented relative to the average severity of sAAa. The amount of AA deposits in these organs (Table 3) is displayed according to increasing severity.

Note: Individual variations were primarily due to sampling limitations and the semi-objective nature of the evaluation method. Patient distribution (n = 34, 21.1% of 161 RA patients with sAAa): Kidney: n = 33; Heart: n = 33; Pancreas: n = 29; GI tract: n = 31; Liver: n = 32; Lung: n = 34; Skin: n = 24; Brain: n = 26.

Abbreviations: AA: Amyloid A; GI: Gastrointestinal; sAAa: Systemic amyloid A amyloidosis.

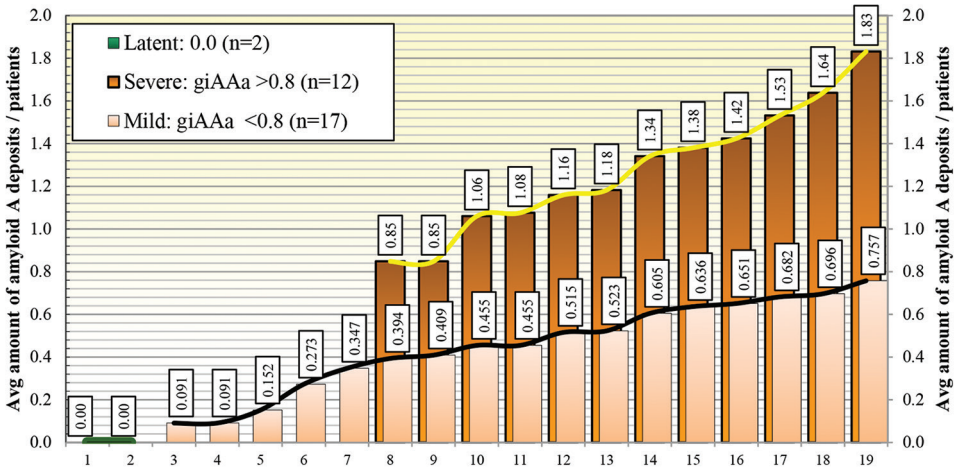

Figure 8. Mean AA deposition in the GI tract across disease stages. The graph illustrates the mean amount of AA deposits in the GI tract during the early, advanced, late, and terminal stages of giAAa, based on increasing severity (i.e., the average amount of AA deposits per patient). This analysis was conducted in a cohort of 31 RA patients with giAAa. Among these 31 patients, two (6.45%) had no detectable AA deposits in the GI tract, indicating a latent stage of GI amyloidosis (AA deposits=0.00). The average AA deposit levels in these two patients with sAAa were 1.097 (237/70) and 0.524 (90/85) (Table 4). In 17 (54.84%) of 31 patients with mild amyloidosis, the AA deposit level was <0.8, whereas in 12 (38.71%) of 31 patients with severe amyloidosis, the AA deposit level was >0.8 (Table 4). In the past four patients among the 12 with severe giAAa, AA deposition became extremely severe, with an average exceeding 1.4. These terminal-stage cases represented end-stage systemic amyloidosis, predicting a fatal outcome. The rate of AA deposition in both mild and severe giAAa followed a linear growth pattern, indicating a consistent rate of AA deposition. However, in the past four patients with extremely severe giAAa, AA deposition increased exponentially.

Abbreviations: AA: Amyloid A; GI: Gastrointestinal; sAAa: Systemic amyloid A amyloidosis; RA: Rheumatoid arthritis; giAAa: GI AA amyloidosis.

steadily continuous, except in the terminal stage when the rate of deposition became exponential. The rate of amyloid deposition in both mild and severe GI amyloidosis cases was parallel throughout disease progression (Table 4 and Figure 8).

The prevalence and amount of AA deposits in different tissue structures of the GI tract followed parallel trends. Tissues that were frequently involved showed marked AA deposition, while those less frequently affected exhibited milder deposits. Notably, the basement membrane of GI glands and small veins

Table 4. Prevalence and amount of amyloid A deposits in different tissue structures of the gastrointestinal tract

Serial number	Pr. n0]/y	f/m	GI-Tract AA amyloidosis											Avg giAAa/Pt	Cause of death	Cl+/Cl-
			a	A	I	ret	VV	AA	V	BM	Myo	v	n			
1	237/70	f	0	0	0	0	0	0	0	0	0	0	0	0	rAAa-U	–
2	90/85	f	0	0	0	0	0	0	0	0	0	0	0	0	–	–
3	155/87	f	0.5	0.5	0	0	0	0	0	0	0	0	0	0.09	–	–
4	243/87	f	0.67	0.33	0	0	0	0	0	0	0	0	0	0.09	cAAa	–
5	322/81	f	1	0.67	0	0	0	0	0	0	0	0	0	0.15	cAAa	–
6	183/92	f	1	1	1	0	0	0	0	0	0	0	0	0.27	–	–
7	240/88	f	0.67	0.33	0.33	1.33	0.33	0.17	0.33	0	0	0.33	0	0.35	–	–
8	287/91	f	2	1.33	0	0	0.33	0.67	0	0	0	0	0	0.39	cAAa	–
9	52/92	f	2	1	0.5	0.5	0	0.5	0	0	0	0	0	0.41	–	–
10	232/74	m	2	1	1	1	0	0	0	0	0	0	0	0.45	rAAa-U	Cl+
11	76/79	f	2	1	1	0	1	0	0	0	0	0	0	0.45	–	–
12	80/80	f	3	0.75	0.5	0.5	0	0	0	1	0	0	0	0.52	rAAa-U	Cl+
13	226/85	f	2	1	1.67	0.67	0.33	0	0	0	0	0	0	0.52	–	–
14	430/80	f	2.33	1.33	1.33	0	0.67	0.33	0.33	0.33	0	0	0	0.61	cAAa	–
15	39/76	f	3	2	0	0	0	1	0	1	0	0	0	0.64	rAAa-U	–
16	174/88	f	2	1	1.5	0.33	0.67	0.33	0.33	1	0	0	0	0.65	rAAa-U	–
17	137/76	f	3	2	1	0.5	0	1	0	0	0	0	0	0.68	rAAa-U	Cl+
18	203/88	f	2	1.33	1.5	1	0.67	0.33	0.33	0	0.5	0	0	0.7	rAAa-U	–
19	245/88	f	2.67	2	0.33	0	0.33	1	0	0	1.67	0	0.33	0.76	cAAa	–
20	45/74	f	3	2	2	0.67	1	0.33	0.33	0	0	0	0	0.85	cAAa	ND
21	342/86	m	2	1.33	2	1	1.33	0	0	1.67	0	0	0	0.85	rAAa-U	–
22	73/87	f	3	2.67	2	0.33	0.83	1.33	0.17	0.33	0.67	0	0.33	1.06	rAAa-U	Cl+
23	395/76	f	2.33	1.17	3	3	1.33	0	1	0	0	0	0	1.08	cAAa	–
24	367/75	f	3	2.5	2	1	1	1.5	0.25	1.5	0	0	0	1.16	cAAa	–
25	162/78	f	3	2	2	1	0	1	1	0	2	1	0	1.18	–	–
26	43/85	m	3	2.5	1.5	0.75	1.5	1.5	1	0.5	1.5	0.5	0.5	1.34	rAAa-U	–
27	181/80	m	3	2	2.67	2.67	0.67	0.33	0.17	1.33	0.67	0	1.67	1.38	rAAa-U	Cl+
28	255/83	f	3	2.33	2	0.67	2	1.33	1	2.67	0	0.33	0.33	1.42	rAAa-U	Cl+
29	101/90	f	2.67	2.33	1.67	2	2.33	1	1.67	1.33	0.67	1.17	0	1.53	rAAa-U	–
30	265/80	f	3	2	2.67	2.67	3	1	2	0.67	0	1	0	1.64	rAAa-U	Cl+
31	53/87	m	3	2.33	2.33	2.33	2.33	1.67	1.33	2.33	1.33	0.33	0.83	1.83	rAAa-U	Cl+
32	266/78[a]	f	NA	NA	NA	NA	NA	NA	NA	NA	NA	NA	NA	NA	–	–
33	V/T[b]	f	NA	NA	NA	NA	NA	NA	NA	NA	NA	NA	NA	NA	rAAa-U	–
34	306/90[c]	f	NA	NA	NA	NA	NA	NA	NA	NA	NA	NA	NA	NA	rAAa-U	Cl+
	Statistics															
	Count		31	31	31	31	31	31	31	31	31	31	31	31	23	8
	Sum		65.84	43.73	37.50	23.92	21.65	16.32	15.66	11.24	9.01	4.66	3.99	23.05	25	9
	Avg		2.124	1.411	1.210	0.772	0.698	0.526	0.505	0.363	0.291	0.150	0.129	0.743	–	–

(Cont'd...)

Table 4. *(Continued)*

f/m	GI-Tract AA amyloidosis											Avg giAAa/Pt	Cause of death	Cl+/Cl-
	a	A	I	ret	VV	AA	V	BM	Myo	v	n			
SD	0.97	0.78	0.93	0.89	0.83	0.56	0.76	0.55	0.57	0.33	0.34	0.51	–	–
"0" *n*	2	2	7	11	12	12	18	16	23	24	25	2	–	–
"+" *n*	29	29	24	20	19	19	13	15	8	7	6	29	–	–
Prev. %	93.548	93.548	77.419	64.516	61.290	61.290	41.935	48.387	25.806	22.581	19.355	93.548	–	–
Sev. %	70.796	47.022	40.323	25.720	23.280	17.548	16.839	12.086	9.688	5.011	4.290	24.782	–	–

Notes: (i) Table 4 is organized based on the increasing values of average AA deposits per patient (vertical columns) and the distribution of AA deposits across gastrointestinal (GI) tissue structures arranged in order of severity (horizontal rows).

(ii) [a]Sporadic vasculitis associated with carcinoma (CA).

(iii) Definition: Pr. n^{0}/y: Protocol number/year; Prevalence/patient in % (Prev. %): positive ("+") cases in % of "count"; Severity in % (Sev. %): "Avg" in % of maximum "3" value of severity; CoD: Cause of death; Cl+: Clinically recognized; Cl-: Clinically not recognized; f: female; m: male; NA: Tissue blocks of GI tract were not available; ND: No data; SD: Standard deviation; "–": Died of other causes or were not diagnosed clinically; Avg: Average; rAAa-U: Uremia due to massive AA deposition in the kidneys (rAAa) with consecutive renal insufficiency (*n*=17); cAAa: Lethal outcome exclusively caused by cardiac amyloidosis (*n*=3) (322/81, 430/80, 45/74); in additional 5 (243/87, 287/91, 395/76, 245/88, 367/75) of 31 patients, cardiac amyloidosis contributed to the death; a: Arteriole; A: Small artery; AA: Medium size artery; v: Venule; V: Small vein; VV: Medium size vein; I: Interstitial collagen fiber; ret: Reticulin fiber (collagen III); BM: Basement membrane of intestinal gland; Myo: Smooth muscle cells of tunica muscularis; n: Nerve.

(iv) In 2 (6.45%) of 31 rheumatoid arthritis patients with sAAa, no AA deposition was detected in the GI tract, representing a latent stage of GI amyloidosis (AA deposits=0.00).

(v) In 17 (54.84%) of 31 patients with mild GI amyloidosis, the AA deposit level was <0,8, classifying them as mild.

(vi) In 12 (38.71%) of 31 patients, the GI AA deposit level was >0.8, which was considered severe.

(vii) sAAa was the cause of death in 23 of 31 patients with GI AA amyloidosis (giAAa); 8 of these 23 cases were clinically diagnosed.

(viii) While GI amyloidosis itself was not a direct cause of mortality, three of the four patients with the most severe giAAa also had the most severe renal amyloidosis. These patients (255/83, 101/90, 265/80, and 53/87) represented the pre-mortem stage of fatal uremia.

Abbreviations: AA: Amyloid A; giAAa: GI AA Amyloidosis.

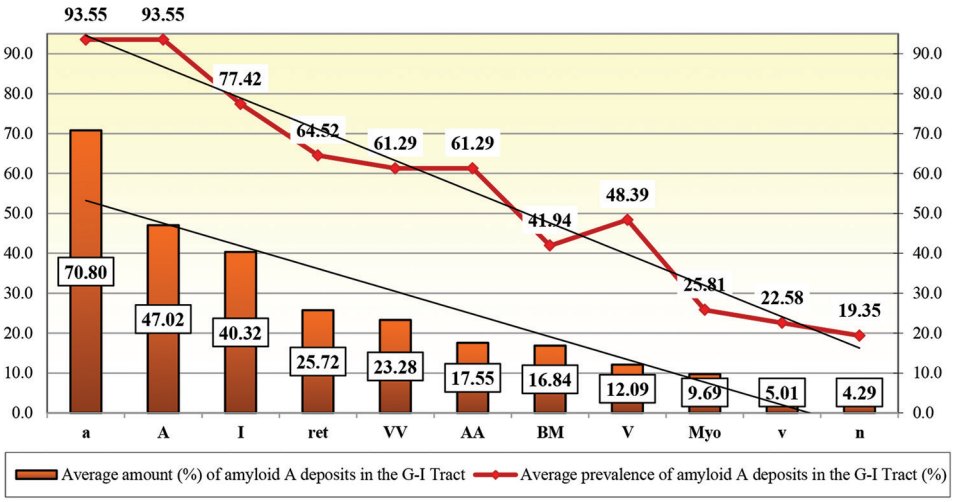

Figure 9. Prevalence and amount of amyloid A (AA) deposits in different GI tissue structures. The graph depicts the average prevalence and amount of AA deposits in different GI tissue structures in 31 rheumatoid arthritis patients. The trends in AA deposition remained generally parallel, except for the basement membranes of the GI glands and small veins, which exhibited an inverse pattern (Table 4).

Notes: a: Arteriole; A: Small artery; AA: Medium size artery; v: Venule; V: Small vein; VV: Medium size vein; I: Interstitial collagen fiber; ret: Reticulin fiber (collagen III); BM: Basement membrane of the intestinal gland; Myo: Smooth muscle cells of tunica muscularis; n: Nerve.

Abbreviations: AA: Amyloid A; GI: Gastrointestinal.

deviated from this trend, demonstrating an inverse relationship (Table 4 and Figure 9). Figure 9 provides a quantitative summary of the prevalence and amount of AA deposits in different GI tissue structures in patients with giAAa.

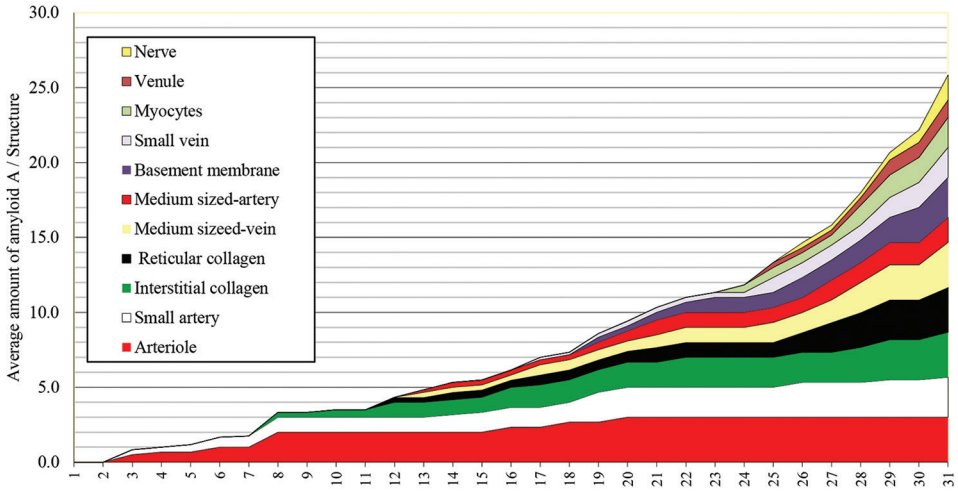

Figure 10. Progression of AA deposition in different GI tissue structures. The graph illustrates the progression of AA deposition across different GI tissue structures in 29 (93.55%) of 31 rheumatoid arthritis patients with GI AA amyloidosis. Tissue structures are arranged according to their decreasing amount of AA deposition, as detailed in Table 4. AA deposition did not begin simultaneously in all GI structures. However, once amyloid accumulation started, the amount of AA deposits in different tissues increased simultaneously at a constant rate, independent of the disease stage. Abbreviation: BM: Basement membrane of the intestinal gland.
Abbreviations: AA: Amyloid A; GI: Gastrointestinal.

Detectable AA deposits in different GI tissue structures did not appear simultaneously. In the early stage of giAAa, amyloid deposits were histologically detectable in only a few structures – specifically, in arterioles, small arteries, and interstitial collagen fibers. As the disease progressed (advanced stages), additional structures became involved, including reticulin fibers, medium-sized veins and arteries, and basement membranes of GI glands. In the late stages, amyloid deposits were observed in structures that had previously remained uninvolved, including small veins, smooth muscle cells, venules, and nerves. This stage was characterized by extensive amyloid deposition in previously affected structures.

Although the amount of deposited AA varied between various GI tissue structures, the proportions of AA deposition remained consistent, indicating that the relative distribution of amyloid among tissue compartments was independent of the disease stage. The distribution of AA deposition in the GI tract is illustrated in Figure 10.

3.7. Mortality of sAAa and/or giAAa

sAAa was lethal in 25 (73.53%) of 34 patients. Among these, extensive AA deposition in the kidneys resulted in renal insufficiency and uremia in 17 (68.0%) of 25 patients. Cardiac AA amyloidosis (cAAa) was the primary cause of death in 3 (12.0%) of 25 patients. In an additional 5 (20.0%), cAAa was associated with systemic vasculitis of autoimmune origin, atherosclerosis, or occlusive bronchiolitis, playing an additive role in mortality.

Nine (26.47%) of 34 patients with sAAa died from other causes, such as autoimmune vasculitis, peritonitis, and lethal septic infections. GI amyloidosis did not play a direct role in the mortality of RA patients (Table 5). sAAa was clinically diagnosed only in 9 (26.47%) of 34 patients, whereas it was missed in 25 patients (73.53%). Neither cAAa nor its pathogenic role in mortality was recognized in clinical diagnoses (Table 5). Similarly, giAAa was not identified as a direct cause of death in any of the patients with sAAa. The basic diseases, complications, and associated conditions of the 34 RA patients with sAAa, as well as the mortality patterns of renal AA amyloidosis (rAAa) and cAAa, are summarized in Table 5.

4. Discussion

Estimating the true prevalence of sAAa in RA is challenging, as it depends on the specificity and sensitivity of the detection methods used. Less sensitive staining techniques may fail to identify some positive cases, while more specific methods can detect earlier stages of amyloid deposition and reveal a higher prevalence. Non-specific staining methods may introduce misleading conclusions regarding the prevalence and mortality of sAAa.[3,50]

The use of a professional polarizing microscope with high brightness (at least 100 W) is also critical for accurate diagnosis.

In early publications, various diagnostic methods with differing levels of specificity and sensitivity were used to identify amyloidosis. As a result, estimates of

Table 5. Mortality of systemic amyloid A amyloidosis (*n*=34), gastrointestinal amyloid A amyloidosis (*n*=31), and their amyloid A deposits per patient

Total	Pr. n^{0}/y	f/m	Basic disease	Complication 1	Complication 2	Cause of death	Accompanying disease	Avg sAAa	Avg giAAa	Cause of death	Cl+/Cl-
1	237/70	f	RA	sAAa	–	Uremia	Atherosclerosis	1.097	0.09	rAAa-U	–
2	45/74	f	RA	sAAa	–	Circulatory failure	–	0.437	0.09	cAAa	–
3	232/74	m	RA	sAAa	–	Uremia	–	0.788	0.45	rAAa-U	Cl+
4	367/75	f	RA	sAAa	–	Myocardial necrosis	DM-atherosclerosis	0.905	0.35	cAAa	–
5	39/76	f	RA	sAAa	–	Uremia	Atherosclerosis	0.593	0.39	rAAa-U	–
6	137/76	f	RA	sAAa	–	Uremia	–	0.963	0.52	rAAa-U	Cl+
7	395/76	f	RA	AV	sAAa	Multifocal myocardiocytolysis	Tuberculosis-Fc-mTb	0.351	0.27	cAAa	–
8	162/78	f	RA-gastric ulcer	Perforation	sAAa	Peritonitis- sepsis	–	0.432	NA	–	–
9	266/78	f	RA	sAAa	–	Sepsis	Atherosclerosis	0.278	NA	–	–
10	76/79	f	RA-duodenal ulcer	Perforation	sAAa	Peritonitis	–	0.10	0.61	–	–
11	80/80	f	RA	sAAa	–	Uremia	Atherosclerosis	0.393	1.08	rAAa-U	Cl+
12	181/80	m	RA	sAAa	–	Uremia	Neurinoma pararenal-JCA	1.834	0.52	rAAa-U	Cl+
13	265/80	f	RA	sAAa	–	Uremia	Pancreas CA	0.856	0.15	rAAa-U	Cl+
14	430/80	f	RA	sAAa	–	Circulatory failure	Gall-bladder CA	0.338	1.18	cAAa	–
15	322/81	f	RA	sAAa	–	Circulatory failure	–	0.426	0.41	cAAa	–
16	255/83	f	RA	sAAa	–	Uremia	DM7	1.271	0.85	rAAa-U	Cl+
17	43/85	m	RA	sAAa	AV	Uremia	DM-hypertension	1.023	0.85	rAAa-U	–
18	90/85	f	RA	sAAa	AV	Myocardial necrosis-CI	DM-atherosclerosis	0.524	0.00	–	–
19	226/85	f	RA	sAAa	mTu-sporadic vasculitis[a]	Bronchopneumonia	Alveolar CA-atherosclerosis	0.252	0.70	–	–
20	V/T	f	RA	sAAa	–	Uremia	–	0.943	0.64	rAAa-U	–
21	342/86	m	RA	sAAa	–	Uremia	Neurinoma n. VIII.-atherosclerosis	0.448	0.76	rAAa-U	–
22	53/87	m	RA	sAAa	–	Uremia	–	1.666	0.45	rAAa-U	Cl+
23	73/87	f	RA	sAAa	–	Uremia	–	0.915	1.64	rAAa-U	Cl+
24	155/87	f	Ependymoma	Vertebral fracture	sAAa	Pulmonary emboli	RA-atherosclerosis-HT	0.022	1.16	–	–
25	243/87	f	RA	sAAa	AV	Circulatory failure	–	0.074	1.06	cAAa	–
26	174/88	f	RA	sAAa	–	Uremia	–	1.025	NA	rAAa-U	–
27	203/88	f	RA	sAAa	Femoral artery & vein thrombosis	Uremia	–	0.569	0.68	rAAa-U	–
28	240/88	f	RA	AV	sAAa	Multifocal myocardiocytolysis	Tuberculosis-Fc-mTb	0.106	1.34	–	–

(Cont'd...)

doi: 10.36922/gtm.5325

Table 5. Mortality of systemic amyloid A amyloidosis (n=34), gastrointestinal amyloid A amyloidosis (n=31), and their amyloid A deposits per patient

Total	Pr. n^0/y	f/m	Basic disease	Complication 1	Complication 2	Cause of death	Accompanying disease	Avg sAAa	Avg giAAa	Cause of death	Cl+/Cl-
29	245/88	f	RA	Bronchiolitis obliterans	sAAa	Multifocal myocardiocytolysis	DM	0.738	0.65	cAAa	–
30	101/90	f	RA	sAAa	–	Uremia	Hypertension	1.193	0.00	rAAa-U	–
31	306/90	f	RA	sAAa	–	Uremia	–	0.325	1.53	rAAa-U	Cl+
32	287/91	f	RA	sAAa	Epicarditis	Circulatory failure	Operated breast cancer	0.172	1.42	cAAa	–
33	52/92	f	Atherosclerosis	Hypertension	sAAa	Bronchopneumonia	RA	0.435	1.83	–	–
34	183/92	f	RA-colitis-nephrolithiasis	sAAa	Penectomy	Peritonitis-sepsis	–	0.258	1.38	–	–
Total	34		34	34	14	34	20	34	31	25	9

Notes: Basic disease: Underlying disease related to death; Complication: A direct consequence of the basic disease that contributed to death; Associated (Accompanying) disease: A significant disorder without a direct causal role in death; Pr. n^0/y: Protocol number/year; CoD: Cause of death – Uremia (U) or Uremia due to massive AA deposition in the kidneys with consecutive renal insufficiency (U-rAAa) (n=17); cAAa – Lethal outcome exclusively caused by cardiac amyloidosis (n=3); contribution of cardiac amyloidosis to the death (n=5); Cl+: Clinically recognized amyloid A amyloidosis in 9 (27.27%) of 34 patients; Cl-: Clinically not recognized 25 (72.73%) of 34 patients; aSporadic vasculitis associated with carcinoma (CA); mTu: Malignant tumor (Alveolar carcinoma of the lungs); bTu: Benign tumor (Ependymoma); AV: Systemic vasculitis of autoimmune origin; SI: Lethal septic infection; Ath: Atherosclerosis; HT: Hypertension; TB: Post-primary (fibro caseous [Fc]) tuberculosis; mTB: Active miliary dissemination of TB; DM: Adult type II diabetes mellitus; Myocardiocytolysis: Multifocal microinfarction of myocardium; NA: Tissue blocks of GI tract were not available; RA: Rheumatoid arthritis; JCA: Juvenil chronic arthritis.

sAAa prevalence and mortality in these studies were often overestimated or underestimated when compared to our results. This discrepancy likely stems from limited microscopic examination of various organs or the application of non-specific staining methods (Table 6).[53-76] Unfortunately, few studies have specifically addressed the relationship between sAAa and AA deposition in different organs. To our best knowledge, no prior study has provided a detailed analysis of the rate of AA deposition in the GI tract, nor its relationship to sAAa and mortality.

The precursors of AA protein fibrils are synthesized by the liver and circulate in the bloodstream, where they are deposited in various organs. The concentration of these precursors in the blood is influenced by the balance between their production and elimination.

Systemic amyloidosis primarily involves the cardiovascular system and spreads through the bloodstream, whereas organ- or tissue-limited (localized) amyloidosis is not directly linked to systemic circulation and remains confined to specific tissues.[74,79] As previously stated: "All forms of amyloidosis related to the circulation of blood are systemic, and all forms of amyloidosis not connected to the circulation are isolated (localized)."[74(p.48),79(pp.67-68),80(pp.212-213)].

The rate and extent of AA deposition in different organs may be influenced by differences in blood supply per unit volume, local tissue factors, and the potential for incidental amyloid elimination.[74,79]

Amyloidosis is a progressive and cumulative process, initially affecting only a few tissue structures in select organs before progressively involving more structures as the disease advances.[3,74,79-82]

The degree of AA deposition – both in terms of prevalence and amount – in various organs and tissue structures follows the same progressive and cumulative pathological process, as demonstrated in Figures 5,7,8 and 10. The steady and continuous (consistently linear) accumulation of AA across different tissue structures and organs suggests a gradual deposition process.

With the exception of the early (latent) and late stages of amyloidosis, AA accumulation in different tissue structures and organs generally follows a linear trajectory. The onset of AA deposition varies across organs, which explains the variability observed in the early stage of amyloidosis.

In the terminal stage, a rapid (exponential) increase in AA accumulation occurs, likely due to massive amyloid deposition in the kidneys, which leads to complete renal failure and the inability to excrete amyloid precursors in end-stage rAAa.

The rate of amyloid deposition was comparable in patients with mild and severe amyloidosis, as well as across

Table 6. Prevalence and mortality of sAAa in rheumatoid arthritis autopsy patients: Impact of sAAa and giAAa on lethal outcomes[42]

References	Year of publication	Autopsy, *n*	Prevalence of sAAa, *n* (%)	Mortality of sAAa, *n*/*N* (%)
Bayles[53]	1943	23	ND	3/23 (13.0)
Baggenstoss and Rosenberg[54]	1943	30	2 (6.6)	1/30 (3.3)
Rosenberg and Baggenstoss5[5]	1943	30	2 (6.6)	1/30 (3.3)
Young and Schwedel[56]	1944	33	5 (15.2)	0/33 (0)
Unger *et al.*[57]	1948	58	4 (6.9)	ND
Teilum and Lindahl[58]	1954	28	17 (60.7)	7v28 (25.0)
Gedda[59]	1955	45	11 (24.4)	9/45 (20.0)
Sinclair and Cruickshank[60]	1956	16	4 (25.0)	0/16 (0)
Missen and Tailor[61]	1956	47	8 (17.0)	4/47 (8.5)
Lebowitz[62]	1963	62	6 (10.0)	ND
Sokoloff[63]	1964	19	0 (0)	0/19 (0)
Cohen[4]	1968	42	11 (26)	ND
Karten[64]	1969	95	1 (1.05)	ND
Gritsman[65]	1969	15	6 (40.0)	ND
Ozdemir *et al.*[66]	1971	47	1 (2.1)	ND
Gardner[67]	1972	142	17 (11.97)	ND
Püschel[68]	1973	143	15 (10.5)	ND
Vroninks *et al.*[69]	1973	62	3 (4.84)	0/62 (0)
Hajzok *et al.*[70]	1976	16	7 (43.7)	ND
Eulderink[71]	1976	111	ND	6/111 (5.4)
Rainer *et al.*[72]	1978	79	ND	4/79 (5.0)
[a]Boers *et al.*[73]	1987	132	14 (10.6)	ND
Bély[74]	1993	161	34 (21.1)	17/161 (11)
Suzuki *et al.*[75]	1994	81	17 (21.0)	6/81 (7.4)
[b]Bély and Apáthy[76]	2006	234	48 (20.5)	20/234 (8.5)

Notes: (i) Amyloid deposits were identified using various staining methods with different specificity and sensitivity, including toluidine blue, crystal violet, Syrius red, and Congo red staining using Romhányi's,[45] Bély and Apáthy's Congo red method,[46] Bennhold's,[77] Puchtler *et al.*,[78]
[a]Boers *et al.*[73] focused exclusively on renal involvement (*n*=132).
(iii) [b]Bély and Apáthy[76] did not explicitly report sAAa prevalence and mortality, which were retrospectively determined for this table.
Abbreviations: ND: No data; giAAa: Gastrointestinal amyloid A amyloidosis; sAAa: Systemic amyloid A amyloidosis.

different tissue structures and organs. This deposition pattern is driven by variations in precursor production, which, in turn, is influenced by RA disease activity.[41]

The prevalence and severity of AA deposits in various organs and tissue structures represent different aspects of the same pathological process, which generally progress parallel (Figures 6,7, 9 and 10).

AA deposition begins in the most frequently affected structures of the most commonly involved organ.[3,74,79] In the GI tract, AA initially accumulates in the walls of arterioles, small arteries, and interstitial collagen fibers. As the disease advances, reticulin fibers (collagen III of adipose tissue), medium-sized veins and arteries, basement membranes of GI glands, and small veins become involved, marking advanced stages of amyloid deposition. The terminal stage is characterized by the involvement of smooth muscle cells in the GI walls, venules, and nerves.

The progression of AA deposition in medium-sized, small veins, and venules of the GI tract may be influenced by stasis and retrograde accumulation of circulating precursors (Figure 9). The role of stasis is further supported by the similar deposition patterns observed in the veins of the pancreas[41] and liver[43]

The consistent relationship between AA deposition across different tissue structures allows for the approximate estimation of amyloid burden in other structures and

organs (Figures 7 and 10), even in cases when some structures are absent in a biopsy specimen.[41,43]

A limitation of this study is that minimal amyloid deposits may go undetected, and a small, randomly selected tissue sample may provide misleading results, particularly in early-stage amyloidosis.

It is essential to consider the following factors:

(i) The staining procedure should be appropriate[46,81]
(ii) Illumination during histological examination is crucial; a highly bright professional polarization microscope is required for reliable amyloid detection.
(iii) The staining intensity of Congo red may degrade over time; thus, freshly stained, high-quality tissue sections are essential for accurate diagnosis.

5. Conclusion

sAAa is one of the most significant and insidious complications of RA, affecting multiple organs with varying prevalence and severity.

sAAa affects the cardiovascular system, and giAAa is closely associated with it. Compared to systemic AA deposition, GI AA deposition occurs after a latent stage. Like systemic amyloid deposition, GI amyloid deposition follows a progressive and cumulative trajectory, initially affecting only a few structures in the GI tract before expanding to involve additional structures as the disease advances. AA deposition begins in the most frequently affected structures of the GI tract, where more extensive deposits are observed.

In this study, giAAa did not play a direct role in the mortality of 34 RA patients with sAAa.

Acknowledgment

We wish to express our gratitude to Károly Balogh, MD, Associate Professor Emeritus of Pathology at Harvard Medical School, for his invaluable contributions over the years to our work with critical advice and professional editing of the English text.

Funding

None.

Conflict of interest

The authors declare no conflicts of interest.

Author contributions

Conceptualization: Miklós Bély
Investigation: Miklós Bély
Methodology: Miklós Bély, Ágnes Apáthy
Writing – original draft: Miklós Bély
Writing – review & editing: Ágnes Apáthy

Ethics approval and consent to participate

This study was conducted in accordance with the local legislation and institution requirements.

Consent for publication

Not applicable.

Availability of data

Data used in this work are available from the corresponding author upon reasonable request.

References

1. Buxbaum JN, Eisenberg DS, Fändrich M, *et al*. Amyloid nomenclature 2024: Update, novel proteins, and recommendations by the International Society of Amyloidosis (ISA) Nomenclature Committee. *Amyloid*. 2024;31(4):249-256.

   doi: 10.1080/13506129.2024.2405948

2. Sipe JD, Benson MD, Buxbaum JN, *et al*. Amyloid fibril proteins and amyloidosis: Chemical identification and clinical classification international society of amyloidosis 2016 nomenclature guidelines. *Amyloid*. 2016;23(4):209-213.

   doi: 10.1080/13506129.2016.1257986

3. Bély, M, Apáthy Á. *Clinical Pathology of Rheumatoid Arthritis: Cause of Death, Lethal Complications and Associated Diseases in Rheumatoid Arthritis*. Akadémiai Kiadó, Budapest, Hungary; 2012. p. 1-440. Available from: https://www.akkrt.hu [Last accessed on 2024 Oct 17].

4. Cohen AS. Amyloidosis associated with rheumatoid arthritis. *Med Clin North Am*. 1968;52:643-653.

5. Gillmore JD, Lovat LB, Persey MR, Pepys MB, Hawkins PN. Amyloid load and clinical outcome in AA amyloidosis in relation to circulating concentration of serum AA protein. Lancet. 2001;358(9275):24-29.

6. Lachmann HJ, Goodman HJ, Gilbertson JA, *et al*. Natural history and outcome in systemic AA amyloidosis. *New Engl J Med.* 2007;356(23):2361-2371.

   doi: 10.1056/NEJMoa070265

7. Simons JP, Al-Shawi R, Ellmerich S, Speck I, Aslam S, Hutchinson WL. Pathogenetic mechanisms of A amyloidosis. *Proc Natl Acad Sci U S A*. 2013;110(40):16115-16120.

   doi: 10.1073/pnas.1306621110

8. Kennedy AC, Burton JA, Allison MEM. Tuberculosis as a continuing cause of renal amyloidosis. *Br Med J*. 1974;3:395-397.

   doi: 10.1136/bmj.3.5934.795

9. Pasternack A. Fine-needle aspiration biopsy of spleen in diagnosis of generalized amyloidosis. *Br Med J*. 1974;3:30-33.

   doi: 10.1136/bmj.2.5909.20

10. Sanz-Martín N, Del Rocío Samillán-Sosa K, De Miguel J, Martínez-Miguel P. Renal amyloidosis in leprosy, an infrequent cause of nephrotic syndrome in Europe. *Br Med Case Rep.* 2016;2016:1-3.

doi: 10.1136/bcr-2016-216038

11. Shuttleworth JS, Ross H. Secondary amyloidosis in leprosy. *Ann Intern Med.* 1956;45(1):23-38.

doi: 10.7326/0003-4819-45-1-23

12. McGlennen RC, Burke BA, Dehner LP. Systemic amyloidosis complicating cystic fibrosis. A retrospective pathologic study*Arch Pathol Lab Med.* 1986;110:879-884.

13. Bontempini L, Ghimenton C, Colombari R, *et al*. Secondary amyloidosis and cystic fibrosis. A morphological and histochemical study of five cases. *Histol Histopathol.* 1987;2:413-416.

14. Lachmann HJ, Hawkins PN. Amyloidosis and the lung. *Chron Respir Dis*. 2006;3(4):203-214.

doi: 10.1177/1479972306070066

15. Gertz MA, Kyle RA. Secondary systemic amyloidosis: Response and survival in 64 patients. *Medicine*. 1991;70:246-256.

16. Punia RS, Dhingra N, Mohan H, D'Cruz S. Amyloidosis secondary to xanthogranulomatous pyelonephritis: A rare association. *Saudi J Kidney Dis Transpl*. 2010;21(4):720-723.

17. Almirall J, López T, Sáez A, Gratacós J, Prats J. Systemic amyloidosis secondary to xanthogranulomatous pyelonephritis. *Nefrologia*. 2001;21(5):505-508.

18. Lauzurica R, Felip A, Serra A, *et al*. Xanthogranulomatous pyelonephritis and systemic amyloidosis: Report of 2 new cases and the natural history of this association. *J Urol.* 1991;6:1603-1606.

doi: 10.1016/S0022-5347(17)38181-8

19. Maury CPJ, Tornroth T, Wegelius O. Is AA (AA) amyloidosis always secondary? *Ann Rheum Dis*. 1985;44:273-276.

doi: 10.1136/ard.44.4.273

20. Apáthy Á, Bély M. AB0737 Aa amyloidosis in rheumatoid arthritis and in psoriatic arthritis-a postmortem clinicopathologic study of 173 patients. *Ann Rheum Dis.* 2017;76:1312.

doi: 10.1136/annrheumdis-2017-eular.1224

21. Apáthy Á, Bély M. AB0164 amyloidosis in progressive systemic sclerosis-a postmortem clinicopathologic study of 12 patients. *Ann Rheum Dis.* 2017;76:1312.

doi: 10.1136/annrheumdis-2017-eular.1226

22. Shorvon JP. Amyloidosis and inflammatory bowel disease. *Am J Digest Dis*. 1977;22:209-213.

doi: 10.1007/BF01072278

23. Gitkind MJ, Wright SC. Amyloidosis complicating inflammatory bowel disease. A case report and review of the literature. *Dig Dis Sci.* 1990;35:906-908.

doi: 10.1007/BF01536807

24. Escribá A, Morales E, Albizúa E, *et al*. Secondary (AA-type) amyloidosis in patients with polymyalgia rheumatic. *Am J Kidney Dis.* 2000;35(1):137-140.

doi: 10.1016/S0272-6386(00)70312-X

25. Tang AL, Davies DR, Wing AJ. Remission of nephrotic syndrome in amyloidosis associated with a hypernephroma. *Clin Nephrol.* 1989;32(5):225-228.

26. Nobata H, Suga N, Itoh A, *et al*. Systemic AA amyloidosis in a patient with lung metastasis from renal cell carcinoma. *Amyloid*. 2012;19(4):197-200.

doi: 10.3109/13506129.2012.712926

27. Fernandez-Miranda C, Mateo S, Gonzalez-Gomez C, Ballestin C. Systemic amyloidosis and ovarian carcinoma. *Postgrad Med J.* 1994;70(825):505-506.

doi: 10.1136/pgmj.70.825.505

28. Thysell H, Ingvar CH, Gustafson T, Holmin T. Systemic reactive amyloidosis caused by hepatocellular adenoma. A case report. *J Hepatol.* 1986;2:450-457.

doi: 10.1016/s0168-8278(86)80056-3

29. Calderaro J, Letouzé E, Bayard Q, *et al*. Systemic AA amyloidosis caused by inflammatory hepatocellular adenoma. *N Engl J Med.* 2018;379(12):1178-1180.

doi: 10.1056/NEJMc1805673

30. Fiever P, Sevestre H, Boudjelal M, *et al*. Systemic AA amyloidosis induced by liver cell adenoma. *Gut.* 1990;31:361-363.

doi: 10.1136/gut.31.3.361

31. Richmond I, Hasleton PS, Samadian S. Systemic amyloid associated with carcinoma of the bronchus. *Thorax*. 1990;45:156-157.

doi: 10.1136/thx.45.2.156

32. Hiasa Y, Konishi N, Kitahori Y, *et al*. Secondary systemic amyloidosis with Hodgkin's disease. *Acta Pathol Jpn*. 1983;33:1069-1077.

doi: 10.1111/j.1440-1827.1983.tb02152.x

33. Lanjewar DN, Raghuwanshi SR, Gupta D, Jain P, Valand AG. Systemic amyloidosis in Hodgkin's disease. *Indian J Pathol Microbiol.* 1998;41(2):169-171.

34. Wens R, Goffin Y, Pepys MB, *et al*. Left atrial myxoma associated with systemic AA amyloidosis. *Arch Intern Med*. 1989;19:453-454.

35. Röcken C, Shakespeare A. Pathology, diagnosis and pathogenesis of AA amyloidosis. *Virchows Arch*. 2002;440:111-122.

doi: 10.1007/s00428-001-0582-9

36. Obici L, Merlini G. AA amyloidosis: Basic knowledge,

unmet needs and future treatments. *Swiss Med Wkly*. 2012;142:w13580.

doi: 10.4414/smw.2012.13580

37. *Amyloidosis Foundation. AA amyloidosis*. Available from: https://www.amyloidosis.org [Last accessed on 2024 Jun 01].
38. Petre S, Shah A, Gilani N. Review article: Gastrointestinal amyloidosis-clinical features, diagnosis and therapy. *Aliment Pharmacol Therapeut*. 2008;27:1006-1016.

doi: 10.1111/j.1365-2036.2008.03682.x

39. Westermark GT, Fändrich M, Westermark P. AA amyloidosis: Pathogenesis and targeted therapy. *Annu Rev Pathol*. 2015;10:321-344.

doi: 10.1146/annurev-pathol-020712-163913

40. Available from: https://www.sciencedirect.com/topics/immunology-and-microbiology/aa-amyloidosis [Last accessed on 2013 Jun 01].
41. Bély M, Apáthy Á. Progression of AA amyloidosis (sequence of AA deposition) in the pancreas-a postmortem clinicopathologic study of 161 patients. *Gastroenterol Hepatol Int J*. 2018;3(2):000143.

doi: 10.23880/ghij-16000143

42. Bély M, Apáthy Á. A comparative postmortem clinicopathologic study of renal and cardiac AA amyloidosis in rheumatoid arthritis. *J Clin Trials Cardiol*. 2019;6(1):1-20.

doi: 10.15226/2374-6882/6/1/00158

43. Bély M, Apáthy Á. AA Amyloidosis of the liver in rheumatoid arthritis-a postmortem clinicopathologic study of 152 autopsy patients. *Arch Gastroenterol Hepatol*. 2020;3(2):1-26.

doi: 10.22259/2639-1813.0302001

44. Aletaha D, Neogi T, Silman AJ, *et al*. 2010 rheumatoid arthritis classification criteria: An American college of rheumatology/european league against rheumatism collaborative initiative. *Ann Rheum Dis*. 2010;69:1580-1588.

doi: 10.1136/ard.2010.138461

45. Romhányi G. Selective differentiation between amyloid and connective tissue structures based on the collagen specific topo-optical staining reaction with Congo red. *Virchows Arch A Pathol Pathol Anat*. 1971;354:209-222.

doi: 10.1007/BF00544254

46. Bély M, Makovitzky J. Sensitivity and specificity of congo red staining according to romhányi-comparison with puchtler's or bennhold's methods. *Acta Histochem*. 2006;108:175-180.

doi: 10.1100/tsw.2006.35

47. Bratthauer GL. The avidin-biotin complex (ABC) method and other avidin-biotin binding methods. *Methods Mol Biol*. 2010;588:257-270.

doi: 10.1007/978-1-59745-324-0_26

48. Romhányi G. Selektive darstellung sowie methodologische möglichkeiten der analyse ultrastruktureller unterschiede von amyloidablagerungen. *Zentralbl Allg Pathol Pathol Anat*. 1979;123:9-16.
49. Bély M. Histochemical differential diagnosis and polarization optical analysis of amyloid and amyloidosis. *ScientificWorldJournal*. 2006;6:154-168.

doi: 10.1100/tsw.2006.35

50. Bély M, Apáthy Á editors. *Differential Diagnosis of Amyloid Deposits by Light, Polarization and Electron Microscopy*. UK London: BP International; 2021. p. 1-253.

doi: 10.9734/bpi/mono/978-93-5547-007-2

51. Lentner C. Statistical methods. In: Lentner C, Compiled, Diem K, Seldrup J, editor. *Geigy Scientific Tables*. Vol. 2. Basle, Switzerland: Ciba-Geigy Limited.; 1982. p. 227.
52. Szentágothai J, Verőerek RM. Visszerek. In: Szentágothai J, editor. *Funkcionális Anatómia II*. Budapest: Medicina; 2002. p. 770-786, 786-788.
53. Bayles TB. Rheumatoid arthritis and rheumatic heart disease in autopsied cases. Am J *Med Sci (AJMS)*. 1943;205:42-48.

doi: 10.1016/S0002-8703(43)90077-8

54. Baggenstoss AH, Rosenberg EF. Visceral lesions associated with chronic infectious rheumatoid arthritis. *Arch Pathol*. 1943;35:503-516.
55. Rosenberg EF, Baggenstoss AH. The causes of death in thirty cases of rheumatoid arthritis. *Ann Intern Med*. 1944;20:903-919.

doi: 10.7326/0003-4819-20-6-903

56. Young D, Schwedel JB. The heart in rheumatoid arthritis. *Am Heart J*. 1944;28:1-23.
57. Unger PN, Zuckerbrod M, Beck GJ, Steele JM. Amyloidosis in rheumatoid arthritis; a report of ten cases. *Am J Med Sci*. 1948;216:51-56.

doi: 10.1097/00000441-194807000-00008

58. Teilum G, Lindahl A. Frequency and significance of amyloid changes in rheumatoid arthritis. *Acta Med Scand*. 1954;149:449-455.

doi: 10.1111/j.0954-6820.1954.tb11456.x

59. Gedda PO. On amyloidosis and other causes of death in rheumatoid arthritis. *Acta Med Scand*. 1955;60:443-452.

doi: 10.1111/j.0954-6820.1955.tb15728.x.

60. Cruickshank B, Sinclair RJ. A clinical and pathological study of sixteen cases of rheumatoid arthritis with extensive visceral involvement ('Rheumatoid disease'). *Quarterly J Med*. 1956;25:313-332.
61. Missen GAK, Taylor JD. Amyloidosis in rheumatoid arthritis. *J Pathol Bacteriol*. 1956;71:179-192.

doi: 10.1002/path.1700710124

62. Lebowitz WB. The heart in rheumatoid arthritis (Rheumatoid disease). A clinical and pathological study of sixty-two cases. *Ann Intern Med.* 1963;58:102-123.

doi: 10.7326/0003-4819-58-1-102

63. Sokoloff L. Cardiac involvement in rheumatoid arthritis and allied disorders: Current concepts. *Mod Concepts Cardiovasc Dis*. 19964;33:847-850.

64. Karten I. Arteritis, myocardial infarction, and rheumatoid arthritis. *JAMA*. 1969;210:1717-1720.

doi: 10.1001/jama.1969.03160350029004

65. Gritsman NN. Morfologicheskaya kharakteristika porazheniya pri infektsionnom nespetsificheskom poliartrite (Morphologic characteristics of heart lesions in infectious nonspecific polyarthritis (rheumatoid arthritis). *Arkh Patol*. 1969;31:49-53.

66. Ozdemir AI, Wright JR, Calkins E. Influence of rheumatoid arthritis on amyloidosis of aging. Comparison of 47 rheumatoid patients with 47 controls matched for age and sex. *N Engl J Med*. 1971;285:534-538.

doi: 10.1056/NEJM197109022851002

67. Gardner DL. Causes of death. In: *The Pathology of Rheumatoid Arthritis*. London: Edward Arnold; 1972. p. 183-197.

68. Püschel W. Sektionsstatistische untersuchungen bei der rheumatoid-arthritis. *Deutsch Gesundheitswesen*. 1972;27:754-756.

69. Vroninks, Ph, Cats, A, Eulderink, F, Goslinks, J. Hartafwijkingen bij rheumatide arthritis, in het bijzonder pericarditis. *Ned Tijdschr Voor Geneeskd*. 1973;117:10-17.

70. Hajzok O, Tomik F, Hajzoková M. Amyloidosis in rheumatoid arthritis. A study of 48 histologically confirmed cases. *Z Rheumatol.* 1976;35:356-362.

71. Eulderink F. Doodsoorzak: Rheumatoide arthritis. *Ned Tijdschr Voor Geneeskd*. 1976;120:357-363.

72. Rainer F, Klein G, Schmid P, Härringer M. Untersuchungen über art und häufigkeit der todesursachen bei chronischer polyarthritis. *Z Rheumatol.* 1978;37:335-341.

73. Boers M, Croonen AM, Dijkmans BA, *et al*. Renal finding in rheumatoid arthritis: Clinical aspect of 132 necropsies. *Ann Rheum Dis.* 1987;46:658-663.

doi: 10.1136/ard.46.9.658

74. Bély M. *Krankheitsmodifizierende Faktoren bei Chronischer Polyarthritis: Über Zusammenhänge Zwischen Generalisierter Vaskulitis, Sekundärer Amyloidose, Septischen Infektionen und Auftreten Von Miliaren Epitheloidzelligen Granulomen. D.Sc. Thesis, Budapest*; 1993.

doi: 10.13140/2.1.3940.7680

75. Suzuki A, Ohosone Y, Obana M, *et al*. Cause of death in 81 autopsied patients with rheumatoid arthritis. *J Rheumatol*. 1994;21:33-36.

76. Bély M, Apáthy Á. Szövődmények és társult megbetegedések rheumatoid arthritisben-a 234 elhunyt beteg patológiai és klinikai adatainak retrospektív elemzése alapján (Complications and associated diseases in rheumatoid arthritis-a retrospective clinicopathologic study of 234 autopsy patients) [Hung]. *Orvosi Hetilap.* 2006;147:1063-1076.

77. Bennhold H. Eine spezifische amyloidfärbung mit Kongorot. *Münchener Medizinische Wochenschrift*. 1922;44:1537-1538.

78. Puchtler H, Sweat F, Levine MJ. On the binding of Congo red by amyloid. *J Histochem Cytochem*. 1962;10(3):355-364.

doi: 10.1177/10.3.355

79. Bely M, Apáthy Á, Pintér T, Ratkó J. Generalized secondary amyloidosis in rheumatoid arthritis. *Acta Morphol Hung.* 1992;40:49-69.

80. Bély M, Apáthy A. Histochemical and immunohistochemical differential diagnosis of amyloidosis--a brief illustrated essay and personal experience with Romhányi's method. *Amyloid*. 2000;7(3):212-217.

doi: 10.3109/13506120009146836

81. Bély M. Identification of amyloid deposits by histochemical methods of romhányi and wright: A comparative histochemical and immunohistochemical study. *Amyloid*. 2001;8(2):177-182.

82. Bély M, Apáthy Á. Differential diagnosis of amyloid and amyloidosis by histochemical methods of Romhányi and Wright. *Acta Histochem*. 2003;105(4):361-365.

doi: 10.1078/0065-1281-00722

ACCSCIENCE PUBLISHING

Global Translational Medicine

ORIGINAL RESEARCH ARTICLE

Predicting magnetic resonance imaging-guided focused ultrasound sonication parameters beyond skull density ratio

Alsu Narkisovna Khatmullina[1]*, Diana Shamilevna Avzaletdinova[1,2], Dinara Ilgizovna Nabiullina[1], Sergey Nikolaevich Illarioshkin[3], Guzaliya Minvazykhovna Sakharova[1,2], Naufal Shamilevich Zagidullin[1,2], Nadezhdina Ekaterina Andreevna[1,2], Shamil Makhmutovich Safin[2], and Rezida Maratovna Galimova[1,2]

[1]Intelligent Neurosurgery Clinic, Ltd., V.S. Buzaev International Medical Center, Ufa, Bashkortostan, Russia

[2]Department of Surgery, Bashkir State Medical University, Ufa, Bashkortostan, Russia

[3]Institute of the Brain, Research Center of Neurology, Moscow, Russia

(*This article belongs to the Special Issue: Special Issue of Global Translational Medicine in the Fourth RCCCDT-2024*)

Abstract

Precise temperature regulation is essential for effective and safe magnetic resonance imaging-guided focused ultrasound (MRgFUS) treatments. Several variables influence the target temperature during sonication, with the energy delivered being a pivotal physical determinant. The skull density ratio (SDR) is utilized to evaluate the feasibility of treatment, with values below 0.3 – 0.4 generally considered contraindications for treatment. This study aimed to develop a robust predictive model for sonication parameters that can accurately achieve the desired temperature within the target tissue region. We obtained 152 treatment log data from the Insightec Exablate workstation. Variables, including power output, sonication duration, stop sonication button activation, SDR, age, sex, and initial sonication (ALIGN) parameters, were used as predictors (x), with the achieved temperature as the response (y), to construct the predictive models. RStudio was used to build linear models, and the TensorFlow library was employed for the neural network models. The linear and neural network models predicted tissue temperature with a mean absolute error of 2.78°C and 1.93°C, respectively, and a coefficient of determination of 0.71 and 0.76, respectively. The neural network model outperformed the linear model, demonstrating a smaller residual dispersion and a lower root-mean-square deviation. While the neural network model is more accurate and reliable for predicting MRgFUS temperatures, the linear model is easier to use. Key factors, such as sex, age, SDR, and the initial tissue response to the first sonication – the energy delivered during this initial treatment and the corresponding temperature – are crucial for optimizing subsequent sonication parameters such as power, energy, and duration.

Keywords: Magnetic resonance imaging-guided focused ultrasound; Skull density ratio; Sonication

***Corresponding author:**
Alsu Narkisovna Khatmullina (info@buzaevclinic.ru)

Citation: Khatmullina AN, Avzaletdinova DS, Nabiullina DI, *et al*. Predicting magnetic resonance imaging-guided focused ultrasound sonication parameters beyond skull density ratio. *Global Transl Med*. 2025:4(1):126-135. doi: 10.36922/gtm.5419

Received: October 22, 2024
Revised: December 28, 2024
Accepted: February 7, 2025
Published online: March 10, 2025

1. Introduction

Magnetic resonance imaging-guided focused ultrasound (MRgFUS) treatment has been approved by the Food and Drug Administration[1] and the European Medical Agency[2] as a non-surgical alternative for treating movement disorders. This technology concentrates ultrasound at specific tissue points in tissue, offering therapeutic potential in various clinical conditions.[3-13] Clinical studies have demonstrated its efficacy in treating essential tremor,[14-16] Parkinson's disease (PD),[17-23] neuropathic pain,[24-27] and psychiatric conditions.[28-32] At present, researchers are exploring the use of MRgFUS in incurable diseases, such as Alzheimer's disease.[33] and other dementias,[34] amyotrophic lateral sclerosis,[35] glioblastomas and brain metastases, and Huntington's disease.

Initially, focused ultrasound treatment systems used ultrasound imaging for treatment, which has limited guidance accuracy and lacked real-time temperature detection. Combining magnetic resonance (MR) imaging with focused ultrasound has significantly improved imaging and enhanced thermometry accuracy to assess the degree of exposure. MR-thermography is used to control the target area temperature.[36]

MRgFUS uses three interrelated parameters: energy (joules), power (watts), and time (seconds).[37,38] During initial sonication, known as ALIGN, the neurosurgeon sets the power to 150 watts for 10 s, resulting in 1,500 joules of energy. We hypothesized that the response to the initial sonication energy can predict the outcomes of subsequent sonications.

When adjusting power during MRgFUS treatments, caution is essential to prevent rapid overheating, which can have irreversible consequences. Excessive power can quickly overheat an area, potentially causing patient discomfort. In addition, higher power levels may increase headaches, causing the patient to stop or decline the procedure. Insufficient power may prolong sonication unnecessarily, causing temporary tissue swelling and altering the neurological condition.

Time plays a critical role in the heating process. Longer durations allow for more energy delivery and intense heating, while shorter duration leads to insufficient energy to heat tissue. Excessive heating time, on the other hand, can lead to patient discomfort and headaches. Reducing the treatment time may improve patient tolerance. It is important to note that different patients require varying durations to heat an area to a specific temperature.

Bone tissue properties, such as the skull density ratio (SDR), are known to affect energy loss. Patients with varying conductivity may require different durations to reach the same target temperature. In addition, the water and oxygen bubbles along the ultrasound path can absorb ultrasound energy, affecting the efficiency of heating. Conductivity is also impacted by tissue conditions along the ultrasound path.

Incorporating additional clinically relevant factors would enhance the construction of a temperature model, enabling more accurate calculations of the target temperature based on power, time, and the bone tissue coefficient.

This study aimed to determine the most accurate temperature calculation model using various models, including linear models and a neural network, considering tissue conductivity and other variables.

2. Methods

We obtained log data of 152 MRgFUS treatments between May 05, 2020, and July 01, 2023, using the Insightec Exablate workstation. According to nosological forms, patients were distributed as follows: PD with predominant tremor phenotype (84 patients), PD with predominant akinetic-rigid phenotype (four patients), essential tremor (45 patients), and various forms of dystonia (19 patients).

The first model was based on power, energy, time, and bone ultrasound conductivity coefficient. A random sample of 782 sonications was used for model training, while 369 sonications were used for testing.

On the test set, the root mean square error (RMSE) was 3.68, the coefficient of determination (R^2) was 0.62, and the mean absolute error (MAE) was 2.78. Training set RMSE was 3.55 with an R^2 of 0.64 and an MAE of 2.67. Figure 1 shows the observed and predicted temperatures plotted against each other. In the second model, all the parameters were included to identify those that significantly affect the temperature. Power ($P < 0.05$), sonication duration, early cessation, bone conductivity coefficient, initial sonication parameters, and results, age, and sex are the key factors that significantly impact temperature in the model.

The third model was constructed by eliminating redundant parameters using the command:

```
lm(formula = max_avg_temp ~ power + stopped + scull_
score + first_measured_energy + first_max_avg_temp +
actual_duration + age + male_sex, data = ds [idx == 1, ])
```

After training, the median of residuals was 0.05 with $P < 2.2 \times 10^{-16}$, which is close to zero as required. However, the model tended to underestimate the temperature. The parameters of the linear model are shown in Table 1.

Recent advances in machine learning enable the development of sophisticated algorithms to construct

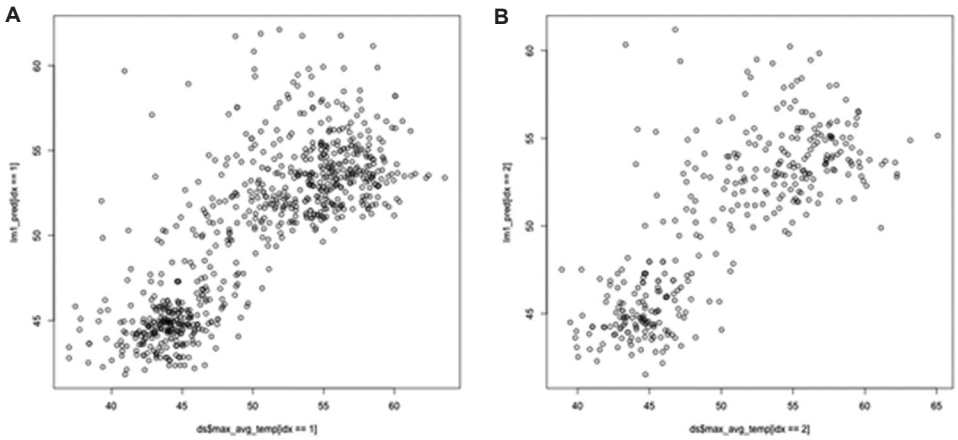

Figure 1. An observation and prediction graph of the model. (A) The training sample has a root mean square error (RMSE) of 3.55, a coefficient of determination (R^2) of 0.64, and a mean absolute error (MAE) value of 2.67. (B) The testing sample has an RMSE of 3.68, R^2 of 0.62, and an MAE of 2.78. The observed temperature is on the x-axis, and the predicted temperature is on the y-axis.

Table 1. Temperature prediction model coefficients

Variable	Estimate	Standard error	*t*-value	Pr (>|*t*|)	*P*
(Intercept)	5.9513128	2.4767214	2.403	0.01651	*
Power	0.0131968	0.0004608	28.637	$<2\times10^{-16}$	***
Duration	0.1706348	0.0168204	10.145	$<2\times10^{-16}$	***
Stopped	1.1448043	0.3413393	3.354	0.000838	***
Scull score	8.4071908	1.4172244	5.932	4.59×10^{-09}	***
Temperature on ALIGN	0.7456789	0.0556243	13.406	$<2\times10^{-16}$	***
Energy on ALIGN	−0.0012530	0.0001831	-6.842	1.64×10^{-11}	***
Age	−0.0190515	0.0078899	-2.415	0.015992	*
Male sex	0.7334997	0.2569256	2.855	0.004426	**

Note: ALIGN refers to the first sonication. Statistical significance determined at $P<0.05$*, $P<0.01$**, and $P<0.001$***.

models that handle multiple variables and uncertainties. Recognizing the limitations of linear models in capturing non-linear relationships, a neural network model was developed using the RStudio 2021.09.2 build 382, R version 4.2.1 environment, which uses the open TensorFlow libraries for high-level machine learning tasks. Specifically, we used Tensorflow R and Keras 2.9.0, an open python library, to facilitate the interaction with various artificial neural networks.

A deep neural network was chosen to determine optimal mathematical computations to derive outputs based on input data, regardless of linear or non-linear regression complexity. To address the problem, we implemented a convolutional neural network (CNN) with hidden layers of neurons representing potential abstract input features. The model was constructed sequentially. The first layer was a standard, fully connected dense layer tailored to the dimensionality of the training input data. Next, a layer of 64 neurons was added with a rectified linear unit (ReLU) activation function. ReLU offers simple computations and binary derivations (0 or 1) based on input negativity to mitigate the exponential computational growth of neural networks. Next, a 128-neuron dense layer and a dropout function were introduced to prevent overfitting by randomly deactivating neurons during training. Two dense layers were added, culminating in a single neuron output layer. The parameters of the neural network are shown in Table 2.

The code snippet shown in the Appendix describes the process of creating and training the neural network using training input data (x_train) and corresponding correct responses (y_train). Training and testing were split into an 80:20 ratio.

The neural network training progress over 200 epochs is shown in Figure 2, demonstrating the regression model error reduction per epoch. The subsequent verification test using a dataset of sonication parameters and temperature resulted in metrics of MAE = 1.93, RMSE = 2.69, and an error rate of 5.37%. Comparable values were obtained with the training dataset, demonstrating the model's consistency. The results were consistent across the cohorts, indicating the effectiveness of the neural network in predicting temperature.

3. Results

Figure 3 shows the accuracy indicators displayed for both the linear and neural network models. The x-axis represents the observed temperature, while the y-axis

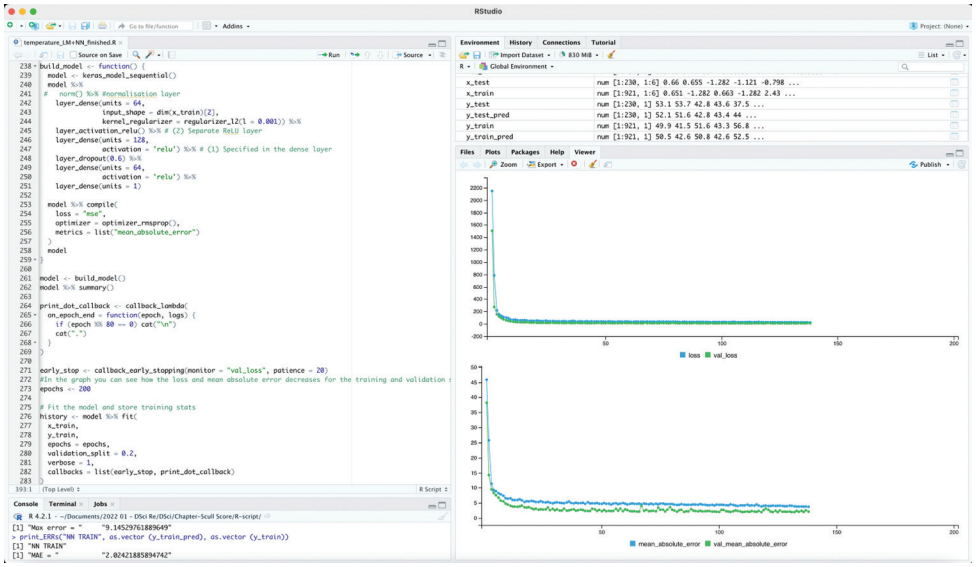

Figure 2. Neural network training

Table 2. Parameters of a multilayer neural network (Model: "sequential_3") for temperature prediction during sonication

Layer (type)	(Output, shape)	Parameter
dense_15 (Dense)	(None, 64)	448
re_lu_3 (ReLU)	(None, 64)	0
dense_14 (Dense)	(None, 128)	8,320
dropout_3 (Dropout)	(None, 128)	0
dense_13 (Dense)	(None, 64)	8,256
dense_12 (Dense)	(None, 1)	65
Total parameters		17,089
Trainable parameters		17,089
Non-trainable parameters		0

Abbreviation: ReLU: Rectified linear unit.

represents the predicted temperature. The training matrix is shown in the left column, and the testing matrix is shown in the right column. The linear model is displayed at the top (Figure 3A), and the neural network model is displayed at the bottom (Figure 3B). The linear model in the training sample has an MAE of 2.32, an RMSE of 3.1, an error rate of 6.3%, and an R^2 value of 0.71. In the test sample, the MAE is 2.2, the RMSE is 3.12, and the error rate is 6.0%.

The graphs indicate that the neural network model has less residual dispersion than the linear model. This is supported by the RMSE parameter, which was higher for the linear (3.12) than the neural network model (2.56). The maximum prediction error was 17.8°C for the linear model and 12.1°C for the neural network model, indicating that the neural network performed better.

Figure 4 presents a density plot of residuals, demonstrating that the neural network model has errors closer to zero. For practicality, if access to a computer with R and libraries is not available, the linear model coefficients can be entered into Microsoft Excel, as shown in Figure 5.

4. Discussion

MRgFUS treatment is a promising innovative treatment for movement disorders, such as essential tremor and advanced PD. However, skull barriers can prevent sufficient temperature elevation in the target area. In a retrospective analysis of 25 patients, Chang *et al.*[39] found that the skull volume and the SDR were associated with the maximum temperature achieved during MRgFUS treatment. These findings may help identify eligible candidates for MRgFUS.

D'Souza *et al.*[40] investigated the impact of cranial bone characteristics on the efficacy and safety of procedures employing an integrated 3T MRgFUS system. The analysis included data from 189 patients diagnosed with essential tremor, with particular emphasis on a subgroup exhibiting low SDR. The results indicated a significant difference in the probability of reaching the target temperature of 54°C between patients with SDR values below 0.45 and those with SDR values of 0.45 or higher.

In a study of 270 patients,[41] researchers compared outcomes based on SDR. Patients were categorized into low SDR (<0.40, n = 31) or high SDR (≥0.40, n = 239) groups. A matched-case analysis (n = 56) showed that patients with low SDR needed greater sonication power and energy, leading to smaller lesion volumes. Despite these differences, both groups achieved similar tremor control. While patients with low SDR experienced slightly more

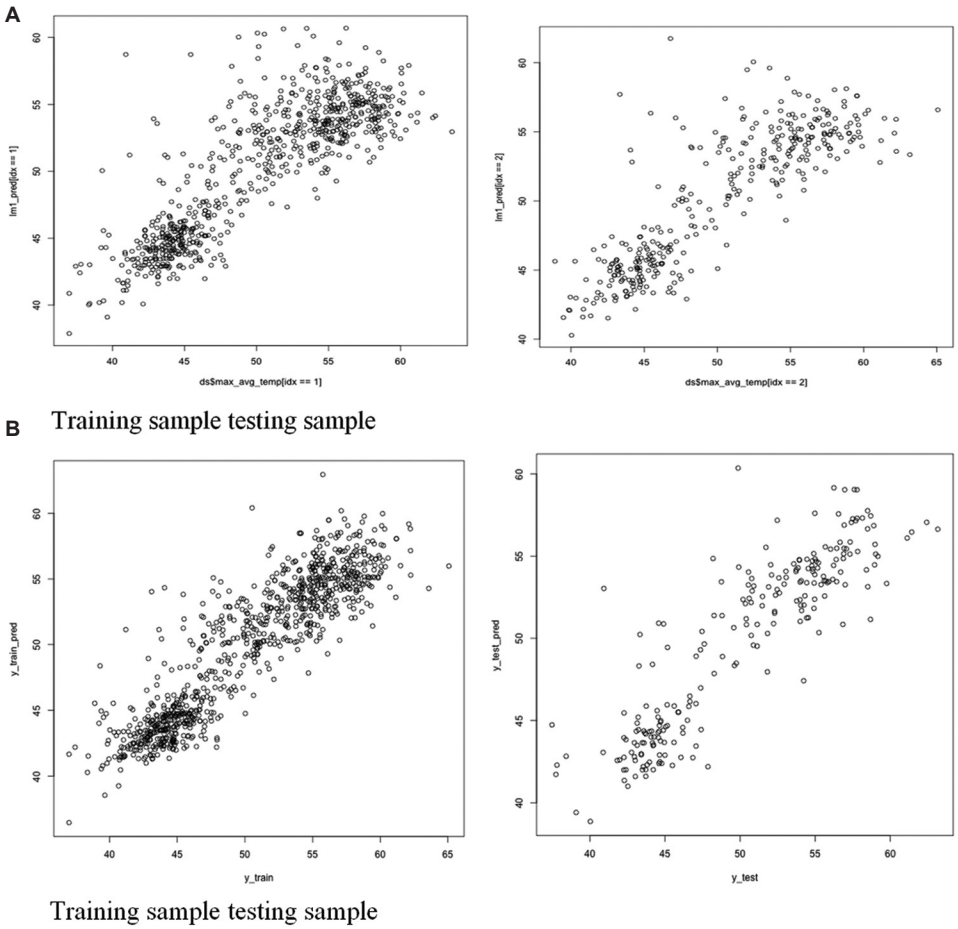

Figure 3. Prediction accuracy indicators for linear and neural network models. (A) The linear model has a determination coefficient value of 0.71, while the (B) neural network model has a determination coefficient value of 0.76. The observed temperature is on the x-axis, and the predicted temperature is on the y-axis.

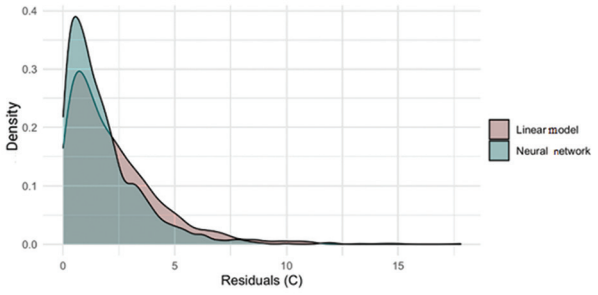

Figure 4. A diagram of the residual distribution density (difference between the predicted and achieved temperature)

side effects, overall tremor reduction was comparable. These findings suggest that MRgFUS is safe for patients with low SDR, although they may be at higher risk for treatment failure and intraoperative discomfort.

Gagliardo *et al.*[23] described the relationships between sonication parameters, emphasizing their significant impact on MRgFUS treatment. They highlighted the importance of skull bone ultrasonic conductivity coefficient in MRgFUS treatment. Gagliardo *et al.* suggested that better control of the procedure can be achieved by prospectively determining ultrasound energy based on energy delivery curves and skull bone ultrasonic conductivity coefficients at each treatment step. However, they did not propose a formula for calculating the heat energy.

Boutet *et al.*[42] also investigated the role of SDR in the effectiveness of MRgFUS for movement disorders in two cohorts. They noted that low SDR values can impede the passage of acoustic energy. In their study, 98 patients who underwent MRgFUS thalamotomy (Cohort 1) were analyzed. While patients with lower SDRs needed higher energy levels for treatment, their overall clinical outcomes were not significantly different. Furthermore, a study of 163 emergency department patients (Cohort 2) showed that approximately one-third had low SDRs, and SDR was not associated with age or gender. This finding suggests that skull density does not vary predictably with these

	A	B	C	D
1		5.9513128	1	5.95131
2	Power	0.0131968	750	9.89760
3	Time	0.1706348	6	1.02381
4	Scull score	8.4071908	0.38	3.19473
5	ALIGN energy	-0.001253	2516	-3.15255
6	ALIGN temperature achieved	0.7456789	39.8	29.67802
7	Age	-0.019052	50	-0.95258
8	Sex	0.7334997	1	0.73350
9				
10	Temperature	46.4		
11	Energy	4500		

Figure 5. An Excel spreadsheet for automatic temperature calculation
Note: ALIGN refers to the first sonication.

demographic factors. Boutet *et al*. concluded that while SDR impacts the energy needed during sonication, it does not accurately predict treatment success in the study population. They proposed that a broader assessment, including local variations in bone density, is necessary to determine which patients are good candidates for MRgFUS.

Yuen *et al*.[43] explored how different skull measurements, especially the SDR, relate to the success of MRgFUS treatment for essential tremor. They reanalyzed the records of 62 patients treated at the Mayo Clinic from 2017 to 2021, examining the association between skull metrics and treatment details, such as the highest power and energy used. The findings show that while SDR is a key predictor of treatment success, other skull features also play a significant role in how the treatment is delivered. Machine learning methods were used to improve predictions of treatment outcomes, with some success. The study results indicated that while SDR was a strong indicator, combining it with other skull metrics could further improve predictive accuracy. Yuen *et al*. concluded that patient selection for MRgFUS should consider multiple skull features, acknowledging that factors beyond just SDR influence treatment outcomes.

In our study, we used three linear models and a CNN to effectively compare and determine the most accurate model for temperature prediction. In the first model, the RMSE was 3.68, the R^2 was 0.62, and the MAE was 2.78. On the training set, the RMSE was 3.55, with an R^2 value of 0.64 and an MAE value of 2.67. In the second model, we identified power sonication duration, early termination, bone tissue coefficient, initial sonication parameters, as well as results, age, and sex, as the key factors that significantly affect temperature within the model ($P < 0.05$). The third model, created by eliminating redundant parameters, tended to underestimate temperature. In the test sample, the MAE was 2.2, the RMSE was 3.12, and the error rate was 6%. In the training sample, the MAE was 2.32, and the RMSE was 3.14. The low RMSE differences between training and test samples indicate that model overfitting was not an issue. For the entire cohort, the MAE was 2.29, the RMSE was 3.13, and the error rate was 6.2%.

In addition, we chose to use a deep neural network for its ability to perform optimal computations based on the input data, regardless of regression complexity. Using a CNN with hidden layers, the model showed promising results with an MAE of 1.93, an RMSE of 2.69, and an error rate of 5.37%. Thus, the consistency of the neural network was validated using the training dataset. Overall, with an MAE of 1.93°C and an R^2 of 0.76, the neural network outperformed the linear models in temperature prediction.

Our study further supports previous findings, demonstrating that the temperature at the target during ultrasonic heating is influenced not only by power, energy, and exposure time but also by the patient's body mass index, sex, and age, which are likely related to the age and sex characteristics of the tissues.

However, our study has several limitations. First, it is based on data obtained from 152 patients who underwent the MRgFUS procedure. These patients had different conditions, such as essential tremor, PD, and various forms of dystonia. Moreover, the distribution of patients by nosology may not account for other potential factors affecting accurate temperature calculation. We did not explore factors such as race, population demographics, or the impact of certain medications on MRgFUS treatment. While the study identified several parameters that significantly affect treatment, there may be other important variables not included in the models that could improve the prediction accuracy.

5. Conclusion

Sex, age, SDR, and the initial tissue response to the first sonication—specifically the energy delivered during this initial treatment and the corresponding temperature—are critical factors in optimizing subsequent sonication parameters, such as power, energy, and duration.

Acknowledgments

We thank the Research Center of Neurology, Moscow, Russia, the National Society of Movement Disorders and Parkinson Disease Research, and Bashkir State Medical University for academic support.

Funding

None.

Conflict of interest

Naufal Zagidullin is an Editorial Board Member of this journal and Guest Editor of this special issue but was not in

any way involved in the editorial and peer-review process conducted for this paper, directly or indirectly. Separately, other authors declared that they have no known competing financial interests or personal relationships that could have influenced the work reported in this paper.

Author contributions

Conceptualization: Naufal Shamilevich Zagidullin, Rezida Maratovna Galimova
Investigation: Rezida Maratovna Galimova
Methodology: Diana Shamilevna Avzaletdinova, Guzaliya Minvazykhovna Sakharova, Shamil Makhmutovich Safin
Visualization: Dinara Ilgizovna Nabiullina, Nadezhdina Ekaterina Andreevna
Writing – original draft: Alsu Narkisovna Khatmullina
Writing – review & editing: Sergey Nikolaevich Illarioshkin

Ethics approval and consent to participate

The study was approved by the Ethical Committee of the Research Center of Neurology (Moscow) (N 1 – 8/23). All patients were informed about the treatment technique. They all signed a written consent to participate in the research and an agreement to share personal data. They signed an informed consent form after being fully informed about the treatment, its results, and risks.

Consent for publication

Patients consented on the publication of their data.

Availability of data

Data are available from the corresponding author upon reasonable request.

References

1. FDA Approves First MRI-guided Focused Ultrasound Device to Treat Essential Tremor; 2016. Available from: https://www.fda.gov/news-events/press-announcements/fda-approves-first-mri-guided-focused-ultrasound-device-treat-essential-tremor
2. Zaaroor M, Sinai A, Goldsher D, *et al*. Magnetic resonance guided focused ultrasound thalamotomy for tremor: A report of 30 Parkinson's disease and essential tremor cases. *J Neurosurg*. 2017;128(1):202-210.

   doi: 10.3171/2016.10.JNS16758
3. Foley JL, Eames M, Snell JW, *et al*. Image-guided focused ultrasound: state of the technology and the challenges that lie ahead. *Imag Med*. 2013;5(4):357.

   doi: 10.2217/iim.13.38
4. Yamaguchi T, Hori T, Hori H, *et al*. Magnetic resonance-guided focused ultrasound ablation of hypothalamic hamartoma as a disconnection surgery: A case report. *Acta Neurochirurg*. 2020;162(10):2513-2517.

   doi: 10.1007/s00701-020-04468-6
5. Parker WE, Weidman EK, Chazen JL, *et al*. Magnetic resonance-guided focused ultrasound for ablation of mesial temporal epilepsy circuits: Modeling and theoretical feasibility of a novel noninvasive approach. *J Neurosurg*. 2019;133(1):63-70.

   doi: 10.3171/2019.4.JNS182694
6. Tierney TS, Alavian KN, Altman N, *et al*. Initial experience with magnetic resonance-guided focused ultrasound stereotactic surgery for central brain lesions in young adults. *J Neurosurg*. 2022;137(3):760-767.

   doi: 10.3171/2021.10.JNS21416
7. Horisawa S, Fukui A, Tanaka Y, *et al*. Pallidothalamic tractotomy (Forel's Field H1-tomy) for dystonia: Preliminary results. *World Neurosurg*. 2019;129:e851-e856.

   doi: 10.1016/j.wneu.2019.06.055
8. Gallay MN, Moser D, Jeanmonod D. MR-guided focused ultrasound central lateral thalamotomy for trigeminal neuralgia. Single center experience. *Front Neurol*. 2020;11:271.

   doi: 10.3389/fneur.2020.00271
9. Ma Y, Hsu G, Zhang F. The applicability and efficacy of magnetic resonance-guided high intensity focused ultrasound system in the treatment of primary trigeminal neuralgia. *Med Hypothes*. 2020;139:109688.

   doi: 10.1016/j.mehy.2020.109688
10. Franzini A, Moosa S, D'Ammando A, *et al*. The neurosurgical treatment of craniofacial pain syndromes: Current surgical indications and techniques. *Neurol Sci*. 2019;40(1):159-168.

    doi: 10.1007/s10072-019-03789-4
11. Cohen-Inbar O, Xu Z, Sheehan JP. Focused ultrasound-aided immunomodulation in glioblastoma multiforme: A therapeutic concept. *J Ther Ultrasound*. 2016;4(1):2.

    doi: 10.1186/s40349-016-0046-y
12. Darrow DP. Focused ultrasound for neuromodulation. *Neurotherapeutics*. 2019;16(1):88-99.

    doi: 10.1007/s13311-018-00691-3
13. Hynynen K, Freund WR, Cline HE, *et al*. A clinical, noninvasive, MR imaging-monitored ultrasound surgery method. *Radiographics*. 1996;16(1):185-195.

    doi: 10.1148/radiographics.16.1.185
14. Martínez-Fernández R, Mahendran S, Pineda-Pardo JA, *et al*. Bilateral staged magnetic resonance-guided focused ultrasound thalamotomy for the treatment of essential tremor: A case series study. *J Neurol Neurosurg Psychiatry*.

2021;92(9):927-931.

doi: 10.1136/jnnp-2020-325278

15. Abe K, Horisawa S, Yamaguchi T, *et al*. Focused ultrasound thalamotomy for refractory essential tremor: A Japanese multicenter single-arm study. *Neurosurgery*. 2021;88(4):751-757.

doi: 10.3390/w12051285

16. Osterholt T, McGurrin P, Bedard P, *et al*. Thalamic tremor following focused ultrasound thalamotomy for the treatment of essential tremor. *Mov Disord Clin Pract*. 2021;8(1):139-141.

doi: 10.1002/mdc3.13097

17. Bond AE, Shah BB, Huss DS, *et al*. Safety and efficacy of focused ultrasound thalamotomy for patients with medication-refractory, tremor-dominant Parkinson disease: A randomized clinical trial. *JAMA Neurol*. 2017;74(12):1412-1418.

doi: 10.1001/jamaneurol.2017.3098.

18. Eisenberg HM, Krishna V, Elias WJ, *et al*. MR-guided focused ultrasound pallidotomy for Parkinson's disease: Safety and feasibility. *J Neurosurg*. 2020;135:792-798.

doi: 10.3171/2020.6.JNS192773

19. Lin F, Wu D, Yu J, *et al*. Comparison of efficacy of deep brain stimulation and focused ultrasound in parkinsonian tremor: A systematic review and network meta-analysis. *J Neurol Neurosurg Psychiatry*. 2021;92(4):434-443.

doi: 10.1136/jnnp-2020-323656.

20. Gallay MN, Moser D, Magara AE, Haufler F, Jeanmonod D. Bilateral MR-gui ded focused ultrasound pallidothalamic tractotomy for Parkinson's disease with 1-year follow-up. *Front Neurol*. 2021;12:601153.

doi: 10.3389/fneur.2021.601153

21. Bellary A, Villarreal A, Eslami R, *et al*. Perfusion-guided sonopermeation of neuroblastoma: a novel strategy for monitoring and predicting liposomal doxorubicin uptake *in vivo*. *Theranostics*. 2020;10(18):8143-8161.

doi: 10.7150/thno.45903

22. Martínez-Fernández R, Máñez-Miró JU, Rodríguez-Rojas R, *et al*. Randomized trial of focused ultrasound subthalamotomy for Parkinson's disease. N Engl J Med. 2020;383(26):2501-2513.

doi: 10.1056/NEJMoa2016311

23. Gagliardo C, Midiri M, Cannella R, *et al*. Transcranial magnetic resonance imaging-guided focused ultrasound treatment at 1.5 T: A retrospective study on treatment-and patient-related parameters obtained from 52 procedures. *Front Phys*. 2020;7:223.

doi: 10.3389/fphy.2019.00223

24. Jeanmonod D, Werner B, Morel A, *et al*. Transcranial magnetic resonance imaging–guided focused ultrasound: Noninvasive central lateral thalamotomy for chronic neuropathic pain. *Neurosurg Focus*. 2012;32(1):E1.

doi: 10.3171/2011.10.FOCUS11248.

25. Martin E, Jeanmonod D, Morel A, Zadicario E, Werner B. High-intensity focused ultrasound for noninvasive functional neurosurgery. *Ann Neurol*. 2009;66(6):858-861.

doi: 10.1002/ana.21801

26. Blomstedt P, Hariz GM, Hariz MI, Blomstedt P. Pallidotomy versus pallidal stimulation. *Parkinsonism Relat Disord*. 2006;12(5):296-301.

doi: 10.1016/j.parkreldis.2005.12.007

27. Corneliuson O, Björk-Eriksson T, Daxberg EL, *et al*. Transcranial magnetic resonance guided focused ultrasound treatment of essential tremor, neuropathic pain and Parkinson's disease. *HTA Cent*. 2015;82:11.

28. Sanguinetti JL, Hameroff S, Smith EE, *et al*. Transcranial focused ultrasound to the right prefrontal cortex improves mood and alters functional connectivity in humans. *Front Hum Neurosci*. 2020;14:52.

doi: 10.3389/fnhum.2020.00052

29. Jung HH, Kim SJ, Roh D, *et al*. Bilateral thermal capsulotomy with MR-guided focused ultrasound for patients with treatment-refractory obsessive-compulsive disorder: A proof-of-concept study. *Mol Psychiatry*. 2015;20(10):1205-1211.

doi: 10.1038/mp.2014.154

30. Davidson B, Hamani C, Meng Y, *et al*. Examining cognitive change in magnetic resonance-guided focused ultrasound capsulotomy for psychiatric illness. *Translat Psychiatry*. 2020;10(1):397.

doi: 10.1038/s41398-020-01072-1

31. Davidson B, Hamani C, Huang Y, *et al*. Magnetic resonance-guided focused ultrasound capsulotomy for treatment-resistant psychiatric disorders. *Oper Neurosurg*. 2020l;19(6):741-749.

doi: 10.1093/ons/opaa240

32. Davidson B, Mithani K, Huang Y, *et al*. Technical and radiographic considerations for magnetic resonance imaging-guided focused ultrasound capsulotomy. *J Neurosurg*. 2020;135(1):291-299.

doi: 10.3171/2020.6.JNS201302

33. Lipsman N, Meng Y, Bethune AJ, *et al*. Blood-brain barrier opening in Alzheimer's disease using MR-guided focused ultrasound. *Nat Commun*. 2018;9(1):2336.

doi: 10.1038/s41467-018-04529-6

34. Dubey S, Heinen S, Krantic S, *et al*. Clinically approved IVIg delivered to the hippocampus with focused ultrasound promotes neurogenesis in a model of Alzheimer's disease. *Proc Nat Acad Sci*. 2020;117(51):32691-32700.

doi: 10.1073/pnas.1908658117.

35. Jones RM, Hynynen K, Jones RM. Advances in acoustic monitoring and control of focused ultrasound-mediated increases in blood-brain barrier permeability. *Br J Radiol*. 2019;92(1096):20180601.

doi: 10.1259/bjr.20180601

36. Galimova R, Illarioshkin SN, Buzaev IV, Kachemaeva OV. Therapy of motor disorders by focused ultrasound under the control of magnetic resonance imaging. Recommendations for neurologists on the selection of patients. *Bull Natl Soc Study of Parkinsons Dis Mov Disord*. 2020;1:9-15.

37. Maesawa S, Nakatsubo D, Tsugawa T, *et al*. Techniques, indications, and outcomes in magnetic resonance-guided focused ultrasound thalamotomy for tremor. *Neurol Med Chir (Tokyo)*. 2021;61(11):629-639.

38. Jolesz FA. MRI-Guided focused ultrasound surgery. *Annu Rev Med*. 2009:60:417-430.

doi: 10.1146/annurev.med.60.041707.170303

39. Chang WS, Jung HH, Zadicario E, *et al*. Factors associated with successful magnetic resonance-guided focused ultrasound treatment: Efficiency of acoustic energy delivery through the skull. *J Neurosurg*. 2016;124:411-416.

doi: 10.3171/2015.3

40. D'Souza M, Chen KS, Rosenberg J, *et al*. Impact of skull density ratio on efficacy and safety of magnetic resonance-guided focused ultrasound treatment of essential tremor. *J Neurosurg*. 2019;132:1392-1397.

doi: 10.3171/2019.2.JNS183517

41. Ng PR, Blitz SE, Chua MM, Rees G. Cosgrove Magnetic resonance-guided focused ultrasound thalamotomy for essential tremor patients with low skull density ratio: A case-matched analysis. *Front Neurol*. 2024;15:1370574.

doi: 10.3389/fneur.2024.1370574

42. Boutet A, Gwun D, Gramer R, *et al*. The relevance of skull density ratio in selecting candidates for transcranial MR-guided focused ultrasound. *J Neurosurg*. 2019;132(6):1785-1791.

doi: 10.3171/2019.2.JNS182571

43. Yuen J, Goyal A, Kaufmann TJ, *et al*. Comparison of the impact of skull density ratio with alternative skull metrics on magnetic resonance-guided focused ultrasound thalamotomy for tremor. *J Neurosurg*. 2022;138(1):50-57.

doi: 10.3171/2022.5.JNS22350

Appendix

The convolutional neural network code snippet to estimate optimal magnetic resonance imaging-guided focused ultrasound temperature.

```
# Function to build the neural network model
build_model <- function() [
model <- keras_model_sequential()
model %>%
layer_dense(units = 64,
        input_shape = dim(x_train)(2),
    kernel_regularizer = regularizer_l2(l = 0,001)) %>%
layer_activation_relu() %>%
layer_dense(units = 128, activation = 'relu') %>%
layer_dropout(0.6) %>%
layer_dense(units = 64, activation = 'relu') %>%
layer_dense(units = 1)
model %>% compile(
        loss = "mse",
        optimizer = optimizer_rmsprop(),
        metrics = list("mean_absolute_error")
model
model <- build_model()
print_dot_callback <- callback_lambda(
        on_epoch_end = function(epoch, logs) [
        if (epoch %% 80 == 0) cat("\n")
        cat(".")
early_stop <- callback_early_stopping(monitor = "val_loss", patience = 20)
epochs <- 200
# Model training
history <- model %>% fit(
        x_train,
        y_train,
        epochs = epochs,
        validation_split = 0,2,
        verbose = 1,
        callbacks = list(early_stop, print_dot_callback)
```

ACCSCIENCE PUBLISHING

Global Translational Medicine

MINI-REVIEW

The potential impact of weight control management on metabolic health during healthy aging

Onur Oral[1]*, Mudasir Maqbool[2], Pramila Thapa[3], Pinar Tatlibal[4], and Mumtaz Enser[5]

[1]Department of Health and Sports, Faculty of Sports Sciences, Ege University, Izmir, Turkey

[2]Department of Pharmaceutical Sciences, Faculty of Pharmacology, University of Kashmir, Srinagar, Jammu and Kashmir, India

[3]Department of Health Sciences, Life Skill Education Institutes/Yeti Health Science Academy, Katmandu, Nepal

[4]Department of Sports and Physical Education, Faculty of Necat Hepkon Sport Sciences, Dokuz Eylul University, Izmir, Turkey

[5]Department of Philosophy, Institute of Social Sciences, Dokuz Eylul University, Izmir, Turkey

Abstract

This review highlights the importance of weight management in supporting metabolic health and healthy aging. By taking into account the genetic, environmental, and behavioral factors, effective weight management strategies can help reduce the risk of metabolic disorders and improve overall quality of life. The aging process is a multifaceted phenomenon influenced by a number of socioeconomic, biological, and psychological factors. In an aging society, the importance of healthy living and the significance of delaying aging process have increasingly gaining traction. The emergence of new medical and technological developments has led to the development of anti-aging methodologies designed to extend a healthy life span. Although aging is a natural process that can be accompanied by health problems, research shows that adopting a healthy lifestyle can help to delay and alleviate the negative effects of aging. Extensive clinical studies emphasize the importance of nutrition and regular physical activity in maintaining metabolic health in the healthy aging process. In summary, this review highlights genetic, environmental, and behavioral factors in weight management to support metabolic health and healthy aging, and evaluates the incorporation of personalized medicine in weight management as promising method of interventions to improve the healthy aging process.

Keywords: Metabolic health; Longevity; Weight control management; Healthy aging; Obesity

***Corresponding author:**
Onur Oral
(onur.oral@ege.edu.tr)

Citation: Oral O, Maqbool M, Thapa P, Tatlibal P, Enser M. The potential impact of weight control management on metabolic health during healthy aging. *Global Transl Med*. 2025:4(1):136-141. doi: 10.36922/gtm.4815

Received: September 10, 2024

Revised: November 8, 2024

Accepted: December 20, 2024

Published online: January 13, 2025

1. Introduction

Aging, a complex phenomenon characterized by the gradual deterioration of metabolic and bodily systems, encompassing a range of dimensions including socioeconomic, biological, and psychological factors,[1,2] is increasingly recognized as a treatable condition thanks to new scientific research.[3] Research has shown that various interventions such

as reducing stress, a balanced diet and regular exercise can positively contribute to the healthy aging process.[4,5] In the medical world, it is apparent that there is an increasing effort in delaying the aging process by promoting a healthy life.[6,7]

Recently, there has been a growing interest in clinical studies on the effects of healthy lifestyle habits on healthy aging. These studies aim to provide further insight into the role of maintaining metabolic health in maintaining healthy aging. Evidence from these studies suggests that dietary habits and physical activity, which are among the leading weight control methods, may play important roles in maintaining metabolic health during the aging process. This has led to valuable insights into the complex relationship among metabolic health and individual quality of life, longevity, and public health policy.[8,9] These studies aim to shed light on the intricate relationships between genetic, environmental, and behavioral factors that influence metabolic health and overall quality of life.[10] In addition, there is a growing recognition of the potential benefits of personalized medicine, which seeks to develop tailored interventions based on individual genetic profiles and lifestyle factors to enhance the healthy aging process.[11,12]

A growing line of evidence has shown that metabolic health covers a broad concept encompassing a range of physiological processes, including glucose metabolism, lipid metabolism, and energy balance. It is widely acknowledged that these processes, which are also influenced by genetic interactions, play a pivotal role in maintaining overall metabolic health, preventing chronic diseases, and ensuring healthy aging.[13] Studies shown that healthy and natural eating habits such as the Mediterranean diet, which forms the basis of effective weight control strategies, may play a role in reducing the risk of metabolic disorders such as type 2 diabetes, cardiovascular diseases, and metabolic syndrome. Based on these findings, it is useful to consider a holistic approach to weight management,[14-16] as these important health contributions may support both the effectiveness of weight control methods and metabolic health and hence, healthy aging.[17,18]

Clinical research in this area aims to gain a deeper understanding of the complex nature of metabolic health and its broader implications for public health policy. This understanding provides insight into how factors such as genetics, environment, and behavior, may potentially influence metabolic health, longevity, and quality of life.[19,20] It is known that weight control methods that are supplemented with healthy nutrition can assist in supporting some physiological processes which contribute to better metabolic health. Therefore, it is thought that a healthy nutrition approach to metabolic health and weight control management, as well as physical activity habits, contributes to the improvement of a person's metabolic health problems.[21,22]

2. Materials and methods

A detailed literature search was conducted using various databases, including the US National Library of Medicine (PubMed), Scopus, MEDLINE, Embase, Web of Science, and SportDiscus. To gain a comprehensive understanding of the subject matter, several keywords were selected for inclusion in the search strategy, including "metabolic health," "longevity," "weight control management," "systemic healthy aging," and "obesity." The studies included in the reference lists of articles identified through the literature review were also examined, resulting in the compilation of more exhaustive literature on the subject matter. The search criteria were narrowed down to peer-reviewed articles published in English between 2004 and 2024 to focus on the results. To gain a detailed understanding of the relationship among metabolic health, obesity, longevity, and various systemic conditions of human physiology, studies involving animal models were excluded from the search. For a study to be included in this review, it had to meet certain criteria. First, a study had to examine the relationship between weight control management and general healthy aging. Second, a study had to be published in a peer-reviewed journal. Third, a study had to be available in English. Following a comprehensive review process, a total of 44 studies were included in this review.

3. Results and discussion

There is a consensus that maintaining a healthy weight is important for a long and quality life in elderly patients and effective weight control management is known to be critical for quality of life and healthy aging. Recent clinical studies conducted primarily among middle-aged and elderly populations have suggested an increased risk of death from cardiovascular disease, which potentially impact the healthy aging process associated with being overweight or obesity. It would be beneficial to highlight these scientific studies as they illustrate the potential advantages of a healthy diet and weight management for optimal cardiovascular health and quality of life.[23,24]

Several studies have indicated the possibility that general dietary patterns may offer benefits for cardiovascular health, though further research is needed to confirm this postulation. Other studies have indicated that a diet rich in plant-based foods may have beneficial effects against the risk of developing cardiovascular disease and diabetes.

In addition, a large-scale prospective cohort study conducted by Satija *et al.*[25] found that a plant-based diet may be associated with lower risk of cardiovascular disease compared to a diet rich in animal products. Thus, it may be helpful to consider some of the promising metabolic and cardiovascular benefits of plant-based nutrition.[26,27] Furthermore, studies by Alvarez-Alvarez *et al.*[28] and Oral *et al.*[29] have suggested that greater compliance with the Mediterranean diet and plant-based eating style were associated with a significant reduction in the risk of developing cardiovascular disease and other metabolic diseases. These studies indicate that a health-oriented, dietary modification holds promise for maintaining metabolic health and healthy aging.

In addition to the general dietary patterns, evidence from research seemed to suggest that weight management may have an important role to play in healthy aging. A growing body of evidence suggests an association between maintaining a healthy weight and healthy aging. This may be due to improved metabolic outcomes and reduced risk of age-related diseases observed in these studies.[30,31] There is a possibility that interventions such as regular physical activity and training programs may improve metabolic health, cardiovascular health, longevity, weight control management, and overall well-being in adults, particularly those associated with inflammatory and degenerative conditions in tissues.[32-36] Furthermore, research suggests that early-life nutritional programs may have effects on individual phenotype programming. The tailored weight management strategies that take into account individual preferences and genetic predispositions could potentially lead to more positive outcomes.[37]

Recent advances in medicine and technology have led to the emergence of new anti-aging strategies aimed at extending healthy lifespans and mitigating the aging process.[38] While the aging process is a natural phenomenon that can potentially lead to various health issues, research suggests that adopting a healthy lifestyle such as a natural, balanced diet, and regular physical activity habits, could potentially play an important role in delaying and reducing its negative effects.[39-41] A number of studies on the potential benefits of a healthy lifestyle showed that healthy nutrition and regular physical activity may play an important role in maintaining metabolic health and extending lifespan, which could be of great importance for the healthy aging process.[42-44]

In light of these findings, it is reasonable to suggest that weight management may have a significant impact on metabolic health during healthy aging. As research continues to elucidate the complex associations between lifestyle and metabolic health, it is increasingly clear that personalized interventions can improve the quality of life and healthy aging process. Therefore, effective weight management, which can be achieved through physical activity and healthy nutrition, can be a valuable approach to improving metabolic health and healthy aging.

4. Conclusion

The aging process is regarded as a multifaceted phenomenon with implications across a range of disciplines, including socioeconomics, biology, and psychology. Some studies suggest that aging may be a treatable disease. Researchers from various studies have proposed that the aging process may be slowed down through the implementation of various measures, including stress reduction, balanced nutrition, and exercise. The concept of healthy aging and the mission to delay the aging process has gained significant attention among the scientific community in recent years, particularly in a world where the population is aging. The objective is to promote healthy aging and enhance the quality of life as people age. Thanks to the advancements in medicine and technology, we have several new methods aimed at prolonging a healthy life by delaying the aging process. While aging is inevitable, some scientists believe that it should be treated as a disease, a suggestion that has led to the development of anti-aging treatments.

Scientists are recognizing the importance of understanding the genetic basis of obesity to develop more effective health strategies to combat this global epidemic. Recent research suggests that there is a complex association between genetic predisposition and environmental factors in obesity. Lifestyle changes have shown promise in better weight management and improving metabolic health. Studying these findings can provide new insights into potential targets for interventions. This knowledge is crucial in minimizing the negative impact of obesity on quality of life and life expectancy. In addition, the influence of socioeconomic status and access to health services are considered important in developing effective public health interventions. Overall, understanding the genetic basis of obesity and the involvement of environmental factors can contribute to more successful prevention and treatment approaches.

During the aging process, recognizing the significant impact of lifestyle choices on overall health is crucial in promoting healthy lifestyle habits. Clinical studies have shown that adopting a healthy lifestyle can help mitigate health problems associated with aging. This review highlights the importance of dietary choices and regular physical activity in maintaining metabolic health. It is important to consider the role of genetic factors in the causation and treatment of obesity when developing

weight management strategies. By adopting healthy eating habits and engaging in physical activity, individuals not only improve metabolic health but also prevent diseases associated with overweight and obesity. These efforts ultimately aim to enhance the overall quality of life.

Acknowledgments

We would like to express our sincere gratitude to Dr. George N. Nomikos for his significant contribution to literature search and academic support in the publication of this review article.

Funding

None.

Conflict of interest

The authors declare that they have no competing interests.

Author contributions

Conceptualization: Onur Oral, Mudasir Maqbool, Pramila Thapa, Pınar Tatlibal
Writing – original draft: All authors
Writing – review & editing: All authors

Ethics approval and consent to participate

Not applicable.

Consent for publication

Not applicable.

Availability of data

Not applicable.

References

1. Martinson M, Berridge C. Successful aging and its discontents: A systematic review of the social gerontology literature. *Gerontologist*. 2015;55(1):58-69.

   doi: 10.1093/geront/gnu037

2. Rowe JW, Kahn RL. Successful aging 2.0: Conceptual expansions for the 21st century. *J Gerontol B Psychol Sci Soc Sci*. 2015;70(4):593-596.

   doi: 10.1093/geronb/gbv025

3. Stambler I. Recognizing degenerative aging as a treatable medical condition: Methodology and policy. *Aging Dis*. 2017;8(5):583-589.

   doi: 10.14336/AD.2017.0130

4. López-Otín C, Blasco MA, Partridge L, Serrano M, Kroemer, G. The hallmarks of aging. *Cell*. 2013;153(6): 1194-1217.

   doi: 10.1016/j.cell.2013.05.039

5. Calder PC, Carding SR, Christopher G, Kuh D, Langley-Evans SC, McNulty H. A holistic approach to healthy ageing: How can people live longer, healthier lives? *J Hum Nutr Diet*. 2018;31(4):439-450.

   doi: 10.1111/jhn.12566

6. Dogra S, Dunstan DW, Sugiyama T, Stathi A, Gardiner PA, Owen N. Active aging and public health: Evidence, implications, and opportunities. *Annu Rev Public Health*. 2022;43(1):439-459.

   doi: 10.1146/annurev-publhealth-052620-091107

7. Schmauck-Medina T, Molière A, Lautrup S, *et al*. New hallmarks of ageing: A 2022 Copenhagen ageing meeting summary. *Aging*. 2022;14:6829-6839.

   doi: 10.18632/aging.204248

8. Dunn SL, Siu W, Freund J, Boutcher SH. The effect of a lifestyle intervention on metabolic health in young women. *Diabetes Metab Syndr Obes*. 2014;7:437-444.

   doi: 10.2147/DMSO.S67845

9. Ford ES, Li C. Metabolic syndrome and health-related quality of life among U.S. adults. *Ann Epidemiol*. 2008;18(3): 165-171.

   doi: 10.1016/j.annepidem.2007.10.009

10. Higuera-Gómez A, Ribot-Rodríguez R, Micó V, Cuevas-Sierra A, San Cristóbal R, Martínez JA. Lifestyle and health-related quality of life relationships concerning metabolic disease phenotypes on the Nutrimdea online cohort. *Int J Environ Res public Health*. 2022;20(1):767.

    doi: 10.3390/ijerph20010767

11. Mangoni AA. Comprehensive geriatric assessment and personalized medicine. In: *Comprehensive Geriatric Assessment*. Cham, Switzerland: Springer International Publishing; 2018. p. 69-77.

12. Martens CR, Wahl D, LaRocca TJ. Personalized medicine: Will it work for decreasing age-related morbidities? In: *Aging*. United States: Academic Press; 2023. p. 683-700.

13. Ordovas JM, Shen J. Gene-environment interactions and susceptibility to metabolic syndrome and other chronic diseases. *J Periodontol.* 2008;79(8 Suppl):1508-1513.

    doi: 10.1902/jop.2008.080232

14. Elfhag K, Rössner S. Who succeeds in maintaining weight loss? A conceptual review of factors associated with weight loss maintenance and weight regain. *Obes Rev.* 2005;6(1):67-85.

    doi: 10.1111/j.1467-789X.2005.00170.x

15. Llewellyn C, Wardle J. Behavioral susceptibility to obesity: Gene-environment interplay in the development of weight. *Physiol Behav*. 2015;152(Pt B):494-501.

    doi: 10.1016/j.physbeh.2015.07.006

16. Ofori SN, Unachukwu CN. Holistic approach to prevention and management of type 2 diabetes mellitus in a family setting. *Diabetes Metab Syndr Obes.* 2014;7:159-168.

doi: 10.2147/DMSO.S62320

17. Ghosh TS, Rampelli S, Jeffery IB, *et al*. Mediterranean diet intervention alters the gut microbiome in older people reducing frailty and improving health status: The NU-AGE 1-year dietary intervention across five European countries. *Gut*. 2020;69(7):1218-1228.

doi: 10.1136/gutjnl-2019-319654

18. Slagter SN, van Vliet-Ostaptchouk JV, van Beek AP, *et al*. Health-related quality of life in relation to obesity grade, type 2 diabetes, metabolic syndrome and inflammation. *PLoS One*. 2015;10(10):e0140599.

doi: 10.1371/journal.pone.0140599

19. Aldhoon-Hainerová I, Hainer V, Zamrazilová H. Impact of dietary intake, lifestyle and biochemical factors on metabolic health in obese adolescents. *Nutr Metab Cardiovasc Dis.* 2017;27(8):703-710.

doi: 10.1016/j.numecd.2017.05.002

20. Govindaraju D, Atzmon G, Barzilai N. Genetics, lifestyle and longevity: Lessons from centenarians. *Appl Transl Genomics*. 2015;4:23-32.

doi: 10.1016/j.atg.2015.01.001

21. Knell G, Li Q, Pettee Gabriel K, Shuval K. Long-term weight loss and metabolic health in adults concerned with maintaining or losing weight: Findings from NHANES. *Mayo Clinic Proc.* 2018;93(11):1611-1616.

doi: 10.1016/j.mayocp.2018.04.018

22. Mathew H, Farr OM, Mantzoros CS. Metabolic health and weight: Understanding metabolically unhealthy normal weight or metabolically healthy obese patients. *Metabolism*. 2016;65(1):73-80.

doi: 10.1016/j.metabol.2015.10.019

23. Franco M, Orduñez P, Caballero B, *et al*. Impact of energy intake, physical activity, and population-wide weight loss on cardiovascular disease and diabetes mortality in Cuba, 1980-2005. *Am J Epidemiol.* 2007;166:1374-1380.

doi: 10.1093/aje/kwm226

24. Karimi M, Brazier J. Health, health-related quality of life, and quality of life: What is the difference? *PharmacoEconomics*. 2016;34(7):645-649.

doi: 10.1007/s40273-016-0389-9

25. Satija A, Bhupathiraju SN, Spiegelman D, *et al*. Healthful and unhealthful plant-based diets and the risk of coronary heart disease in U.S. adults. *J Am Coll Cardiol.* 2017;70(4):411-422.

doi: 10.1016/j.jacc.2017.05.047

26. Chen B, Zeng J, Qin M, *et al*. The Association between plant-based diet indices and obesity and metabolic diseases in Chinese adults: Longitudinal analyses from the China health and nutrition survey. *Front Nutr*. 2022;9:881901.

doi: 10.3389/fnut.2022.881901

27. Kahleova H, Levin S, Barnard N. Cardio-metabolic benefits of plant-based diets. *Nutrients*. 2017;9(8):848.

doi: 10.3390/nu9080848

28. Alvarez-Alvarez I, de Rojas JP, Fernandez-Montero A, *et al*. Strong inverse associations of Mediterranean diet, physical activity and their combination with cardiovascular disease: The Seguimiento Universidad de Navarra (SUN) cohort. *Eur J Prev Cardiol*. 2018;25(11):1186-1197.

doi: 10.1177/2047487318783263

29. Oral O, Rezaee Z, Stavropoulou E. The role of vegan diet on health and fitness. *Biomed J Sci Tech Res.* 2022;43(3):34557-34560.

doi: 10.26717/BJSTR.2022.43.006899

30. Alley DE, Ferrucci L, Barbagallo M, Studenski SA, Harris TB. A research agenda: The changing relationship between body weight and health in aging. *J Gerontol A Biol Sci Med Sci*. 2008;63(11):1257-1259.

doi: 10.1093/gerona/63.11.1257

31. Han TS, Wu FC, Lean ME. Obesity and weight management in the elderly: A focus on men. *Best Pract Res Clin Endocrinol Metab.* 2013;27(4):509-525.

doi: 10.1016/j.beem.2013.04.012

32. Gill LE, Bartels SJ, Batsis JA. Weight management in older adults. *Curr Obes Rep.*, 2015;4(3):379-388.

doi: 10.1007/s13679-015-0161-z

33. Hall ME, Cohen JB, Ard JD, *et al*. Weight-loss strategies for prevention and treatment of hypertension: A scientific statement from the American Heart Association. *Hypertension*. 2021;78(5):e38-e50.

doi: 10.1161/HYP.0000000000000202

34. Oral O, Rezaee Z, Thapa P, Tatlibal P. The positive impact of regular physical activity on metabolic health and healthy aging: A narrative review. *Int J Case Rep Case Res.* 2024;1(2):1-4.

doi: 08.2024/IJCRCR/006

35. Rezaee Z, Javaheri S, Rashidlamir A, Oral O, Stavropoulos E. Effects of BFR training in serum NRG-1 and IL-6 in overweight postmenopausal women. *Sci Chronic.* 2022;27(4):541-554.

36. Szychowska A, Drygas W. Physical activity as a determinant of successful aging: A narrative review article. *Aging Clin Exp Res.* 2022;34(6):1209-1214.

doi: 10.1007/s40520-021-02037-0

37. Buchanan KL, Meillère A, Jessop TS. Early life nutrition

and the programming of the phenotype. In: *Development Strategies and Biodiversity: Darwinian Fitness and Evolution in the Anthropocene*. Cham: Springer International Publishing; 2022. p. 161-214.

38. Juengst ET. Anti-aging research and the limits of medicine. In: *The Fountain of Youth: Cultural, Scientific, and Ethical Perspectives on a Biomedical Goal*. New York: Oxford Academic; 2004. p. 321-339.

39. Daskalopoulou C, Stubbs B, Kralj C, Koukounari A, Prince M, Prina AM. Physical activity and healthy ageing: A systematic review and meta-analysis of longitudinal cohort studies. *Ageing Res Rev.* 2017;38:6-17.

doi: 10.1016/j.arr.2017.06.003

40. Sánchez-González D, Rojo-Pérez F, Rodríguez-Rodríguez V, Fernández-Mayoralas G. Environmental and psychosocial interventions in age-friendly communities and active ageing: A systematic review. *Int J Environ Res Public Health*. 2020;17(22):8305.

doi: 10.3390/ijerph17228305

41. Taylor AH, Cable NT, Faulkner G, Hillsdon M, Narici M, Van Der Bij AK. Physical activity and older adults: A review of health benefits and the effectiveness of interventions. *J Sports Sci*. 2004;22(8):703-725.

doi: 10.1080/02640410410001712421

42. Xu F, Cohen SA, Lofgren IE, Greene GW, Delmonico MJ, Greaney ML. The Association between physical activity and metabolic syndrome in older adults with obesity. *J Frailty Aging*. 2019;8(1):27-32.

doi: 10.14283/jfa.2018.34

43. Yao S, Colangelo LA, Perry AS, *et al*. Implications of metabolism on multi-systems healthy aging across the lifespan. *Aging Cell*. 2024;23(4):e14090.

doi: 10.1111/acel.14090

44. Johnson AA, Stolzing A. The role of lipid metabolism in aging, lifespan regulation, and age-related disease. *Aging Cell*. 2019;18(6):e13048.

doi: 10.1111/acel.13048

ACCSCIENCE PUBLISHING

Global Translational Medicine

LETTER TO EDITOR

Comment to the manuscript "chronic positive mass balance is the actual etiology of obesity: A living review"

Nikolaos Theodorakis[1,2]*

[1]NT-CardioMetabolics, Clinic for Metabolism and Athletic Performance, Palaio Faliro, Greece

[2]Department of Cardiology and Preventive Cardiology Outpatient Clinic, Amalia Fleming General Hospital, Melissia, Greece

Dear Editor,

The perspective manuscript titled "Chronic positive mass balance is the actual etiology of obesity: A living review" makes an important distinction between mass balance and energy balance in obesity, emphasizing the role of nutrient mass in body weight regulation.[1] This is an insightful argument, as the physical mass of ingested nutrients is directly linked to body mass changes. However, dismissing the energy balance theory as fallacious oversimplifies the complex interplay between mass and energy in biological systems.

Body weight regulation is fundamentally governed by the interconnected processes of mass balance and energy balance, both of which must be understood within the framework of thermodynamics. According to the First Law of Thermodynamics (conservation of energy), energy in a closed system cannot be created or destroyed but is instead transformed into various forms. In the human body, energy derived from food is metabolized into usable energy (e.g., adenosine triphosphate [ATP]), heat, and metabolic byproducts (e.g., CO_2, water, urea). Simultaneously, the Law of Conservation of Mass governs nutrient flow, with body mass changes reflecting the net balance of ingested, metabolized, stored, or excreted nutrients.

Metabolism transforms nutrients into usable energy (e.g., ATP, guanosine triphosphate), "waste" energy (heat), and byproducts (e.g., CO_2, water, urea, uric acid). These metabolic processes, which are influenced and regulated by multiple factors (e.g., genetics, lifestyle, hormones), determine the fate of nutrients, which may be:

- Converted into usable energy (e.g., ATP) for immediate utilization in cellular functions (e.g., Na^+/K^+ pump activity)
- Stored as fat or lean tissue (a process that also requires ATP utilization)
- Dissipated as heat (e.g., via uncoupling of oxidative phosphorylation), or
- Excreted as metabolic byproducts.

While the manuscript correctly identifies limitations in the rigid application of energy balance models – such as their inability to account for the effects of macronutrient distribution on body composition – its assertion that energy balance has no impact on body mass is scientifically inaccurate. A positive energy balance drives fat storage, increasing body mass, whereas a caloric deficit mobilizes stored fat, reducing body mass. Energy balance and mass balance are not mutually exclusive but rather complementary and interdependent. Neglecting this interrelationship misrepresents physiological reality. However, it is important to acknowledge that traditional energy balance models,

***Corresponding author:**
Nikolaos Theodorakis
(n.theodorakis@flemig-hospital.gr)

Citation: Theodorakis N. Comment to the manuscript "chronic positive mass balance is the actual etiology of obesity: A living review". *Global Transl Med*. 2025:4(1):142-143. doi: 10.36922/gtm.8079

Received: December 19, 2024

Accepted: January 10, 2025

Published online: March 20, 2025

when applied rigidly, have limitations. For example, they often fail to predict how macronutrient composition (e.g., low-carbohydrate or high-protein diets) affects energy expenditure, fat oxidation, and storage efficiency. This limitation underscores the need for a more integrative approach.

The interdependence between nutrient mass (mass balance) and energy content (energy balance) becomes particularly evident when considering how they interact to regulate body weight. While nutrient mass determines the physical input and output of body weight, the energy derived from this mass dictates how it is processed, stored, or excreted. For instance, 1 g of carbohydrate or protein provides approximately 4 kcal, whereas 1 g of fat provides 9 kcal. These differences in caloric density illustrate why equal masses of macronutrients can lead to vastly different metabolic outcomes.

A caloric surplus of 500 kcal/day would theoretically result in a fat gain of approximately 65 g/day, or about 2 kg over a month. This estimate is based on the energy density of body fat, where 1 g of fat tissue corresponds to roughly 7.7 kcal (accounting for water and other components). However, this calculation assumes no compensatory metabolic adjustments and that all surplus energy is stored as fat with 100% efficiency. In reality, the process is far more complex and influenced by various factors. Notably, some of the surplus energy may contribute to lean mass (especially in individuals engaged in resistance training or consuming a high-protein diet), support cellular functions, or be dissipated as heat through the uncoupling of oxidative phosphorylation. In addition, mechanisms such as "luxurious energy expenditure" can elevate basal metabolic rate in response to increased energy intake, primarily by enhancing oxidative phosphorylation uncoupling through complex mechanisms such as increased peripheral conversion of T4 to T3. This process reduces the efficiency of fat storage.[2]

These metabolic processes exhibit significant individual variability and are strongly influenced by both genetic and lifestyle factors, with the latter inducing epigenetic modifications that alter metabolic pathways and hormonal regulation. For instance, a recent study showed that an approximately 1,000 kcal/day surplus resulted in only about 1 kg of fat gain over 28 days – approximately four times less than the theoretical prediction of 4 kg.[3] These findings highlight the dynamic and adaptive nature of metabolism, demonstrating that neither mass balance nor energy balance models alone can fully capture the complexities of weight regulation.

By combining mass balance for nutrient flow and energy balance for metabolic regulation, a robust framework for understanding obesity can emerge. Such a framework acknowledges that while nutrient mass determines physical weight change, the energy derived from these nutrients governs the metabolic pathways that dictate their ultimate fate – storage, oxidation, or excretion.

In conclusion, the manuscript provides valuable insights into the role of nutrient mass in obesity but would benefit from a more nuanced discussion of the interplay between mass and energy. Recognizing their interdependence could help bridge the gap between traditional energy-centric approaches and emerging mass-focused paradigms, fostering a deeper understanding of obesity and its management. Addressing these aspects would strengthen the manuscript's scientific rigor and enhance its practical relevance.

Conflict of interest

The author declares no conflict of interest.

References

1. Manninen AH. Chronic positive mass balance is the actual etiology of obesity: A living review. *Glob Transl Med*. 2023;2(1):222.

   doi: 10.36922/gtm.222

2. Theodorakis N, Kreouzi M, Pappas A, Nikolaou M. Beyond calories: Individual metabolic and hormonal adaptations driving variability in weight management-A state-of-the-art narrative review. *Int J Mol Sci*. 2024;25(24):13438.

   doi: 10.3390/ijms252413438

3. Morrison DJ, Kowalski GM, Bruce CR, Wadley GD. Modest changes to glycemic regulation are sufficient to maintain glucose fluxes in healthy young men following overfeeding with a habitual macronutrient composition. *Am J Physiol Endocrinol Metab*. 2019;316(6):E1061-E1070.

   doi: 10.1152/ajpendo.00500.2018

Our Journals

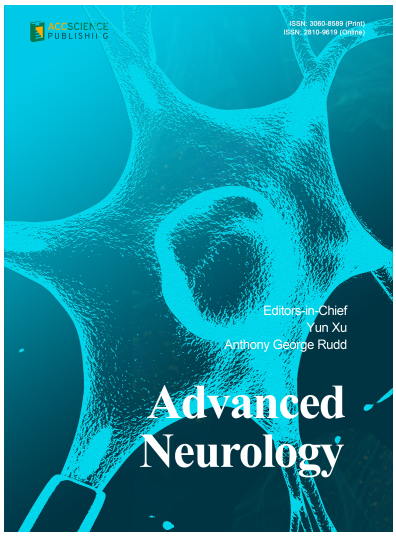

Advanced Neurology is a peer-reviewed and open-access journal that aims to publish and disseminate novel research in the breadth of neurology and neuroscience. The journal aims to advance our understanding in the nervous system and provide a platform to neuroscientists and physicians to showcase their findings in original fundamental and clinical research as well as to present new ideas that highlight the changes in the neurological clinical practice.

Advanced Neurology covers subject areas, including but not limited to the following:

- Neurological disorders
- Neurodegenerative disease
- Cerebrovascular disease
- Epilepsy and movement disorders
- Neuroimmune disease
- Neurological infections
- Muscle disease
- Molecular and cellular neuroscience
- Systems neuroscience
- Cognitive neuroscience
- Computational modeling of nervous system

Gene & Protein in Disease publishes rigorously peer-reviewed and high quality original articles and authoritative reviews that focus on the latest development in multidisciplinary areas in biology and biomedicine, with an emphasis on gene and protein research. The journal has worldwide authorship, and a broad scope in basic and translational biomedical research of genetics, biochemistry, biophysics, oncology, immunology, cell biology, molecular biology, developmental biology, microbiology, neuroscience, stem cell, protein science, structural biology, regenerative medicine and translational medicine.

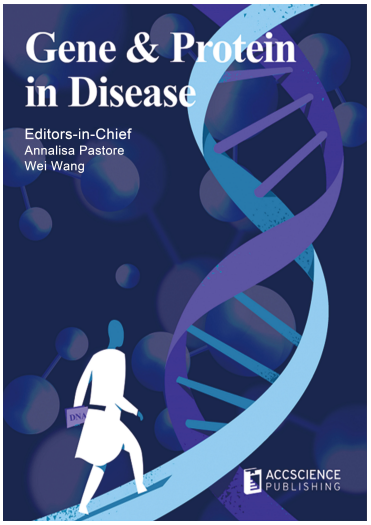

Start a new journal

Write to us via email if you are interested to start a new journal with AccScience Publishing. Please attach your CV, professional profile page and a brief pitch proposal in your email. We shall inform you of our decision whether we are interested to collaborate in starting a new journal.

Contact: info@accscience.com

https://accscience.com/journal/GTM

Contact
www.accscience.com
8 Burn Road, #15-03 Trivex, Singapore 369977
Email: editorial@accscience.com
Phone: +65 8182 1586